IN VITRO GENERATION OF A BILAYERED DENSE COLLAGEN /CHITOSAN HYDROGEL SCAFFOLD AS AN OSTEOCHONDRAL MODEL

Florencia Chicatun

Department of Mining and Materials Engineering

McGill University, Montreal, QC, Canada

August 2013

A thesis submitted to McGill University in partial fulfillment of the requirements of the degree of Doctor of Philosophy

ABSTRACT

Tissue engineering (TE) is an interdisciplinary research field that is emerging as an alternative approach to traditional surgical strategies in repairing damaged tissues. Thus far, efforts have resided in achieving functionally engineered grafts based on homogeneous scaffolds seeded with a single cell source. However, a current challenge for TE is the development of scaffolds with heterogeneous structural organization seeded with multiple cell types for replacing more complex tissues, such as the osteochondral interface in joints.

Success of osteochondral tissue regeneration therapies in clinical practice require *a priori* development of experimental *in vitro* models as tools to comprehensively study their complex physiological and pathological mechanisms. In this regard, stratified scaffolds have been designed to mimic and recreate, to a certain extent, the biochemical and biophysical composition of the intricate cellular environment of the two dissimilar tissues (*i.e.* cartilage and subchondral bone). The osteochondral interface is composed of adhesive and mineral-binding proteins and proteoglycans (glycosaminoglycans; GAGs), in addition to collagen fibrils. The highly challenging problem of interfacing one tissue with another has led to the development of bilayered constructs to satisfy the demand of multiple cell types and to promote their simultaneous growth and differentiation within discrete layers.

In vitro reconstituted collagen type I (Coll) hydrogels are widely used as biomimetic scaffolds for TE as well as for *in vitro* three-dimensional tissue-equivalent models. Although Coll gels offer many biochemical benefits, a major factor that limits their therapeutic use is the low protein concentration that results from their highly-hydrated nature (> 99 wt. % water), thus conferring geometrical instability and poor mechanical properties. Highly-hydrated Coll hydrogels collapse in an unconfined environment due to gravitational forces, a process identified as self-compression (SC), which can be accelerated through the controlled application of an external load (plastic compression; PC). PC is a simple, rapid and reproducible technique that generates dense scaffolds with

increased solid weight percent (~8 %), approaching those of native tissues, along with improved mechanical properties.

The aim of this doctoral research was to develop and characterize a bilayered model system for osteochondral TE applications based on the incorporation of a GAG-analog within a dense Coll hydrogel, to closely mimic the native extracellular matrix (ECM) of both cartilage and subchondral bone at the osteochondral interface. Chitosan (CTS) is a natural polysaccharide, which structurally and compositionally resembles the GAGs present within native tissues. It was therefore hypothesized that ECM-like scaffolds can be optimized by the incorporation of CTS within dense Coll gels, thus mimicking the roles of the fibrillar protein network and GAGs found in native cartilage and bone ECMs. Within this doctoral research, five different objectives were established.

The first objective was to develop and optimize a co-gelling system for the generation of highly-hydrated Coll/CTS hybrid gels with different CTS proportions, which could be subjected to PC to achieve dense scaffolds with compositions closer to native tissue. In this respect, PC was shown to be an effective and rapid process able to generate, within minutes, dense Coll/CTS hybrid gels with increased solid weight percent, compressive modulus and resistance to enzymatic degradation, as dictated by CTS content.

As a second objective, the effect of CTS incorporation on modulating MC3T3-E1 pre-osteoblast seeded-cell function within dense Coll gels was investigated, and compared to Coll alone. Dense Coll/CTS hydrogels supported MC3T3-E1 cell viability, proliferation, and differentiation under osteogenic-inducing conditions. The incorporation of CTS within dense Coll gels effectively modulated cell-based remodeling *via* the action of MC3T3-E1 secreted proteases (*i.e.* MMP-13) and by their forces exercised on the substrate (*i.e.* cell-mediated contraction). Furthermore, the potential of MC3T3-E1 pre-osteoblasts to mineralize the osteoid-like matrix was investigated. Measurements of alkaline phosphatase activity, MMP-13 expression, and phosphate concentration showed that hybrid scaffolds supported osteoblastic differentiation and mineralization,

resembling nascent bone tissue. These findings demonstrated that dense Coll/CTS hybrids provide a novel approach for the assembly of osteoid-like structure with biomimetic function as an *in vitro* model for bone TE.

As a third objective, the effect of CTS incorporation into dense Coll gel discs and cylindrically shaped constructs was investigated to serve as a chondroprotective material to support RCJ3.1C5.18 chondroprogenitors (RCJ) differentiation and cartilage-like ECM production. Seeded RCJ cell metabolic activity, cell-mediated gel contraction, viability and morphology, and cartilage-like aggregate formation within dense Coll/CTS discs, were compared to cells seeded into dense Coll gels alone. Coll/CTS hydrogel discs resulted in higher RCJ viability and metabolic activity as well as lower cell-mediated gel contraction. In addition, immunohistochemistry for collagen type II, in combination with Safranin O staining and GAG quantification, indicated greater chondroprogenitor differentiation within Coll/CTS scaffolds. Furthermore, the complex interplay between scaffold geometry, microstructure, composition, and mechanical properties with chondroprogenitor function was assessed on cylindrically shaped constructs of clinically relevant dimensions (3 to 5 mm in diameter and 9 mm in height). While GAG content decreased over time and reduced cell viability was observed within the core regions of all cylindrical rolls, the incorporation of CTS diminished both these effects. Together these findings provide a framework for understanding the interactions between chondrocytes and the macromolecular components and morphometric parameters of dense Coll/CTS scaffolds.

The fourth objective was to develop a bilayered dense Coll/CTS hydrogel with ratios approaching those of Coll/GAGs found in native cartilage (Coll/CTS 1:1) and bone (Coll/CTS 33:1) ECM at the osteochondral interface. Bilayered dense scaffolds having two distinct but integrated layers were rapidly produced, by means of plastically compressing co-gelled bilayered hydrogels, achieving solid weight percent in the physiological range. In addition, the optimization of the co-culturing conditions to maximize and maintain the simultaneous differentiation of chondro- and osteoprogenitor cells was investigated. The *in vitro* work demonstrated that by modulating the medium and supplement

concentrations, bilayered dense Coll/CTS hydrogel supported concurrent chondrogenesis and osteogenesis within each layer, while maintaining the integrity of the scaffold. These results demonstrated the potential of bilayered dense Coll/CTS hydrogel to be used as effective *in vitro* osteochondral models for the study of cell-cell interactions and the production of multilayered scaffolds that resemble complex native tissues.

As the fifth objective, the effect of CTS on Coll gel consolidation during SC and PC was investigated by monitoring the microstructural evolution of Coll/CTS hydrogels through the detection of the spatiotemporal distribution of fluorescent beads using confocal microscopy. The Happel model was used to theoretically predict the hydraulic permeability (k) of pre- and post-compressed hydrogels. In addition, the effect of CTS fixed charge on dense Coll/CTS hydrogels was investigated through structural, mechanical and swelling characterizations under isotonic and hypertonic conditions. The results showed that bead density correlated with gel solid weight percent, thus validating the fluorescent-based imaging method. k decreased with increasing CTS content, resulting in a concomitant increase in scaffold compressive modulus. In addition, the screening of electrostatic forces from CTS repulsive charges was evident by the decrease in the swelling ratio of Coll/CTS scaffolds in hypertonic when compared to isotonic conditions. These results indicate the ability of a charged GAG-analog to tailor the biophysicochemical properties of Coll hydrogels, thus providing a reliable 3D *in vitro* tissue model with similar cues to the *in vivo* environment that may be adapted to optimize TE scaffold design and improve therapeutic outcomes.

In conclusion, the integrated bilayered dense Coll/CTS construct developed and characterized in this doctoral research effectively provided a tailored *in vitro* cell culture milieu that closely mimics a complex physiologic ECM – with collagen mimicking the fibrillar protein network and CTS fulfilling the specific role of the GAGs found in native tissues – to be used as a three-dimensional experimental tissue model and with the potential for clinical use as a biomimetic implant with osteochondral regenerative capacity.

RESUME

Le génie tissulaire est un champ de recherche interdisciplinaire qui émerge en tant qu'approche alternative aux stratégies chirurgicales traditionnelles pour la réparation des tissus endommagés. À ce jour les efforts ont été concentrés sur la réalisation de greffons fonctionnels basés sur une matrice homogène ensemencée d'une source cellulaire unique. Cependant le défi actuel du génie tissulaire est le développement de matrices avec une organisation structurale hétérogène ensemencées de plusieurs types de cellules afin de remplacer des tissus plus complexes comme l'ostéochondral.

Le succès de la thérapie de régénération du tissu ostéochondral en pratique clinique requiert le développement de modèles in vitro expérimentaux en tant qu'outil afin d'en étudier les complexes physiologiques et pathologiques complexes. Dans cette optique des matrices stratifiées ont été conçues afin d'imiter et recréer, jusqu'à un certain point, la composition biochimique et biophysique de l'environnement cellulaire complexe des deux différents tissus, soient le cartilage et l'os sous-chondral. L'interface de l'osteochondral est composée de protéines adhésives, protéines liées aux minéraux et de protéoglycans (glycosaminoglycanes; GAGs) en plus de fibrilles de collagène. Ce problème a mené à l'élaboration d'une construction à deux couches afin de répondre à la demande des multiples types de cellules et de promouvoir leur croissance simultanée et leur différentiation dans les différentes couches.

Les hydrogels de collagène de type I (Coll) reconstitués *in vitro* sont grandement utilisés en tant que matrices biomimétiques pour le génie tissulaire et en tant que modèle de tissus *in vitro* tridimensionnel. Malgré que les gels de collagène offrent de nombreux avantages biochimiques un facteur majeur limite leur utilisation thérapeutique soit leur faible concentration en protéines qui résulte de leur nature hautement hydratée (> 99% massique d'eau) qui cause une instabilité géométrique et de mauvaises propriétés mécaniques. Les hydrogels de collagène hautement hydratés s'affaissent en l'absence de support externe à cause des forces gravitationnelles, un procédé appelé auto-compression (SC), qui peut

être accéléré par l'application d'une charge externe contrôlée (compression plastique; CP). La CP est un procédé simple, rapide et reproductible qui génère des matrices denses offrant un pourcentage massique de solide plus élevé (~8%) se rapprochant du taux de solide des tissus naturels et offrant de meilleurs propriétés mécaniques.

Cette recherche de doctorat a pour but de développer et caractériser un modèle à deux couches pour des applications en génie tissulaire ostéochondral basés sur l'incorporation de GAGs analogiques dans un hydrogel Coll dense afin de reproduire de près la matrice extra-cellulaire (MEC) naturelle du cartilage et de l'os sous-chondral à l'interface ostéochondrale. Le chitosan (CTS) est un polysaccharide naturel qui se rapproche des GAGs présents dans les tissus naturels structurellement et au niveau de la composition. Une hypothèse a donc été émise : les matrices de type MEC peuvent être optimisées en incorporant des CTS dans des gels Coll denses reproduisant ainsi le rôle du réseau de protéines fibrillaires et des GAGs se retrouvant dans la MEC naturelle des os et du cartilage. Dans le cadre de ce doctorat cinq objectifs ont été établis.

Le premier objectif était de développer et d'optimiser un système co-gélifiant pour la génération de gels hybrides de Coll/CTS hautement hydraté avec diverses proportions de CTS et soumis à une CP afin d'obtenir des matrices avec une composition plus près des tissus naturels. In a été démontré que la CP est un procédé rapide et efficace capable de générer en quelques minutes des gels hybrides de Coll/CTS dense avec un taux de solide accru, un module de compression et une résistance à la dégradation enzimatique, le tout dicté par la teneur en CTS.

Comme second objectif l'effet de l'incorporation de CTS sur la modulation de la fonction de cellules ensemencées pré-ostéoblastes MC3T3-E1 à l'intérieur de gels Coll denses a été étudié et comparé au Coll seul. Les hydrogels de Coll/CTS dense ont permis la viabilité et la prolifération de cellules MC3T3-E1 ainsi que leur différentiation dans des conditions ostéogéniques. L'incorporation de CTS aux gels Coll denses a modulé de manière efficace le remodelage basé sur

les cellules par l'action de protéases MC3T3-E1 sécrétées (*i.e.* MMP-13) et par leurs forces exercées sur le substrat (*i.e.* contractions par les cellules). De plus, le potentiel des pré-ostéoblastes MC3T3-E1 à minéraliser la matrice de type ostéoïde a été étudié. Des mesures d'activité de la phosphatase alcaline, l'expression de MMP-13 et la concentration de phosphatase ont démontré que les matrices hybrides supportent la différentiation et la minéralisation ostéoblaste, se rapprochant des tissus naissants. Ces résultats démontrent que les hybrides de Coll/CTS denses sont une nouvelle approche pour l'assemblage de structures de type ostéoïdes avec des fonctions biomimétiques en tant que modèle *in vitro* pour l'ingénierie tissulaire.

En tant que troisième objectif l'effet de l'incorporation de CTS à des disques et des constructions cylindriques de gel Coll dense afin de servir comme matériel chondro-protecteur pour supporter la différentiation de chondro-progéniteurs RCJ3.1C5.18 (RCJ) et de la production de MEC de type cartilage a été étudié. L'activité métabolique de RCJ ensemencées, la contraction de gel induite par les cellules, sa viabilité et sa morphologie et la formation d'agrégats dans les disques de Coll/CTS dense ont été comparés à des cellules ensemencées dans du gel Coll dense seul. La structure hybride a montré une plus grande viabilité et une meilleure activité métabolique en plus de diminuer la contraction du gel par les cellules. De plus, l'immunohistochimie du colagène de type II, combiné avec la coloration avec du Safranin O et la quantification des GAGs, ont indiqué que la différentiation des chondro-progéniteurs est meilleures avec les matrices de Coll/CTS. Également, la relation complexe entre la géométrie, la microstructure, la composition et les propriétés mécaniques de la matrice avec la fonction des chondro-progéniteurs a été adressée sur des structures cylindriques aux dimensions cliniquement utiles (3 à 5 mm de diamètre et 9 mm de hauteur). Alors que le contenu en GAGs diminuait avec le temps et qu'un diminution de la viabilité ont été observés dans les régions centrales de tous les rouleaux cylindriques, l'incorporation de CTS a permis de diminuer ces deux effets. Ensemble ces résultats procurent un cadre afin de comprendre l'interaction entre

les chondrocytes et les composantes macro-moléculaires et les paramètres morphométriques des matrices de Coll/CTS denses.

Le quatrième objectif était de développer une structure à deux couches d'hydrogel de Coll/CTS denses avec des ratios se rapprochant celui de Coll/GAGs se retrouvant dans le cartilage naturel (Coll/CTS 1:1) et dans la MEC de l'os à l'interface ostéochondrale (Coll/CTS 33:1). Des matrices possédant deux couches distinctes mais intégrées ont rapidement été produites par compression plastique d'hydrogels co-gélifiés à deux couches permettant d'atteinte un pourcentage de solide dans la plage physiologique. De plus l'optimisation des conditions de co-culture permettant de maximiser et de maintenir la différentiation simultanée de cellules chondro- et ostéo-progénitrices a été étudiée. Le travail *in vitro* a permis de démontrer que les structures d'hydrogel à deux couches supportent les réactions concurrentes de chondrogénèse et d'ostéogénèse dans chaque couche en modulant la concentration du milieu et des suppléments. Ces résultats démontrent la possibilité d'utiliser les hydrogels de Coll/CTS denses à deux couches en tant que modèles ostéochondraux *in vitro* pour l'étude de l'interaction inter-cellulaire ainsi que pour la production de matrices à multiples couches s'approchant de la structure de tissus complexes.

En tant que cinquièmes objectif l'effet des CTS sur la consolidation du gel de colagène durant la SC et la CP a été étudié en surveillant l'évolution de la microstructure des hydrogels de Coll/CTS par la détection de la distribution spatiotemporelle de billes fluorescentes par microscopie confocale. Le modèle de Happel a été utilisé afin de prédire de manière théorique la perméabilité hydraulique (k) des hydrogels avant et après compression. Aussi l'effet de la charge fixe des CTS sur les hydrogels Coll/CTS a été étudié par leur caractérisation structurelle, mécanique et de gonflement dans des conditions isotoniques et hypertoniques. Les résultats ont montré que la densité de billes était corrélée au taux de solide du gel validant ainsi la méthode d'imagerie par fluorescence. k diminuait avec l'augmentation de la quantité de CTS résultant en une augmentation du module de compression de la matrice. De plus, le dépistage des forces électrostatiques provenant des charges répulsives des CTS a été mis en

évidence par la réduction du ratio de gonflement des matrices de Coll/CTS en hypertonique comparé à des conditions isotoniques. Les résultats ont indiqué la capacité d'un analogue de GAG chargé à s'adapter aux propriétés biophysicochimiques des hydrogels Coll, offrant un modèle de tissus 3D *in vitro* avec des signals similaires dans l'environnement *in vitro* pouvant être adapté afin d'optimiser le design de matrices en génie tissulaire et améliorer les aboutissements thérapeutiques.

En conclusion la structure à deux couches de Coll/CTS dense développée et caractérisée dans le cadre de ce doctorat a procuré un milieu de culture de cellules *in vitro* reproduisant la MEC complexe avec le collagène reproduisant le rôle du réseau de protéines fibrillaires et les CTS remplissant le rôle spécifique des GAGs se trouvant dans les tissus naturels. Cette structure est utilisée en tant que modèle expérimental tridimensionnel de tissus et pourrait potentiellement être utilisé cliniquement en tant qu'implant biomimétique avec des capacités régénératrices ostéochondrales.

ACKNOWLEDGEMENTS

It is with immense gratitude that I acknowledge my supervisor, Dr. Showan N Nazhat, for his guidance, encouragement, patience, trust and understanding throughout the course of this research. I am also thankful to my co-supervisor Dr. Marc D McKee who was insightful, motivating and very supportive towards my academic pursuits; as well as Dr. Mari Kaartinen for having her doors always open for advice. Their generosity in providing all of the necessary facilities, equipment and training, as well as imparting valuable knowledge for my research is deeply appreciated.

Special thanks are extended to Dr. Thomas Quinn, not only for providing access to the facilities in his lab and kind collaboration, but also for his guidance regarding professional and personal matters.

I owe my deepest gratitude to Dr. Claudio Pedraza and Dr. Naser Muja from whom I have gained invaluable experience in many experimental skills. Their commitment to teaching and sharing their expertise with me, along with their technical assistance and constructive advice, is deeply appreciated. Thanks also for the countless philosophical discussions on relevant and non-relevant topics.

I would like to acknowledge those who have provided technical assistance toward this dissertation over the years, which include Lydia Malynowsky and Line Mongeon for assistance with the microscopy and protocol design.

I would also like to thank all my lab members in Dr. Nazhat's laboratory. In particular, Vahid Serpooshan, Maziar Shah Mohammadi and Christopher Stähli for their help and support throughout the most rigorous phase of my research. Further acknowledgements go to Aisha Mousa and Betty Hoac for the continuous exchange of ideas and providing help on countless occasions with many protocols. Special thanks are extended to Aisha for sharing her expertise, wisdom and friendship with me.

This thesis would not have been possible without the generous funding support, scholarships and awards. In particular, I would like to express my

gratitude to the Fondation Pierre Arbour for their generous scholarship, and the Faculty of Engineering for the continuous recognition of my efforts during these years, through the Recruitment Excellence Fellowship 2007 and 2008, McGill Engineering Doctoral Award 2008-2011, McGill Engineering Vadasz Faculty Fellowship 2008, McGill Engineering Hatch Faculty Fellowship 2009, Graduate research enhancement and travel award 2010, 2011 and 2012, Principal Graduate's Fellowship 2011 and non-conference travel award 2012.

I wish to express my deep love and appreciation to my dearest parents Daniel Chicatun and Isabel Tipping, my sister Victoria and my brothers Martin and Pablo for their unconditional love, care and support. *Muchísimas gracias por su sacrificio, por creer en mi y por haberme dado la oportunidad de realizarme como profesional; por alentarme día a día y, por sobre todas las cosas, por haber estado presente en cada momento de mi vida a pesar de la distancia*.

Last, I am greatly indebted to my husband Martin who held my hand through this challenging journey and never let it go. Words cannot express my love and gratitude towards him, who encouraged and believed in me at all times. This work is dedicated to him and to the greatest project of my life - my son Benjamin - who I deeply love and who has endured his mother finishing her PhD in his first months of life.

TABLE OF CONTENTS

LIST OF FIGURES

LIST OF TABLES

GLOSSARY OF ABBREVIATIONS AND SYMBOLS

μ	Micro
μ	Dynamic viscosity
ρ	Fluid density
σ	Solid volume fraction
k	Hydraulic permeability
t	Time
2D	Two-dimensional
3D	Three-dimensional
α-MEM	Alpha-Minimum essential medium
α-MEM-LDEX	Alpha- Minimum essential medium supplemented with 10^{-9} dexamethasone
βGP	Beta-Glycerol phosphate
a	Rod hydrodynamic radius
AA	Ascorbic acid
AC	Articular cartilage
Acan/AGG	Aggrecan gene/protein
ALP	Alkaline phosphatase
ATR-FTIR	Attenuated Total Reflectance Fourier Transform Infra Red
BTE	Bone tissue engineering
BSA	Bovine serum albumin
CTE	Cartilage tissue engineering

CTS	Chitosan
Coll/CTS	Collagen/Chitosan
CFD	Collagen fibrillar density
Coll	Collagen type I
Coll II	Collagen type II
CLSM	Confocal laser scanning electron microscopy
DDA	Degree of deacetylation
DEX	Dexamethasone
DMMB	Dimethyl-methylene blue
dH_2O	Distilled water
DMEM	Dulbecco's modified Eagle medium
ECM	Extracellular matrix
EDX	Energy-dispersive X-ray microanalysis
EthD, EthD-1	Ethidium homodimer-1
ESCs	Embryonic stem cells
FBS	Foetal bovine serum
FDA	Food and drug administration
GAGs	Glycosaminoglycans
H&E	Haematoxylin/eosin
HA	Hydroxyapatite
HHG	Highly hydrated gel
kPa	Kilo Pascal
MMP-13	Matrix metalloproteinase-13
MPa	Mega Pascal

MSCs	Mesenchymal stem cells
micro-CT	Micro-computed tomography
MEM	Minimum essential medium
MEM-HDEX	Minimum essential medium supplemented with 10^{-7} dexamethasone
MEM-LDEX	Minimum essential medium supplemented with 10^{-9} dexamethasone
OCP	Octacalcium phosphate
OTE	Osteochondral tissue engineering
Pi	Phosphate
PBS	Phosphate-buffered saline
PC	Plastic-compression
RCJ	RCJ3.1C5.18 chondroprogenitors
RT-PCR	Reverse transcription polymerase chain reaction
SC	Self-compression
SEM	Scanning electron microscopy
SDS-PAGE	Sodium dodecyl sulphate polyacrylamide gel electrophoresis
SVF	Solid volume fraction
TRITC	Tetramethylrhodamine isothiocyanate
TE	Tissue engineering
TEM	Transmission electron microscopy
UT	Untreated
wt. %	Weight percent

CONTRIBUTIONS OF AUTHORS

This dissertation is presented as a collection of four published and submitted manuscripts written by the candidate under the supervision of Dr. Showan N Nazhat and Dr. Marc D McKee. As the first author of all the manuscripts, I proposed, designed and conducted the bulk of the experiments. In addition, material preparation and testing, data collection and analysis, and manuscripts draft writing have been my commitment. Dr. Showan N Nazhat and Dr. Marc D McKee guided the candidate throughout the whole process and extensively reviewed all the manuscripts.

From a tissue-engineering standpoint, the development of a construct for tissue repair implicates a multidisciplinary approach that involves engineering, chemistry, materials science and cell biology. Consequently, the collaboration with other scientists in the above-mentioned fields was essential. The role of each collaborator or co-author of the manuscripts presented in this doctoral research is explained below.

- **Dr. Claudio Pedraza**, worked as a research associate in the Department of Dentistry at McGill University in Dr. Marc D McKee's lab. He significantly contributed to interpreting osteoblast cell culture assays, in particular, for the investigation of MMPs within dense scaffolds over time. These results are incorporated into manuscript 1 (*Chapter 4*). Moreover, his guidance for chondrocyte culture for their use in dense hybrid scaffolds for cartilage tissue engineering (CTE) applications was essential (*Chapter 5*).
- **Dr. Naser Muja**, is a research associate in the Department of Materials Engineering at McGill University in Dr. Showan N Nazhat's laboratory, whose expertise is centered in cell biology. His help was crucial for the confocal microscopy studies, as well as, for revision of manuscripts (*Chapter 5, 6* and *7*).
- **Chiara E Ghezzi**, is a PhD candidate in the Department of Mining and Materials Engineering at McGill University in Dr. Showan N Nazhat's laboratory who works on the development of tubular dense Coll scaffolds for

various applications (*e.g.* airway and blood vessel substitutes). She provided significant knowledge and technical expertise in the experimental design, collection and analysis of data for the mechanical tests (*Chapters 4* and *5*).

- **Dr. Benedetto Marelli** is a former PhD candidate in the Department of Mining and Materials Engineering at McGill University in Dr. Showan N Nazhat's laboratory who worked on the *in vitro* mineralization of dense Coll scaffolds as an osteoid model. He contributed with his expertise to the micro-CT analyses (*Chapter 4*).

- **Dr. Mari T Kaartinen** is an associate professor in the Faculty of Dentistry at McGill University. She reviewed and commented on manuscripts 1 and 3 (*Chapters 4* and *6*, respectively).

- **Antoine Charbonneau** is an undergraduate student doing a summer internship in the Department of Mining and Materials Engineering at McGill University in Dr. Showan N Nazhat's laboratory. I trained and supervised him during his stay and helped with conducting the enzymatic degradation of the dense hybrids in manuscript 1 (*Chapter 4*).

- **Dr. Thomas Quinn** is an associate professor in the department of Chemical Engineering at McGill University, whose expertise is centered in soft tissue mechanics and the development of cell-based biomedical technologies. His contribution was essential for the measurement of the hydraulic permeability of Coll/CTS hydrogels. He also reviewed and commented on manuscript 4 (*Chapter 7*).

- **Dr. Vahid Serpooshan** is a former PhD candidate in the Department of Materials Engineering at McGill University in Prof. Showan N Nazhat's laboratory who worked on developing micromechanical models to measure hydraulic permeability of Coll hydrogels undergoing gravity-driven consolidation (self-compression) and accelerated consolidation by the application of a compressive stress (plastic compression). He contributed with his expertise to establishing the experiments to measure hydraulic permeability of the Coll/CTS hydrogels (*Chapter 7*).

CHAPTER 1: GENERAL INTRODUCTION

1.1 INTRODUCTION

The field of tissue engineering (TE) endeavours to regenerate living tissue with compositions, structures and functions comparable to native tissues by combining approaches used in multiple disciplines and fields (*e.g.* engineering, biology and medicine) for collaboration [1]. TE involves the assembly of a tissue equivalent by combining cells and a porous scaffold. Although a wide variety of materials have been investigated to provide form and mechanical support to the newly developed tissue, the above description provides a relatively simplistic definition of what a scaffold should be, and in practice, the simple addition of cells to a porous scaffold is frequently insufficient for developing a functional tissue-equivalent [2]. Developing three-dimensional (3D) constructs with both the microarchitecture and microenvironment appropriate to surround cells and mimicking natural tissues is one approach to increasing the functionality of these scaffolds [2]. Subsequently, in the last decade, TE has shifted from the use of classic biomaterials that statically substitute a tissue defect, to the use of biomaterials that present biochemical, cellular and physical stimuli to seeded cells and interact with the surrounding tissue in a more complex and dynamic fashion [2, 3].

Compared to metallic and ceramic-based scaffolds, polymeric scaffolds are able to better respond to changes dictated by cells, such as remodelling of the extracellular milieu [4]. In particular, natural-based polymers offer distinct advantages of having biological properties, including cell-mediated degradation and remodelling [4]. These materials can be classified as proteins (*e.g.* collagen, gelatin, silk, elastin), polysaccharides (*e.g.* chitosan, chitin, cellulose, glycosaminoglycans) or polynucleotides (*e.g.* DNA, RNA) [5].

In an effort to mimic the molecular and structural properties of the extracellular matrix (ECM) of native tissues, collagen has been widely used as a

biomaterial in a range of different TE applications, including those related to cartilage, bone and osteochondral joints [6-8]. Collagen is the most abundant protein in vertebrates, comprising approximately 30 % of the total protein mass of the body, with collagen type I (Coll) being predominant [9]. Collagen plays an important role in maintaining the biological and structural integrity of the ECM and in providing the tissue with the necessary physical attributes [10].

Among the various processed forms of Coll scaffolds, hydrogels have played an increasing role in the field of TE [9]. Hydrogels have the advantage of being able to homogeneously accommodate cells as part of their processing route. In addition, they can be shaped into different forms to fill complex defects [11]. The combination of high water content and porous structure results in high hydraulic permeability (k ~ 6-60 μm^2) that allows for the transport of solutes, nutrients and wastes in and out the hydrogels [12, 13]. However, while high water content is beneficial for engineering tissue-like matrices, it lowers the collagen fibrillar density (CFD) to less than 1 % and decreases the mechanical properties of the scaffold (compressive modulus (E) ~ 4-6 kPa) [14, 15]. Under unconfined conditions, these Coll hydrogels tend to collapse under their own weight and undergo a gravity-driven consolidation process (self-compression; SC) that increases the CFD after several minutes. By applying an external load, Brown *et al.* [16] developed plastic compression (PC) - an accelerated scaffold processing technique. PC rapidly increases the CFD of highly-hydrated Coll gels to approximately 10 % and subsequently improves its mechanical properties (E ~ 18 kPa) [14]. This technique negates the potential toxicity of chemical cross-linking agents used to increase scaffold stiffness and enables the production of scaffolds with CFDs approaching those of native tissue in a matter of minutes, compared to weeks/months via cell-action [17]. Furthermore, PC limits the high extent of cell-mediated contraction, which significantly alters the original scaffold geometry and which can lead to an undesired mismatch between the defect and the scaffold after implantation. Plastically compressed dense Coll gel scaffolds have been shown to allow for the organization of seeded cells in 3D by providing the space

for their growth and differentiation without compromising their viability [18]. However, the ECM of tissues is a complex cellular environment that is composed not only of collagen fibrils but also contains other macromolecules such as adhesive and mineral-binding proteins, proteoglycans and other soluble molecules [19]. One such example is the proteoglycans, composed of a complex carbohydrate with linear disaccharides glycosaminoglycans (GAGs) side chains covalently bound to a core protein molecule. GAGs are an essential component of the ECM of both bone and cartilage.

Disruption of the cartilage ECM often leads to the clinical syndrome of osteoarthritis (OA) [20]. OA is a degenerative joint disease characterized by a progressive loss of articular cartilage (AC) often associated with the ageing process. Tissue damage due to OA frequently traverses the articular surface to reach the underlying supporting subchondral bone through the osteochondral interface, causing severe pain and malfunction [21, 22]. OA affects approximately 28 million people in the USA alone (and an estimated 4 - 13 % of the world's population) causing an annual financial burden of approximately USD$128 billion in the USA alone [23]. Current clinical treatments often contribute to the formation of fibrocartilage, which does not possess the endurance and function of hyaline cartilage, and therefore gradually deteriorates with time [24]. In this regard, osteochondral tissue engineering (OTE) holds promise for use in full-thickness AC defect repair based on the greater integration of bone-to-bone interfaces as compared to creating a cartilage-to-cartilage interface alone [25, 26].

As a consequence of the complexity of the osteochondral tissue (being a hybrid of both cartilage and bone) the design of an osteochondral-mimicking scaffold requires the use of an integrated bilayered matrix that promotes the simultaneous growth of both tissues [27]. Attempts to successfully produce these complex scaffolds have resulted in the proposal of different strategies involving the use of one or more cell types cultured into a homogeneous or heterogeneous scaffold [28]. However, despite the significant advances in OTE to date,

developing a tailored *in vitro* cell culture milieu that closely mimics the complex ECM of both the bone and cartilage still remains a challenge.

1.2 AIM, RESEARCH HYPOTHESIS AND OBJECTIVES

The principal aim of this doctoral research was to develop an integrated bilayered system for OTE applications based on the incorporation of a GAG-analog within a dense Coll hydrogel to closely mimic the native ECM of both cartilage and bone at the osteochondral interface, a junction that ultimately defines the physical morphology and the local environment, and in which cells reside.

It was therefore hypothesized that ECM-like scaffolds can be optimized by the incorporation of chitosan (CTS) within dense Coll gels, thus mimicking the roles of the fibrillar protein network and the GAGs found in native tissues. Moreover, the addition of CTS allows for tailoring the bioactivity, biodegradability, hydraulic permeability and, structural and mechanical properties of the scaffolds for the development of a tissue-equivalent matrix that possess characteristics of native cartilage and bone ECM.

Within this research, five different objectives were established, which were to:

1. Design and optimize a co-gelling system for the development of Coll/CTS hybrid gel scaffolds with different CTS proportions with enough capacity to be plastically compressed, in order to achieve a 3D tissue-equivalent with CFDs and solid weight percent values approaching those found in native ECM.
2. Characterize the dense Coll/CTS gels to serve as a bone osteoid-like scaffold and investigate the effect of CTS incorporation within dense Coll gels on the function of MC3T3-E1 pre-osteoblast seeded-cells.

3. Characterize the dense Coll/CTS gel scaffold to serve as an *in vitro* model scaffold directed towards the clinical repair of critical-sized AC defects; investigate the effect of CTS content on RCJ3.1C5.18 chondroprogenitors function within dense Coll gels; and design and characterize dense Coll/CTS gel scaffolds with clinically relevant diameters (3-5 mm) and study the interactions between their macromolecular components and morphometric parameters, and cell function.
4. Develop and characterize a bilayered dense Coll/CTS hydrogel to be used as an *in vitro* model that resembles the complex osteochondral structure and supports the regeneration of AC and the underlying subchondral bone; and optimize the co-culturing conditions to maximize the simultaneous differentiation of RCJ3.1C5.18 and MC3T3-E1 seeded-cells within each distinct layer with long-term stability.
5. Investigate the effect of incorporating CTS (*i.e.* a charged polysaccharide GAG-analog) within a highly-hydrated Coll hydrogel on the gravity-driven consolidation process (SC); evaluate the consolidation process under the application of a compressive stress (PC); assess the hydraulic permeability (k) of the highly-hydrated and dense Coll/CTS hydrogels; and study the effect of CTS fixed charge on dense Coll/CTS hydrogels physicochemical and biomechanical properties.

In order to meet the first objective, the process of CTS incorporation into a Coll acidic solution was investigated. The use of PC to remove the excess fluid that results from casting a mixture of protein and polysaccharide-based hydrogel has not been previously reported in the literature. Coll/CTS hybrid hydrogels were developed by using two different proportions of CTS (2:1 and 1:1 w/w), allowing for the formation of a tissue-equivalent matrix with CFD (~8 %) approaching physiological values. The mechanical, structural and biodegradability properties of the dense Coll gel scaffolds were evaluated as a function of CTS content.

To achieve the second objective and develop a bone osteoid-like model, the effect of CTS content when incorporated within a dense Coll network on MC3T3-E1 pre-osteoblastic cell-induced contraction, viability, proliferation, matrix remodelling, differentiation and mineralization under osteogenic-inducing conditions, was evaluated. The immortalized MC3T3-E1 clonal cell line was established from newborn mouse calvaria and can be readily differentiated into osteoblasts upon the supplementation with ascorbic acid and β-glycerolphosphate [29]. These cells display a time-dependent and sequential expression of osteoblast characteristics, analogous to osteoblast *in vivo* during bone formation [30, 31].

In order to meet the third objective and develop a cartilage-like model to assess AC repair, the effect of CTS content within dense Coll hydrogels on RCJ3.1C5.18 chondroprogenitor viability, proliferation, differentiation, biosynthesis of cartilage-specific ECM components and cartilage-like aggregate formation, was investigated. RCJ3.1C5.18 cells, a non-transformed clonal chondrogenic cell line from rat calvaria widely used for growth plate chondrocyte research and cartilage TE, were chosen here because of their capacity to undergo a cell differentiation sequence similar to that observed in cartilage *in vivo* [32, 33]. The motivation behind this objective was the limited capacity of AC to self-repair. In particular, AC defects that penetrate the subchondral bone and present diameters larger than 2 mm where self-repair is compromised [34]. Consequently, the potential of Coll/CTS cylindrically shaped constructs to fill defects of up to 5 mm in diameter was investigated by rolling dense planar Coll/CTS hydrogels into sheets. More importantly, the complex interplay between scaffold geometry, microstructure, composition, mechanical properties and chondrocyte function was evaluated.

To meet the fourth objective and develop an *in vitro* model as an approach towards improved AC repair, a bi-layered dense Coll/CTS hybrid gel was generated by simultaneously co-gelling two hydrogel layers. The stratified construct, having weight ratios approaching those of Coll/GAGs in the native

ECM of cartilage (Coll/CTS 1:1) and bone osteoid (Coll/CTS 33:1), was seeded with RCJ3.1C5.18 chondroprogenitor and MC3T3-E1 pre-osteoblast cells, respectively. The use of a bilayered scaffold presents the advantage of promoting a better integration of the cartilage as a consequence of the improved scaffold fixation in the subchondral region, as well as, optimizing the repair of both the cartilage and bone tissues. The motivation behind this objective was an anticipated rapid integration of bone-to-bone interfaces compared to cartilage-to-cartilage interfaces [25, 26]. Optimization of the co-culturing conditions was performed to identify an optimal medium formulation to maintain both chondrogenic and osteogenic phenotype.

To achieve the fifth objective, the microstructural evolution of Coll/CTS hydrogels undergoing a gravity-driven (SC) or an accelerated consolidation (PC), was investigated by collecting 3D image stacks of the spatiotemporal distribution of seeded fluorescent beads during the collapse process. The contribution of a charged macromolecule to the *k* of Coll hydrogels, based upon the incorporation of CTS, a cationic polysaccharide, was evaluated to further mimic the *in vivo* cellular microenvironment of native tissues. The Happel model [35], a microstructurally-based model, was used to calculate *k*, a property that correlates with a porous material to allow for the inflow of nutrients and oxygen as well as the outflow of metabolic waste and biodegradation by-products within a hydrogel [36]. The effect of CTS fixed charge on the structural, mechanical and swelling properties of dense Coll/CTS hydrogels and its contribution to *k* was investigated under two conditions: an isotonic solution (physiological salt concentration; 0.15M NaCl) and a hypertonic solution (1.5M NaCl).

1.2 THESIS OUTLINE

The present chapter (*Chapter 1*) consists of a general overview of the TE field and its limitations. *Chapter 2* provides a detailed review of the fundamental engineering and biological principles underlying the field of TE along with an

exhaustive description of the current state-of-the-art. Topics discussed include bone, cartilage and osteochondral biology, biomaterials for TE and their particular applications for bone, cartilage and osteochondral joint repair. In particular, this C*hapter 2* outlines the specific biomaterials, fabrication methods and cell sources used within this thesis. In addition, the aim, research hypothesis and objectives are described, followed by a thesis outline and a summary of original contributions. *Chapter 3* offers a description of the statement of the problem, highlighting the motivations behind this doctoral research.

Chapter 4 introduces the mechanism of production of dense Coll/CTS hybrid gels via the PC technique. In particular, the weight loss attributable to the applied load versus time and final hydration state are evaluated. The morphology and structure of as-made acellular hybrid gels are investigated, together with their mechanical properties. Additionally, their biodegradability via enzymatic degradation over time is studied. The suitability of these scaffolds for bone tissue engineering applications is evaluated in relation to osteoblast function. More specifically, it addresses the viability, metabolic activity, cell-mediated contraction, differentiation and mineralization of collagen and hybrid scaffolds. Finally, a detailed characterization on the mineral phase deposited within the hybrid scaffold is presented. This manuscript has been published in the peer-reviewed journal *Biomacromolecules*.

Chapter 5 deals with the versatility of the Coll/CTS hybrid gels to be used for cartilage tissue engineering applications. Based on the benefits of CTS in supporting chondrocyte growth and morphology, as well as its reported "chondroprotective" properties, Coll/CTS scaffolds are seeded with chondroprogenitor cells and evaluated for their ability to behave as chondrocyte-like cells for their potential use as models for AC repair. The complex interaction between chondroprogenitor cells, macromolecular components and scaffold morphometric parameters is investigated in scaled-up gels, necessary to treat large AC defects. For this purpose, ~200 μm-thick Coll/CTS sheets are scaled up into

cylindrically shaped roll scaffolds measuring 3-5 mm in diameter, a dimension relevant to critical-sized AC defect repair in the clinical setting. This manuscript has been published in the peer-reviewed journal *Tissue Engineering Part A*.

Chapter 6 investigates the fabrication of a dense bi-layered construct by co-gelling cartilaginous- (Coll/CTS 1:1) and osteoid-like (Coll/CTS 33:1) layers, seeded with RCJ3.1C5.18 chondroprogenitors and MC3T3-E1 pre-osteoblast, respectively, for their potential use as models for full-thickness osteochondral defects repair in osteochondral tissue engineering. To maintain both chondrogenic and osteogenic phenotypes, culturing conditions are optimized. The bilayered scaffold is investigated in terms of morphology and microstructure, cell viability, histochemical and biochemical analyses, as well as, biosynthesis by immunostaining and gene expression. This manuscript is under review in a peer-reviewed journal.

An investigation on the highly-hydrated Coll/CTS consolidation process undergoing SC or PC is reported in *Chapter 7*. The effect of CTS incorporation into a Coll hydrogel on k properties, estimated by the Happel model, is reported here. The effect of CTS fixed charge on the structural, mechanical and swelling properties of dense Coll/CTS hydrogels and its contribution to k was investigated under isotonic and hypertonic conditions for charge screening. This manuscript has been published in the peer-reviewed journal *Soft Matter*.

Chapter 8 provides a general discussion of the work undertaken in this thesis. Finally, in *Chapter 9*, the overall conclusions and future perspectives are presented.

1.3 SUMMARY OF ORIGINAL CONTRIBUTIONS

The original contribution to the advancement of knowledge in the research area of tissue engineering are summarized by the following publications:

- **Chicatun F.**, Pedraza C., Ghezzi C.E., Marelli B., Kaartinen M.T., McKee M.D. and Nazhat S.N., *Osteoid-mimicking dense collagen/chitosan hybrid gels*. **Biomacromolecules**, 2011, 12 (8), pp.:2946-2956.

This article (*Chapter 4*) provides a novel approach for the assembly of an osteoid-like structure with biomimetic properties, with collagen serving as a substrate for cell adhesion and proliferation, and CTS fulfilling the role of GAGs in native ECM. The results demonstrated that the incorporation of CTS improves the morphological and mechanical properties of as-made Coll/CTS scaffolds with CFDs closely mimicking the osteoid for their potential use in BTE applications. The concomitant increase of compressive modulus with CTS content has been correlated to the extent of contraction, which has not been previously reported. In addition, an increase in the CFD to physiological range resulted in a slower and less contraction extent compared to previously reported highly hydrated Coll/CTS gels. The osteoblastic differentiation results showed for the first time that MC3T3-E1-seeded cells within a 3D dense Coll/CTS hybrid support the normal *in vivo* osteoblast differentiation sequence. An extensive characterization of the mineral deposited by MC3T3-E1 is described here for the first time.

- **Chicatun F.**, Pedraza C., Muja N., Ghezzi C.E., McKee M.D. and Nazhat S.N., *Effect of chitosan incorporation and scaffold geometry on chondrocyte function in dense collagen type I hydrogels*. Published in **Tissue Engineering Part A.**

The development of dense Coll/CTS hydrogels as a model scaffold directed towards the clinical repair of AC is introduced here for the first time. In particular, this study focused on dense scaffolds with CFD approaching physiological levels. The results demonstrated that the incorporation of CTS to dense Coll gels has a stimulatory effect on seeded cells towards chondrocyte-like cells. The use of CTS to stimulate cartilage ECM production within dense Coll gel scaffolds has not been previously reported. Furthermore, this work provides new insights into the

development of Coll/CTS cylindrically shaped constructs with clinically relevant diameters (> 2 mm diameter) and their potential as *in vitro* models to assess the repair of critical-sized AC defects. It was demonstrated that, although the GAG content between cylindrical rolls declined over time and cell viability was reduced within the core regions of all constructs, the incorporation of CTS diminished both of these effects. Overall, the findings reported herein provide valuable design information for the development of model scaffolds directed towards the clinical repair of critical-sized AC defects; as well as the framework for understanding the interactions between chondroprogenitor cells, macromolecular components and morphometric parameters of dense Coll/CTS scaffolds. It is expected that this study will provide new perspectives regarding the translation of *in vitro* results into *in vivo* clinical applications.

- **Chicatun F.,** Muja N., Kaartinen M.T., McKee M.D. and Nazhat S.N., *A bilayered dense collagen/chitosan hydrogel as a three-dimensional tissue model for osteochondral tissue engineering.* Submitted to a peer-reviewed journal.

The feasibility to develop an integrated bilayered dense Coll/CTS hybrid gel scaffold, with ratios approaching those of Coll/GAG in the native ECM of cartilage and bone, by means of an innovative method that combines the simultaneous co-gelling of two hydrogel layers and a PC technique, was demonstrated here. This study circumvented the problem of scaffolds delamination, which arises from independently culturing each layer, or from substantial differences in the mechanical properties of each layer when using different materials. The results demonstrate two distinctive but integrated layers with unique morphologies with CFD closely mimicking both cartilage and bone native ECM. The optimization of the culture conditions for the simultaneous co-culturing of RCJ3.1C5.18 and MC3T3-E1 cells resulted in the maintenance of both chondrogenic and osteogenic phenotype within each layer.

- **Chicatun F.,** Muja N., Serpooshan V., Quinn T., McKee M.D. and Nazhat S.N. *Effect of CTS incorporation on the consolidation process of highly-hydrated Coll/CTS hydrogels*. Published in **Soft Matter**.

A novel methodology based on the quantification of fluorescent bead density both temporally and spatially was reported here for the first time to investigate the microstructural evolution of hybrid gels when undergoing consolidation. The use of the Happel model to measure *k* of hydrogels was used here to predict the effect of CTS on *k* properties of dense Coll hydrogels. The results show a previously unreported decrease in *k* with higher contents of CTS, and a concomitant increase in the scaffolds compressive modulus. It was demonstrated that the incorporation of CTS within dense Coll hydrogels modifies the biophysicochemical properties of the hydrogel, providing a reliable 3D *in vitro* tissue model that may be adapted to optimize TE scaffold design and potentially improve therapeutic outcomes.

CHAPTER 2: BACKGROUND AND LITERATURE REVIEW

2.1 BONE

2.1.1 Bone function and structure

Bone is a rigid skeletal tissue whose major function includes the provision of structural support for body tissues and organs, protection for vital organs, structure for muscle attachment, as well as, serving as a mineral ion reservoir for calcium homeostasis in the body [37]. By weight, bone is composed of ~60 % of inorganic mineral salts, ~30 % of an organic extracellular matrix (ECM) and ~10 % water [38].

Osteogenic cells are committed progenitors that are derived from pluripotent mesenchymal stem cells (MSCs). Mature osteoblasts, which arise from these progenitors, are highly differentiated cells that present a distinctive phenotype, morphology and biosynthetic activity, depending on the stage of functional differentiation (*i.e.* active osteoblasts, osteoclasts and lining cells) [37]. Active osteoblasts synthesize collagen type I, glycoproteins, cytokines and growth factors into a non-mineralized region, the osteoid [37]. These cells are also responsible for the subsequent mineralization of the osteoid by producing calcium phosphate minerals directly in the ECM and in small vesicles called matrix vesicles [38]. Osteocytes are highly specialized and differentiated cells deriving from osteoblasts. They are smaller in size, compared to osteoblasts, and the most abundant cell type in adult bone. Osteocytes are strategically located in lacunae within the mineralized matrix and act as mechanosensory cells in order to respond to changes in physical forces on bone, and to pass on messages to osteoblasts located on bone surfaces, leading to its resorption or formation [39]. Therefore, strains due to fluid flow or local deformation mechanically stimulate osteocytes, leading to bone formation/remodelling. The diffusion of oxygen and nutrients is achieved through canaliculi contained in long cell process extensions [40]. Lining cells cover over 90 % of the adult bone surface and are thought to be responsible

for the transfer of mineral in and out of bone and also in the sensing of mechanical strains [41]. Bone is therefore a dynamic tissue that is constantly remodelled throughout life, involving both bone resorption and formation through intercellular communications between osteoblasts and osteoclasts to achieve a balance between both processes to maintain bone's structural and functional integrity [37, 42].

Bone is characterized by a complex hierarchical structure as shown in *Figure 2.1* [43]. At the macrostructural level, bone is generally classified as being cortical (or compact bone) or cancellous (or trabecular) bone comprising 80 % and 20 % of the total mass of the skeleton, respectively [44]. The main difference between these two configurations is the degree of porosity or density. While compact bone has 10 % porosity, cancellous bone can have up to 90 % interconnected porosity, which is filled with marrow. This dissimilarity, leads to different mechanical properties in bones (*e.g.* modulus of elasticity and ultimate compressive strength) [45]. At the microstructural level, bone consists of cylindrical structures called osteons or Harvesian systems, with an average diameter of 200 μm. Osteons have Harvesian vascular canals in the center, which accounts for their porosity, and cement lines in their boundary [43, 44]. Cancellous/trabecular bone consists of an interconnected framework of plates and rods that are between 30 and 500 μm in diameter, named trabeculae. From a sub-micron standpoint, the osteon is composed of mineralized collagen fibre sheets that are between 4 and 7 μm in width. In cortical bone, these cylindrically shaped mineralized sheets are either perpendicular, parallel or alternating to the long axis of the bone [41]. At the nanostructural level, bone is composed of collagen fibres with diameters ranging from hundreds to thousands of nanometers and embedded within a mineral matrix. Lastly, the main sub-nanostructural components of the bone family are collagen, proteoglycans (*e.g.* glycosaminoglycans (GAGs)), non-collagenous proteins, carbonated hydroxyapatite crystals and water [46].

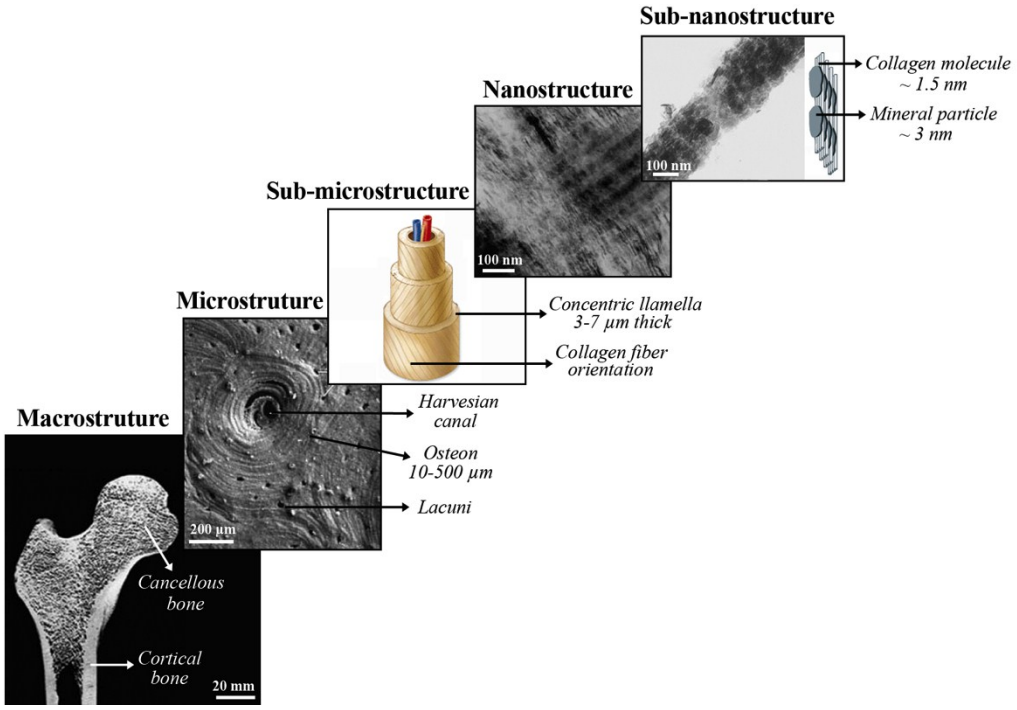

Figure 2.1: Hierarchical organization of bone from macro- to sub-nanoscale. Macrostructure – section through a femoral head showing the shell of cancellous and cortical bone. Microstructure – SEM of a Harvesian system or osteoid. Sub-microstructure – Typical concentric lamellar organization of bone. Nanostructure – TEM micrograph of a thin section of turkey tendon showing bundles of mineralized collagen fibres. Sub-nanostructure – TEM micrograph of a thin section of turkey tendon showing a mineralized collagen fibril and the schematic of the collagen molecules arrangement and mineral crystallites. Adapted from [39, 43, 47-49] Copyright © 2001 Springer-Verlag. Copyright © 1998 Elsevier Science Ltd. Copyright © 2010 The McGraw-Hill Companies, Inc. Copyright 2004© The Royal Society of Chemistry. Copyright © 1998 Annual Reviews.

The osteoid, which is the synthetized matrix prior to its mineralization, is comprised of 90 % collagen type I, and is responsible for providing mechanical and structural integrity to the ECM, as well as, regulating cell attachment and spreading [50]. Along with the collagen, the osteoid is also composed of GAGs and more than 200 non-collagenous proteins, which account for < 10 % of the total protein content by weight [49]. Phosphoproteins such as osteopontin, bone sialoprotein, osteonectin and osteocalcin are believed to be involved in regulating the size and orientation of the mineral crystals. This mineral phase – carbonated hydroxyapatite – provides the hardness, stiffness and rigidity of bone, and is composed of calcium (Ca^{2+}) and phosphate (PO_4^{3-}) with carbonate (CO_3^{2-}) substitutions. These crystals are plate-shaped and are found within discrete spaces (called hole or gap zones) within the collagen fibrils, growing in a specific

crystalline orientation [43]. The third major component of the ECM is water, which is located within the collagen fibrils, in the gaps, between the triple-helical molecules and fibres, and in the interfibrillar compartment [49].

2.1.2 Bone lesions

There are several clinical conditions that involve bone defects and failures due to traumatic injuries, genetic bone disorders (*e.g.* osteogenesis imperfecta) or pathological fractures caused by osteoporosis, cancer or infection [46]. It has recently been reported that the lifetime risk of major bone fractures in Caucasian women and men at the age of 50 is between 40 and 46 % and 13 and 22 %, respectively, and this is expected to reach 4.5 million worldwide by 2050 [44].

In many cases bone is capable of self-regeneration. The bone-healing mechanism involves a blood vessel ingrowth at the injury site, followed by the formation of a fibrin network. A granular or early tissue is then formed, aided by signal emissions from the fibrin clot and surrounding cells, to induce the migration of other cell types towards the wound. Functional bone reconstruction involves cleaning the damaged entities by macrophages, the initiation of neo-vascularization by the invasion of other cell types, and the synthesis of an ECM consisting of an assembly of numerous proteins such as collagen, proteoglycans, fibronectin and hyaluronic acid [38]. However, in many cases the size of the fracture or defect is bigger than the critical size for bone self-repair and surgical intervention is needed [45].

2.1.3 Current treatment options and limitations

Various techniques have been developed for the repair of large bone defects. The preferred procedure is the autologous bone graft, where the bone to be implanted is taken from the same patient in order to provide the initial structural stability [44, 45]. Autografts are commonly harvested from the iliac crest and this technique is considered as the “gold standard” because of the osteogenic, osteoconductive and osteoinductive properties of this bone grafts. Although the percentage of successful implants is high, autologous bone grafting is limited by

certain factors, such as limited quantity, risk of infection, nerve damage, and loss of function, among others [51]. Another option available for bone grafting is the allograft, where the bone to be implanted is taken from a different person. However, the success of these implants is limited as a consequence of the inflammatory and immune responses and the risk of disease transmission [52, 53].

2.2 CARTILAGE TISSUE

2.2.1 Cartilage function and structure

Cartilage is an avascular, aneural and alymphatic specialized connective tissue in which the ECM organization is responsible for bearing mechanical stresses without permanent distortion. As a result of its avascular condition, cartilage is nourished by the diffusion of nutrients through nearby capillaries located in the perichondrium, adjacent to the cartilage [47].

As a consequence of the different functional requirements, there are three distinct types of cartilage: elastic, fibrocartilage and hyaline (*Figure 2.2*).

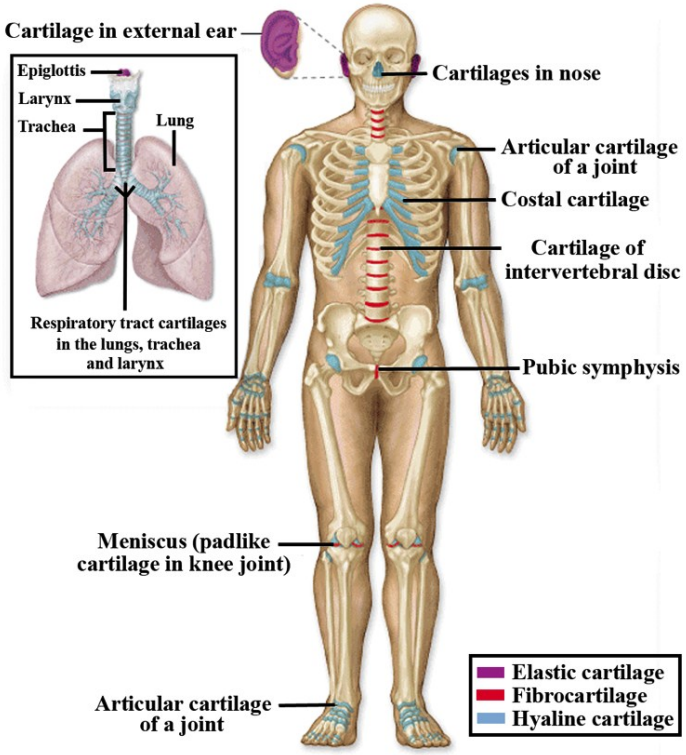

Figure 2.2: Sketch of the distribution of cartilage in adults. There are three types of cartilage distributed in the body: elastic, fibrocartilage and hyaline, each of which has distinct ECM composition and organization. Adapted from [47]. Copyright © 2010 The McGraw-Hill Companies, Inc.

Elastic cartilage is present in the epiglottis, auricle of the ear, Eustachian tubes and larynx. It is composed of collagen (mainly type II) and fine elastic fibres of elastin. Fibrocartilage is permanently found in the intervertebral disk of the spine, at the mandibular condyle in the temporomandibular joint, in the attachments of certain ligaments, and in the meniscus of the knee. Fibrocartilage cells have a rounded morphology and are considered to be a cross between fibroblast and chondrocytes, as they produce both collagen types I and II [54].

Hyaline cartilage is the most abundant type of cartilaginous tissue. In the embryo it serves as a provisional skeleton until it is progressively replaced by bone. In adult mammals, hyaline cartilage is mainly present in the articular surfaces of the joints, named articular cartilage (AC), as well as in the walls of respiratory passages and in the ventral ends of ribs [47]. Approximately 12 to 24 % of the wet weight of the tissue is collagen type II, 3 to 6 % is proteoglycans and

70 to 85 % is water [55]. By dry weight, 60 to 70 % is composed of collagen type II and ~30 % proteoglycans [56]. Proteoglycans contain many GAGs, such as keratin sulphate, chondroitin 4-sulfate and chondroitin 6-sulfate, which are covalently linked to the core proteins. These proteoglycans bind to long molecules of hyaluronic acid via a link protein and form proteoglycan aggregates, such as aggrecan, which is the major proteoglycan in cartilage ECM [47].

At the macroscale, AC is a porous/permeable, fibre-reinforced composite that exhibit high strength and stiffness, as well as presenting outstanding friction, lubrication and wear characteristics. At the microstructural level, cartilage is composed of three distinct yet integrated zones having different cellular phenotypes and ECM organization: superficial (or tangential), middle (or transitional) and deep (or basal) (*Figure 2.3*). These three zones are determined by collagen fibre orientation, and the density depends on the tissue depth, being highest at the surface zone and lowest at the inner zone adjacent to bone. In addition to collagen, the AC matrix is composed of GAGs where the concentration is highest in the inner zone and lowest at the surface [57]. The superficial zone is composed of small, disc-shaped chondrocytes and collagen fibres packed in bundles oriented parallel to the articulating surface. This zone is densely packed in order to avoid the permeation of unwanted molecules from the synovial fluid. Unlike the superficial zone, the middle zone presents larger and more rounded chondrocytes within a randomly oriented collagen network. Cells in the deep zone are oval in shape and oriented along the collagen fibres in vertical columns perpendicular to the articulating surface. These cells secret greater amounts of collagen and GAGs compared to cells in the superficial or middle zones. The deep zone is followed by a tidemark that separates it from the calcified zone, which eventually interfaces with the subchondral bone [58]. At the nanostructural level, cartilage is composed of a solid phase of collagen fibrils, proteoglycans, and non-collagenous proteins, and a fluid phase that includes water and electrolytes. The biomechanical properties of the AC depend on the interaction of its two major load-bearing macromolecules; the collagen fibrils and

GAGs. [59]. The net negative charged proteoglycans, due to the presence of GAGs, attract cations and water that repel each other. This repelling effect allows the GAG monomers to be extended and fill the collagen network with water. This swelling is then counteracted by the collagen network [58]. While the cross-linked collagen network is responsible for providing the tensile strength, the proteoglycans and water within the collagen network provide resistance to compressive loading, which on average is three times the body weight, and can approach 10-20 times the body weight during running or jumping, respectively [59].

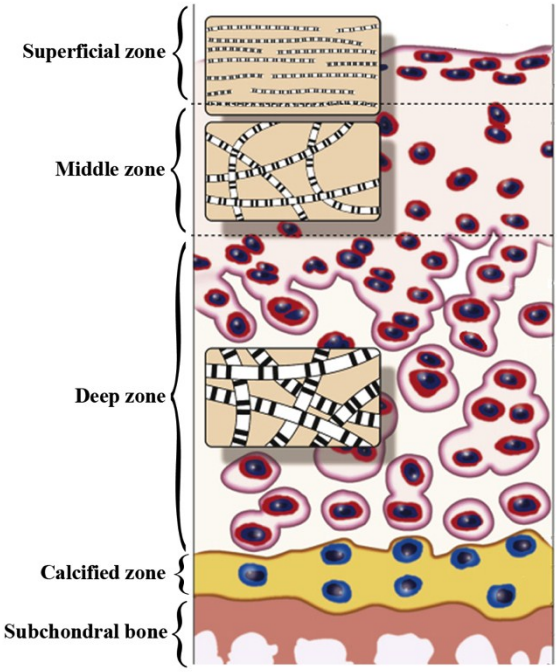

Figure 2.3: Cartilage micro-structural level. Cross-section of articular cartilage showing the micro-structural level. Adapted from [60]. Copyright © 2011 Elsevier Ltd.

2.2.2 Cartilage lesions

Cartilage tissue can become injured due to disease or trauma. The most common cartilage disease is osteoarthritis (OA). OA is a debilitating, progressive joint disease that leads to tissue softening and degeneration, which is initiated by the loss of GAGs from the ECM and followed by the disruption of the collagen network, leading to deterioration of the functional tissue [20]. OA is manifested

by morphologic, biochemical, molecular and biomechanical changes of both cells and matrix [61]. Although OA is not a consequence of ageing, ageing is the greatest identified risk factor for its development [61]. In addition, single or multiple joint overloading can cause tissue damage by microfracture or disruption.

In general, cartilage tissues exhibit limited capacity for self-repair as a consequence of their avascular nature. In particular, AC defects that penetrate the subchondral bone (that include osteochondral fractures) rely on the formation of a blood clot and an inflammatory response to recruit blood vessels and MSCs from the bone marrow to stimulate tissue regrowth [24, 62, 63]. However, the repair of these lesions is limited to defects with diameters smaller than 2 to 3 mm in diameter [34, 64]. For larger lesions the healing process is compromised, leading to the development of a rough AC surface that causes pain and malfunctions [65].

2.2.3 Current treatment options and limitations

Currently, the primary approaches to restore injured AC include the stimulation of bone marrow through surgical microfracture or tissue transplantation. Surgical microfracture consists of performing a micro-penetration of the subchondral bone plate for the formation of a fibrin clot and subsequent migration of bone marrow MSCs for cartilage repair [66]. Microfracturing is by far the most commonly used method for symptomatic chondral defects [67]. Although the microfracture technique have shown initial symptomatic improvement in younger patients [68], studies have demonstrated that this surgical technique often contributes to the formation of fibrocartilage tissue, which gradually deteriorates [38, 69, 70]. Moreover, the success of tissue regeneration is limited to small defects with less than 3 mm in diameter [71].

Tissue transplantation can be subdivided into autologous and allograft transplantation. Autografts involve harvesting cartilage from areas of low loading, usually taken from the patella or the femoral condyle or the proximal fibula, and transplanting it into high loading areas. However, as is the case for bone, this technique can cause donor site morbidity and is limited by the small amount of

cartilage available in the body for transplantation [71]. Allografting can overcome this problem by replacing the lesion with a cartilage segment obtained from an organ donor, however, the limitations of this technique include graft availability and possible disease transmission [24].

2.3 THE OSTEOCHONDRAL JUNCTION

2.3.1 Osteochondral function and structure

The foremost region of osteochondral tissue is the cartilage layer and the lattermost region is the subchondral bone (*Figure 2.4*). The osteochondral junction is the interface between bone and cartilage, which is structurally weaker than the transitions within the cartilage superficial, middle and deep zones since there are no continuous collagen fibres between the calcified cartilage and the subchondral bone [72].

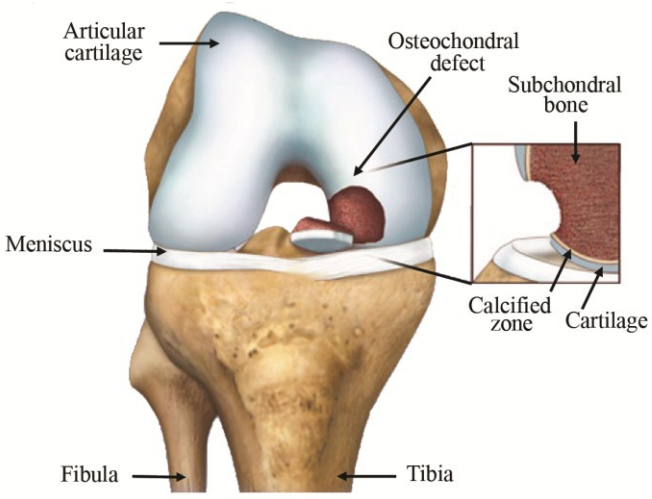

Figure 2.4: Schematic representation of an osteochondral defect. Adapted from [73]. Copyright © 2012 The journal of bone and joint surgery, Incorporated.

2.3.2 Osteochondral lesions

AC defects are classified as either chondral or osteochondral depending on the depth of the defect. Osteochondral defects involve damage to both the cartilage and the underlying subchondral bone [74]. Although knee osteochondral defects are very common, osteochondral defects can occur in any joint in the

body. When a defect crosses the tidemark (*Figure 2.3*), it allows the migration of bone marrow MSCs to the defect, leading to the formation of a fibrocartilage tissue. As previously stated, fibrocartilage is biochemically and structurally inferior to hyaline cartilage and unsuitable for load-bearing functions [66]. Defects with > 100 mm^2 are less likely to heal. In particular, studies on horses have revealed that only defects with a diameter < 3 mm are able to completely heal [66]. Osteochondral lesions, as a result of trauma, ischemia, genetics, abnormal vasculature or metabolic disorders, often lead to joint malfunction, and ultimately, to degenerative diseases such as premature osteoarthritis (OA) [75].

2.3.3 Current treatment options and limitations

Although many different treatments are currently available for osteochondral repair, an optimal solution still needs to be found to fulfil all the necessary requirements for a long-term effective regeneration [75]. Current clinical treatments for osteochondral repair includes those for AC repair (*Section 2.2.3*), in addition to the following methods:

1. Mosaicplasty, which is a method based on the implantation of an osteochondral plug previously harvested from a low-weight-bearing area of the knee joint, creating a “mosaic” pattern [76].
2. Autograft and allograft plugs, a technique where osteochondral plugs are harvested from a non-weight-bearing site in the knee and are pressed into a prepared site in the lesion. Depending on the size of the lesions, an allograft may be used instead of an autograft to minimize donor site morbidity [77, 78].
3. Cell-based techniques such as autologous chondrocyte implantation (ACI), which involves the implantation of expanded chondrocytes that have been enzymatically isolated from a small cartilage piece harvested from a low-load-bearing area of the knee joint [76].

4. Matrix-induced autologous chondrocyte implantation (MACI), a method that involves seeding chondrocytes into a type I /type III collagen bilayer membrane, or a synthetic material [79].

5. Total joint replacement.

Clinical use of autologous osteochondral plugs present numerous disadvantages that includes limited material availability, donor site morbidity and a mismatch between the graft and the defect morphologies [28]. Likewise, autologous osteochondral grafts deteriorate because of their limited integration between the host and donor plug [78]. Moreover, ACI has not shown significant improvement when compared to the microfracture technique, although the graft survival after 10 years of implantation has been shown to be significantly higher than those of the mosaicplasty technique [76, 80].

2.4 TISSUE ENGINEERING APPROACHES

Tissue engineering (TE) has in the past two decades been developing as an alternative approach for bone and cartilage tissue regeneration. This approach, pioneered by Langer and Vacanti [1], draws support from multiple disciplines and fields, including engineering, biology and medicine. The main challenge in TE is the regeneration of a tissue with the composition, structure and function comparable to that of the lost or defective native tissue.

TE has shown tremendous promise in the creation of tissues, with applications involving the fabrication of skin [81], liver [82], nerves [83], valve leaflet [84], ligament [85], tendon [86], cartilage and bone [87-89]. The overall concept of TE involves four stages (*Figure 2.5*) [1, 90]:

1. Isolation of appropriate cells for culture from a tissue harvest, and subsequent subculture for cell expansion (*Figure 2.5 a, b*).

2. Homogenous cell seeding in or onto an engineered 3D scaffold that mimics the dynamic *in vivo* environment for cell attachment, proliferation

and differentiation by allowing the diffusion of signalling molecules and nutrients (*Figure 2.5 c*).

3. *In vitro* culture in an environment that promotes the tissue substitute growth. This stage involves the addition of signalling molecules such as proteins and growth factors (*Figure 2.5 d*).

4. Integration into living systems using *in vivo* animal studies followed by human clinical trials, a stage that needs to meet the challenge of efficacy, long-term patency and immune acceptance (*Figure 2.5 e*).

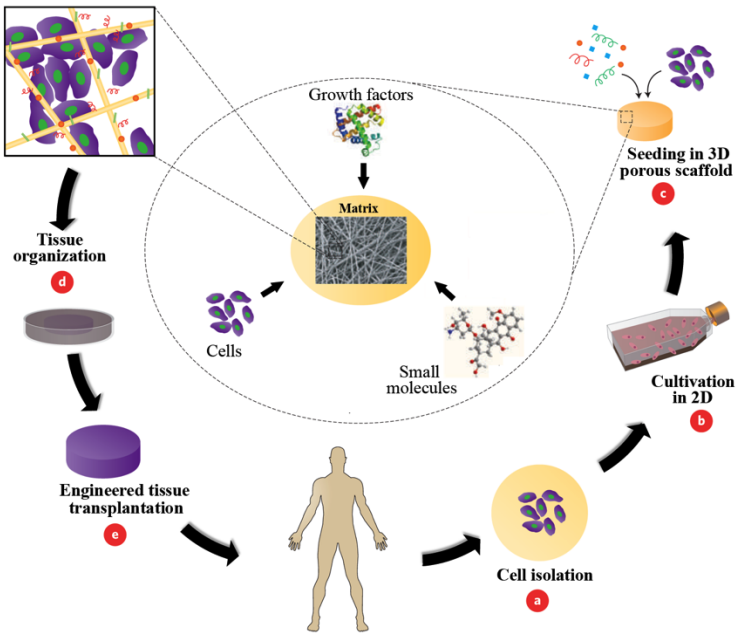

Figure 2.5: Tissue engineering stages. (a) Cells isolation from the patient. (b) Subsequent cell culture and expansion. (c) Cell seeding into 3D engineered scaffold mimicking the dynamics of the *in vivo* environment. (d) Addition of growth factors and signalling molecules to promote tissue growth. (e) Integration to *in vivo* system. Adapted from [91]. Copyright © 2011 McMillan Publishers Limited.

2.4.1 Biomaterials for tissue engineering

The development of a tissue-like matrix is directly related to both the properties of the materials and the tissue to be reconstructed. Therefore, it is of utmost importance to select the appropriate material to engineer scaffolds. The desirable characteristics of these materials include biocompatibility, vascular support, non-immunogenicity, sterility and biodegradability with degradation rates matching the formation of the newly build tissue [90].

A wide variety of materials are currently being investigated to produce porous 3D scaffolds. The basic spectrum of materials includes both synthetic and natural organic and inorganic materials, as well as their composites. Although metals and ceramics have been extensively used in TE, their use has been limited due to their lack of biodegradability and reduced processability. In particular, metallic scaffolds present the disadvantage of being of high density and have a high risk of corrosion, while ceramics are brittle materials with relatively poor tensile properties, presenting low mechanical stability [92]. As a consequence, many studies are focused on the use of polymers, and composites for TE applications.

The most widely used synthetic polymers in tissue engineering include poly(α-hydroxy ester)s such as poly(lactic acid) (PLA), poly(lactic-co-glycolic acid) (PLGA), and co-polyesters of the lactic acid and glycolic acid. PLA is currently the most-used synthetic material. Depending on the ratio of lactide/glycolide copolymers it is possible to obtain a wide range of physical properties and degradation rates [93]. Other materials that have long been applied for replacements of tissues and organs are silicone, poly(ethylene terephthalate) (PET), polyethylene and poly(methyl methacrylate), among others. Synthetic polymers have many advantages. First of all, they can be formed with different shapes and good mechanical strength. Secondly, when degradable (*e.g.* PLA, PLGA) their degradation rate can be easily controlled by varying the molecular weight and copolymer ratio [94]. However, these synthetic materials have the disadvantage of potential side effects if they undergo degradation in the body. In particular, PGA, polyhydroxyalkanoate, and poly-4-hydroxybutyrate are potentially immunogenic, show toxic degradation and induce inflammatory reactions [95].

Materials of natural origin have several advantages over synthetic materials, because of their similarity to the biological environment [96]. In the last decade, TE has evolved from using classic biomaterials that statically replace a diseased

or damaged tissue, to using biomaterials that dynamically interact with the tissue [3]. An extensive variety of natural polymers are potentially suitable for tissue scaffolding [4]. The most widely used are collagen [6, 10, 97], chitosan [98-101], fibrin [102-104], starch [105], hyaluronic acid [106-108] and alginate [109].

2.4.1.1 Collagen as a biomaterial for tissue engineering

Collagen is the most abundant protein in vertebrates and makes up approximately 30 % of the total protein mass (*e.g.* ~90 % in tendon and bone and ~50 % in skin) [9]. Collagen plays an important role in maintaining the biological and structural integrity of the ECM, which provides the physical support to tissues [10]. In the body there are different types of connective tissues and all of them have different biological features. These distinct features result from the existence of at least 28 genetically distinct collagens, where 80-90 % of the collagen in the human body consists of type I, II and III [6, 110]. Type I collagen is the primary structural element in ECMs and is found throughout the body except in cartilaginous tissues, where type II collagen is present. Type III collagen is found in blood vessels and other hollow organs.

There are many reasons why collagen is widely used as a biomaterial. First, on account of its protein nature, it has a repetitive sequence of amino acids, specific size and structure, defining its basic qualities. Secondly, it is a biodegradable and bioresorbable molecule. The biodegradability of the collagen can be controlled by cross-linking the polypeptide chains [111]. This is an important issue during implantation where the degradation rate needs to be tuned. It has high affinity for water and has a very low antigenicity attributable to the similarity in the amino acid sequence between species and the low content of aromatic amino acids [9, 112]. Moreover, it is a non-toxic and biocompatible material and it has the ability to promote blood coagulation (haemostatic). Lastly, it is highly available.

Depending on the process of extraction, collagen may be soluble or insoluble, denatured or maintain their triple helical structure [113]. The combination of acid

and enzymatic treatments allows the development of highly purified solubilized collagen, which can yield fibrillar collagen hydrogels by pH and temperature adjustments [114]. Collagen may also be isolated by decellularization of collagen-rich tissues (*e.g.* small intestinal submucosa). The different steps involved in this process may affect both their structure and the type of host response to these materials when used as scaffolds for TE [115]. All these different extraction processes allow the production of collagen with different configurations such as sheets, tubes, sponges, powders, solutions, discs and hydrogels. These systems have been used for drug delivery, wound and burn dressings, and TE of skin, cartilage, bone and other tissues [112, 116].

2.4.1.1.1 In vivo collagen biosynthesis and degradation

The unique physiological characteristic of collagen is derived from the structural complexity of the collagen molecule (*Figure 2.6*). Based on their structure and supramolecular organization, collagens can be classified into different groups: fibril-forming collagens (type I-V, XI), fibril-associated collagens (type IX, XII, XIV, XX, XXI), network-forming collagens (type VI, VIII, X), transmembrane collagens (XIII, XVII), and others with unique functions [117]. Differences in collagen types arise from the presence of additional non-helical domains, their assembly and their function. The most abundant family of collagens is the fibril-forming collagens. The primary structure of collagen type I is a polypeptide consisting of a repeating sequence of more than 1000 amino acids of the repeated sequence: Gly – X – Y, where Gly is glycine, present at every third position and X and Y are frequently proline and hydroxyproline, respectively. The helical nature of the polypeptide chain defines the secondary structure of collagen, which is dictated by intra-molecular hydrogen bonding. When the resulting molecule twists into an elongated left-handed helix, the secondary structure of the collagen is formed. The tertiary structure is a right-handed triple helix formed by three polypeptide chains, called procollagen, which is characteristic of all collagen types. The stability of the triple helix depends on the intra- and inter-molecular hydrogen bonds. Other hydrogen bonds are also

formed between water molecules and the hydroxyl groups of collagen [118]. The amino acid responsible for the closed package of the chains is the glycine.

In particular, collagen type I has two identical chains (α1(I)) and one (α2(I)) chains, whereas type II collagen is characterized by having three identical chains (α1(II)) [117, 119]. Compared to type I collagen, type II collagen chains contain a higher content of specific residues that mediate the interaction with proteoglycans. The procollagen in type I and II collagens is 280 nm long and 1.5 nm diameter and contain telopeptides on their ends. The telopeptides do not present a repeating sequence of amino acids and are present at the amino (N-) and carboxyl (C-) terminal chain ends of the molecule [9, 120]. The N- and C-terminus are cleaved by peptidases to form the tropocollagen. Procollagen molecules overlap with their neighbours by about 67 nm, producing the characteristic banded pattern of the fibrils as can be observed by scanning electron microscopy (SEM), transmission electron microscopy (TEM) or atomic force microscopy (AFM). This structure is known as the quaternary structure of the collagen. These fibrils can reach up to 500 nm in diameter depending on the tissue type. The covalent bonds between adjacent tropocollagen molecules gives the high strength to collagen fibres [118].

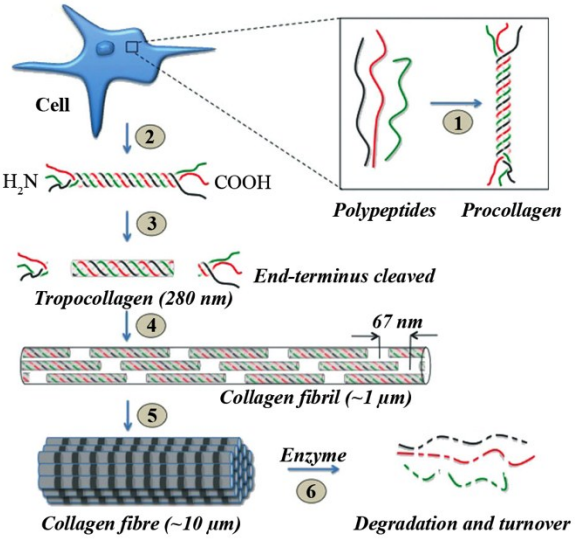

Figure 2.6: Hierarchical structure of collagen type I. (1) The polypeptides are assembled inside the cell into triple helical procollagen. (2) The procollagen molecule is secreted outside the cell. (3) The N- and C-terminus are cleaved to form the tropocollagen. (4) The tropocollagen is then assembled as fibrils by covalent cross-links. (5) Fibrils are structured into collagen fibres. (6) Collagenases present in the body enzymatically catabolize the collagen and cleave the peptides linkages. Adapted from [121]. Copyright © 2011 John Wiley & Sons, Inc.

In account of being the primary structural protein in the body, collagen is very resistant to neutral proteases. *In vivo*, collagen is broken down by catabolic processes that includes the collagenases that cleave the native helix and phagocytosis [9, 116]. Once the triple helix has been cleaved, the collagen is further degraded to small peptides and amino acids by enzymes, such as gelatinases, and non-specific proteinases [9]. *In vitro* degradation is usually simulated by the incorporation of collagenase, cathepsin, pepsin or trypsin. The degradation rate depends on the implantation site and can be tuned by the incorporation of cross-links between the polypeptide chains [116].

2.4.1.1.2 In vitro reconstitution of collagen

A number of techniques have been proposed for collagen type I extraction, providing an acidic environment [122, 123], neutral salt solutions [122, 124] or proteolytic solutions [125]. However, the latter method reduces the self-assembly capacity of the tropocollagen molecules to form fibrils, as a result of the terminal telopeptide cleavage [126]. The addition of pepsin reduces this effect, yet some

telopeptides are cleaved or partially denatured [125]. The most common technique of collagen extraction is acid treatment with acetic acid, where the collagen is extracted from different animal sources, mainly from the dermis or tendon. Briefly, collagen is extracted by grinding the tissue at low temperature, washing with neutral saline for the removal of proteins and polysaccharides and extracting the collagen by adding a low-ionic-strength acid solution [9]. Acidic extractions of collagen yield mainly monomers with a variable amount of dimers, trimers and some higher molecular-weight components [120]. Collagen is not soluble in organic solvents and its solubility in water depends on the type of collagen and the age of the animal from which it is extracted from [9]. Only 2 % of collagen can be solubilized with acid solutions, hence, the remaining 98 % needs to be dissolved with a strong alkali, such as sodium hydroxide [9]. The low dissolution of collagen is attributable to the presence of covalent cross-links between the molecules.

Reconstituted collagen type I can be obtained from this solution by adjusting the pH (5.0-9.0) and temperature (15-37 ^{o}C) to produce a hydrogel with the characteristic ~67 nm D-periodic fibrils [127, 128]. The formed fibrils are unipolar, meaning that all molecules are in the same direction and present two smoothly tapered ends. Collagen fibrillogenesis is a thermally driven process, which is favoured by positive entropy attributable to the displacement of structured water in between collagen molecules [128]. The principal effect that governs collagen fibril formation is the hydrophobic interactions between non-polar regions of adjacent molecules [128]. The rate of assembly of fibril formation follows a near-sigmoidal curve. Depending on the collagen fibril formation process (temperature and pH), collagen can form different aggregation states, with the occurrence of non-banded filaments [120].

Since collagen type II is very insoluble, its extraction requires the elimination of the N- and C-terminal regions by enzymatic digestion with papain or pepsin [129]. This method makes the *in vitro* reconstitution of native-type banded fibrils

a difficult task. For this reason, acid-extracted collagen type I as a biomaterial for TE applications.

2.4.1.2 Chitosan

Chitosan (CTS) is a biodegradable linear polysaccharide that is a partially deacetylated derivative of chitin (*Figure 2.7*), the structural element in the exoskeleton of crustaceans (*e.g.* shrimps, crabs, krill), fungi and insects [121, 130]. Chitin is the second-most naturally occurring polymer in Nature after cellulose, and it is composed of N-acetylglucosamine and glucosamine [130]. It is usually isolated from waste produced in the food industry. The extraction process of chitin involves decalcification, deproteination, and decolorization by a sequential treatment with 5 % HCl solution, 5 % NaOH, 0.5 % $KMnO_4$ and oxalic acid [131]. The degree of CTS deacetylation (DDA) depends on the molar ratio of these glucosamine units to all repeating units on the molecule, which can vary from 50 % up to 95 %. The deacetylation process involves the treatment of chitin with an aqueous NaOH solution at high temperatures (90-120 °C) for 4-5 h. The CTS molecular weight (M_w) and DDA are determined by the alkali treatment conditions [130].

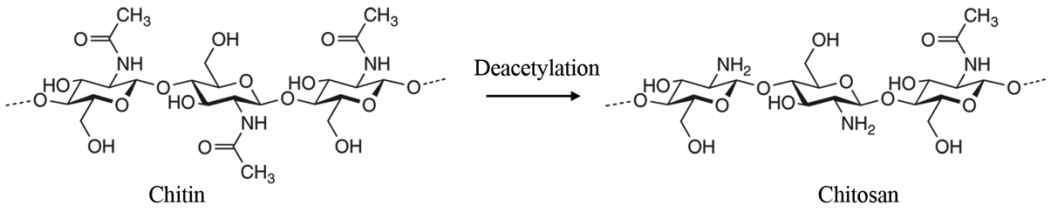

Figure 2.7: Molecular structure of chitin and its deacetylated derivative, chitosan. Adapted from [121].

CTS belongs to the family of polysaccharide-based materials for TE applications and is commonly used because of its biological activity to form hydrogels [132]. CTS is positively charged because of its amine groups, and it can be water-soluble up to pH~6.3 where the free amino groups are protonated [130]. At higher pH, CTS amines become deprotonated, lose their charges and become more insoluble. The charge density depends both on pH and DDA. If NaOH is

added, then the amino groups will be neutralized and this will lead to gel formation. The gel is formed as a consequence of the elimination of the repulsive electrostatic forces of the positive amino groups, leading to hydrogen bonding and hydrophobic interactions between the CTS chains [3, 133].

2.4.1.2.1 Chitosan as a glycosaminoglycan analog

Because CTS is comprised of N-acetylglucosamine and glucosamine units, it is structurally very similar to the GAGs found in native tissue and can be identified as an innocuous component of the ECM. GAGs are linear heteropolysaccharides that are covalently attached to a core protein to form the proteoglycan (*Figure 2.8*). They consist of repeated disaccharide units with the general structure (uronic acid-amino sugar)$_n$ [132]. In addition, GAGs are responsible for water molecular retention, conferring tissue resistance to compression [49]. The family of GAGs includes chondroitin 4-sulfate (glucuronic acid and N-acetyl-galactosamine with an SO^-_4 on the 4-carbon position), chondroitin 6-sulfate (glucuronic acid and N-acetyl-galactosamine with an SO^-_4 on the 6-carbon position) and keratan sulfate (galactose and N-acetyl-glucosamine with an SO^-_4 on the 6-carbon position) [134].

Since GAGs can interact with growth factors, cellular receptors and adhesion properties, it is expected that the analogous structure in CTS may also have similar bioactivities [132]. However, CTS is positively charged, unlike GAGs, which is negatively charged. Nevertheless, CTS can interact with cellular receptors and with matrix proteins in distinct way by stereospecific glycan binding and non-specific charge interactions [135]. Moreover, it has been postulated that CTS may bind and interact with negatively charged GAGs, and has a stimulatory effect on macrophages, which has been attributed to the acetylated residues [136].

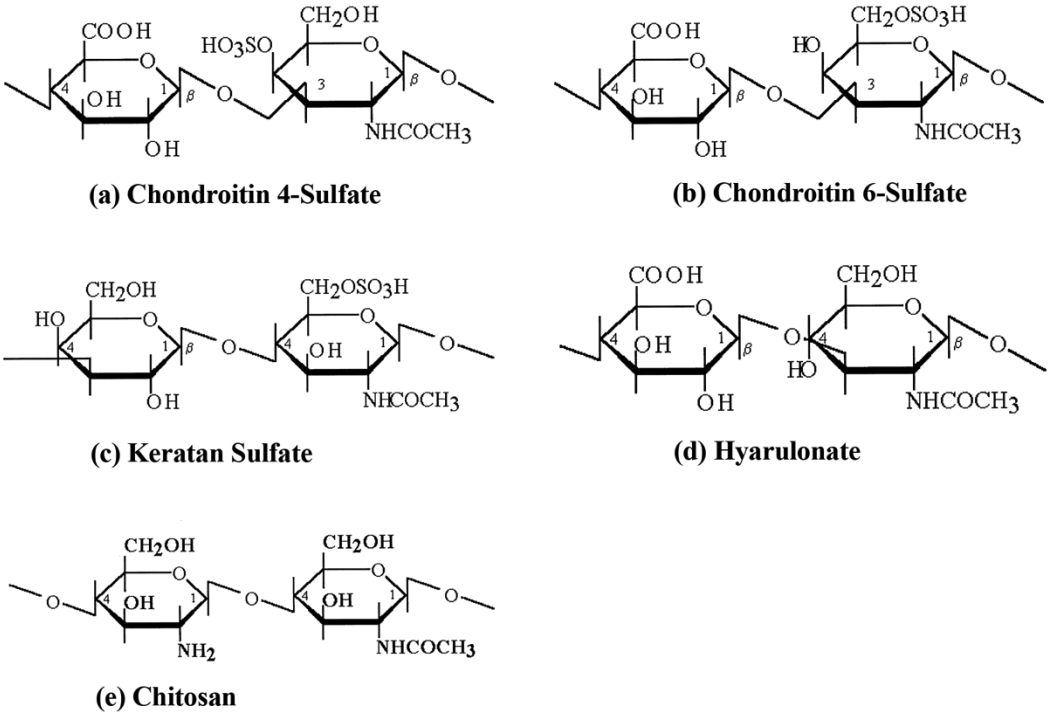

Figure 2.8: Molecular structure of the various members of the GAGs family. (a-d) GAG-analogs, CTS (e). Adapted from [132]. Copyright © 2000 Elsevier Science Ltd.

2.4.1.2.2 Biocompatibility and degradation

CTS has the advantage of being biodegradable [131], biocompatible, non-immunogenic, non-toxic and bio-functional, making it a suitable natural polymer for TE applications [98, 137]. Due to its chemical similarity to GAGs, cellulose and hyaluronate, CTS is generally considered non-toxic. It is Food and Drug Administration (FDA) approved for the use in wound dressing and it has been approved in a few countries for dietary applications [138, 139]. *In vivo* toxicity has been tested intravenously, subcutaneously and orally with no signs of toxicity [140]. It has been used as a haemostatic agent, by agglutinating red blood cells [141]. CTS has also been implicated in fat binding in the intestine when orally administered, being a potential treatment for hypercholesterolemia [142]. Moreover, it has also been used for the treatment of skin lacerations, showing good results in wound healing [143]. In addition, CTS has proven to be capable of hormone releasing in a controlled manner, being suitable for drug delivery [138].

Finally, CTS has also demonstrated its potential to serve as a scaffolding material in a wide range of TE applications [98, 132, 144, 145].

A very important aspect in the selection of a biomaterial is its metabolic fate in the body [140]. Enzymatic degradation of CTS depends on the hydrolization of the glucosamine-glucosamine, glucosamine-N-acetyl-glucosamine and N-acetyl-glucosamine- N-acetyl-glucosamine linkages [140]. The degradation rate is inversely related to the DDA and the main degradation products are CTS oligosaccharides of variable length [146, 147]. In crustaceans, CTS is degraded by chitinases. Interestingly, eight human chitinases (in the glycoside hydrolase 18 family) have so far been identified, three of which have shown enzymatic activity [148]. However, these active forms have not been investigated with respect to the degradation of CTS. In an attempt to provide an insight into the *in vivo* degradation of CTS, this polysaccharide was intravenously injected in rabbits [149]. The results presented in this study shows that the level of lysozyme in blood was up-regulated, indicating that this enzyme may be involved in the degradation process of CTS. The proposed mechanism of degradation involves first the permeation of water and lysozyme into the CTS structure to induce its swelling [150]. The degradation then takes place in the β-(1-4) glycosidic bond to form low M_w CTS, chito-oligomers and N-acetyl-D-glucosamine residues. Higher DDA CTS are more difficult to be hydrolyzed by the enzyme and consequently the rate of degradation is lower. The final residues are small fragments of glucosamine, which can be excreted from the body in urine. Apart from lysozyme, CTS is known to be degraded by bacteria in the colon, which produces enzymes that hydrolyze CTS [150].

2.4.2 Bone tissue engineering

Bone tissue regeneration and repair remains an important challenge. Ideally, a scaffold for bone tissue engineering (BTE) applications should facilitate cell infiltration, attachment, matrix deposition, vascularization, integration and remodelling [151]. BTE involves the development of a scaffold that mimics the

native ECM and supports the three different biological mechanisms that favours bone regeneration [151-154]:

Osteogenesis, which refers to the formation or development of new bone cells and ECM (and mineral) within the scaffold.

Osteoconduction, which refers to the ability of a material to allow cell attachment, migration and support new tissue growth. Osteoconductive scaffolds should provide a structural template and degrade at a rate matching that of bone formation. An osteoconductive material would allow bone formation in a site where normal healing will occur if left untreated.

Osteoinduction, which refers to the capacity of the material to cause pluripotential cells, from a non-osseous environment, to differentiate and regenerate healthy bone tissue. An osteoinductive material would allow bone formation in a site that would normally not regenerate.

2.4.2.1 Collagen-based scaffolds for bone tissue engineering

Collagen-based scaffolds have been widely used for bone regeneration on account of their osteoinductive activity. Collagen has been used as a gene delivery carrier for bone inducing proteins (*e.g.* recombinant human bone morphogenetic protein 2 (rhBMP-2)), as well as bone substitutes [112]. Composites of rhBMP-2 and collagen have been developed as films and sponges to monitor bone development. When implanted, film scaffolds indicated active bone formation in contrast to acellular collagen [155, 156]. Use in humans involved the implantation of collagen/rhBMP-2 sponges, which resulted in the stabilization of dental implants in bony areas and normal bone formation [157].

Different approaches have been used to develop collagen-based scaffolds as bone substitutes. One approach involves a decellularized ECM, which preserves the original tissue shape and ECM structure; however, its use is limited because of immunological, physical scaffold size and availability aspects [158]. The other approach relies on the extraction (*Section 2.3.1.1.2*), purification, and

polymerization of collagen. The use of purified collagen has the advantage of being reconstituted into different products, have low immunogenicity, controlled porosity, retention of cell-matrix interactions, and the ease of processing into a shape [6].

Although collagen-based scaffolds have been extensively experimented on for BTE, the lack of mechanical strength for load bearing applications has lead to various investigations into increasing their strength, including cross-linking or reinforcing with bioceramics. Cross-linking of collagen-based scaffolds has been widely used in an effort to improve their physical properties, control their biodegradation rate upon implantation, and minimize their antigenicity and cell-mediated contraction during cell growth. In order to improve the physical properties of natural polymers, different methods have been studied: physical, chemical and enzymatic cross-linking. Physical methods directed at cross-linking collagen-based scaffolds include photooxidation [159], thermal treatments [160], and ultraviolet irradiation [161]. Chemical cross-linking, on the other hand, are able to reach a high degree of cross-linking. Usual cross-linking agents includes, glutaraldehyde [162, 163], 1-ethyl-3-(3-dimethylaminopropyl)-carbodiimide (EDAC) [164, 165], dimethyl 3,3'-dithiobisprpionimidate (DTBP) [166], dimethyl buberimidate (DMS) [167] and diphenylphosphorylazide (DPPA) [168]. In comparison to chemical cross-linking, physical cross-linking methods do not introduce any potential cytotoxic chemical residuals. However, they cannot achieve a high enough degree of cross-linking. An alternative approach to enhance the tensile strength and enzymatic resistance of collagen-based scaffolds is enzymatic cross-linking by transglutaminase [158, 169, 170]. This technique has the advantage of not producing any chemical residues or by-products within the scaffold structure, therefore reducing the cytotoxic effects [158].

Scaffolds for BTE have involved hardening the scaffold by the incorporation of bioceramics such as calcium phosphate [171-173], hydroxyapatite [174, 175], brushite [176] or bioactive glass (*e.g.* Bioglass®) [177, 178] into the collagen

structure. This approach not only enhances the mechanical properties of the scaffolds but also introduces the mineral component, characteristic of bone. Whereas some attempts are simple mixtures of the above components, others are optimized systems where several parameters are controlled, such as concentration, pH and/or temperature [179]. Other techniques involve soaking the collagen matrix in a super-saturated calcium phosphate solution [180-182] or functionalizing the collagen [183-185].

2.4.2.2 Cells for bone tissue engineering applications

As an alternative to the addition of a mineral phase to collagen-based scaffolds, and on account of its biomimetic properties, collagen gel scaffolds are suitable matrices for bone cell cultivation, allowing the generation of a cell-mediated mineralized tissue both *in vitro* and *in vivo* [186-189]. This approach involves osteoblast-like cell seeding into a scaffold and subsequent culture with specific additives to promote functional differentiation and eventual mineralization of the scaffold. Through this, the *in vivo* osteoblastic sequence for bone generation can be closely mimicked. The osteoblastic differentiation sequence can be subdivided into three consecutive, yet overlapping, phases: cell proliferation, cell differentiation and ECM assembly and maturation, and mineralization (*Figure 2.9*) [190].

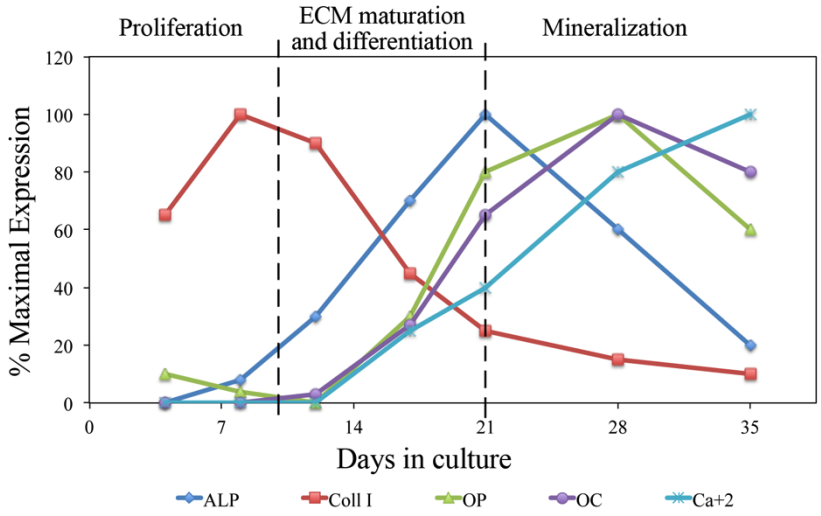

Figure 2.9: Cell growth and phenotype related genes expression for up to 35 days during the osteoblast development sequence. The three principle periods are designated with dashed vertical lines: proliferation, ECM maturation and differentiation, and mineralization. Adapted from [190, 191]. Copyright © 1993 The Endocrine Society. Copyright © 1990 Wiley-Liss Inc.

Following the initial proliferative period, cell matrix synthesis, secretion, and assembly occur to form the ECM. An increase in alkaline phosphatase (ALP) activity is associated with this process and is often considered to be an early marker of the committed osteoblast lineage progression, with subsequent abundant expression and secretion of collagenous and non-collagenous matrix molecules such as bone sialoprotein, osteopontin, and osteocalcin, along with the accumulation of mineral [191]. Finally, at later phases, ongoing synthesis of matrix components and their modification by cell-secreted enzymes leads to ECM mineralization, which completes key osteoblast functions within bone.

Therefore, in order to develop a biomimetic scaffold for *in vitro* BTE, it is necessary to select the proper cell source and type that allows the study of the bone cell response to and interaction with the biomaterial. The selection of an appropriate *in vitro* experimental design will contribute to a better understanding of bone physiological, pathological and regenerative processes [192]. Primary cells present many advantages in terms of presenting cell behaviour more reflective of the *in vivo* scenario. Primary cells may be isolated from human or animals, followed by limited expansion *in vitro*. The main advantage of primary

human cells is their clinical applicability and reduced immune response after transplantation [192]. However it presents numerous disadvantages, including a low number of cells that can be harvested from the patient tissue, a low rate of expansion, and the time required for cell expansion. In addition, cells taken from elderly patients biopsies may not be suitable for transplantation [193, 194]. Moreover, primary human cell functions are influenced not only by age, but also by site of isolation and gender differences [192]. As an alternative to the above method, non-human cells (xenogeneic cells) are being used where genetically engineered animals are used to obtain a high number of cells by xenotransplantation. The main limitation of this method is the possibility of transmission of infectious agents. Moreover, the ethical, moral and social concerns have discouraged its use [194].

In order to overcome the above limitations, stem cells and/or progenitor cells can be used as an alternative. MSCs are unspecialized cells able to differentiate, or specialize in function, into multiple cell types and, as a consequence, regenerate different tissues [195]. The phenotype of these cells depends on their maturation during differentiation. Stem cells have two characteristics: they are capable of self-renewal and differentiation. However, when cultured in 2D, these cells differentiate as they are grown artificially, unlike *in vivo*, where they grow in 3D and cells can be in contact with the matrix in all directions. In contrast, 3D culture is able to maintain the phenotype but presents a low cell expansion rate [196].

As an alternative, various established immortalized cell lines have been developed on account of their many advantages, including ease of maintenance, unlimited number of cells and ability to retain key features of their phenotype [192]. The most commonly used bone cell line is the MC3T3-E1 line. These cells are an immortalized clonal line established from newborn mouse calvaria that can be differentiated into osteoblasts, leading to a mineralized collagenous ECM, when cultured under specific conditions (ascorbic acid and ß-glycerolphosphate),

while expressing osteoblast-related gene products in a temporal sequence (*e.g.* Coll, ALP, osteopontin) [29]. MC3T3-E1 cells are able to display a time-dependent and sequential expression of osteoblast characteristics, analogous to osteoblasts *in vivo* during bone formation [30, 31]. Mouse-derived cell lines are particularly convenient to use because of the widespread use of mice as the prototype mammalian system for genetic manipulation [42]. The MC3T3-E1 cell line has been extensively characterized by Franceschi *et al*. [197-199] and it has been postulated that they provide one of the most convenient and physiologically relevant culture systems for the study of transcriptional control in calvaria osteoblasts and the study of *in vitro* osteogenesis [40, 198].

MC3T3-E1 osteoblasts have been used for various BTE studies [42]. In particular, studies on the biological activity of MC3T3-E1 cell-seeded natural polymer-based scaffolds, such as collagen type I [187, 200, 201] and CTS [202-204] have been previously performed. Although this cell line is not appropriate for *in vivo* therapeutic applications, it enables studies on the differentiation of osteoprogenitor cells in 3D scaffolds, leading to its mineralization [29]. The advantage of their differentiation into osteoblasts, ready maintenance and the reproducibility of their behaviour *in vitro*, make this cell line a popular choice for *in vitro* studies of 3D model systems [42].

2.4.2.3 Commercially available collagen-based scaffolds for bone tissue engineering

Commercially available collagen-based scaffolds for bone repair include Bio-Gide® and Collagraft®. Bio-Gide® consists of a highly purified collagen types I and III of porcine origin [205]. The main function of this matrix is to serve as a matrix for soft tissue support and provide a barrier to the ingrowth of overlying soft tissue into underlying bony defects (*Figure 2.10*). It consists of two layers: a dense membrane and a porous membrane. The dense layer is next to the soft tissue and prevents the invasion of soft connective tissue cells. The second layer is a porous layer that is close to the bone defect and it consists of loosely arranged collagen fibres, acting as a stabilizer and enabling bone cells to become integrated

into the scaffold. This porous layer aims to promote osseo-progenitor cell proliferation. Collagraft® is a combination of highly purified type I bovine dermal fibrillar collagen and hydroxyapatite/tri-calcium phosphate ceramic (approx. 65 % hydroxyapatite and 35 % tri-calcium phosphate) [206]. Collagraft® is biocompatible, closely resembles natural bone and eliminates donor site morbidity problems. It is indicated for use in long bone fractures and traumatic osseous defects to provide a matrix for the repair process of bone.

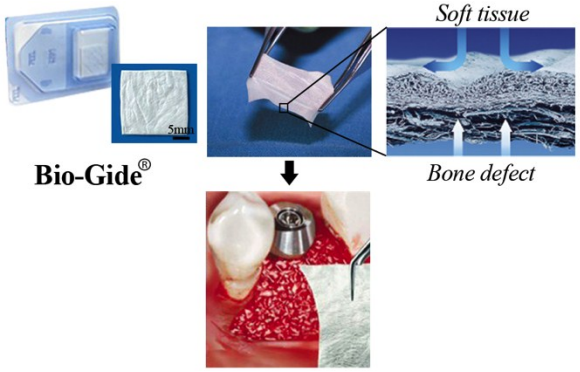

Figure 2.10: Commercial bone graft Bio-Gide®. Bi-layered collagen membrane. The upper part acts as a guide for fibroblast attachment leading to gingival tissue, whereas the dense bottom layer acts as a guide for osteoblasts, supporting bone healing. Adapted from [207]. Copyright © Geistlich Pharma AG.

2.4.2.4 Chitosan scaffolds for bone repair

Over the last few decades, CTS has played a major role in the field of TE, mainly due to the plethora of advantages listed in *Section 2.4.1.2*. In particular, CTS has been demonstrated to serve as an osteoconductive material, mimicking the natural function of bone and activating *in vivo* mechanisms of tissue regeneration, making it an effective template for bone repair [99]. Studies have also shown that CTS has the potential to promote growth and mineral matrix deposition and enhance bone formation both *in vitro* and *in vivo* [208, 209].

While CTS has been processed in various forms for BTE applications (*Figure 2.11*), most studies have focused on the development of sponges, as CTS possesses an excellent ability to create porous scaffolds via freeze-drying or lyophilisation [209-212]. Another possible matrix preparation is wet spinning, which involves the formation of fibres by dissolution in a suitable solvent and

coagulation in a bath [213-215]. CTS has also been demonstrated as a potential temperature-responsive injectable matrix for the delivery of drugs and therapeutic cells [216-219].

Composite materials are now playing a predominant role as scaffolds in BTE. Materials such as calcium phosphate [220-223], gentamicin-conjugated reinforced with beta-tri-calcium phosphate [223, 224], hydroxyapatite [225], and calcium phosphate cements [226], have been tested in combination with CTS for BTE applications.

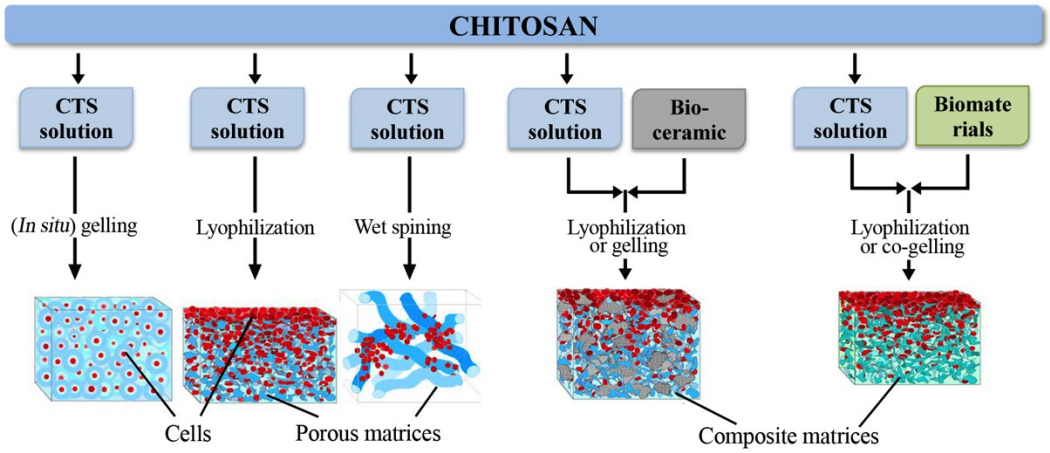

Figure 2.11: CTS processing for bone tissue engineering. Cells may be seeded within a gel-like scaffold, lyophilized sponge or fibrous structure. CTS has been combined with bioceramics (*e.g.* calcium phosphate, hydroxyapatite) or biomaterials (*e.g.* gelatin, alginate, collagen) to develop composite material to modify the biomechanical and biological properties of the scaffolds. Adapted from [99]. Copyright © 2005 Elsevier Ltd.

2.4.2.5 Collagen/Chitosan scaffolds as in vitro osteoid models

In an effort to create an *in vivo*-like environment suitable for bone cell attachment, proliferation, differentiation and mineralization, collagen-based scaffolds have been combined with different biomolecules that mimic the native components of the ECM. As previously stated, along with abundant collagen type I, bone ECM is also composed of adhesive and mineral-binding proteins, as well as, polysaccharides such as GAGs [46]. As a consequence of its structural analogy to GAGs and its osteoconductive properties, CTS has been combined with collagen in different forms for BTE [227]. Most studies have focused on the

development of collagen/chitosan (Coll/CTS) scaffolds via a freeze-drying process. Arpornmaeklong *et al.* [201, 228] investigated the effect of Coll/CTS sponges on the osteogenic differentiation of rat bone marrow stromal cells (BMSCs), as well as mouse pre-osteoblast MC3T3-E1. Attachment of BMSCs and expression of ALP and osteocalcin was observed to be higher when compared to CTS alone. Moreover the combination of these two natural polymers resulted in a greater uptake of water and resistance to enzymatic degradation compared to collagen alone. MC3T3-E1-seeded Coll/CTS sponges also promoted cell growth and showed higher degree of differentiation when compared to CTS alone sponges. However, as a consequence of the freeze-drying process these scaffolds rely on cell seeding post-fabrication, which is time consuming as it involves the addition of a cell suspension onto all surfaces of the sponge, leading to a heterogeneous cell distribution [229].

Coll/CTS hydrogels provide an *in vivo*-like environment in which the cell-seeding process is part of the scaffold fabrication, allowing a homogenous cell distribution in a short time frame. Tan *et al.* [230] pioneered the development of Coll/CTS hydrogels, where K565 cells were cultured within a 3D scaffold with different CTS proportions. Increasing amount of CTS led to a decrease in cell proliferation, however, cell function, based on cytokine-release, was greatly augmented. Recently, Wang and Stegemann [231] developed a thermogelled Coll/CTS scaffold via a sol-gel process by the use of β-glycerolphosphate. The addition of CTS to collagen hydrogels resulted in higher expression of osterix and sialoprotein of human BMSCs-seeded scaffolds when compared to collagen alone. Moreover, an increase in ALP and calcium deposition was also noted, making them a suitable matrix for tissue repair.

2.4.3 Cartilage tissue engineering

Since cartilage is a predominantly avascular, aneural and an alymphatic tissue, unlike bone, it lacks regenerative capabilities. Thus, it is crucial to develop novel approaches for its regeneration. To date, two different approaches have

been developed for cartilage tissue engineering (CTE) applications. One involves a scaffold-free approach, where the constructs are developed *in vitro* by the cells alone [232-234]. However, this technique is time-consuming, as the cells need to generate sufficient ECM in order to provide the mechanical stability when implanted into the defect. The traditional approach, on the other hand, involves the development of a 3D scaffold, which fundamental requirements include lack of immune response and inflammation, adherence and integration with the surrounding native cartilage, adhesion of chondrocytes and maintenance of the chondrocyte phenotype. Moreover, they should possess initial mechanical stability within the defect and have directed and controlled degradation (slow degradation may hinder cartilage formation, whereas fast degradation may compromise the structure and shape of the scaffold) [58, 235].

2.4.3.1 Collagen-based scaffolds for cartilage tissue engineering

Collagen types I and II are natural polymers widely used in CTE that present inherent biological cues that allow chondrocyte interaction with the scaffold, as well as providing the necessary space for the growing tissue. This is attributed to collagen recognition by cellular enzymes [88].

Nehrer *et al.* [236] reported different behaviour when seeding canine chondrocytes within Coll I and Coll II constructs. While seeded cells in Coll I gels exhibited a more fibroblastic phenotype, cells within Coll II retained chondrocyte morphology and characteristic biosynthesis. Coll I destabilization of seeded chondrocytes towards a fibroblastic phenotype and reduced the synthesis of cartilage-specific components, believed to be caused by their interaction with Coll I fibrils in highly hydrated gels [236-239]. However, because of the limited processing of Coll II into gel-like scaffolds [129, 240-242], as a result of the proteolytic cleavage of its telopeptides during extraction, Coll I-modified scaffolds are more frequently used [112, 114, 243, 244].

Acellular Coll I gels and sponges have been characterized *in vivo* in rabbit osteochondral defects and shown to enhance its spontaneous healing [245].

However, most studies have focused in the use of Coll I scaffolds as cell carriers for chondrocytes or MSCs. Allograft AC chondrocytes have been embedded within Coll I gels and transplanted into full-thickness defects in rabbit AC, resulting in a defect filled with hyaline cartilage 24 weeks after transplantation, compared to defects without seeded gels which were filled with fibrocartilage [7]. In a similar study, osteochondral progenitor cells were seeded into Coll I gels and transplanted into defects of up to 6 x 3 x 3 mm^3 in size in the medial femoral condyle of rabbits. After 2 weeks of implantation, cells differentiated into chondrocytes throughout the defect [246].

2.4.3.2 Cells for cartilage tissue engineering applications

The concept of engineering a scaffold that resembles the native ECM of cartilage involves seeding suitable cells able to synthesize the cartilage-specific ECM components (*e.g.* Coll II and GAGs), which play a critical role in regulating the expression of chondrocyte phenotype, in addition to supporting chondrogenesis − a process by which cartilage is developed by the creation of chondrocytes during embryogenesis and skeletal repair in the adult [130, 247]. Through this, the *in vivo* chondrogenic sequence for AC generation can be closely mimicked.

The chondrocytic differentiation sequence in embryonic stem cells (ESCs), can be subdivided into five consecutive, yet overlapping, phases: condensation of progenitor, chondrocyte differentiation, cartilaginous ECM deposition, hypertrophy and cartilage degradation, and bone replacement [248]. During the first phase, ESCs differentiate into chondrocytes and start to produce an ECM rich in *Coll2a1* (IIb) and *aggrecan*. This stage is highly proliferative. Following differentiation, cartilage formation occurs, and characteristic chondrocyte marker genes are expressed (*Sox9*, *Coll2a1* (IIb) and *aggrecan*). When chondrocytes start undergoing hypertrophy, the genes that encode *Coll2a1* (IIb) and *aggrecan* are repressed and the gene for *Coll10a1* is activated. In cartilage (*e.g.* AC), chondrocyte differentiation ends at this stage and chondrocytes undergo apoptosis

followed by cartilage degradation. In long bones, the process continues as chondral ossification occurs. At this stage, terminally differentiated hypertrophic chondrocytes express the matrix-degrading enzyme MMP-13, controlling the process preceding bone formation [249].

An optimal cell source for CTE applications should be easily isolated, capable of being expanded without cell de-differentiation, as well as synthesizing all the cartilage-specific components. To date, several cell sources have been investigated, including chondrocytes [250, 251] and MSCs [235].

Chondrocytes are the first choice of cells, as they are naturally found in native cartilage. They are characterized by their rounded morphology and their synthesis of ECM components. However, chondrocytes are limited in number (5-10 % of cartilage tissue) and need to be expanded to high quantities. Their expansion in monolayers causes de-differentiation into a fibroblastic phenotype, characterized of lower Coll II synthesis and increased Coll I production, as well as a change from rounded to polygonal morphology [235]. Moreover, the use of autologous AC chondrocytes involves harvesting the joint cartilage which causes tissue morbidity, loss-of-function, and low cell yield and bioactivity [235]. In an effort to prevent de-differentiation process, chondrocytes have been cultured in 3D constructs, such as agarose [252], alginate beads [253] and fibrin glue [254], which have been shown to preserve the chondrocyte phenotype. A promising cell source for CTE, as an alternative to autologous chondrocytes, is autologous MSCs. Recent studies have focused on its differentiation toward the chondrocyte lineage when cultured in chondrogenic medium within collagen-based scaffolds [255, 256]. Sources of MSCs investigated for cartilage repair in collagen scaffolds include bone marrow [257], muscle [258, 259] and synovium [260]. However, the differentiation of MSCs results in an uncommon differentiation pathway different to endochondral ossification or permanent cartilage formation where markers of hyaline cartilage, hypertrophy and bone are expressed simultaneously [261].

As an alterative to cell sources listed above, chondroprogenitor cell lines have been developed on account of their various advantages that arise from their ability to retain key features of their phenotype [32]. In particular, RCJ3.1C5.18 − a non-transformed clonal chondrogenic cell line from rat calvaria − is a lineage-restricted cell line able to express several chondrogenic markers and form cartilage nodules in culture [32]. RCJ3.1C5.18 cells have been used to test the suitability of fibrin hydrogels as scaffolds for AC regeneration [262]. Fibrin-encapsulated RCJ3.1C5.18 cells secreted an ECM containing Coll II and aggrecan, both components of hyaline cartilage [263].

2.4.3.3 Commercially available collagen-based scaffolds for cartilage tissue engineering

Commercially available collagen-based scaffolds for cartilage repair include MACI®, Novocart®3D and CaReS®, all associated with autologous cell transplantation (*Figure 2.12*) [69, 264]. MACI® (Genzyme, USA, former Verigen, Germany) is a collagen type I/III membrane seeded with autologous cells isolated from the patient biopsy. Novocart®3D is a bi-phasic 3D collagen-based sponge containing chondroitin-sulfate. This graft is produced by isolating the patient's chondrocytes from a full-thickness defect followed by expansion in a monolayer without passaging. Cells are then seeded into the scaffold and cultured for another 2 days before being implanted.

Another commercial product available is CaReS® (Arthro Kinetics Biotechnology GmbH; Austria). This graft is composed of autologous cells embedded within a Coll gel. As opposed to other grafts, CaReS® gel is immediately mixed with the isolated cells after the biopsy, followed by 2 weeks of culture. A recent study comparatively investigated the gene expression and chondrocyte differentiation from patient's biopsies implanted within MACI®, Novocart®3D and CaReS® [264]. None of the transplanted scaffolds, including a hyaluronan-based graft (Hyalograft®) reached the levels of hyaline cartilage. The highest differentiation of cells was found to be in CaReS® scaffolds, followed by Novocart®3D, Hyalograft® and MACI®.

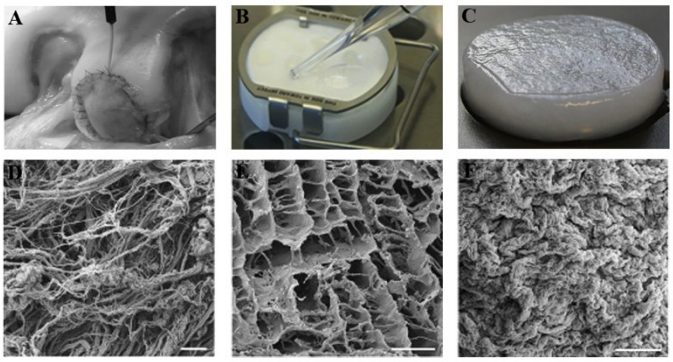

Figure 2.12: Commercially available collagen-based cartilage grafts. (A,D) MACI®, (B, E) Novocart®3D and (C, F) CaReS® scaffolds and SEM micrographs. Adapted from [264-267]. Copyright © 2011 TETEC- a B. Braun Company. Copyright © 2005 British Editorial Society of bone and Joint Surgery. Copyright © 2008 Macmillian Publishers Limited. Copyright © 2011 Osteoarthritis research Society International.

2.3.3.4 Chitosan scaffolds for cartilage repair

CTS has the potential to serve as a material for CTE applications, on account of its structural analogy to GAGs found in native cartilage [132, 268]. Since GAGs are known to be involved in regulating chondrocyte differentiation, morphology and biosynthesis, Suh and Matthew [132] noted that CTS may be able to fulfill the role of GAGs by mimicking certain biological activities, such as binding growth factors and adhesion proteins [131]. The cationic nature of CTS allows cell adhesion and electrostatic interactions with GAGs, promoting their retention within CTS scaffolds, as suggested by Roughley *et al.* [136]. In addition, the culture of chondrocytes on CTS substrates has been shown to maintain a rounded morphology as well as preserve the synthesis of their characteristic ECM molecules [268].

CTS scaffolds can be prepared by a freeze-drying process, and the effect of pore size on the behaviour of cultured chondrocytes within the scaffolds has been determined [269]. Compared to pores of < 10 μm in diameter, scaffolds with pore sizes between 70 and 120 μm exhibit higher chondrocyte proliferation, as well as Coll II and GAGs biosynthesis [270]. Furthermore, it has been demonstrated that CTS has an effect on the differentiation of MSC into chondrocytes. The results show that the synthesis of Coll II by the MSCs seeded within 3D freeze-dried CTS scaffolds increased after 3 weeks in culture, indicating the beginning of

differentiation [271]. Lu *et al.* [272] demonstrated that CTS can be prepared as a hydrogel and injected into knee articular defects of rats to stimulate chondrocyte growth, suggesting their potential benefit for wound healing. Furthermore, it has been reported that the combination of CTS-glycerolphosphate with autologous blood in ovine cartilage defects are able to repair with higher content of hyaline cartilage compared to microfracture alone in an ovine model [217, 273]. This result suggested that CTS has the ability to stabilize the blood clot formed in the defect and stimulate the wound healing process [130]. CTS effect on cartilage repair was validated within marrow-stimulated chondral defects in rabbits [274].

An example of cartilage treatment using CTS is a product based on a liquid scaffold named BST-Cargel® [217]. This novel chitosan-based scaffold is intended to promote hyaline cartilage formation when incorporating autologous whole blood into a debrided cartilage defect. The BST-Cargel® hybrid clot is able to guide the repair of cartilage by stem cells that migrate from the bone marrow. Clinical trials of BST-Cargel® have proven superior outcomes compared to microfracture alone [275].

2.4.3.5 Collagen/Chitosan scaffolds for cartilage tissue engineering

Since collagen and GAGs are the two main ECM macromolecules found in native cartilage, the use of collagen/CTS-based scaffolds for the regeneration of injured cartilage has received much attention [276-282]. Coll/CTS-based scaffolds have been produced as cell carriers for CTE by freeze-drying in order to produce porous scaffolds that support chondrocyte attachment, proliferation and differentiation. Coll/CTS hybrid scaffolds have also been combined with different materials such as hyaluronan (HA) [278, 282] or GAGs [276, 280] in an effort to closely mimic the naturally occurring environment in the cartilage ECM. Coll/CTS/GAG scaffolds have been shown to support chondrocyte proliferation and ECM biosynthesis when implanted for 12 weeks in the dorsum of athymic nude mice [277]. Similar results were obtained in Coll/HA/CTS scaffolds seeded with chondrocytes from articular cartilage of rabbits when cultured for 21 days.

DNA and GAG contents were significantly higher during culture periods when compared to collagen alone, and most seeded cells preserved their chondrocytic phenotype during culture [278]. In order to improve the mechanical strength and tune their degradation, Coll/CTS-based scaffolds have been chemically cross-linked with a natural cross-linker named genipin [276, 281].

2.4.4 Osteochondral tissue engineering

Progress made in both bone and cartilage tissue engineering has led to the advancement of osteochondral tissue engineering (OTE). This technique aims to promote superior cartilage integration and repair of osteochondral defects [27]. When attempting to repair injured cartilage by the implantation of a scaffold that mimics the native cartilage ECM within a full-thickness defect, a problem of fixation and integration with the surrounding host tissue is usually encountered [8]. The lack of integration is attributable to the differences in the structural and mechanical properties between the engineered construct and the subchondral bone. Even in partial-thickness defects the integration of the construct with the surrounding tissue may be a problem; therefore, an alternative strategy is to create a full-thickness defect followed by the implantation of an osteochondral implant [26]. This approach is based on a better and faster integration of bone-to-bone interface compared to cartilage-to-cartilage interface [283].

Engineering complex tissues is one of the most ambitious goals of all TE disciplines, as it includes the development of a stratified scaffold with two or more discrete layers with specific physical and chemical properties [74]. The different approaches investigated so far for the development of osteochondral scaffolds can be classified in a combination of a scaffold strategy (*Figure 2.13 (A-D)*) and a cellular strategy (*Figure 2.13 (I-IV)*) [28].

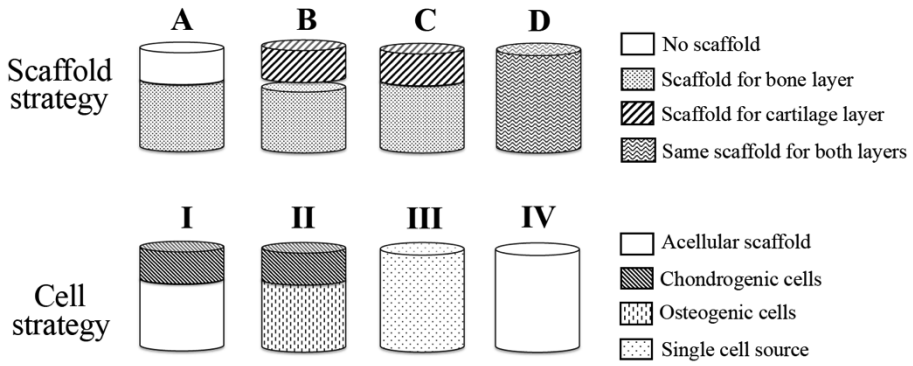

Figure 2.13: Schematic diagram of the strategies used to develop osteochondral scaffolds. Broadly, it can be classified based on a combination of a scaffold strategy (A-B) and cell strategy (I-IV). Adapted from [28]. Copyright © 2006 Elsevier Ltd.

From the scaffold point of view, an osteochondral construct can be generated by [28]:

A. A bone layer with a cartilaginous scaffold-free layer

B. A bone and cartilaginous layer cultured in separate media and conditions, and joined prior to implantation.

C. A bilayered scaffold with a bone and cartilage layer as a single heterogeneous scaffold cultured using the same conditions.

D. A single homogenous scaffold for both bone and cartilage repair.

Strategies B and C are based on the development of bi-layered scaffolds (*Figure 2.14 A*). The use of a bi-layered scaffold presents the advantage of promoting a better integration of the cartilage as a consequence of the improved scaffold fixation in the subchondral region, as well as optimizing the repair of both the cartilage and bone tissues [27]. Cartilage and bone-like layers can be cultured separately and combined into a single construct by either suturing, or gluing with a fibrin sealant, or simply by press-fitting [26, 28, 283]. Nonetheless, their implantation has shown poor integration between layers, often leading to implant failure [27, 284]. Thus, some attempts have been made to achieve well-integrated cartilage- and bone-like layers based on polymeric and ceramics layers

(*Figure 2.14 B-D*) [27, 171, 285, 286]. Coll I bi-layered scaffolds have been created by layering different concentrations of Coll I, followed by freeze-drying (*Figure 2.14 B*). A dense Coll I layer was used to be in contact with the bone and a porous Coll I layer was used to be in contact with the cartilage. Histological data showed that seeded scaffolds presented better results compared to the cell-free scaffolds [287]. Chen *et al.* [8] combined a cartilaginous layer of Coll I and a bone layer of Coll I in combination with PLGA for the development of a bi-phasic scaffold (*Figure 2.14 C*). Osteochondral tissue was regenerated four months after implantation in the knee of a 1-year old beagle. In addition, Harley *et al.* [171, 173] developed a bilayered osteochondral scaffold based on a mineralized collagen type I-GAG scaffold by nanoparticulates of calcium-phosphate precipitated within the collagen network, designed to regenerate the underlying subchondral bone, and a non-mineralized collagen type II-GAG scaffold, designed to regenerate cartilage. The scaffolds were prepared via a liquid-phase cosynthesis technique, which allowed the simultaneous formation of the bilayered scaffold with a gradual interface. Another example of a natural polymer used for osteochondral repair involves the use of an HA scaffold partially impregnated with a viscous CTS solution [288]. CTS has also been used in a bi-phasic scaffold in combination with D, D-L, L-polylactic acid impregnated with HA for the regeneration of bone and a hydrogel of HA and CTS for the regeneration of cartilage. These scaffolds were implanted in rabbits and the results show that the constructs were capable of maintaining hyaline-like cartilaginous tissue at 24 weeks [289]. In another study, a bi-phasic scaffold comprised of a polymer and a ceramic such as (polyethylene oxide/polybutylene terephthalate)/HA-tri-calcium phosphate scaffold was used (*Figure 2.14 D*). Polyethylene oxide/polybutylene terephthalate has been shown to have mechanical properties similar to cartilage tissue, whereas HA/tri-calcium phosphate, has shown to present both osteoconductive and osteoinductive properties [28].

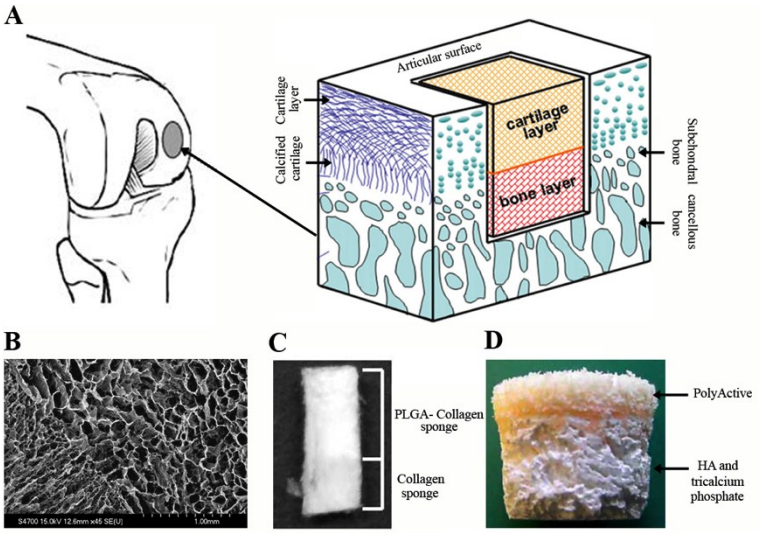

Figure 2.14: Osteochondral tissue engineering. (A) Schematic of a defect in articular knee joint injury and implanted bi-layered scaffold. (B) SEM micrograph of a bilayered Coll I freeze-dried scaffold with two concentrations. (C) Poly(DL-lactic-co-glycolic acid) (PLGA)-Coll I sponge layer for bone engineering and Coll I sponge for cartilage engineering. (D) A cartilaginous top layer of the elastomeric copolymer poly(ethylene glycol)-terephthalate/poly(butylene)-terephthalate (PolyActive) and a bottom bony-layer composed of hydroxyapatite (HA) and tri-calcium phosphate. Adapted from [8, 26-28, 290].

From a cell point of view, OTE scaffolds can be seeded with [28]:

A. A single source with chondrogenic differentiation capacity

B. Two sources with chondrogenic and osteogenic differentiation capacity, seeded respectively in each layer.

C. A single source with both chondrogenic and osteoblastic differentiation capacity.

D. A cell-free approach.

Acellular scaffolds can be modified by incorporating growth factors or vascularization barriers to prevent the growth of blood vessels within the cartilaginous layer [290]. The cellular approach involves the seeding of cells that differentiate into chondrocyte and/or osteoblasts, which are the two main cells that comprise the osteochondral tissue. The different osteoblasts and chondrocytes available for the simultaneous repair of bone and cartilage has already been introduced earlier in *Section 2.3.1.4* and *2.3.2.2*, respectively. The most direct

source involves the isolation of both cell types from a patient biopsy, followed by their expansion *in vitro*. However, the number of cells that can be harvested and expanded is low. MSCs are an alternative option, since these cells present a nearly unlimited-self renewal capacity and can be harvested into the scaffold before or after their differentiation into chondrogenic or osteogenic phenotype [26, 290].

2.5 HYDROGELS AS EXTRACELLULAR MATRIX-MIMICKING SCAFFOLDS

2.5.1 Hydrogel structure

Since the development of methacrylate-based hydrogels in the early 1960s, hydrogels have been used in an effort to better mimic the native ECM of tissues [291]. A large variety of natural and synthetic hydrogels have been investigated for their use as surface modification of biomedical implants, drug delivery and TE [291, 292]. Hydrogels have the advantage of being able to homogeneously accommodate cells as part of their processing. In addition, they can be formed *in situ* within a defect site in the body by injecting a thermo-responsive solution that can easily fill complex shapes [11]. Hydrogels can be defined as three-dimensional cross-linked polymeric networks that contain either covalent bonds between one or more co-monomers, physical cross-links due to chain entanglements, hydrogen bonds or strong van der Waals interactions, or crystallites bringing together two or more macromolecular chains [293]. They can be classified as physical (*i.e.* reversible) or chemical (*i.e.* permanent) depending on their network [294]. Physical gels are networks that are held together by only secondary forces such as, ionic, hydrogen-bonding or hydrophobic forces. These type of gels are usually not homogenous as they may contain clusters of molecular entanglements, or hydrophobic or ionic domains [294]. Chemical gels, on the other hand, are covalently cross-linked networks. Hydrogels can be classified into different categories depending on their method of preparation (*e.g.* homo-polymer, co-polymer), charge (*e.g.* neutral, anionic, cationic) and physical

structure (*e.g*. amorphous, semi-crystalline, hydrogen-bonded, supra-molecular, or hydro-colloidal) [293].

2.5.2 Hydrogel properties

The potential advantages of hydrogels are numerous, including their capability of imbibing large amounts of water or biological fluids, thus resembling natural living tissues [295]. These hydrophilic networks are able to absorb from 10-20 % to about thousands of times their dry weight without polymer dissolution [294]. The first water molecules that bind to a dry gel, called "primary bound water", hydrates the most polar, hydrophilic sites of the gel. As the hydrophilic groups bind to water, the gel starts to swell and the hydrophobic groups are exposed, which can also interact with water molecules, called "secondary bound water". The additional imbibed water, because of the osmotic driving force of the network chains towards infinite dilution, is opposed by the covalent or physical cross-links, leading to an elastic network retraction force and a state of swelling equilibrium. The water molecules that follow the imbibed ionic, polar and hydrophobic bound water are called "free water" or "bulk water". The free water fills the space between the macro-pores or voids of the network [294]. The high water content of these materials contributes to their biocompatibility, as the low dry mass causes little irritation and low quantities of degradation products [296]. However, the biocompatibility depends on several properties, including polymer type, cross-linking method, degradation rate, and its by-products [291].

2.5.2.1 Hydraulic permeability

The water content found in hydrogels mimics the interstitial fluid found in tissues, which provides several important biomechanical functions [297-300]. The high water content along with the hydrogels porous structure allows for the transport of low-molecular-weight solutes and nutrients into the hydrogel as well as cellular waste out of it [12]. Moreover, the fluid flow provides a mechanical environment for interstitial cells, which sense mechanical forces via integrin

receptors through the cell-ECM signalling [297, 298, 301]. Hydraulic permeability (*k*) is defined as the ability of a porous structure to transfer a fluid under an applied pressure [302]. *k* is an intrinsic parameter that describes the scaffolds microstructure independent of its size and type of fluid use [297, 298, 301]. In particular, the fluid flow in hydrated soft tissues and hydrogel scaffolds is the major factor modulating its poroelastic response, thus influencing the mechanical properties of tissues [303, 304]. A well-known theoretical model for the calculation of *k* is the Happel model, which is a continuum approximation that relates permeability to physical and geometrical parameters. The Happel model is a simplified model that describes the relationship between *k* of a random array of long cylindrical rods and its geometry [35]. This model has been particularly useful in fibrillar structures, such as connective tissues (*e.g.* cartilage) and collagen-based hydrogel scaffolds. The total hydraulic permeability of the fibrillar structure can be calculated by:

$$k = \frac{2}{3}k_{\perp} + \frac{1}{3}k_{\parallel} \tag{1}$$

Where $k_{\parallel}$and $k_{\perp}$ are the contributions of the parallel and perpendicular fibres to permeability, respectively, [35, 298] as a function of fibre hydrodynamic radius (a) and the construct solid volume fraction (σ):

$$k_{\parallel} = \frac{a^2}{8}\left[4 - \sigma + \frac{1}{\sigma}\left\{2ln\left(\frac{1}{\sigma}\right) - 3\right\}\right] \tag{2}$$

and

$$k_{\perp} = \frac{a^2}{8}\left[\frac{1}{\sigma}ln\left(\frac{1}{\sigma}\right) - \frac{1}{\sigma}\frac{1-\sigma^2}{1+\sigma^2}\right] \tag{3}$$

This model applies several assumptions, including uniform fibrillar density and random orientation of fibres, constant fibre cross-sectional area along the direction of the flow, yielding no inertia in terms of the Navier-Stokes equations, and a weighted averaging method giving twice the weight for perpendicular fibres than for parallel fibres [35].

2.5.2.2 Mechanical properties

Although a high content of water is beneficial for tissue production, it decreases the mechanical properties of the scaffolds. These properties are controlled by the polymer concentration and cross-linking density, two important physical properties of hydrogels [291]. On account of their low mechanical strength, hydrogels are usually chemically cross-linked, cell-remodelled with bioreactors or combined with other polymers or bioceramics (*Section 2.4.2.1 and Section 2.4.2.2*).

Since 1962 following the development of Coll I gels by Grillo and Gross [305], through the adjustment of the pH of acidic solutions of Coll I to physiological pH, these gels have been extensively studied and used in many biomedical applications (*Section 2.5.1.1*). Coll I fibrillogenesis results in a highly-hydrated gel with low collagen fibrillar density (CFD; < 1 %) with poor mechanical properties (E ~ 4-6 kPa, strength ~ 2-8 kPa) [14]. Plastic compression (PC) is a scaffold-processing technique developed by Brown *et al.* [16] to increase rapidly the CFD of highly-hydrated gels and subsequent increase in their modulus and strength (*Figure 2.15*).

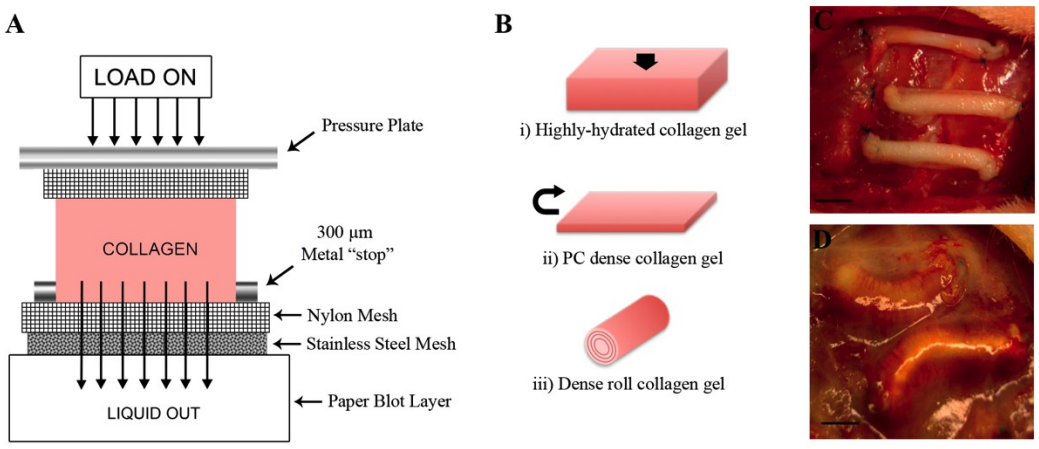

Figure 2.15: Plastic compression technique. (A) Schematic showing a highly-hydrated gel on a series of metal and nylon meshes and paper blot. (B) Schematic representation of the collagen gel before and after PC and subsequent rolling process for the development of a dense cylindrical roll. (C) *In vivo* implantation of three PC constructs sutured in transversal intercostal space. (D) Constructs prior to harvesting after 5 weeks of implantation. Adapted from [14, 16, 17].

By removing the excess fluid that results from casting, this technique allows for the development of a dense collagen gel with CFD approaching the native ECM. This controllable process not only enables the production of collagen scaffolds with increased biomechanical properties but also allows for the organization of seeded cells in 3D by providing the space for their growth and differentiation without compromising their viability [306]. Dense gels are achieved by placing the highly-hydrated gels on a series of plastic and metal meshes and paper blot and subjected to a compressive load for a 5 min period to expel more than 90 % of the fluid content, thus increasing the CFD 40-fold from 0.3 to 12 % (*Figure 2.15 A*).

Abou Neel *et al.* [14] reported that collagen gels with improved tensile properties can be produced through the PC technique. By using this method, the authors were able to measure the weight loss of highly-hydrated, single (SC) and double compressed (DC) sheets under various conditions: self compression, compression with an external load and capillary action. Results showed that under creep stress gels with different hydration levels have different responses. Highly-hydrated gels showed a poroelastic response, where the fluid flow dominated and no immediate recovery was observed. SC scaffolds resulted in a greater strain than the DC scaffolds showing a clear dependence between the strain under creep and the collagen concentration. Unlike the highly-hydrated gel, both the SC and the DC scaffolds exhibited a viscoelastic recovery phase with time.

Since the development of the PC technique, dense collagen scaffolds have been shown to support numerous cell sources in different geometries. Dense collagen scaffolds have been shown to improve cell metabolic activity [307] and have been proven to be a versatile scaffold for the potential repair of various tissues, including bone [187, 307-309], skin [310, 311], bladder [312], spinal cord [313], corneal epithelial [314, 315] and temporomandibular joint [316]. On account of its versatile processability, dense collagen scaffolds have been produced as sheets [187], rolls [16], and tubes [317]. Dense, rolled scaffolds have

been tested *in vivo* in intercostal spaces in a rabbit model in order to evaluate their integration, cell ingrowth and angiogenic response over a period of 5 weeks (*Figure 2.15 B and C*) [17]. Scaffolds were seeded with allogenic rabbit flexor tendon cells and rolled to obtain cylindrical rolls 2.5 mm in diameter and 20 mm in length. The results showed that revascularization rates, inflammation, collagen remodelling and recovery of tensile mechanical strength were all improved and/or faster for cell-seeded constructs, compared to acellular rolls.

2.5.2.3 Cell-mediated contraction

Along with low mechanical strength and stiffness, highly-hydrated gels present limitations associated with extensive cell-mediated contraction. Cells respond to external tension by adjusting their geometry, and connections to the substratum and other cells (*Figure 2.16 A*). In general, cells contract hydrogels as they are not in mechanical equilibrium. In other words, gels contract if the traction forces exerted by seeded cells are greater than the elastic forces of the hydrogel, then the gel contracts. This phenomenon continues until the cell traction force is counterbalanced by the resisting elastic force (stiffness) in the gel. The mechanism involved in this phenomenon is not clearly understood, however it is believed that the cell traction remains approximately constant, while the elastic force of the gel increases until reaching an equilibrium [318]. Therefore, depending on their external tension, cells develop a pre-stress level to modulate their cell-matrix contacts, pseudopod lengths, cytoskeletal organization and modulus of elasticity (*Figure 2.16 A*) [319].

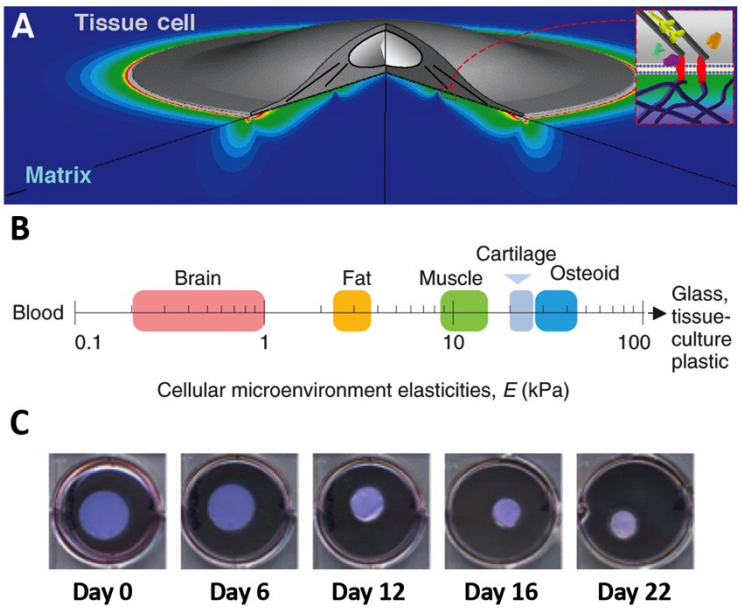

Figure 2.16: **Cell-mediated contraction**. (A) Strain distribution computed in a soft matrix beneath a cell. The cell has a contractile pre-stress from the edge to near the nucleus. (B) Cellular microenvironment elasticity for a variety of tissue cells from soft brain through the intermediate stiffness of muscle to relatively rigid cartilage and osteoid. (C) Pre-osteoblasts contraction of dense Coll scaffolds through 22 days in osteogenic medium. Adapted from [320, 321]. Copyright © 2005 Science. Copyright © 2010 Journal of Cell Science.

The mechanical tension generated by the contractile activity of the cells, plays an important role in cell differentiation, migration, morphogenesis and tissue remodelling [322]. Cytoskeletal assembly and gene expression during differentiation of cells, such as muscle cells, osteoblasts and MSCs have shown to be directed by the elasticity (E) of the tissue through myosin-dependent mechanism (*Figure 2.16 B*) [321]. For example, MSCs can initiate osteogenesis when seeded on a firm collagen-coated gel mimicking the osteoid (E~ 35 kPa), and myogenesis on softer collagen-coated gels mimicking the muscle (E~ 10 kPa) [321].

In particular, collagen hydrogels, on account of their low solid volume fractions, have shown high volume reduction attributable to different cell sources, including endothelial, smooth muscle cells, fibroblasts and osteoblasts [323]. Pioneering work in investigating collagen gel contraction was reported by Bell *et al.* [324] in the late 1970s. This work focused on the study of collagen contraction by fibroblasts to gain insight into wound contraction and suggested their use as

tissue equivalents for skin grafts [325]. It has been described by Vernon *et al*. [326] that the migration of endothelial and fibroblast cells on top of Coll I hydrogels generates a significant distortion of the substrate when they move on top of the gels. In this case, each cell pulls the ECM toward itself in a continuous manner, accumulating ECM around them. This process of pulling on the substrate is known as traction. The traction that the cells apply has been studied by using the fibrillar collagen gel contraction assay embedded with cells (*Figure 2.16 C*). Gel contraction increases the collagen density, and therefore its mechanical strength. In the case of osteoblasts, Qi and co-workers [327] investigated the contraction of collagen gels by osteoblast-like cells and the role of adenosine triphosphate (ATP) in bone remodelling. The results indicated that ATP may act as a regulator and/or transducer of mechano-signal transduction by regulating a cell's set-point for pre-stress.

2.6 FUTURE CHALLENGES

Clinical translation and feasibility of tissue-engineered scaffolds depend on several key issues related to biocompatibility, biodegradability, cell source, mechanical strength and functional integration. Biopolymer-based hydrogels are being increasingly investigated as a consequence of their water-absorbing capacity and native ECM-mimicking property. Although many hydrogel systems have been developed, several biopolymers and proteins will need to be combined to mimic the ECM properties [293]. In this respect, few studies have focused on the development of stratified scaffolds for the repair of cartilage and osteochondral defects with different cell sources.

Hydrogels have long been popular as 3D networks filled with fluid that are able to exchange nutrients, oxygen and waste. However, for large defects it is critical to promote blood vessel formation to enhance the exchange of these molecules. Moreover, successful integration of the engineered tissue with the patient's defect at the injury site also relies on vessel and tissue integration [328].

As a consequence, greater attention is given to the local delivery of angiogenic factors (*e.g.* vascular endothelial growth factors) or blood vessel forming cells (*e.g.* endothelial cells) within the hydrogels [292].

Finally, an ideal hydrogel should initially support loads found in the tissue to be replaced, in order to gradually degrade and transfer the load to the neo-tissue [291]. Much attention has been devoted to developing hydrogels with increased mechanical strength and stiffness without compromising the synergistic beneficial aspects of the hydrogel [12]; however, very few have reported to have achieved both properties. Future studies should address methods to generate scaffolds zonally organized that can better mimic the native tissue and withstand the everyday loads until the neo-tissue is developed.

CHAPTER 3: STATEMENT OF THE PROBLEM

Over the last two decades, OTE has been driven by the demand for alternative treatments to repair full-thickness AC defects and to provide an osteochondral interface that supports the rapid integration of a structurally preferable bone-to-bone interface rather than a cartilage-to-cartilage interface [25, 26]. Initially, OTE involved a relatively simplistic concept based on cell seeding on a homogeneous static carrier that functioned independently and exhibit mechanical properties and characteristics similar to those of one particular tissue [2]. During the past decade, OTE has advanced towards the use of layered constructs with biomaterials that interact with the surrounding tissue in a more complex and dynamic manner [2, 3].

A layered approach comprises the adhering of specific tissue layers that have been independently developed to mimic the particular requirements of each tissue type (*i.e.* cartilage and bone) [329]. This approach often involves the use of adhesives or suturing techniques to join the independently developed constructs together [26, 28, 283]. However, this strategy may result in implant failure caused by poor integration between layers [27, 284]. Several attempts have been made to achieve integrated cartilaginous and bony layers based on polymers and ceramics [27, 285, 286]. However, because of the significant differences in the starting mechanical properties of each layer, current constructs often exhibit a weak mechanical interface, which can lead to the premature failure of the scaffold. Hence, there is a significant need for development of integrated layered scaffolds that do not require a joining mechanism and mimic the complex structure of osteochondral tissue by providing an appropriate structural framework for chondrogenic and osteogenic differentiation during co-culture.

In this doctoral research, the development of an integrated bilayered hydrogel scaffold was proposed as an *in vitro* model to potentially overcome the above-mentioned challenges; with a cartilage-like layer contributing to the repair of

damaged articulating joint tissues and an osteoid-like layer enabling integration of the graft-to-recipient bone interface.

Developing a scaffold that closely mimics the microstructure and microenvironment of each particular native ECM remains to be accomplished since no homogeneous material currently available provides all the essential features [330, 331]. Thus, a reasonable approach would be to design a hybrid scaffold that maximizes the advantageous properties of each material. Attempts to do so involve the use of separate materials that closely mimic the extracellular milieu of bone and cartilage. Reconstituted Coll hydrogels allow for the transport of nutrients, oxygen and waste in and out of the hydrogel, however, this highly-hydrated system presents CFD (< 0.1 %) significantly below physiological values [12, 16]. Herein, a method to produce dense scaffolds was proposed by using a previously reported PC technique [16].

Beside abundant collagen, the ECM of tissues is also composed of non-fibrillar proteins, as well as polysaccharides, such as GAGs. Since CTS is a biodegradable polysaccharide structurally similar to the GAGs found in native tissues [130], it is expected here that CTS may also have similar bioactivities to GAGs [132]. Therefore this doctoral research proposed engineering a novel system for OTE applications based on the incorporation of a GAG-analog to a Coll hydrogel with Coll/CTS ratios approaching those of Coll/GAG found in native bone and cartilage (*Figure 3.1*).

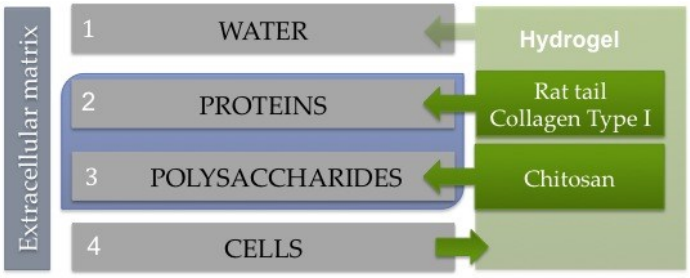

Figure 3.1: **Schematic of the ECM-mimicking strategy of this doctoral research.**

This dissertation also investigated the effect of CTS incorporation on the biophysicochemical properties of hybrid scaffolds, including hydraulic

permeability (*k*), swelling and mechanical properties. It is expected that the incorporation of CTS will modulate Coll hydrogels microstructure and biochemical composition, allowing the controlled production of tissue equivalent dense hydrogels with tailored physicochemical and mechanical properties for each specific application.

Chapter 4 validates the use of PC to obtain dense Coll/CTS hydrogels with CFD approaching those of native tissues. Moreover, it describes the generation of an osteoid-like model for bone repair, and investigates the effect of CTS incorporation on the scaffolds morphological and mechanical properties, including resistance to enzymatic degradation as well as cell-based remodelling and contraction. In addition, the ability of Coll/CTS to support osteoblast viability, growth, differentiation and mineralization is investigated. For the purpose of studying the osteogenic potential of these constructs, osteoid-mimicking hybrid scaffolds were seeded with a well-characterized pre-osteoblastic cell line, and its differentiation along with extensive mineral characterization was investigated.

Chapter 5 evaluates the concept of engineering a scaffold as an *in vitro* model for AC repair, which involves the use of biomaterials that mimic the collagenous protein and GAGs present in the native cartilage ECM. Since collagen type II (Coll II) is difficult to be processed into gel-like scaffolds [129, 240-242], acid extracted Coll was used instead [112, 114]. Based on previous reports on chondrocyte phenotype destabilization toward fibroblasts when seeded within highly-hydrated Coll hydrogels [236-239], it was proposed here that the incorporation of CTS, a polysaccharide with reported "chondroprotective" properties, into collagen type I gels with fibrillar densities approaching physiological levels, would support chondrocyte function and increase cartilage-like ECM production. *Chapter 5* also proposed the use of cylindrically shaped dense constructs of clinically relevant diameters (3-5 mm) to study the complex interplay between scaffold geometry, microstructure, composition, and

mechanical properties with chondroprogenitor function. These constructs are proposed as potential *in vitro* models for critical-sized AC defects for CTE, giving significant insight into the challenges involved when scaling up scaffolds designed and optimised *in vitro* for tissue repair.

In view of dense Coll/CTS scaffolds to individually support bone- and cartilage-like formation, *Chapter 6* builds upon these findings and proposes the combination of the co-gelling and PC techniques to develop an integrated dense bilayered hybrid gel, with weight ratios approaching those of Coll/GAGs in the native ECMs of cartilage (Coll/CTS 1:1) and bone (Coll/CTS 33:1).

Finally, *Chapter 7* evaluates the effect of CTS, a charged macromolecule, on the microstructural evolution of highly-hydrated Coll hydrogels when undergoing a gravity-driven or an accelerated consolidation process due to an external compressive stress. Herein, the use of a novel technique, based on detecting the spatiotemporal distribution of fluorescent beads within Coll/CTS hydrogels using confocal microscopy, is proposed to measure the effect of CTS on Coll gels consolidation process involved in SC and PC. *Chapter 7* also uses the Happel model to calculate the hydraulic permeability of Coll/CTS hydrogels pre- and post-consolidation and describes the relationship between CTS content, biomechanical properties and hydraulic permeability in analogy to GAG content in cartilage tissue. Moreover, the effect of CTS fixed charge on dense Coll/CTS hydrogels was investigated through structural, mechanical and swelling characterizations under isotonic and hypertonic conditions.

CHAPTER 4: OSTEOID-MIMICKING DENSE COLLAGEN/ CHITOSAN HYBRID GELS

Since the ECM is by definition Nature's ideal scaffold biomaterial, the concept of bone healing has evolved from the use of a static carrier, to the use of biomaterials that interact with the surrounding tissue in a more complex and dynamic manner [2, 332]. One such approach is to custom-design a scaffold that mimics the structural and functional molecules of the ECM, which includes, along with abundant Coll, adhesive and mineral-binding proteins and proteoglycans (*e.g.* GAGs). Owing to their biodegradability, biocompatibility, non-toxicity, low antigenicity and hydrophilicity, among other qualities, Coll hydrogels have been extensively used for many different TE applications [9, 112]. However, like most hydrogels, the major disadvantage of Coll is their lack of mechanical strength, as a result of its highly hydrated nature.

Since no single material currently available provides all the essential features for the development of a tailored *in vitro* cell culture milieu that closely mimics the complex ECM [331], it is hypothesized here that the incorporation of a GAG-analog, such as the polysaccharide CTS, into a dense Coll hydrogel with collagen fibrillar density values approaching those of the ECM, will result in an osteoid-like model for the study of osteoblast differentiation and BTE applications. Since GAGs can interact with growth factors, receptors and adhesion proteins [333], it is expected here that the analogous structure in CTS may also have similar bioactivities. The osteoid-like model may be achieved by plastically compressing Coll/CTS highly-hydrated gels in order to achieve scaffolds with protein collagen fibrillar density closer to that of the osteoid, and increased mechanical properties. Their suitability was tested by seeding pre-osteoblasts within dense Coll/CTS scaffolds and monitoring their viability, proliferation, differentiation and mineralization over time.

This work was reported in a manuscript published in the peer-reviewed journal *Biomacromolecules* and is reproduced below.

Osteoid-Mimicking Dense Collagen/Chitosan Hybrid Gels

Florencia Chicatun,[1] Claudio E. Pedraza[2], Chiara E. Ghezzi[1], Benedetto Marelli[1], Mari T. Kaartinen[2], Marc D McKee [2,3] and Showan N Nazhat [1]*

[1]Department of Mining and Materials Engineering, Faculty of Engineering, [2]Faculty of Dentistry, [3]Department of Anatomy and Cell Biology, Faculty of Medicine, McGill University, Montreal, Quebec, Canada H3A 2B2

**Corresponding author:* Showan N. Nazhat, Department of Mining and Materials, Engineering, McGill University, 3610 University Street, Montreal, Qc, Canada, H3A 2B2, Tel: 1-514-398-5524, Fax: 514-398-4492, E-mail. showan.nazhat@mcgill.ca

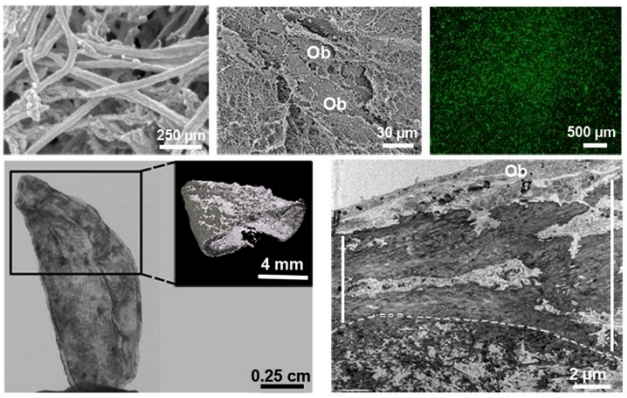

Keywords: Collagen, chitosan, dense hybrids, extracellular matrix, mineralization, osteoblast differentiation, *in-vitro* tissue models.

4.1 ABSTRACT

Bone extracellular matrix (ECM) is a 3D network, composed of collagen type I and a number of other macromolecules, including glycosaminoglycans (GAGs), which stimulate signalling pathways that regulate osteoblast growth and differentiation. To model the ECM of bone for tissue regenerative approaches, dense collagen/chitosan (Coll/CTS) hybrid hydrogels were developed using different proportions of CTS to mimic GAG components of the ECM. MC3T3-E1 mouse calvaria pre-osteoblasts were seeded within plastically compressed Coll/CTS hydrogels with solid content approaching that of native bone osteoid. Dense, cellular Coll/CTS hybrids were maintained for up to 8 weeks under either basal or osteogenic conditions. Higher CTS content significantly increased gel resistance to collagenase degradation. The incorporation of CTS to collagen gels decreased the apparent tensile modulus from 1.82 to 0.33 MPa. In contrast, the compressive modulus of Coll/CTS hybrids increased in direct proportion to CTS content exhibiting an increase from 23.50 to 55.25 kPa. CTS incorporation also led to an increase in scaffold resistance to cell-induced contraction. MC3T3-E1 viability, proliferation, and matrix remodelling capability (via matrix metalloproteinase expression) were maintained. Alkaline phosphatase activity was increased up to two-fold, and quantification of phosphate mineral deposition was significantly increased with CTS incorporation. Thus, dense Coll/CTS scaffolds provide osteoid-like models for the study of osteoblast differentiation and bone tissue engineering.

4.2 INTRODUCTION

Bone tissue engineering (BTE) is an alternative regenerative approach that may overcome host rejection and sourcing problems associated with allografts and autografts, respectively [1]. BTE is based on a 3D biomimetic scaffold that models the extracellular matrix (ECM) of bone by providing favourable environmental cues that support osteoblast attachment, proliferation, and differentiation. Reconstituted nanofibrillar collagen gel scaffolds are biocompatible, biodegradable, and exhibit low antigenicity [305]. However, these hydrogels are highly hydrated (>99 % fluid) and therefore lack control in structure and exhibit poor mechanical properties for tissue replacement applications. Plastic compression (PC) has recently been developed by Brown *et al.* [16] to increase rapidly the collagen fibrillar density (>10 wt. %) by removing the excess fluid that results from casting. This controllable process not only enables the production of collagen scaffolds with increased biomechanical properties but also allows for the organization of seeded cells in 3D by providing the space for their growth and differentiation without compromising their viability [18]. The application of PC enabled the development of tissue-equivalent matrices that have been demonstrated to influence osteoblastic differentiation by the expression of markers such as alkaline phosphatase (ALP), bone sialoprotein, and osteopontin as well as collagen matrix remodelling (MMP-13) [187, 307-309].

Along with abundant collagen type I, bone ECM is also composed of adhesive and mineral-binding proteins, polysaccharides such as glycosaminoglycans (GAGs), and proteoglycans, constituting 66, 33, and 1 wt. % water, collagen, and proteoglycans, respectively [46]. Fibrillar proteins are known to provide mechanical and structural integrity to the ECM and regulate cell attachment and spreading [50]. GAGs are unbranched disaccharides composed of N-acetylglucosamine or N-acetylgalactosamine that are responsible for growth factor binding, interactions with cellular receptors and adhesion proteins, and water molecular retention that confers tissue resistance to compression [333].

Chitosan, a polysaccharide produced via the partial deacetylation of chitin, also possesses N-acetylglucosamine and glucosamine in its structure, and therefore, at least conceptually, can be used as a substitute for GAGs. Therefore, the incorporation of CTS into collagen scaffolds better mimics the native composition of bone osteoid for osteoblast differentiation in hydrogel scaffolds for BTE. However, whereas collagen/GAG and collagen/chitosan (Coll/CTS) matrices have been developed as tissue replacements, these scaffolds commonly rely on cell seeding post-fabrication as a consequence of freeze drying process [111, 200]. Whereas direct cell seeding within highly hydrated gels has been reported, [230, 334] these scaffolds do not fully mimic the osteoid in terms of solid volume fraction and mechanical properties and have limitations associated with extensive cell-induced contraction.

In an effort to overcome these limitations, this study reports on dense Coll/CTS hybrid hydrogel scaffolds produced by PC to mimic bone osteoid, where cell-seeding is part of the processing route. The effect of CTS incorporation on modulating MC3T3-E1 osteoblastic cell-based remodelling of the scaffolds was related to their morphological and mechanical properties. In addition, osteoblastic differentiation and matrix mineralization were evaluated for up to 8 weeks. In this regard, it is expected that dense Coll/CTS hydrogels reflect natural bone ECM macromolecular components and qualities, offering an in vitro model for constructing tissue-like structures with biomimetic function.

4.3 MATERIALS AND METHODS

4.3.1 Preparation and characterization of acellular scaffolds

Sterile, rat-tail tendon-derived type I collagen (2.11 mg/mL of protein in 0.6 % acetic acid, First Link) and ultrapure chitosan powder (79.8 % deacetylated, molecular weight 328 kDa, Ultrasan, BioSyntech) were combined to prepare Coll/CTS hybrids. Coll/CTS scaffolds of relative compositions of 2:1 and 1:1 (w/w) were prepared and compared with Coll gel scaffolds. CTS (13.5 and 27 mg for 2:1 and 1:1, respectively) was dissolved in acetic acid (2.2 mL/0.1 M) at 4°C

and stirred overnight. Coll/CTS solutions were prepared by the addition of 12.8 mL collagen solution under gentle stirring on ice. Coll/CTS self-assembly was achieved by mixing the solution with X10 minimum essential medium (MEM) at a ratio of 4:1 and neutralized with 5 M NaOH. Gels were cast in either rectangular moulds (43 X 50 X 7 mm^3) or four-well plates (A = 2 cm^2) by pouring 15 mL/mould or 0.9 mL/well, respectively, and allowing to set at 37°C in a 5 % CO_2 incubator for 30 min.

After setting, gels were removed from the mould, and dense scaffolds were produced by a standardized PC protocol [16]. In brief, highly hydrated gels were placed on a stack of blotting paper, nylon, and metal meshes to allow for capillary fluid flow in combination with an unconfined compressive stress of 0.5 kN/m^2 for 5 min to remove the excess casting fluid. The efficacy of processing in generating dense scaffolds was assessed gravimetrically by measuring the weight loss in the gels as a function of compression time (n = 3). In brief, as-prepared gels were weighed for their initial weight, and the weight loss attributable to PC was measured at 1 min intervals. The percentage weight loss and solid content in compressed scaffolds were also confirmed by mass measurements after freeze-drying (BenchTop K freeze-dryer, VirTis, n = 3). These data were used to calculate the increase solid weight % due to PC.

4.3.2 Morphological and structural characterization

Scaffolds were morphologically assessed by scanning electron microscopy (FEG-SEM Hitachi S-4700 microscope). Gels were fixed overnight at 4°C in a solution of 4 % paraformaldehyde and 2 % glutaraldehyde in 0.1 M sodium cacodylate buffer. Fixation was followed by dehydration over 15 min in a series of graded ethanol solutions and critical-point drying. SEM was carried out on Au/Pd sputter-coated samples. Attenuated total reflectance Fourier-transform infrared spectroscopy (ATR-FTIR, model Spectrum 400, PerkinElmer Instruments) equipped with a ZnSe diamond-coated ATR crystal was used to analyze scaffold composition. ATR-FTIR was performed in transmittance mode

at 4 cm^{-1} resolution over a range of 4000-650 cm^{-1} (16 scans). Spectra were baseline-corrected for comparison (Spectrum software, Perkin-Elmer).

4.3.3 Mechanical analyses

Quasi-static tensile and compressive mechanical tests were performed on as-prepared acellular dense hydrogel scaffolds using a Bose ElectroForce BioDynamic instrument equipped with a 20N load cell. All tests were carried out in displacement control at 0.01 mm/sec. Measurements were conducted at room temperature while maintaining constant sample hydration using drops of distilled water (dH_2O). Tensile tests were performed on cylindrical-shaped specimens (n = 4) prepared by rolling compressed rectangular sheets along their long axis. Spiral constructs were used because they facilitated better handling and gripping when hydrated as compared with sheets of between 100 and 300 μm in thickness. Specimen dimensions (lengths of 10 ± 2 mm and diameters of 1.5 ± 0.1, 1.8 ± 0.1, and 2.4 ± 0.2 mm for Coll, Coll/CTS 2:1 and 1:1, respectively) were measured using a digital calliper and confirmed by optical microscopy. Test specimens were gripped in small metal screw tension chucks in between silicon carbide paper [335, 336]. The break strength and strain values were defined as the stress and strain, respectively, at the corresponding maximum load. The average apparent modulus was computed from the slope of the linear phase subsequent to the toe region. Compression testing was performed on cylindrical specimens prepared by rolling compressed sheets along their short axis (n = 6-8) of 2.8 ± 0.2 mm in height and 2.6 ± 0.1, 3.5 ± 0.1, and 4.6 ± 0.2 mm in diameter for Coll and Coll/CTS 2:1 and 1:1, respectively. Tests were carried out using two parallel nonporous platens up to 80 % strain. The compressive modulus of all samples was calculated from the slope of the initial linear region (< 20 % strain) of the stress-strain outputs [337].

4.3.4 Accelerated collagenase degradation

Accelerated degradation of dense hydrogel discs was investigated in the presence of collagenase type I (Worthington Biochemical, 270 U/mg) at a

concentration of 15 U/mL in phosphate-buffered saline (PBS, Wisent) incubated at 37°C and pH 7.4. Digested specimens were collected after specific time intervals using a nylon mesh, washed with dH_2O, and weighed after freeze-drying (n = 3).

4.3.5 Preparation and characterization of cellular scaffolds

MC3T3-E1 murine calvarial osteoblasts (subclone 14) were a gift from Dr. R.T. Franceschi (University of Michigan, Ann Arbor, MI) and were used from passages 10 to 16. Cells were cultured and passaged once a week in MEM (Gibco-Invitrogen) containing 1 % penicillin/streptomycin (Gibco), 2 mM L-glutamine (Gibco), 0.225 mM aspartic acid (Sigma), and 10 % v/v of foetal bovine serum (PAA Laboratories). Cells were incubated at 37°C in a 5 % CO_2 humidified incubator and the medium was changed every 48 h.

MC3T3-E1 cells were seeded within the scaffolds at a density of $3x10^5$ cells/mL prior to gelling. Subsequently, gels were cast into four-well plates to give an estimated pre-compression density of $2.16x10^5$ cells/gel, and PC was then applied. Scaffolds were cultured in six-well plates using basal, complete MEM (untreated, UT), complete MEM supplemented with 50 μg/mL ascorbic acid (AA) to enhance collagen synthesis, or AA plus 10 mM β-glycerolphosphate (βGP, an osteogenic medium, Sigma) to enhance mineralization. Scaffolds were transferred into new culture plates at weekly intervals.

4.3.6 Assessment of cell metabolism, viability and morphology

The metabolic activity of the seeded cells was evaluated for up to 3 weeks in culture using the AlamarBlue assay (Biosource) [338]. At days 1, 3, 5, 10, 14, and 21, the culture medium was replaced with MEM containing 5 % by volume AlamarBlue reagent and incubated for 4 h. Aliquots (100 μL) of the supernatants (n = 3) of each well were pipetted into 96-well plates, and the absorbance at 562 and 595 nm was spectrophotometrically measured using a microplate reader (model EL800; Bioinstruments). Acellular scaffolds were used as negative controls.

Cell viability was assessed using the Live/Dead cell viability-cytotoxicity assay (Invitrogen). Scaffolds were incubated at 37°C for 40 min in 2 μM calcein AM and 4 μM ethidium homodimer (EthD) in PBS and examined with a Leica DM-IL fluorescence microscope. Green-labeled cells represent viable cells with no membrane disruption, and red-labeled nuclei indicate cell necrosis.

The morphology of seeded cells within the core of the scaffolds was assessed through FEG-SEM after 3 weeks in culture. Samples were prepared as described above.

4.3.7 Assessment of cell induced contraction

Cell-induced contraction of highly hydrated (non-compressed) and of dense compressed hydrogels was determined by measuring the reduction in the surface area (initially at 2 cm^2) of disk-shaped scaffolds as a function of time in culture. Free-floating scaffolds (n = 3) were incubated at 37°C with 5 % CO_2 in either UT, AA-, or βGP-treated culture conditions. Acellular scaffolds were used as controls. Each plate was scanned (300 dpi resolution) initially (day 0) and at 2-day intervals up to day 22 in culture. The surface areas at each time point were normalized and expressed as a percent of initial area. Images were analyzed using ImageJ software (v1.42q, National Institutes of Health). At day 22, samples were freeze-dried for 48 h, and the final solid weight percentage was measured.

4.3.8 Measurement of matrix metalloproteinase (MMP-13) activity

MC3T3-E1 cell-seeded scaffolds were cultured up to day 21 in βGP. At days 4, 10, and 21, scaffolds were rinsed with PBS and incubated in serum-free medium for 24 h. Conditioned media were collected, centrifuged, and concentrated (Amicon Ultra, Ultracel 10 000 MWCO, Millipore). The protein content of the conditioned media was determined using the Micro BCA protein assay kit (ThermoScientific). Zymographic analysis [339] was carried out by subjecting 15 μg of conditioned media to 10 % sodium dodecyl sulfate polyacrylamide gel electrophoresis (SDS-PAGE) in the presence of 1 % gelatin (Fisher). The gels were then washed in 2.5 % Triton X-100 for 30 min. Gels were

further incubated in 50 mM Tris-HCl, pH 7.6, and 2.5 % Triton X-100 for 30 min, followed by incubation in the same buffer containing 5 mM $CaCl_2$ and 0.5 μM $ZnCl_2$. Gels were incubated overnight at 37°C in the same buffer without Triton-X-100, followed by staining with GelCode (ThermoScientific) and de-staining with dH_2O.

Western blot analysis was carried out for the immunologic detection of MMP-13 expression. Concentrated conditioned media (15 μm) were subjected to 10 % SDS-PAGE with or without reduction by D-L-dithiothretiol (Sigma). Proteins were transferred electrophoretically to nitrocellulose blotting membrane (Pall Corporation). Proteins reacting with a mouse monoclonal antibody [Lipco IID1] to MMP-13 (Abcam) were visualized with ECL-antimouse IgG, horseradish peroxidase-linked species-specific whole antibody from sheep (GE Healthcare). Acellular scaffolds maintained under identical conditions were used as controls. Developed films were scanned, and the intensity of the bands was analyzed using ImageJ software.

4.3.9 Alkaline phosphatase activity and phosphate quantification

Scaffolds were washed thoroughly with PBS and solubilized in 10 mM Tris, pH 7.4, 0.2 % IGEPAL (Sigma), and 2 mM phenylmethylsulfonyl fluoride for 10 min on ice. After 15 s of sonication and 10 min of centrifugation at 10 000 rpm, the supernatant was extracted and used for ALP activity, and the cell lysate was used for phosphate quantification at days 3, 21, and 35 in culture. ALP activity was determined colorimetrically by mixing 10 μL of supernatant (n = 3) with 200 μL of a freshly prepared substrate solution (SIGMAFAST p-nitrophenyl phosphate and Tris buffer tablets, Sigma). After 30 min of incubation in the dark at 37°C, 0.5 M NaOH was added, and an absorbance reading was taken at 405 nm using a microplate reader. Calf intestinal ALP (Sigma) was used as a standard.

To assess phosphate levels, samples were incubated in 15 % trichloroacetic acid for 1 h. After centrifugation at 10 000 rpm for 10 min, the supernatant was assayed by adding 50 % acetone, 2.5M sulfuric acid, and 2.5 mM ammonium

molybdate (Sigma). Color development was stopped by adding 1 M citric acid, and absorbance was measured at a wavelength of 355 nm.

4.3.10 Histological, morphological and structural characterization of mineralized scaffolds

Coll/CTS 2:1 hybrid scaffolds were selected for qualitative assessment of mineralization in longer-term cultures with added βGP. For histological assessment, scaffolds were fixed for 4 h, as described above for SEM, followed by staining with osmium tetroxide/potassium ferrocyanide and dehydration for 15 min in a series of graded ethanol solutions, infiltration, and embedding in LR White acrylic resin (London Resin Company) or Epon 812 epoxy resin (Electron Microscopy Sciences). Sample blocks were polymerized at 55°C for 48 h and cut with a diamond knife on an ultramicrotome (model EM UC6; Leica Microsystems) as 1 μm thick sections, mounted on glass slides, stained with von Kossa reagent for mineral presence, and counterstained with toluidine blue. Specimens were examined using a Leitz DMR optical microscope.

Transmission electron microscopy (TEM) was used to analyze cellular morphology and additionally to examine mineralization of the scaffolds. Fixation was carried out as described above for SEM. Ultrathin (80 nm thick) sections of selected regions were placed on Formvar- and carbon-coated nickel grids, stained with uranyl acetate and lead citrate and examined in a Philips Technai TEM operating at 120 kV. Energy-dispersive X-ray microanalysis (EDX) of mineralized scaffolds at day 35 of culture was performed using a Philips CM200 TEM.

Mineral phase and distribution was characterized through ATR-FTIR and X-ray-based micro-computed tomography (micro-CT). Samples were washed in PBS, frozen at -80°C, and freeze-dried. ATR-FTIR analysis was performed as described above. After baseline correction and normalization at absorbance 1.5 on the amide I peak (Spectrum software, Perkin-Elmer), a curve-fitting of the PO_4^{3-} peak was performed and the individual Gaussian components were obtained

(Origin 7.5, peak-fitting module). The method was iterated until the best fit was obtained with the minimum number of components. The integrated ratio of phosphate (900-1180 cm^{-1}) to amide I (1590-1710 cm^{-1}) bands was used to indicate the mineral-to-matrix ratio. Samples for micro-CT measurements were freeze-dried and a 360° radiologic data set was obtained with no filter applied, a step size of 0.3° and a spatial resolution of 7 μm (SkyScan model 1172). Data were reconstructed and analyzed with CTAn software (Skyscan) to differentiate between non-mineralized and mineralized phases [335]. 3D reconstruction of the scans was obtained with CTVol software (Skyscan) and volumetric analysis function of CTAn was used to estimate mineralized collagen volume fraction.

4.4 STATISTICAL ANALYSIS

All data were presented as mean values ± standard deviation (±SD). Statistically significant differences between scaffold compositions and between time points were determined using a one-way ANOVA with a Tukey-Kramer's post-hoc multiple comparison of means. The level of statistical significance was set at $p = 0.05$.

4.5 RESULTS AND DISCUSSIONS

4.5.1 Weight loss measurement of dense Coll/CTS hybrid scaffolds in response to PC

CTS addition to collagen resulted in a decrease in the amount of fluid removed due to PC, which was related to CTS content (Fig. 4.1). After 5 min, Coll, Coll/CTS 2:1 and 1:1 underwent 97.8 ± 0.3, 95.7 ± 0.1, and 94.5 ± 0.1 % weight loss, which corresponded with a 46.8 (± 5.7), 23.5 (± 0.3) and 18.2 (± 0.1) fold increase in solid weight percentage, respectively. (Refer to Table 4.1 in the Supporting Information). Optical microscopy measurements indicated that the thickness of the plastically compressed scaffolds corresponded to the extent of weight loss, which were 135 (± 14), 179 (± 29), and 249 (± 28) μm for Coll and Coll/CTS 2:1 and 1:1, respectively.

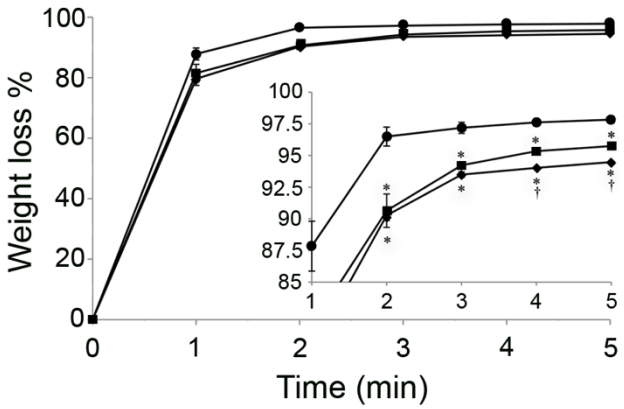

Figure 4.1: Effect of PC on weight loss of Coll (●), Coll/CTS 2:1 (■), and Coll/CTS 1:1 (◆) hydrogels. Weight percentage loss as a function of time under 0.5 kN/m^2. *p < 0.05 statistically significant when compared with Coll; † p < 0.05 statistically significant when compared with Coll/CTS 2:1. Data represented as mean ± SD, *n* = 3.

Differences in weight loss can be attributed to a number of factors, including the water retention capacity of CTS, which is dependent on the polymer macromolecular structure and the state of water [340]. The addition of CTS increases the resistance to compression and decreases the extent of fluid loss. The hydrophilicity and strength of intermolecular hydrogen bonding dictates the amount of water bound to the hydroxyl and amine groups within CTS and collagen [341]. Water uptake of CTS-based hydrogels follows the order: non-freezable bound water, freezable bound water, and free-freezable water [342]. This suggests that during compressive loading, the free and loosely bridged water is expelled. Therefore, the reduction in the extent of weight loss with higher CTS content can be attributed to a combination of higher compressive stiffness and the remaining water molecules that are bound to the hydrophilic sites as well as the free water molecules that have restricted mobility.

4.5.2 Morphological and structural characterization of dense Coll/CTS hybrid scaffolds

SEM micrographs of the internal morphology of dense Coll scaffolds revealed randomly oriented nanofibrils of collagen with their characteristic banding pattern (Fig. 4.2A and inset). In contrast, CTS consisted of interconnected globules with fine intervening strands (Fig. 4.2B and inset). Upon

incorporation of CTS into Coll and PC, dense hybrid scaffolds showed a homogeneous open-pore microstructure with a high degree of interconnectivity (Fig. 4.2C,D and insets, respectively, and Supplementary Fig. 4.1, Supporting Information). CTS addition did not compromise the quaternary structure of the collagen nanofibrils.

Fig. 4.2E shows representative FTIR spectra of Coll, CTS, as well as Coll/CTS hybrids. The N-H and C-H stretching frequencies of Coll corresponding to amide A and B bands were located at 3325 and 3090 cm^{-1}, respectively. The C-N stretching and N-H in plane bending, corresponding to the amide III, was located at 1244 cm^{-1}. The maintenance of the collagen triple helix in all scaffolds was confirmed by the presence of amide I (C=O stretching) and II (N-H deformation) peaks at 1650 and 1558 cm^{-1}, respectively. Typical CTS bands were also displayed, for example, C=O stretching from amide I at 1655 cm^{-1}, N-H bending from amine and amide II at 1590 cm^{-1}, N-H bending from amide at 1560 and CH_3 symmetrical deformation at 1380 cm^{-1} [343, 344]. The peaks corresponding to the glycosidic linkages were observed between 1160 and 1030 cm^{-1} and are associated with antisymmetric stretching of C-O-C bridge and skeletal vibrations of C-O stretching [345, 346]. Both the Coll/CTS 2:1 and 1:1 hybrids displayed bands corresponding to collagen and CTS; however, the amide A shifted to 3310 cm^{-1}, which may result from the overlapping of the amide bands of collagen and the -OH group of CTS [347]. The addition of CTS to Coll gels increased the absorbance bands of the glycosidic linkages and decreased the bands of amide I and II. In sum, FTIR analysis showed that the interactions between the macromolecules were electrostatic, possibly attributable to positively charged NH_3^+ and negatively charged COO^- groups in CTS and collagen, respectively. This result is in accordance with previous work that showed that collagen is able to interact with CTS at the molecular level by forming polyanion-polycation complex or hydrogen bonding [348].

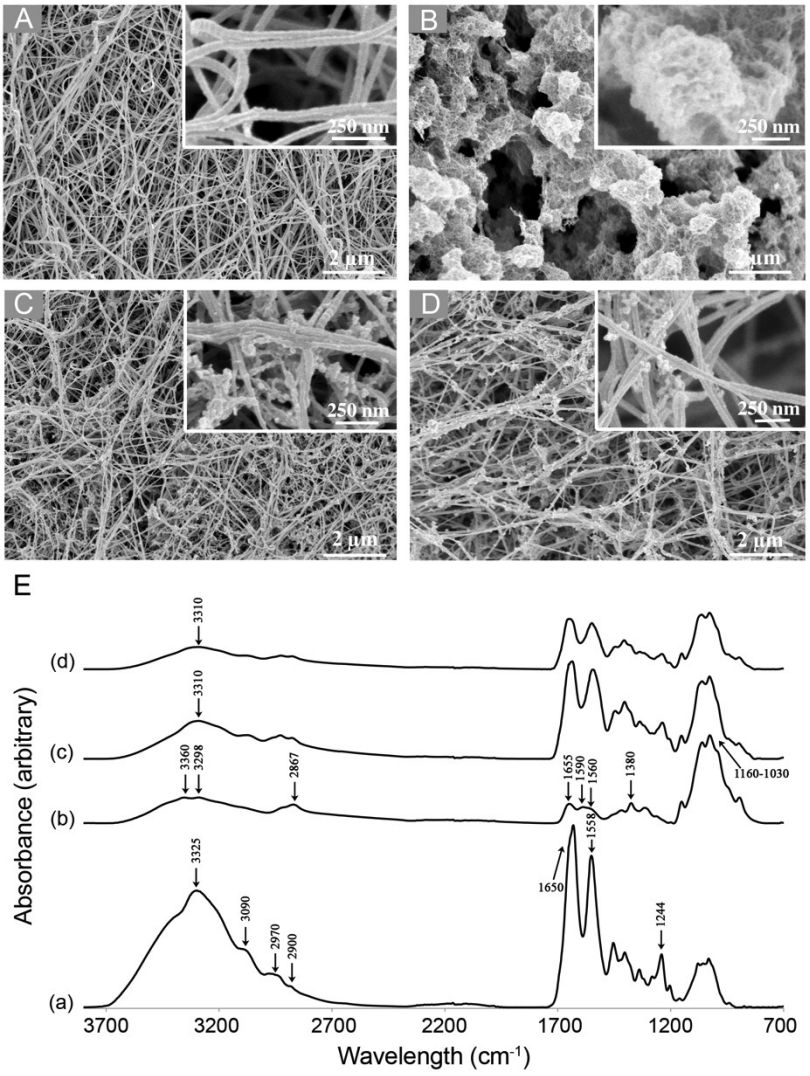

Figure 4.2: Morphological and structural characterization of acellular dense Coll, CTS and Coll/CTS hybrid scaffolds. SEM micrographs of (A) Coll, (B) chitosan, (C) Coll/CTS 2:1, and (D) Coll/CTS 1:1 scaffolds. (E) FTIR spectra of (a) Coll, (b) CTS, (c) Coll/CTS 2:1, and (d) Coll/CTS 1:1 scaffolds.

4.5.3 Mechanical analyses of dense Coll/CTS hybrid scaffolds

Mechanical analysis was carried out to investigate the effect of CTS incorporation into PC Coll scaffolds. The use of cylindrical-shaped spiral constructs allowed for reproducible data as previously reported [14, 16, 231]. Carefully developed specimen preparation protocols ensured that no voids were present between the individual sheets. The addition of CTS to Coll significantly

altered the mechanical properties of the gel scaffolds and had contrasting roles in tension when compared with compression.

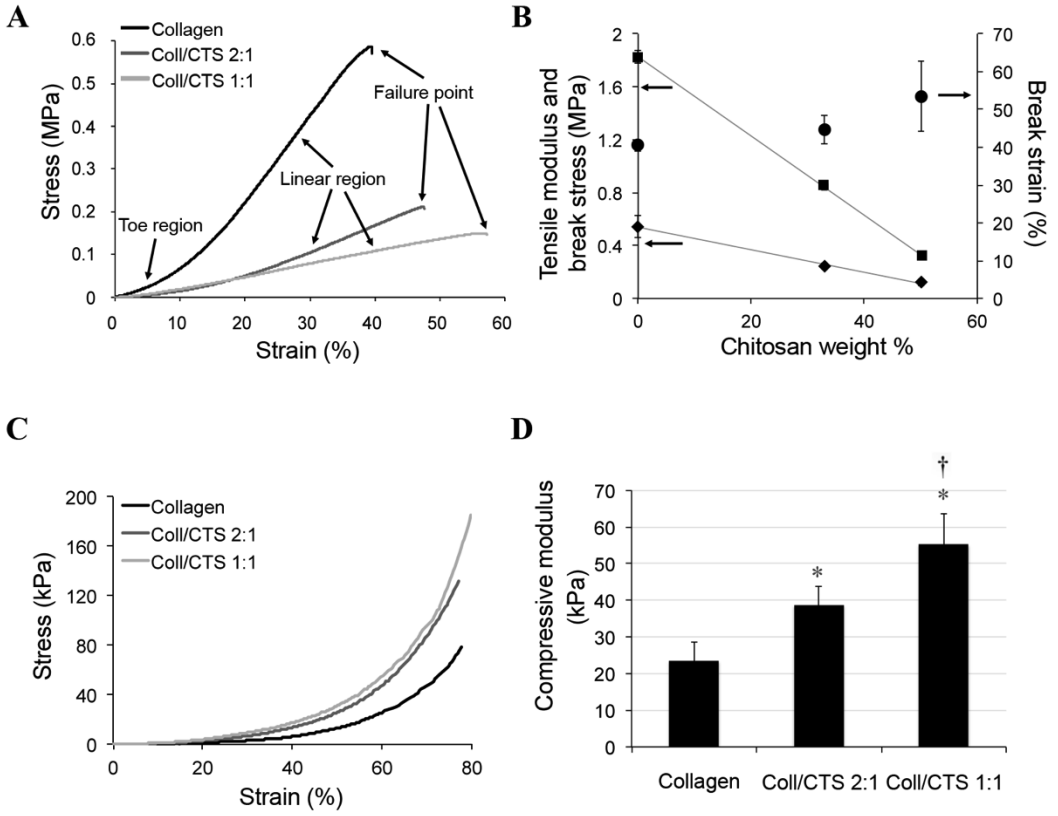

Figure 4.3: Mechanical analyses of acellular scaffolds. (A) Representative tensile stress-strain curves demonstrating toe, linear, and failure regions; (B) relationship between tensile modulus (■), break stress (◆), and strain at failure (●) with CTS weight %; (C) representative compressive stress-strain curves; and (D) compressive modulus of the various scaffolds. Data represented as mean ±SD, n=6_8. *$p < 0.05$ statistically significant when compared with Coll. † $p < 0.05$ statistically significant when compared with Coll/CTS 2:1.

Representative tensile stress-strain curves of Coll and hybrid scaffolds are shown in Fig. 4.3A. Collagen spiral cylinders showed three distinct regions: an initial nonlinear stress-strain response (toe region), a linear region, and a failure region [14]. At low stress levels, the toe region was more evident in Coll gels, which decreased following CTS incorporation. The linear region represents the stretching of the aligned fibrils and provides an indication of the apparent modulus. As shown in Fig. 4.3B, increasing the CTS content significantly decreased the apparent modulus (0.85 ± 0.02 and 0.33 ± 0.02 MPa for Coll/CTS 2:1 and 1:1, respectively, compared with 1.82 ± 0.05 MPa for Coll) as well as the

break stress (0.24 ± 0.02 and 0.12 ± 0.03 MPa for Coll/CTS 2:1 and 1:1, respectively, compared with 0.54 ± 0.08 MPa for Coll). There was no significant change in the break strain with CTS incorporation.

Representative compressive stress-strain curves of Coll and hybrid scaffolds are shown in Fig. 4.3C, displaying typical densification behaviours [14]. The compressive modulus, calculated from the initial region, increased significantly with CTS incorporation (38.75 ± 5.07 and 55.25 ± 8.26 kPa for Coll/CTS 2:1 and 1:1, respectively, compared with 23.5 ± 4.97 kPa for Coll (Fig. 4.3D)). This contrasting behaviour, compared with tensile modulus, can be attributed to the different roles that collagen, CTS, and water play in tension when compared with compression. As in native tissue, collagen fibrils are designed to perform best under tension, and the interstitial fluid does not contribute to the tensile behaviour of the gels [14]. The addition of CTS physically constrains the collagen fibrils, therefore preventing the uncrimping and alignment of the fibrils and consequently reducing the apparent modulus and break stress. Under compression, however, water has an important role when bearing the load through both the frictional resistance to fluid as a result of the ECM small pore size and the pressurization of the entrapped water within the matrix [59]. The role of CTS in compression can be linkened to that of GAGs in the ECM in terms of interlinking with the collagen network and providing an increased resistance to fluid flow [230]. Incorporation of CTS to Coll gel improved the compressive modulus by up to 2.4-fold and was found to be within the range characterized for the osteoid (~ 35 kPa) [349].

4.5.4 Acellular enzymatic degradation of dense Coll/CTS hybrid scaffolds

Accelerated collagenase digestion of the scaffolds indicated a significant reduction in the degradation extent with higher CTS content (Fig. 4.4). Dense Coll and Coll/CTS 2:1 scaffolds completely degraded after 6 h. However, a further increase in CTS content resulted in a decrease in the degradation rate, where at 8 h, 28 wt. % of the Coll/CTS 1:1 scaffold remained. This reduction in biodegradation is important because it provides control over the biological

stability of the hydrogels and will directly affect scaffold behaviour during bone formation *in vivo*.

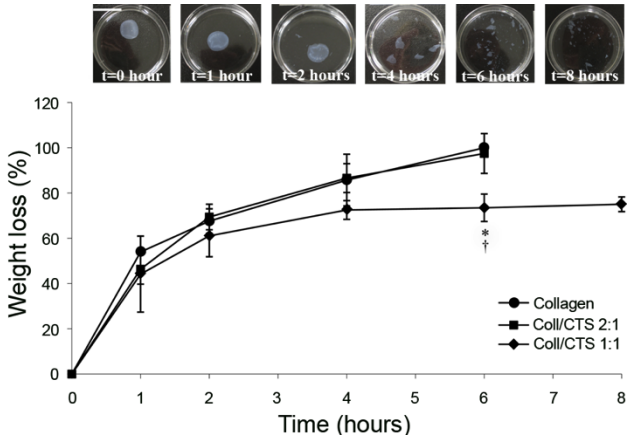

Figure 4.4: Accelerated enzymatic degradation of acellular dense scaffolds by collagenase digestion. Weight percentage loss as a function of time. * $p < 0.05$ significant compared with Coll; † $p < 0.05$ statistically significant when compared with Coll/CTS 2:1. Data represented as mean ± SD, n = 3. Scale bar: 1 cm.

4.5.5 MC3T3-E1 cell growth, viability, and morphology within dense Coll/CTS hybrid scaffolds

AlamarBlue reduction was used to examine the metabolic activity of MC3T3-E1 cells seeded within the dense Coll and hybrid scaffolds for up to 21 days (Fig. 4.5A). Cell metabolic activity within all scaffolds increased up to days 3 and 5 for Coll and hybrids, respectively. Whereas Coll scaffolds showed a decrease after 5 days, the hybrid scaffolds maintained their respective metabolic activities up to day 21. Although a decrease in metabolic activity in Coll/CTS 1:1 was observed at day 10, this drop was overcome at day 14, and the metabolic activity level was maintained up to day 21. The dramatic decrease in Coll scaffolds at day 10 may be attributable to either contact-mediated cell inhibition or a reduction in actual cell number because cells were found to migrate out of the gels (inset, Fig. 4.5B). The metabolic activity of MC3T3-E1 osteoblasts in the hybrids may have been enhanced by the attraction between the positively charged CTS surface and the negatively charged cell surface [350].

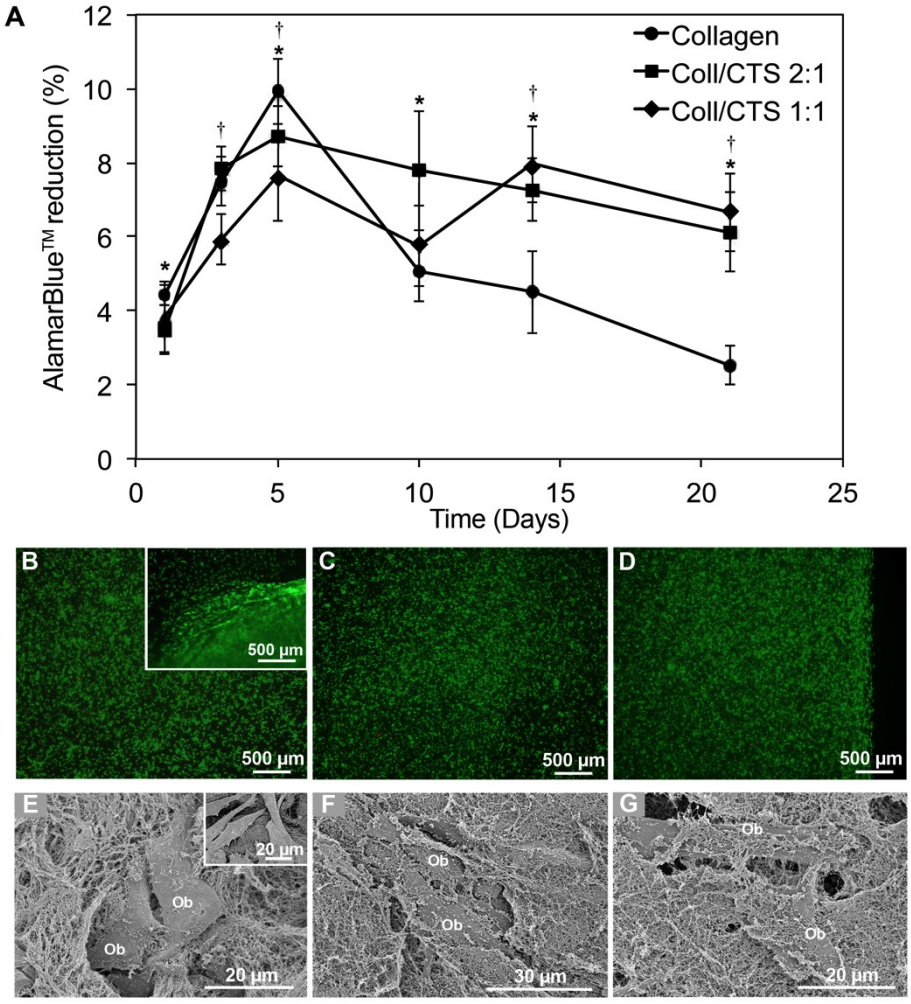

Figure 4.5: Proliferation, viability, and morphology of 3D-seededMC3T3-E1 osteoblastic cells within dense scaffolds. (A) AlamarBlue reduction to indicate the metabolic activity of seeded cells within Coll (•), Coll/CTS 2:1 (■), and Coll/CTS 1:1 (◆) scaffolds when cultured up to day 21 in complete medium (UT, n = 3, error bars ± SD). * indicates statistically significant differences between Coll and Coll/CTS 2:1, $p<0.05$; † indicates statistically significant difference between Coll and Coll/CTS 1:1, $p < 0.05$. (B-D) Live/Dead staining, at day 22, of cells seeded within (B) Coll, with inset showing cells migrating out of a Coll gel scaffold, (C) Coll/CTS 2:1, and (D) Coll/CTS 1:1 scaffolds. (E-G) SEM micrographs of cellular scaffolds of (E) Coll, (F) Coll/CTS 2:1, and (G) Coll/CTS 1:1 at day 22 (Osteoblast: Ob).

Live/Dead staining of MC3T3-E1 seeded in the various gels at day 1 after PC showed that cells were viable and well-distributed within the scaffold (Supplementary Fig. 4.2). Assessment of the viability of cells within the gel scaffolds at day 22 indicated that both Coll and hybrid scaffolds presented a predominantly viable cell population throughout the total thickness of the various scaffolds, as evidenced by the green-stained cell cytoplasm (Fig. 4.5B-D).

MC3T3-E1 cells displayed well-spread morphology with abundant cytoplasmic extensions interacting with structural elements within the scaffolds (Fig. 4.5E-G). Osteoblasts within interior regions of the scaffold were polymorphic and closely apposed to and surrounded by the Coll/CTS network. At the uppermost surface of the scaffolds (inset in Fig. 4.5E), cells were more abundant and spindle-shaped. Cells were mostly evenly distributed throughout the scaffold; however, on some occasions, cells accumulated at the edge/surface, presumably reflecting greater access to nutrients and oxygen [187].

4.5.6 Assessment of cell-induced contraction of Coll/CTS hybrid scaffolds

Cell-induced contraction of non-compressed and compressed hydrogels as a result of cell-generated forces and movements achieved through cell-fibril connections [327, 351] was measured up to day 22 under UT culture conditions (Fig. 4.6A). Compressed gels displayed a sigmoidal surface area reduction versus time relationship, featuring three different contraction phases: a lag phase, a linear rapid contraction phase, and a slow contraction phase. In contrast, non-compressed highly hydrated gels demonstrated immediate rapid contraction resulting in a higher rate and extent of contraction, which can be related to their significantly lower stiffness [14, 352]. Acellular scaffolds demonstrated no contraction. Fig. 4.6B demonstrates that the concomitant increase in scaffold compressive modulus with CTS content can be correlated with a decrease in the extent of contraction. Higher CTS content also led to a significantly longer lag phase and a decrease in the rate of contraction [353, 354]. Therefore, increasing CTS content may delay the onset of initiation and overall extent of gel contraction by increasing the compressive modulus values of hybrid scaffolds. The correlation between the lag phase up to day 5 and the increase in cell metabolic activity up to day 5 (Fig. 4.5A) may indicate that critical cell numbers were required to exert enough contractile forces to contract stiffer hydrogels. Indeed, cell seeding density has been shown to influence contraction in dense Coll hydrogels [355]. Although cell-induced contraction is an important component of cell remodelling,

excessive contraction of Coll-based scaffolds for BTE can significantly distort and reduce the size of implants [356]. Therefore, by incorporating CTS, it is possible to tune the contraction extent and control scaffold distortion (Fig. 4.6).

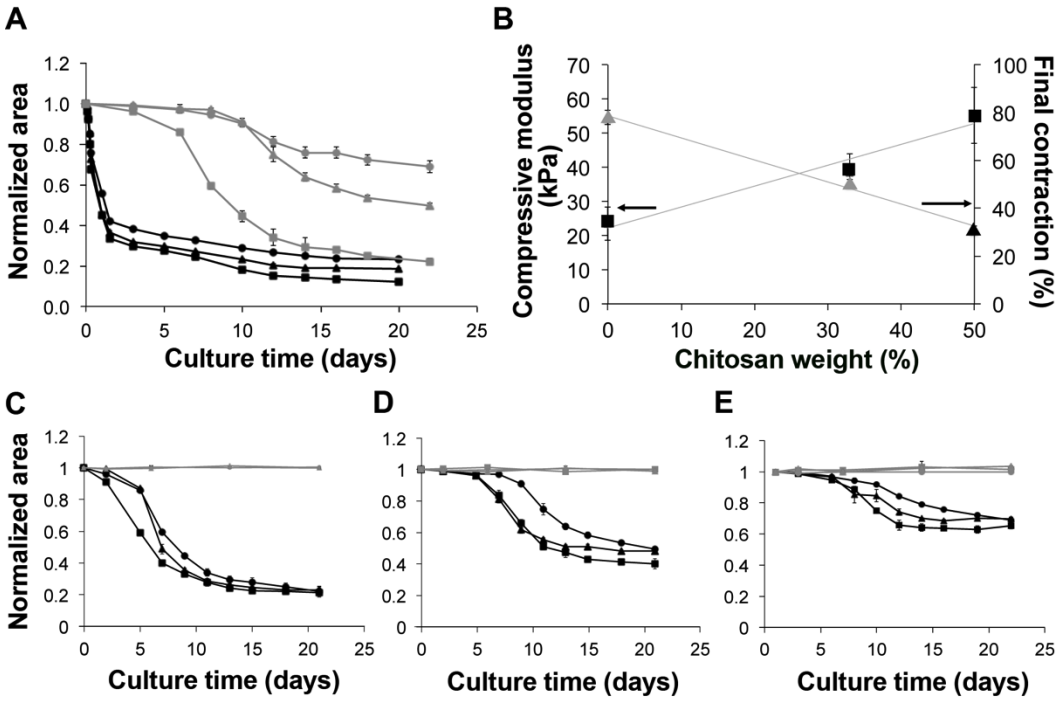

Figure 4.6: Cell-induced contraction of scaffolds. (A) Compressed (gray) and noncompressed (black) Coll (■), Coll/CTS 2:1 (▲), and Coll/CTS 1:1 (•) scaffolds for up to 22 days (n = 3) in UT. (B) Compressive modulus (■) and final contraction percent after 22 days (▲) versus chitosan weight %. Cellular (black) and acellular (gray) (C) Coll, (D) Coll/CTS 2:1, and (E) Coll/CTS 1:1 scaffolds contraction for up to 22 days (n = 3), incubated with complete medium (UT, •), medium supplemented with ascorbic acid (AA, ■), or osteogenic medium supplemented with both AA and β-glycerol phosphate (βGP, ▲). The surface areas at each time point were normalized to the initial surface area (t = 0).

The effects of AA and βGP treatment on cell-induced gel contraction were also investigated (Fig. 4.6C-E). Whereas the culture conditions exerted an effect on the contraction lag phase of Coll alone, cell-induced contraction of the hybrids under all conditions was similar up to day 6. Beyond 6 days, the contraction rate in UT scaffolds was reduced compared with those where cells grown in scaffold supplemented with AA or βGP, which may be associated with cell proliferation [357]. At longer times, culture conditions had no effect on the extent of contraction. At day 22, acellular and cellular scaffolds were weighed before and after freeze-drying to calculate the final solid-weight percentage, which indicated

a 3.1-, 2.8-, and 2.3-fold increase for Coll and Coll/CTS 2:1 and 1:1 scaffolds, respectively.

4.5.7 MMP-13 activity within dense Coll/CTS scaffolds

Cell-induced contraction is an important component of ECM remodelling. Remodelling also involves degradation of the collagenous ECM, which is dependent on the function of MMPs, such as MMP-13 [358, 359]. Zymography revealed the presence of multiple metalloproteinase isoforms whose major gelatinase activity corresponded to proteins with molecular weights between 37 and 100 kDa (4.7A). To characterize further and identify MMP-13, conditioned media from the various scaffolds were concentrated and analyzed by Western blotting. Under both reducing (Fig. 4.7B, bottom) and non-reducing (unpublished observations) conditions, two bands of MMP-13 immunoreactivity were detected at ~ 60 and 54 kDa, which correspond to the pro-enzyme and active forms of MMP-13, respectively [360]. The pattern of MMP-13 immunoreactivity closely corresponds with two of the bands displaying MMP activity detected by zymography. Concentrated media from acellular scaffolds, used as controls, did not exhibit any immunoreactivity for MMP-13.

The sustained expression of MMP (estimated by densitometric analysis of protein bands reacting with MMP-13 monoclonal antibody) suggested that secreted MMP-13 is partially responsible for scaffold remodelling. At day 21, MMP-13 expression was more evident in the hybrid scaffolds, which may be attributed to a reduction in cell number in Coll scaffolds. The differences in the extent of cell-induced contraction may also contribute to restricting the proliferation of cells within the scaffold.

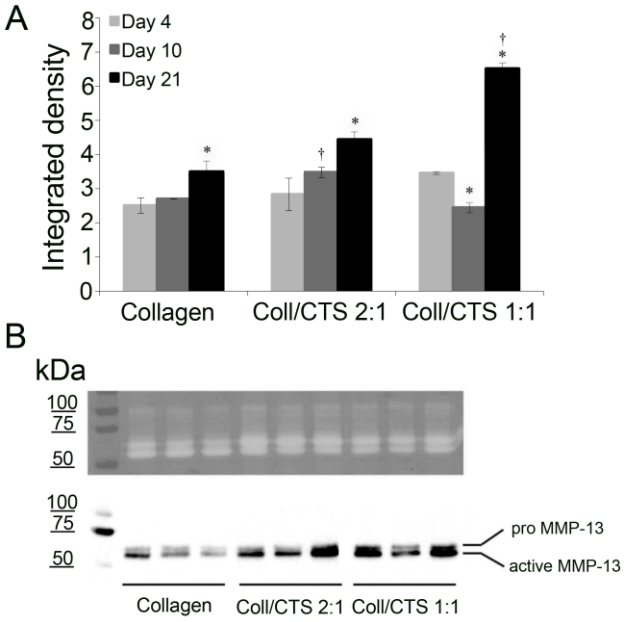

Figure 4.7: MMP-13 activity and densitometric analysis of Western blots for protein bands reacting with MMP-13 antibody of MC3T3-E1 cells seeded within dense Coll and Coll/CTS hybrid scaffolds. (A) Integrated density of conditioned medium from scaffolds up to day 21 in culture (n = 3). (B) Representative gelatin zymogram and Western blot analysis showing the active and pro-active form of MMP-13 activity. * indicates statistical significant difference against day 1, $p < 0.05$. † indicates statistical significant difference when compared with Coll, $p < 0.05$.

4.5.8 Osteoblastic ALP activity and phosphate quantification within dense Coll/CTS hybrid scaffolds

The osteogenic differentiation of seeded MC3T3-E1 pre-osteoblasts was assessed by measuring ALP activity within the scaffolds. There was a significant increase in ALP activity up to day 21 (Fig. 4.8A), which decreased in both Coll and Coll/CTS hybrids at day 35 (~50 % less). This may be correlated with the onset of biomineralization *in vivo* [361]. Compared with Coll/CTS 1:1, cells seeded in dense Coll alone expressed significantly ($p < 0.05$) lower levels of ALP activity beyond day 3. At days 3 and 35, significant higher levels of ALP activity were observed in Coll/CTS 2:1 compared with Coll alone. No statistical differences were observed between ALP activities of cell seeded in both hybrids at all times.

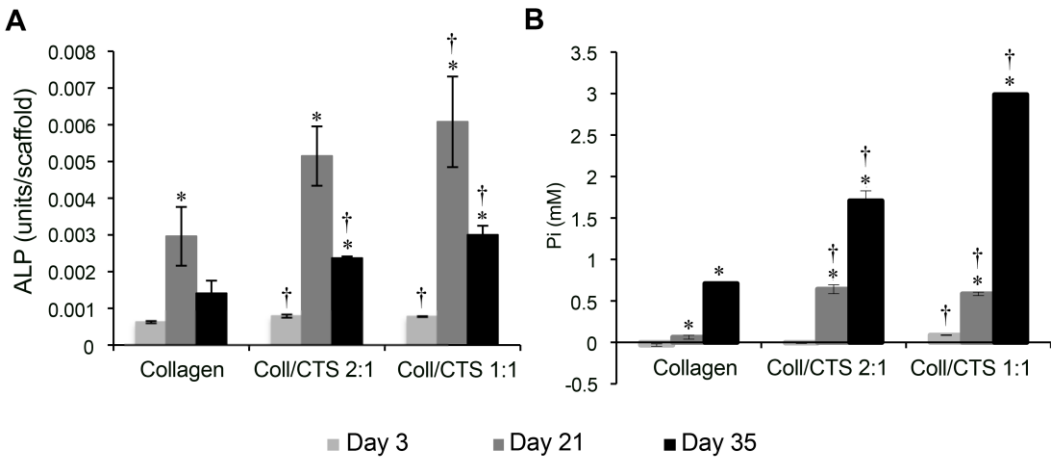

Figure 4.8: Osteogenic differentiation ofMC3T3-E1 cells seeded in dense Coll, Coll/CTS 2:1 and Coll/CTS1:1 scaffolds up to 35 days in βGP (n=3) as assessed by: (A) ALP activity, and (B) phosphate levels. * indicates statistical significant difference against day 3, $p < 0.05$; † indicates statistical significant difference when compared to Coll, $p < 0.05$.

The down-regulation of ALP activity was correlated with an increase in phosphate concentration (accumulating as mineral) within the scaffolds over time in culture, reaching a maximum at day 35 (Fig. 4.8B). Interestingly, at all time points, both ALP activity and phosphate concentration were significantly elevated within the Coll/CTS hybrids compared with Coll scaffolds. Positively charged CTS may electrostatically interact with anionic molecules such as GAGs, which are associated with factors which stimulate cell growth, proliferation, and differentiation [100].

4.5.9 Histological, morphological and structural characterization of mineralized hybrids

The mineralization of dense Coll scaffolds has been previously extensively characterized [187, 309]. Qualitatively, mineralization in both hybrids was similar, and this study focused on presenting the data of Coll/CTS 2:1. Fig. 4.9A shows positive von Kossa staining for mineral in the hybrid gel at week 5 in culture. Intense and sporadically distributed mineral deposits were detected in the core and on the surface of the scaffold. Subsequent histological evaluation revealed that foci of mineral formation were mainly associated with regions containing a high density of osteoblasts. In addition, the mineralized matrix

presented two distinctive patterns of staining: a relatively smooth-textured mineral region surrounding the osteoblasts that was associated with nascent collagen fibrils and a granular mineralized region found toward the center of the scaffold. TEM of the mineralized scaffold readily confirmed the presence of these two distinct patterns of mineralization (Fig. 4.9B). Overall, these data support the notion that the scaffold mineralized most readily adjacent to the " bone-forming" regions.

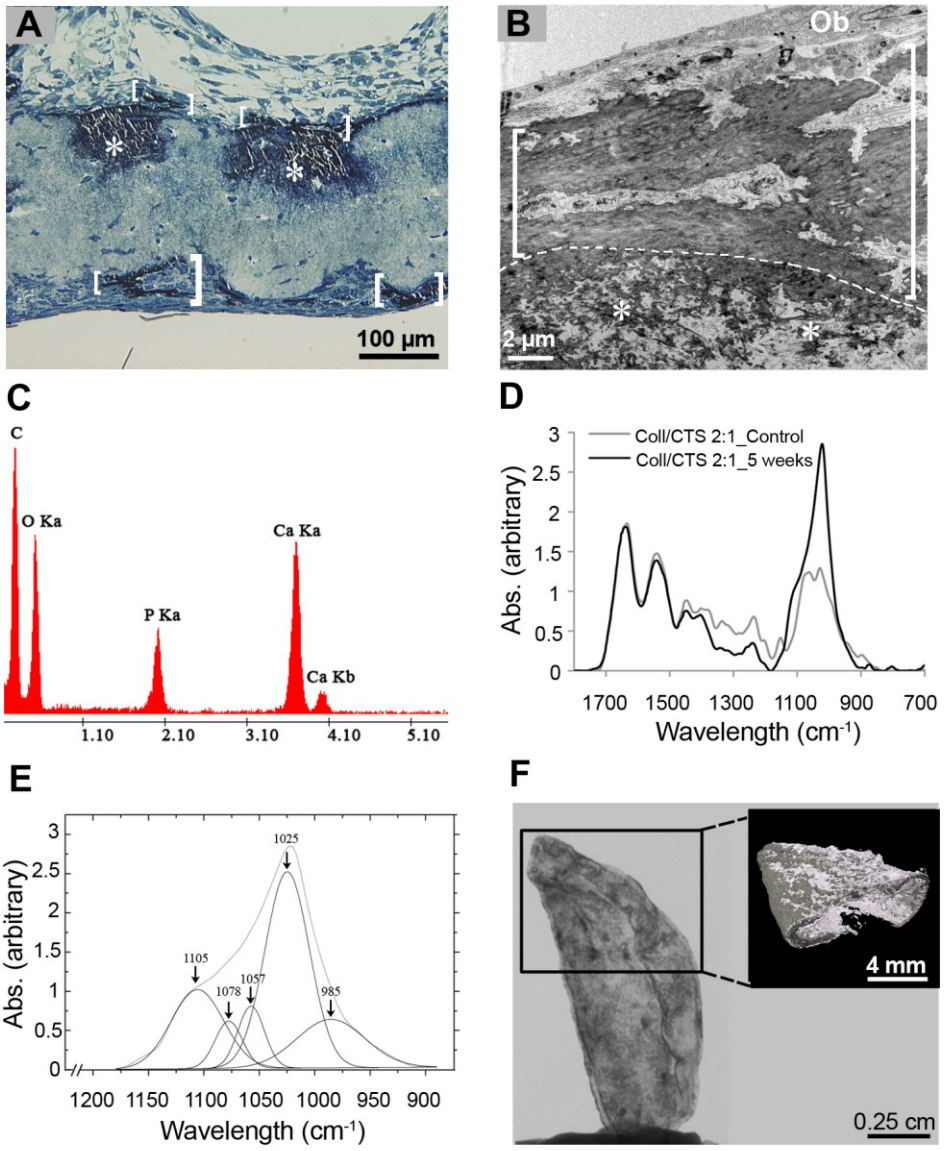

Figure 4.9: Assessment of MC3T3-E1 cell-induced mineralization in Coll/CTS 2:1 scaffold treated with osteogenic medium (βGP) in longer-term culture. (A) Light micrograph of sectioned scaffold stained with von Kossa for mineral after 5 weeks in culture. Formation of mineralized bone-like tissue (between brackets) is present at the surface of the scaffolds, and subjacent regions of the scaffold are also mineralized (asterisks). (B) TEM micrograph showing the ultrastructure of the mineralized areas, where two distinct regions having different textures are apparent (separated by dashed line): an upper region (brackets) resembling a bone-like tissue and a lower region (asterisks) showing mineral with a highly granular texture. (C) EDX compositional analysis of these mineralized areas showing strong Ca and P peaks. (D) ATR-FTIR spectra of hybrid scaffolds at 5 weeks and as prepared. (E) Curve fitting of the PO_4^{3-} peak and the individual Gaussian components. (F) Micro-CT 2D slice and 3D reconstruction (inset) of mineralized scaffold after 8 weeks in culture.

EDX analysis of mineralized areas showed the presence of calcium and phosphorus with a ratio of 1.3 ± 0.05 (Fig. 4.9C), indicating that another mineral phase, such as octacalcium phosphate of amorphous calcium phosphate (OCP), a potential precursor of hydroxyapatite (HA) [362], may be present. Therefore, the incorporation of CTS may increase the net positive charge from abundant NH_3^+ groups, which can contribute to the adsorption of negatively charged OCP crystals (attributable to orthophosphate ions HPO_4^{2-}) [363]. *In vitro*, CTS has been shown to influence calcium phosphate nucleation and growth in 3D scaffolds [231, 364], but not in 2D monolayer models where it did not promote osteogenesis [365]. However, the mechanism of mineral nucleation by CTS is not fully understood, and careful mineral characterization coupled with anhydrous and cryo-techniques to preserve mineral precursor phases is required for these and additional studies. Nevertheless, FTIR spectra provided some evidence that the HA may have been precipitated via an OCP precursor [366] (Fig. 4.9D). The transformation from OCP to substituted HA would give rise to carbonate incorporation [367], as evidenced by the ν_2 CO_3^{2-} stretching peak at 880 cm^{-1} [368]. Moreover, reductions in the intensities of the amide II and III of the mineralized scaffolds can be attributed to the enveloping of the carboxyl and carbonyl groups by mineral crystals [369]. Curve fitting of the $\nu_1\nu_3$ PO_4^{3-} peak at 1022 cm^{-1} and examination of the individual components revealed sub-peaks at 1078, 1057, and 1025 cm^{-1} corresponding to the ν_3 P-O antisymmetric stretching mode of the apatitic class of phosphate (Fig. 4.9E). The presence of the 1078 cm^{-1} peak as a shoulder suggests that an OCP phase converted into a more bone-like apatitic form [370], and the presence of the 1105 cm^{-1} peak corresponds to non-apatitic phosphate or HPO_4^{2-} in poorly crystalline apatite [371, 372]. Micro-CT radiographic image of a scaffold at week 8 and a 3D reconstruction of its apex demonstrated the extent of collagen mineralization (dark gray phases in Fig. 4.9F). Volumetric analysis indicated a mineralized volume fraction of 0.22, which was consistently distributed throughout much of the scaffold.

In vivo, the osteoblastic differentiation sequence can be subdivided into three consecutive, yet overlapping, phases: cell proliferation, cell differentiation, and ECM assembly and maturation, and mineralization [190]. Following the initial proliferative period, cell matrix synthesis, secretion, and assembly occur to form the ECM. An increase in ALP activity is associated with this process and is often considered to be an early marker of the committed osteoblast lineage progression, with subsequent abundant expression and secretion of collagenous and non-collagenous matrix molecules such as bone sialoprotein, osteopontin, and osteocalcin, along with the accumulation of mineral [191]. Finally, at later phases of osteoblast development, ongoing synthesis of matrix components and their modification by cell-secreted enzymes leads to ECM mineralization, which completes key osteoblast functions within bone. When seeded within hybrid Coll/CTS scaffolds, MC3T3-E1 proliferation, ALP activity, MMP-13 expression, and matrix phosphate (mineral) concentration displayed trends that were similar to the *in vivo* sequence of osteoblast differentiation (Fig. 4.10). Therefore, the results of this study indicate that Coll/CTS hybrids support the normal pattern of development of bone-like tissue, signifying its suitability as a potential *in vitro* osteoid model and scaffold for BTE.

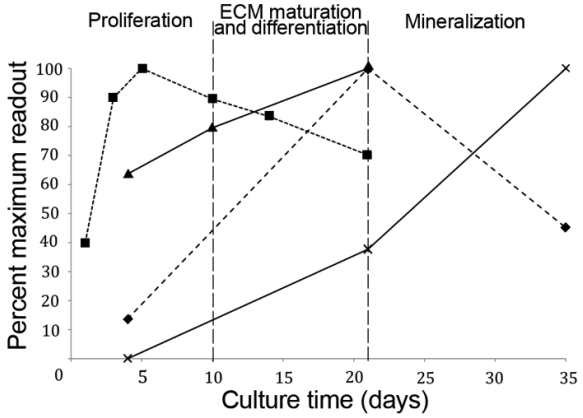

Figure 4.10: Summary of the osteoblast differentiation sequence of the MC3T3-E1-seeded Coll/CTS 2:1 hybrid scaffold showing three distinct periods: proliferation, ECM maturation and differentiation, and mineralization. The seeded cells undergo an initial rapid increase in proliferation (as indicated by the metabolic activity by AlamarBlue reduction, ■), which is then down-regulated by the organization and maturation of an initial bone-like ECM. In a second phase, proteins associated with the osteoblast phenotype, such as MMP-13 (▲) and ALP (•), can be detected. Finally, the ECM becomes permissive to mineral deposition (x).

4.6 CONCLUSIONS

Cell-seeded, osteoid-like scaffolds can be rapidly produced by plastically compressing self-assembled Coll/CTS hydrogels. CTS incorporation improves scaffold morphological and mechanical properties including resistance to collagenase degradation as well as cell-based remodelling and contraction. Dense Coll/CTS hybrid scaffolds support MC3T3-E1 osteoblast cell viability, proliferation, and differentiation under osteogenic-inducing conditions. In addition, measurements of ALP activity, MMP-13 expression, and phosphate concentration showed that the hybrid scaffolds support osteoblastic differentiation and mineralization, which resembled nascent bone-like tissue. Coll/CTS hybrids provide a novel approach for the assembly of osteoid-like structures with biomimetic function for BTE.

4.7 ACKNOWLEDGEMENTS

This work was supported by funds from Canadian Natural Sciences and Engineering Research Council (Strategic Research Grant number 350725-07, with BioSyntech as partner; and Discovery Grant number RGPIN 341235-2007), the Canadian Foundation for Innovation (Leaders Opportunity Fund project number 13054), and the McGill University Faculty of Engineering Hatch Faculty Fellowship (in support of SNN). Florencia Chicatun is also partly supported by McGill Engineering Doctoral Awards, Vadasz and Hatch fellowships and a Bourses Fondation Pierre Arbour scholarship. Technical assistance was provided by Line Mongeon (SEM analyses), Antoine Charbonneau (degradation assay), and Lydia Malynowsky (TEM analyses). The authors would like to thank Dr. Naser Muja for useful discussions.

4.8 APPENDIX: SUPPORTING INFORMATION

Table 4.1: Percentage weight loss of Coll and Coll/CTS scaffolds attributable to PC, gravimetrically measured, and verified through freeze-drying pre- and post-compression. Solid weight percent pre- and post-compression and corresponding fold-increase due to PC.

Sample	Weight loss measurement	Freeze drying method	Solid weight % before PC	Solid weight % after PC	Fold increase
	% Weight loss	% Weight loss			
Collagen	97.8± (0.25)	98.00 ± (0.26)	0.17± (0.01)	8.13± (1.2)	46.82± (5.7)
Coll/CTS 2:1	95.7± (0.06)	95.96± (0.06)	0.22± (0.01)	5.26± (0.3)	23.51 ± (0.3)
Coll/CTS 1:1	94.5± (0.05)	94.85± (0.004)	0.35± (0.01)	6.38± (0.24)	18.23 ± (0.06)

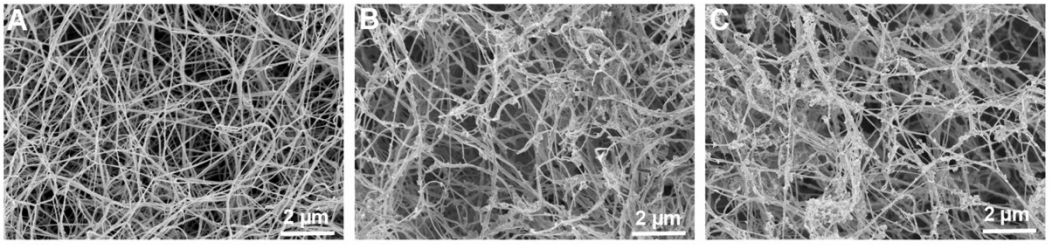

Supplementary Figure 4.1: SEM micrographs of Coll (A), Coll/CTS 2:1 (B) and Coll/CTS 1:1 (C) scaffolds before plastic compression.

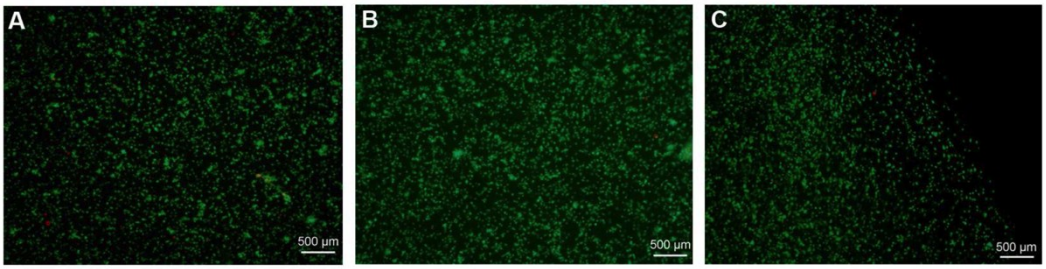

Supplementary Figure 4.2: Live/Dead® staining of MC3T3-E1 seeded in dense Coll (A), Coll/CTS 2:1 (B) and Coll/CTS 1:1 (C) at day 1 in culture.

CHAPTER 5: EFFECT OF CHITOSAN INCORPORATION AND SCAFFOLD GEOMETRY ON CHONDROCYTE FUNCTION IN DENSE COLLAGEN TYPE I HYDROGELS

In *Chapter 4* the assembly of an osteoid-like structure with biomimetic properties was investigated, with collagen serving as a substrate for cell adhesion and proliferation, and CTS fulfilling the GAGs role in native osteoid. It was demonstrated that the incorporation of CTS into dense Coll hydrogels increased the gel's resistance to enzymatic degradation, compressive modulus of as-made scaffolds, resistance to cell-mediated contraction and osteoblast differentiation.

In view of the results mentioned above and the fact that natural polymers such as, collagen and CTS are either an actual component or structurally similar to natural occurring macromolecules in the cartilage ECM (*i.e.* GAGs), this study hypothesized that these complex 3D dense hybrid scaffolds may be used as *in vitro* tissue models for the repair of AC.

The response of RCJ.3.1.C5.18 chondroprogenitor cells to CTS content in terms of cell growth, viability and differentiation within a dense Coll hydrogel, was investigated here. Additionally, the production of model constructs on a scale necessary to repair AC critical-sized defects (> 2 mm diameter) was explored. On this point, cylindrically shaped constructs having clinically relevant diameters (3-5 mm diameter) were characterized in terms of viability, GAG production, temporal changes in mechanical properties and cell-mediated contraction. It is hypothesized that this study will provide valuable design information to the understanding of the interactions between chondrocyte-like cells, macromolecular components and morphometric parameters of dense Coll/CTS scaffolds for the development of three-dimensional AC-ECM mimicking scaffolds.

A manuscript based upon these findings has been published in *Tissue Engineering Part A* and is reproduced below.

Effect of chitosan incorporation and scaffold geometry on chondrocyte function in dense collagen type I hydrogels

Florencia Chicatun,[1] Claudio E. Pedraza[2], Naser Muja,[1] Chiara E Ghezzi,[1] Marc D McKee [2,3] and Showan N Nazhat [1]*

[1]Department of Mining and Materials Engineering, Faculty of Engineering, [2]Faculty of Dentistry, [3]Department of Anatomy and Cell Biology, Faculty of Medicine, McGill University, Montreal, Quebec, Canada H3A 2B2

**Corresponding author:* Showan N. Nazhat, Department of Mining and Materials, Engineering, McGill University, 3610 University Street, Montreal, Qc, Canada, H3A 2B2, Tel: 1-514-398-5524, Fax: 514-398-4492, E-mail. showan.nazhat@mcgill.ca

Keywords: Dense collagen hydrogels, extracellular matrix, articular cartilage, plastic compression, chitosan, critical-sized defect

5.1 ABSTRACT

Tissue engineering approaches for articular cartilage (AC) repair using collagen type I (Coll)-based hydrogels are limited by their low collagen fibrillar density (CFD; < 0.5 wt. %) and their poor capacity to support chondrocyte differentiation. Chitosan (CTS) is a well-characterized polysaccharide that mimics the glycosaminoglycans (GAGs) present in native AC extracellular matrix and exhibits chondroprotective properties. Here, dense Coll/CTS hydrogel discs (16 mm diameter, 140-250 μm thickness) with CFD (~ 6 wt. %) approaching that of AC were developed to investigate the effect of CTS content on the growth and differentiation of three-dimensionally seeded RCJ.3.1.C5.18 chondroprogenitor cells. Compared to dense Coll alone, cells seeded within Coll/CTS showed increased viability and metabolic activity as well as a decrease in cell-mediated gel contraction. Immunohistochemistry for collagen type II, in combination with Safranin O staining and GAG quantification, indicated greater chondroprogenitor differentiation within Coll/CTS, compared to cells seeded within Coll alone. The complex interplay between scaffold geometry, microstructure, composition, mechanical properties and cell function was further evaluated by rolling dense planar sheets to prepare cylindrically shaped constructs having clinically relevant diameters (3-5 mm diameter, 9 mm height). The compressive modulus of the cylindrically shaped constructs decreased significantly after 7 days in culture, and remained unchanged up to 21 days for each scaffold composition. Unlike Coll, cells seeded within Coll/CTS showed greater viability along the entire radial extent of the cylindrical rolls and increased GAG production at each time point. While GAG content decreased over time and reduced cell viability was observed within the core region of all cylindrical rolls, the incorporation of CTS diminished both these effects. In summary, these findings provide insight into the challenges involved when scaling up scaffolds designed and optimised *in vitro* for tissue repair.

5.2 INTRODUCTION

The repair of critical-sized articular cartilage (AC) defects (> 2 mm diameter) is limited due to the low vascular supply of cartilaginous tissues [64]. Cartilage tissue engineering strategies seek to overcome this biological limitation through the development of cellular scaffolds that closely mimic the complex structure of AC, which consists of a dense fibrillar network of collagen type II (Col II; 12-24 %) and abundant proteoglycans containing charged glycosaminoglycan (GAG; 3-6 %) side chains that entrap substantial fluid volume (70-85 %) [64, 88]. By dry weight, 60 to 70 % of cartilage is composed of collagen type II and 30 % proteoglycans, giving a Coll/GAGs ratio of 2:1 [56].

Hydrogels exhibit a biomolecular structure that is similar to native tissue and, unlike freeze-dried scaffolds, these fully hydrated matrices allow direct cell seeding and homogeneous cell distribution during scaffold preparation and processing [296]. In particular, acid-extracted collagen type I (Coll) hydrogels have been extensively used as scaffolds for cartilage tissue engineering applications [112, 114] primarily because of the difficulties associated with processing isolated Coll II protein extractions into gel-like scaffolds [129, 240]. However, Coll hydrogels exhibit poor mechanical properties attributable to their low collagen fibril density (CFD, < 0.5 wt. %) and undergo a high level of cell-mediated contraction which causes a physical mismatch between the dimensions of the defect and the graft [373]. In order to overcome both these limitations, plastic compression (PC) of Coll hydrogels has been developed as a method to rapidly increase the CFD by expelling unbound fluid immediately after cell seeding to produce dense hydrogels with increased biomechanical properties and decreased cell-mediated contraction [14, 16, 374].

Differentiated chondrocytes seeded within Coll scaffolds have been shown to lose their cartilage-like characteristics as they undergo dedifferentiation towards a fibroblastic phenotype [236, 238]. Therefore, improved scaffold compositions are necessary to ensure the long-term maintenance of the chondrocytic characteristics.

Chitosan (CTS) is a polysaccharide composed of randomly distributed N-acetylglucosamine and glucosamine units, which structurally and compositionally resembles the GAGs present within native tissues. The incorporation of CTS within various types of hydrogels has been found to stimulate chondrogenesis by supporting chondrocyte growth and differentiation as well as the production of cartilage-specific extracellular matrix (ECM) components such as Coll II and GAGs [132, 279, 375]. A number of studies have examined the *in vivo* biological performance of chitosan hydrogel implants in both animal and human cartilage defects. No major foreign body reaction has been observed and, in general, these scaffolds have been found to present the formation of hyaline-like cartilage as well as improve the integration of repaired cartilage within the lesion [376]. However, the effect of CTS on chondrocyte function within dense Col I gels has not been determined.

The present study tests the hypothesis that the incorporation of CTS into dense Coll gels serves as a chondroprotective material that supports chondrocyte differentiation and increases cartilage-like ECM production. Dense Coll/CTS scaffolds with weight ratios approaching those of Coll/GAGs [56] in the native ECM of AC (relative compositions of 2:1 and 1:1 by weight) were prepared and compared with Coll hydrogels. A mesenchymal chondrogenic cell line RCJ3.1C5.18 (RCJ) developed from cells isolated from rat calvaria was used in view of its capacity to undergo a cell differentiation sequence similar to that observed in cartilage *in vivo* [32, 33]. Moreover, the RCJ cell line has been widely used for chondrocyte research, which demonstrates its utility as a model cell line for articular cartilage tissue engineering [262, 263, 377]. Seeded RCJ cell metabolic activity, cell-mediated gel contraction, viability and morphology, and cartilage-like aggregate formation within dense Coll/CTS gels, were compared to cells seeded into dense gels made of Coll alone. In addition to support of cell phenotype, the production of constructs of a scale necessary to repair critical-sized clinical defects is a major challenge for cartilage tissue engineering. In this regard, the viability of RCJ cells and GAG content within each specimen was

investigated on cylindrically shaped constructs measuring 3 to 5 mm in diameter, depending upon scaffold composition. The study of three-dimensional (3D) AC-ECM mimicking scaffolds, designed according to the structure and properties of native AC, provides a framework for understanding the interactions between chondrocytes and the macromolecular components and morphometric parameters of dense Coll/CTS scaffolds.

5.3 MATERIALS AND METHODS

5.3.1 Cell culture

The nontransformed RCJ3.1C5.18 mesenchymal clonal chondrogenic cell line isolated originally from foetal rat calvaria was kindly provided by Dr. Jane E. Aubin (University of Toronto, Ontario, Canada). Cells from passages 9 to 20 were cultured in α-minimum essential medium (α-MEM; Gibco-Invitrogen, Grand Island, NY, USA) with ribonucleosides and deoxyribonucleosides containing 1% penicillin/streptomycin (Gibco), 10^{-7} M dexamethasone (Sigma, St. Louis, MO, USA), 50 μg/ml ascorbic acid (AA; Sigma) and 15 % v/v of foetal bovine serum (Hyclone, Thermo Scientific, Logan, UT, USA). Cells were incubated at 37 °C, in a 5 % CO_2 humidified incubator, and the medium was changed at 2-day intervals.

5.3.2 Preparation of dense Coll and Coll/CTS gel discs and cylindrical rolls

Sterile, rat-tail tendon-derived type I collagen (2.10 mg/ml of protein in 0.6 % acetic acid, First Link Ltd., West Midlands, UK) and ultrapure CTS powder [(79.8 % DDA, Ultrasan™, BioSyntech Ltd., Montreal, QC, Canada (now Piramal Healthcare, Laval, QC, Canada)] were used as starting materials. Coll/CTS hybrid gels having relative compositions of 2:1 and 1:1 (w/w) were developed as previously described [374]. Briefly, CTS (13.5 and 27 mg for 2:1 and 1:1, respectively) was dissolved in acetic acid (2.2 ml/0.1 M) at 4 °C and stirred overnight, followed by the addition of collagen solution (12.8 ml) under gentle stirring. Coll and Coll/CTS self-assembly were achieved by mixing the solution with 10 X MEM (Sigma Aldrich, Ottawa, ON, CA) at a ratio of 4:1 and

neutralized with 5 M NaOH. For cellular gels, RCJ cells were seeded within the hydrogels at a density of $3x10^5$ cells/ml of Coll, or Coll/CTS solution, immediately prior to gel polymerization.

Neutralised Coll or Coll/CTS solutions were poured in either four-well plates (0.9 ml/well of 4.5 mm height x 16 mm diameter) or rectangular moulds (4.5 ml/mould of 18 mm width x 40 mm length x 6.2 mm height) to produce dense planar discs and cylindrical rolls, respectively. Gelation was achieved by allowing the solutions to set at 37 °C in a 5 % CO_2 incubator for 30 min. Hydrogels were removed from the moulds and dense gels with CFD of 8.13, 5.26 and 6.38 % for Coll, Coll/CTS 2:1 and Coll/CTS 1:1, respectively, were produced by PC as previously reported [16, 374]. Briefly, highly hydrated gels were placed on a stack of blotting paper, nylon mesh and metal mesh, and subjected to PC using an unconfined compressive stress of 0.5 kPa for 5 min, to remove the excess casting fluid (Fig. 5.1). After compression, dense discs (16 mm diameter with approximate thicknesses of 140, 180 and 250 μm for Coll, Coll/CTS 2:1 and 1:1, respectively) were transferred to 12-well plates and cultured under static conditions for 21 days with medium changes at 2-day intervals. To obtain cylindrically shaped constructs (9 mm height x 3-5 mm diameter), rectangular sheets (18 mm width x 40 mm length x 140-250 μm thick) were plied through the middle along the short axis and rolled along their long axis.

5.3.3 Scanning electron microscopy

Acellular and cell-seeded gels were morphologically assessed by scanning electron microscopy (SEM, FEG-SEM Model S-4700, Hitachi High Technologies America, Pleasanton, CA, USA). Gels were fixed overnight at 4 °C in 0.1 M sodium cacodylate buffer containing 4 % paraformaldehyde and 2 % glutaraldehyde. Fixation was followed by dehydration in a series of increasing ethanol concentrations for 15 min each and critical-point drying (Ladd Research Industries, Williston, VT, USA). SEM was carried out on Au/Pd sputter-coated samples (Hummer VI Sputter Coater, Ladd Research Industries).

5.3.4 Cell metabolic activity in dense gel discs

Seeded cell metabolic activity was evaluated up to day 21 in culture using the AlamarBlue™ assay (Molecular Probes™, Invitrogen, Carlsbad, CA, USA). Dense gel discs were incubated in complete culture medium containing 10 % AlamarBlue™ for 4 h at 37 °C at days 2, 5, 8, 11, 14, 17 and 21. Aliquots (200 µl) of the supernatants (n = 3) of each well were pipetted into 96-well plates and the absorbance at 562 and 595 nm was spectrophotometrically measured using a microplate reader (Model EL800; BioInstruments, Winooski, VT, USA). The background absorbance of the assay medium was accounted for by subtracting the values obtained for acellular gels.

5.3.5 Cell-mediated gel contraction

Cell-mediated contraction of free-floating dense gel discs and cylindrical rolls was determined by measuring the scaffold surface area as a function of time in culture, which was normalized to the initial area at day 0 (n = 3). Acellular gels were used as controls. Culture plates were scanned with a Canoscan 8600F (300 dpi resolution) at different time points up to day 21 in culture. Images were analyzed using ImageJ software (1.42q, Rasband W, National Institutes of Health, Bethesda, MD, USA).

5.3.6 Cell viability

Cell viability within discs and cylindrical rolls was performed using the Live/Dead® assay (Invitrogen, Carlsbad, CA, USA). Gels seeded with 3 x 10^5 cells/ml of Coll or Coll/CTS solution were incubated for 40 min in phosphate buffered saline (PBS; Wisent, St. Bruno, QC, Canada) containing 1 µM calcein AM and 2 µM ethidium homodimer-1 (EthD-1). Cylindrical rolls were carefully unrolled at each time point prior to staining. Scaffolds were transferred to a glass dish (35 mm in diameter, MatTek, Ashland, MA, USA) and Live/Dead staining was detected using a confocal laser scanning microscope (CLSM, Carl Zeiss, LSM5 Exciter, Toronto, ON, Canada). Unrolled constructs were partitioned into three subdivisions of approximately 13 mm in length (periphery, middle and core)

for analysis. Images from each subdivision were obtained through random sampling. Maximum intensity projections of the confocal z-stacks along the entire thickness of the dense gels were obtained using ImageJ software.

5.3.7 Biochemical analyses

Quantification of GAGs and DNA content was performed at days 1, 7, 14 and 21 (n = 6). Samples were freeze-dried (BenchTop K freeze dryer, VirTis, SP Industries, Gardiner, NY, USA) and digested with papain (Papain from papaya latex (Sigma) for 18 h at 60 °C, as previously reported [378]. The supernatant of papain-digested constructs was immediately used for DNA quantification. Unused supernatant volume was stored at -80 °C for GAG quantification. DNA content was determined by detection of HOECHST 33258 (Sigma) staining (FLUOstar OPTIMA, BMG Labtech, Offenburg, Germany; 360 nm excitation/460 nm emission) using a calf thymus DNA standard curve. Background fluorescence was accounted for by subtracting the values obtained from extracts of acellular gels.

Total GAG content was measured both within the discs and in the surrounding medium at each time point. Culture medium was collected and concentrated by centrifugation using a Centricon YM-10 filter (Millipore). GAG content was determined by adding dimethyl-methylene blue (DMMB) to all samples followed by taking readings with a microplate reader equipped with two onboard reagent injectors (FLUOstar OPTIMA) at 520 nm. Measured values were compared with that of a GAG standard (chondroitin sulfate from shark cartilage; Sigma) determined for the same wavelength. For the cylindrical rolls, the GAG content within the gels was assessed at days 1, 7, 14 and 21 as explained above.

5.3.8 Histological analyses

Histological analyses were performed at day 21 using Safranin O/Fast Green staining to localize sulfated GAGs within discs. Gels were rinsed with PBS, fixed in 10 % neutral buffered formalin overnight at 4 °C, and dehydrated in a series of graded ethanol solutions prior to embedding in paraffin. Sections (5 μm) were

obtained from middle regions of the samples and mounted on positively charged glass slides, followed by staining with Safranin O/Fast Green.

5.3.9 Immunohistochemical analyses

Paraffin-embedded sections (5 μm) were used for Coll II and aggrecan immunohistochemistry. The sections were deparaffinised with xylene and ethanol, and rehydrated in a graded ethanol solution series. Antigen retrieval was performed by immersing slides in Tris/EDTA at pH 9.0 for 24 h at 60 °C. Heat-induced epitope retrieval was followed by digestion in 2 % hyaluronidase (Sigma) for 30 min. The sections were permeabilized with 0.25 % Triton X-100 (Sigma) for 10 min, placed in 2 % bovine serum albumin (blocking buffer; Sigma) for 30 min and then incubated overnight with rabbit anti-Coll II (1:100, Millipore) and rabbit anti-aggrecan (1:100, Millipore) antibodies. The slides were then incubated with Alexa 488-labelled goat anti-rabbit IgG (Invitrogen) for 1 h followed by nucleic acid staining with EthD-1 (1:3000). Finally, samples were coverslipped with mounting medium (Geltol, Thermo Electron Corporation, Pittsburgh, PA, USA). Z-stacks of fluorescent immunoreactivity towards Coll II and aggrecan of each specimen were acquired using a CLSM. Maximum intensity projections of each scaffold were generated using ImageJ. Negative controls were performed in the absence of primary antibody.

5.3.10 Mechanical analysis

Compressive mechanical tests were carried out on cylindrically shaped constructs using a Bose® ElectroForce® BioDynamic® (Model 5160, Bose Corp., Eden Prairie, MN, USA) instrument equipped with a 20 N load cell [335, 374]. Cell-seeded and acellular cylindrical rolls were assessed at days 1, 7, 14 and 21 in culture. All tests were carried out in displacement control with a cross-head speed of 0.01 mm/sec. Measurements were conducted at room temperature while maintaining constant sample hydration using drops of distilled water. The specimens' diameter (2.92 ± 0.23, 3.79 ± 0.13 and 5.21 ± 0.35 mm for Coll, Coll/CTS 2:1 and Coll/CTS 1:1, respectively) and height (3.61 ± 0.21 mm) were

measured using a digital calliper and confirmed with a Leitz DMR optical microscope (Leica, Wetzlar, Germany). Specimens were tested using two parallel nonporous compression platens at up to 80 % strain without any evidence of specimen unfolding (n = 3-4). The stress was calculated by normalizing the recorded force against the initial resistance area of the specimen, and the strain was calculated by normalizing the displacement against the initial height of the specimen. The compressive modulus values were computed from the slope of the initial linear region (< 20 % strain) of the stress-strain outputs. [335, 374].

5.3.11 Statistical analysis

All data are presented as mean values ± standard deviation of the mean (± SD). Statistical significance between groups and between time points was determined using a one-way ANOVA with a Tukey-Kramer's post-hoc multiple comparison of means. The level of statistical significance was set at $p = 0.05$.

5.4 RESULTS

5.4.1 Morphological characterization of dense Coll and Coll/CTS gel discs and cylindrical rolls

As-made acellular gels were morphologically characterized by SEM (Figs. 5.1A-C and E). Micrographs of the internal morphology revealed a porous network of randomly oriented nanofibrils of collagen (Fig. 5.1 A). Incorporation of CTS into Coll, followed by PC, maintained the homogeneous open-pore structure with a high degree of interconnectivity (Figs. 5.1 B and C). Rolling dense sheets along the long axis resulted in cylindrical shaped constructs of 9 mm height and 3 to 5 mm diameter depending upon scaffold composition (Fig. 5.1 D). A low magnification SEM micrograph demonstrates the continuous spiral layers of the rolls (Fig. 5.1 E).

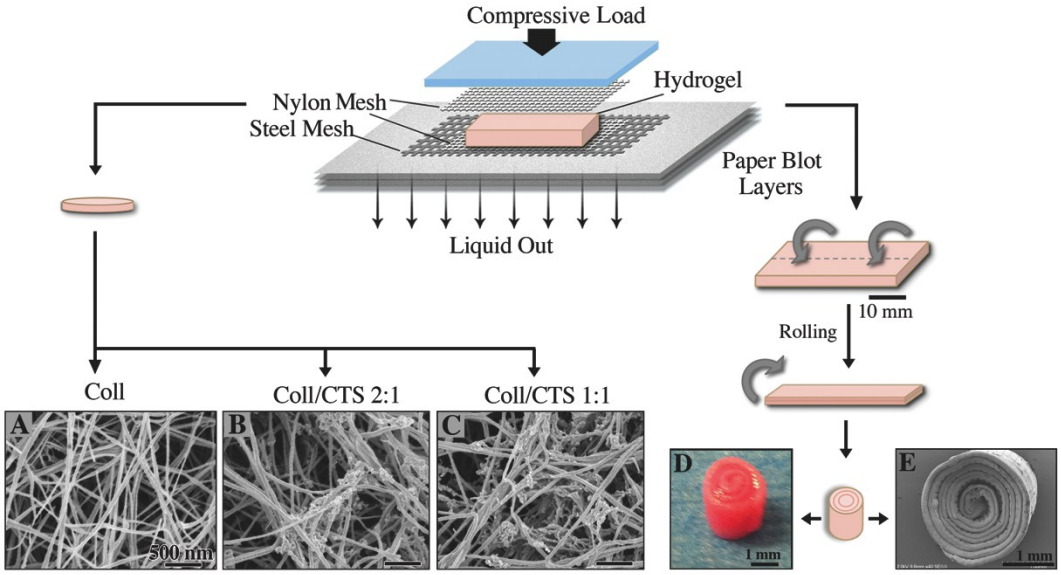

Figure 5.1: Schematic of production of dense Coll/CTS discs and cylindrical rolls. Dense Coll and Coll/CTS hybrid gels were produced by plastic compression using 0.5 kPa for 5 min. (A-C) Morphological characterization by SEM reveals a porous network with a randomly oriented nanofibrillar structure. Incorporation of CTS into the Coll network maintains a homogeneous open-pore structure with a high degree of interconnectivity. (D) Cylindrically shaped constructs were achieved by plying rectangular dense gels through the middle along the short axis and rolling them along their long axis. (E) Low magnification of SEM micrograph shows the continuous spiral layers of the rolls.

5.4.2 Cell metabolic activity and cell-mediated contraction in dense Coll and Coll/CTS gel discs

Cell metabolic activity measured by AlamarBlue™ was significantly reduced in Coll gels after 8 days when compared to the hybrid Coll/CTS gels ($p < 0.05$, Fig. 5.2 A). In Coll/CTS 2:1 and 1:1 gels, cell metabolic activity increased up to day 5 and remained unchanged at days 8 and 14, respectively, at which point cell metabolic activity decreased.

Cell-mediated contraction of dense discs displayed a sigmoidal relationship between scaffold surface area and time, featuring three contraction phases: an initial lag phase, followed by a linear contraction phase and then a slow contraction phase (Fig. 5.2 B). Coll/CTS 2:1 and 1:1 gels were significantly less contracted (55 and 50 %, respectively) compared to Coll (65 %). The extent of contraction between the two Coll/CTS hybrids was not significantly different ($p > 0.05$). No significant changes in scaffold surface area were observed in acellular gel discs with respect to day 0 ($p > 0.05$).

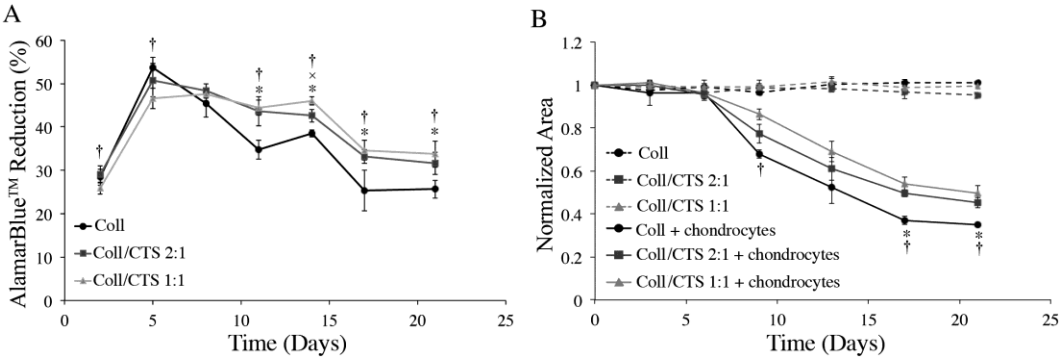

Figure 5.2: Metabolic activity of seeded RCJ cells and cell-mediated Coll and Coll/CTS gel disc contraction up to 21 days in culture. (A) Cell metabolic activity, as indicated by AlamarBlue™ reduction, in Coll (●), Coll/CTS 2:1 (■), and Coll/CTS 1:1 (▲) gels significantly increased up to day 8. Cell metabolism in Coll significantly decreased after 8 days compared to hybrid gels (ANOVA, $p < 0.05$). (B) Measurement of cell-mediated gel disc contraction. Discs display a sigmoidal surface area reduction versus time relationship. All constructs show contraction preceded by a 6-day lag-phase. Contraction of Coll discs is significantly greater than that observed for Coll/CTS 2:1 and 1:1 discs. * indicates a significant difference ($p < 0.05$) between Coll and Coll/CTS 2:1. † indicates a significant difference ($p < 0.05$) between Coll and Coll/CTS 1:1. × indicates a significant difference ($p < 0.05$) between hybrid gels. Acellular gels (indicated by dashed lines) were used as negative controls. Data are represented as the mean ± SD, n = 3.

5.4.3 Cell viability and morphology within dense Coll and Coll/CTS gel discs

CLSM of calcein-AM labelled cells was used to monitor cell viability over time. As indicated by green fluorescent cytoplasmic labelling and negligible EthD-1 binding to nucleic acids (red) in maximum intensity projections, all scaffold compositions supported cell viability both immediately after gelation and during subsequent cell culture (Fig. 5.3). At day 1, all compositions contained uniformly distributed viable cells that displayed a rounded morphology. At day 7, cell density increased throughout the entire thickness, and RCJ cells seeded in hybrid gels formed cartilage-like aggregates with spherical morphology (indicated by white arrows). Aggregate formation progressed up to day 21 with hybrid gels showing a greater tendency to support this.

SEM micrographs at day 21 in culture displayed extensive cytoplasmic extensions of seeded RCJ cells integrated within scaffolds. Cells in Coll exhibited a mixture of flat, polygonal cells combined with rounded cells. In comparison, cells with a rounded morphology were more frequently observed in Coll/CTS hybrids. Quantitative analyses of cell spreading (surface area) using ImageJ

software (n = 10) showed that the average cell surface area within Coll was significantly higher (197 ± 48 μm^2) compared to Coll/CTS 2:1 and 1:1 (110 ± 35 and 83 ± 25 μm^2, respectively) ($p < 0.05$).

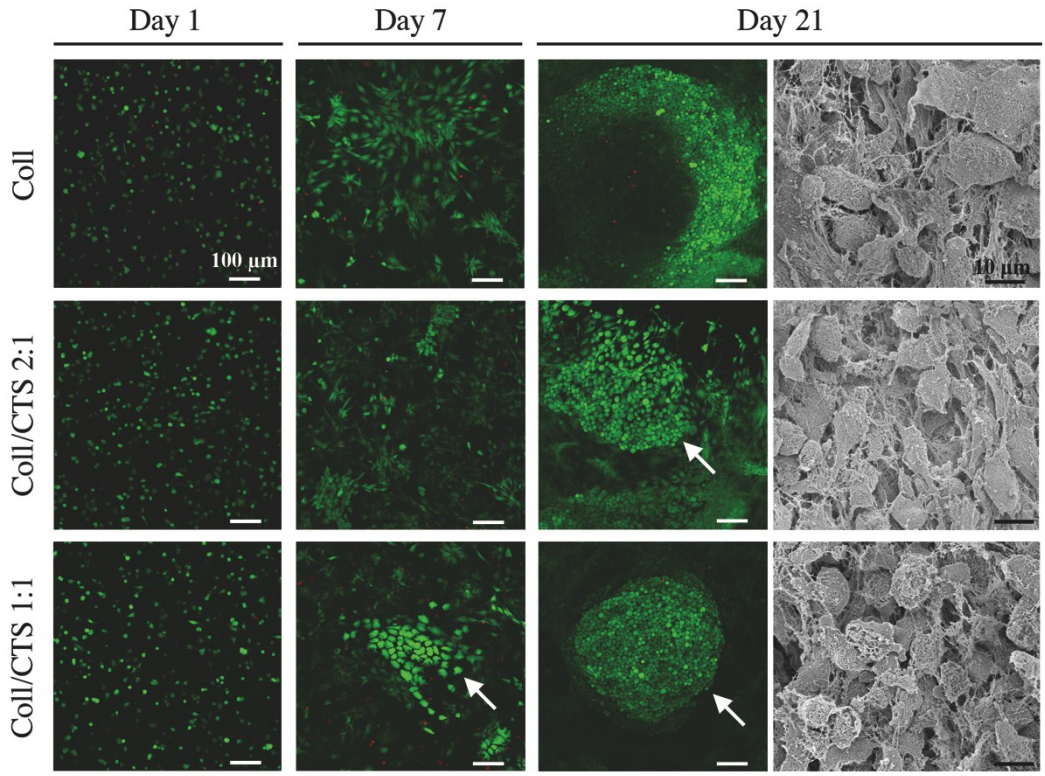

Figure 5.3: Analysis of RCJ cells viability and morphology within dense Coll, Coll/CTS 2:1 and Coll/CTS 1:1 discs. CLSM maximum intensity projection images covering the entire thickness were collected at days 1, 7 and 21. Green fluorescent calcein-AM-labelled cells represent viable cells with no membrane disruption, and red fluorescent EthD-1 positive nuclei indicate cell necrosis and late apoptosis. Aggregates of cells (white arrows) are detected as early as day 7 within Coll/CTS hybrid gels. SEM micrographs obtained at day 21 in culture show the distribution and morphology of seeded RCJ cells within the matrix, with differences in the extent of cell spreading and integration between the different compositions.

5.4.4 Quantification of GAG synthesis and DNA content within dense Coll and Coll/CTS gel discs

Since CTS binds negatively charged GAGs [379], the total GAG content was quantified both within the discs and the surrounding media. GAG synthesis significantly increased in all compositions with incubation time up to day 21, except for Coll where it peaked at day 14 ($p < 0.05$, Fig. 5.4 A). The production of GAGs in Coll, Coll/CTS 2:1 and 1:1 constructs increased by a factor of 1.7, 1.8 and 2.4, from days 7 to 14, respectively. Increasing CTS content led to an increase

in GAG retention as indicated by a decrease in its content within the surrounding medium ($p < 0.05$). The total amount of secreted GAGs in both Coll/CTS 2:1 and 1:1 hybrid gels was significantly higher compared to Coll beyond day 7 ($p < 0.05$).

DNA content significantly increased over the 21-day culture period, except for Coll where it significantly decreased at day 21 ($p < 0.05$, Fig. 5.4 B). ANOVA indicated no significant differences between hybrids at any given time point ($p > 0.05$). In addition, the total GAG synthesis normalized to DNA content showed that the incorporation of CTS into dense Coll gels significantly enhanced GAG secretion at all times following day 1 ($p < 0.05$, Fig. 5.4 C).

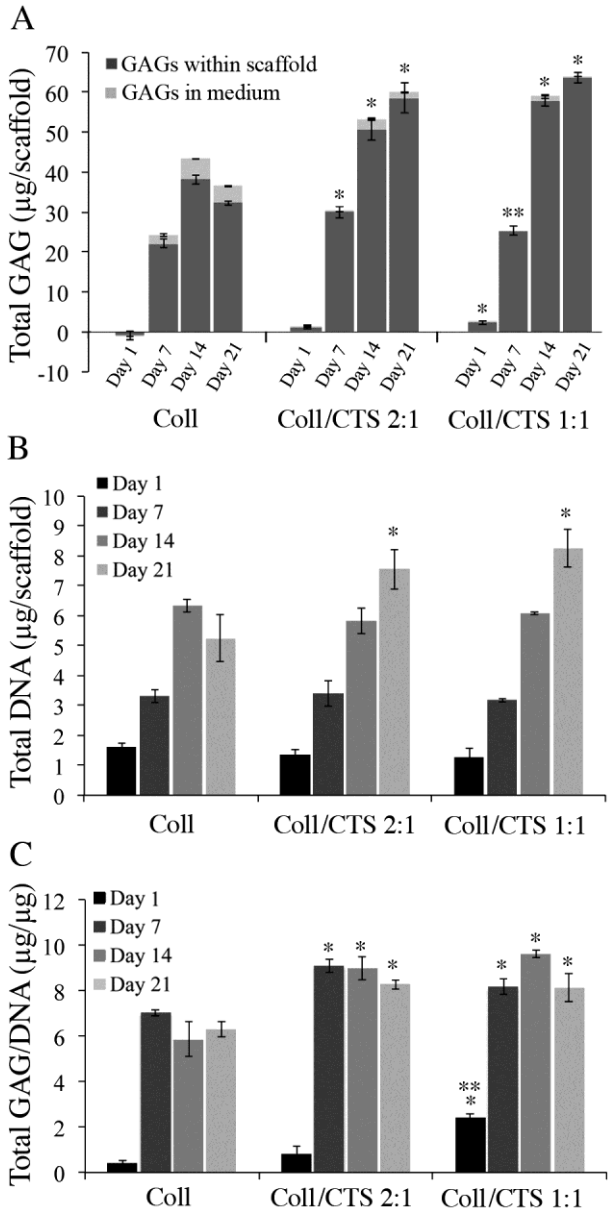

Figure 5.4: GAG synthesis by differentiated RCJ cells within dense Coll, Coll/CTS 2:1 and Coll/CTS 1:1 gel discs up today 21 in culture. (A) DMMB assay for quantification of total GAG within scaffolds and in surrounding medium, (B) Hoechst 33258 fluorimetric detection of total DNA content, and (C) normalized total GAG/DNA content. GAG retention within the discs increases with increasing CTS content. Following day 1 in culture, the amount of total GAG/DNA content remains significantly higher in the hybrid gels compared to Coll alone (ANOVA, $p < 0.05$). * indicates a significant difference ($p < 0.05$) when compared to Coll. ** indicates a significant difference ($p < 0.05$) between hybrid gels 1. Data are represented as the mean ± SD, of three independent experiments performed in duplicate, n = 6.

5.4.5 Histological and immunohistochemical analysis of dense Coll and Coll/CTS gel discs

ECM secretion by RCJ cells within the different specimens was assessed through histochemical and immunohistochemical analysis at day 21 (Fig. 5.5). Sections were histologically stained using Safranin O/Fast Green (Figs. 5.5 A-C) to detect sulfated GAGs. Histological findings in the middle region of the various gel discs showed differences in cartilage-like matrix deposition between all compositions. Coll/CTS 1:1 gels revealed GAG-rich ECM within aggregates, as indicated by intense Safranin O staining, and round chondrocyte-like cells within lacunae characteristic of native cartilage. Staining in the control group (acellular gel) was negative and showed only a light green background counterstaining (data not shown). Differences in the counterstain intensity are attributable to the anionic Fast Green stain having a strong affinity for positively charged CTS [379]. The effect of CTS incorporation into Coll gels was assessed by aggrecan (Figs. 5.5 D-F), and Coll II (Figs. 5.5 G-I) immunostaining. Coll/CTS 1:1 showed stronger positive staining for aggrecan and Coll II compared to Coll/CTS 2:1 and Coll gels.

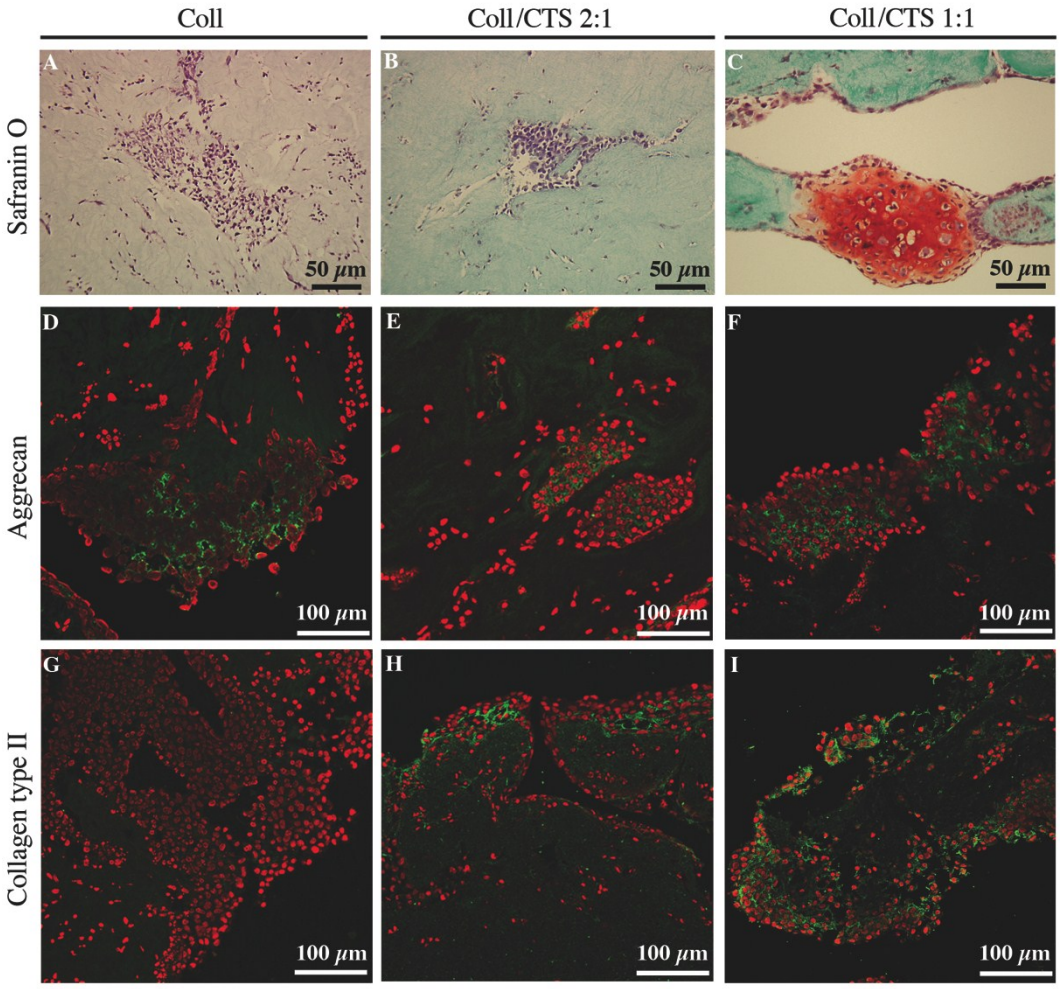

Figure 5.5: Histological and immunohistochemical analyses of ECM synthesis by differentiated RCJ cells seeded within dense Coll, Coll/CTS 2:1 and Coll/CTS 1:1 gel discs in paraffin embedded sections at day 21 in culture. (A-C) Safranin O/Fast Green staining for GAG detection shows strong positive Safranin O staining (red/purple) in Coll/CTS 1:1. (D-I) CLSM maximum intensity projections images of positive immunostaining for (D-F) aggrecan and (G-I) Coll II. Nucleic acid staining was performed with EthD-1 (red).

5.4.6 Mechanical properties of cell-seeded and acellular gel cylindrical rolls

At the earliest time point (day 1), the incorporation of CTS into Coll significantly increased the compressive modulus of both cellular and acellular rolls (Fig. 5.6 A and B, respectively) from 11.7 ± 2.2 kPa for Coll alone, up to 20.5 ± 1.4 kPa for acellular Coll/CTS 1:1 ($p < 0.05$). At day 7, both cell-seeded and acellular hybrid gels showed a decrease in the compressive modulus, a level that was maintained throughout the 21-day culture period. No significant

differences were observed within each group between cellular and acellular cylindrical rolls ($p > 0.05$).

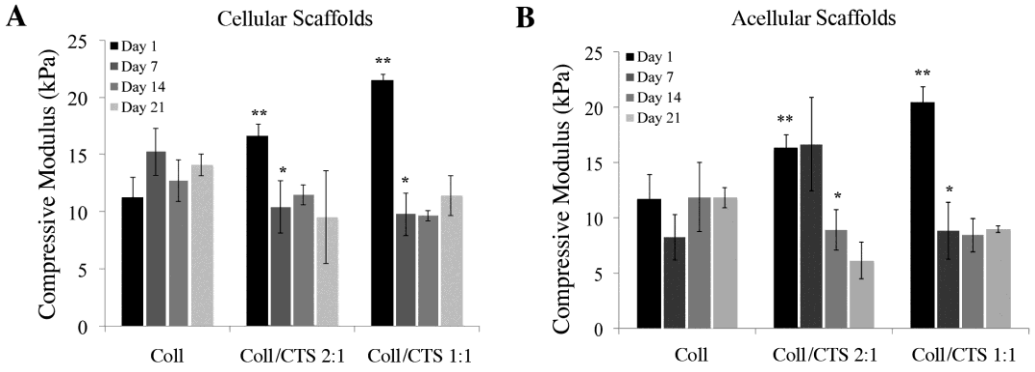

Figure 5.6: Compressive modulus of (A) cellular and (B) acellular dense cylindrically shaped constructs up to day 21 in culture. There is a significant increase in the compressive modulus at day 1 with increasing CTS content. No significant difference is observed in the acellular and cellular cylindrical rolls for all specimens at any given time point (ANOVA, $p > 0.05$). A significant decrease is observed in all constructs following day 1. The compressive modulus remains unchanged up to day 21. * indicates a significant difference ($p < 0.05$) compared to previous time point. ** indicates a significant difference ($p < 0.05$) compared to Coll. Data is represented as mean ± SD, n = 3-4..

5.4.7 CLSM analysis of cell viability within gel cylindrical rolls

RCJ cell viability in cylindrical rolls was investigated by CLSM detection of Live/Dead® staining in unrolled constructs at different time points (Figs. 5.7 A-B). Confocal image z-stacks of the peripheral, middle and core regions of the constructs were acquired at days 1, 7, 14 and 21 from randomly selected regions within three equally spaced, consecutive regions along the construct, and assembled into maximum intensity projection images (Fig. 5.7 C). At day 1, all constructs showed a rounded morphology and a homogenous distribution of viable cells in all regions. At day 7, all constructs exhibited increased cell growth throughout the rolls as well as initial signs of aggregate formation (red arrows). In addition, the amount and size of aggregates increased with CTS content. At day 14, Coll gels showed a decrease in cell growth, in particular after 13 mm from the periphery. In contrast, hybrid gels showed an increase in cell number up to 26 mm from the periphery, followed by a decrease thereafter.

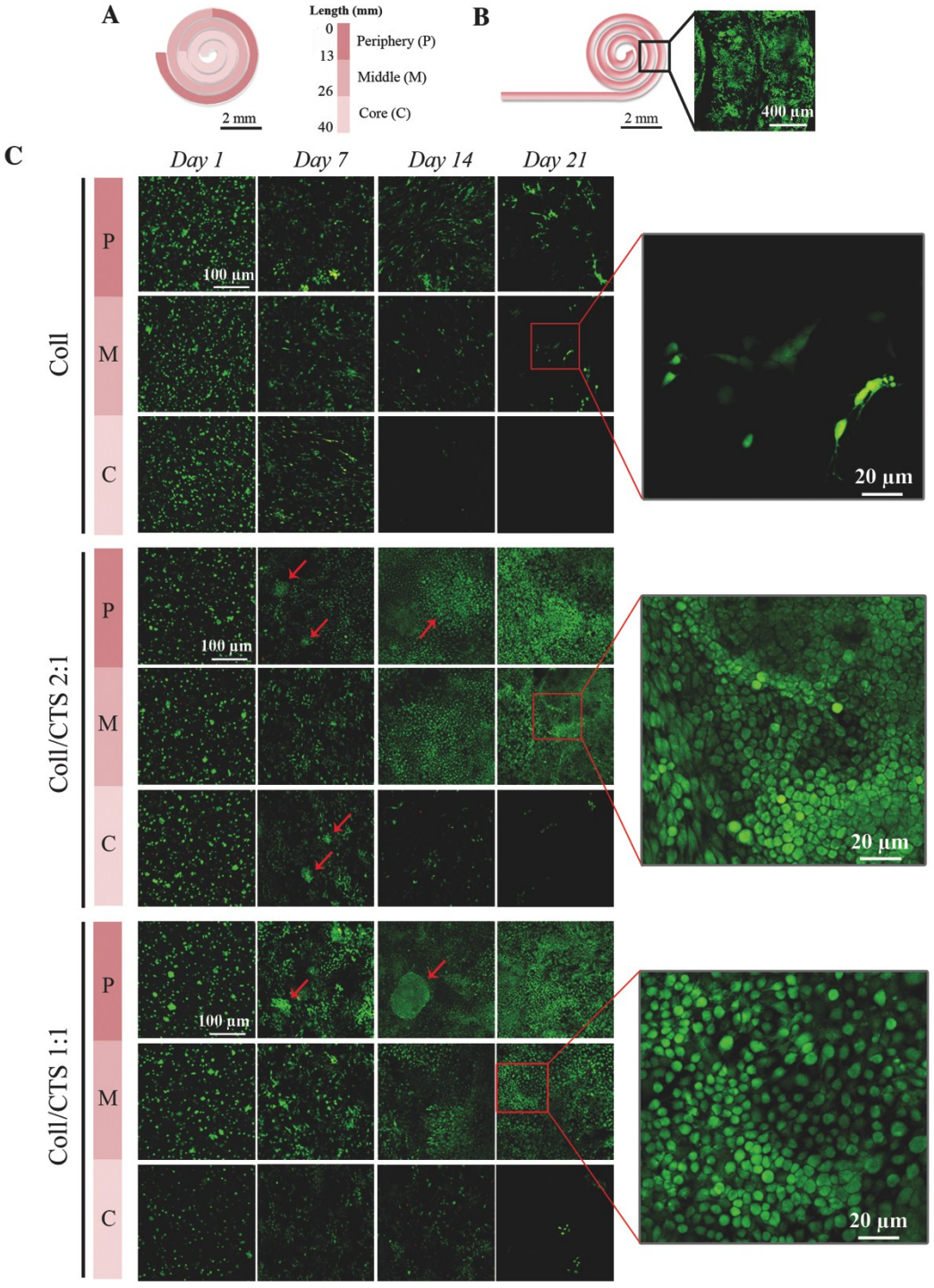

Figure 5.7: CLSM analysis of RCJ cells viability within Coll, Coll/CTS 2:1 and Coll/CTS 1:1 cylindrical rolls up to day 21 in culture. (A, B) Constructs were unrolled and stained for Live/Dead® analyses at days 1, 7, 14 and 21. Confocal images were taken at the periphery, middle and core regions of dense cylindrical rolls. (C) Green-fluorescently labelled cells represent viable cells with no membrane disruption, and red-fluorescently labelled nuclei indicate cell necrosis and late apoptosis. Right panel, high-magnification images of stained cells in the middle region of the cylindrical roll depict details of cell morphology at day 21.

5.4.8 Quantification of GAG synthesis and DNA content within gel cylindrical rolls

Based on the fact that a maximum of 12 % of the total GAGs produced by Coll discs was released to the medium and that this amount decreased with the incorporation of CTS and time, GAG content was only quantified within the cylindrical rolls. GAG synthesis (Fig. 5.8 A) and DNA content (Fig. 5.8 B) in all compositions exhibited a similar trend over time. A significant increase in all compositions was observed up to day 14 ($p < 0.05$). GAG and DNA levels at day 21 remained elevated in the hybrid gels compared to Coll where it decreased significantly. GAG content normalized to DNA significantly decreased with time in all compositions ($p < 0.05$); however, the level of GAGs in hybrid gels was higher than in Coll at all measured times, except at day 21, where there was no significant difference between Coll and Coll/CTS 1:1 (Fig. 5.8 C).

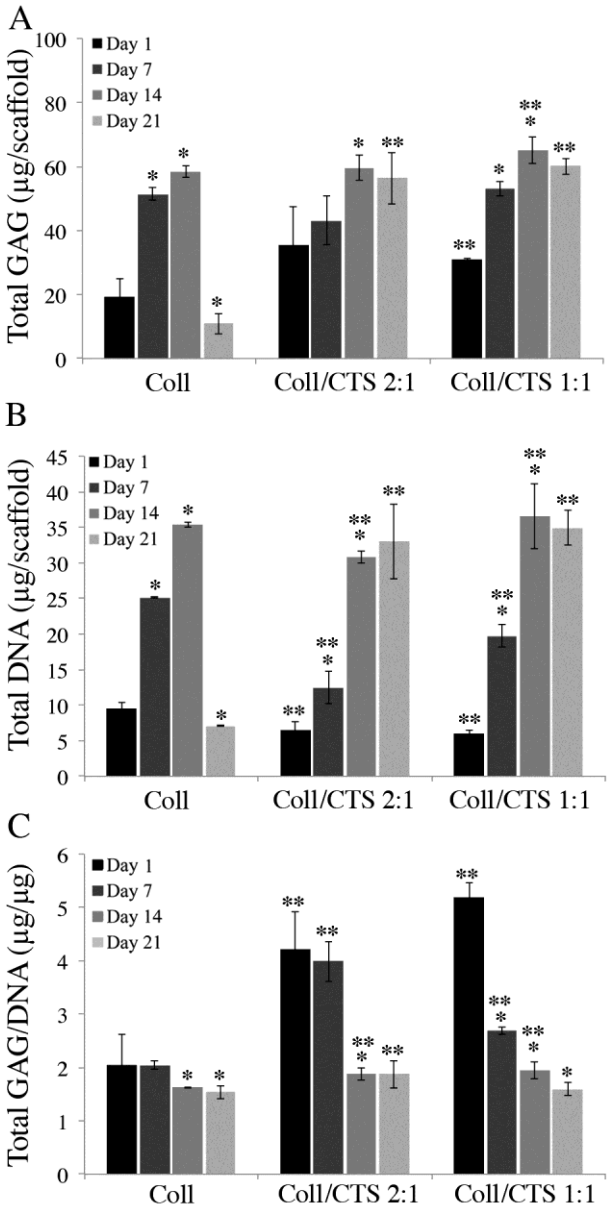

Figure 5.8: GAG synthesis by differentiated RCJ cells within Coll, Coll/CTS 2:1 and Coll/CTS 1:1 cylindrical rolls up to day 21 in culture. (A) DMMB assay quantification of total GAGs, (B) Hoechst 33258 fluorimetric detection of total DNA content, and (C) normalized total GAGs/DNA content within cylindrical rolls. Normalized GAG content is found to be statistically higher in the hybrid constructs after 1 day of cell seeding when compared to Coll (ANOVA, $p < 0.05$). Normalized GAG content within all cylindrical rolls is significantly reduced with time; however, the total GAG content in the hybrids is higher than the Coll gels throughout the time course, except at day 21 where there is no significant difference ($p > 0.05$) between Coll and Coll/CTS. * indicates a significant difference ($p < 0.05$) within a given group, compared to previous time point. ** indicates a significant difference ($p < 0.05$) when compared to Coll cylindrical rolls. Data is represented as mean ± SD, n=3.

5.5 DISCUSSION

Collagen-based hydrogels are attractive scaffolds for AC repair as they present both microstructural and compositional similarities to native cartilage, and allow for homogenous cell seeding within a highly hydrated environment [380]. However, despite the prevalent use of Coll for tissue engineering purposes, numerous *in vitro* studies have reported the phenotypic instability of chondrocytes within these scaffolds [236, 238]. In this study, CTS, a well-known GAG-analog and chondroprotective material [132], was incorporated into a physiologically relevant, dense Coll nanofibrillar gel, which mimics the major structural component of the extracellular milieu, in order to determine its effect on RCJ cell function relative to cells grown in dense Coll alone.

RCJ cells seeded into dense hydrogel discs exhibited a higher level of metabolic activity in Coll/CTS compared to Coll from days 8 to 14. The maximum cell metabolic activity of all gels closely corresponded with the onset of cell-mediated disc contraction at day 6, indicating that a minimum threshold cell density was attained in order to exert sufficient forces required to induce gel contraction [374]. At day 21, the final contraction differed significantly according to CTS content, indicating that RCJ cells in Coll scaffolds may have dedifferentiated into fibroblast-like cells, which exert higher contractile forces compared to chondrocytes. [381]. Moreover, the increased extent of contraction observed for RCJ cells in Coll gels, compared to that seen in Coll/CTS gels, may be related to a collagen-type effect, which is greater when these cells are in contact with Coll than with Coll II [382].

Quantification of DNA showed that RCJ cells seeded within dense Coll/CTS hydrogels proliferated during the 21-day culture period, in contrast to Coll, which demonstrated a significant reduction at day 21. Differences in the metabolic activity results and DNA quantification may be explained by the fact that the Alamarblue™ assay is not a direct cell counting technique, as the absorbance signal is affected not only by the number of cells, but also by cell metabolism. In

particular, the metabolic activity varies greatly depending on the life-cycle of the cell, thus the presence of cells in different phases of cell growth results in different oxidative metabolism [383].

RCJ cells seeded within dense Coll/CTS discs were viable and formed aggregates of spherical cells that are characteristic of differentiated chondrocytes [384], confirming the morphological features observed by SEM. In contrast, cells seeded in Coll alone exhibited a flattened and stellate morphology, with a significantly higher cell surface area that is characteristic of fibroblasts, indicating that cell de-differentiation may have occurred [208]. Increasing CTS content supported the sustained upregulation of secreted cartilage-specific GAGs, as demonstrated by GAG quantification within the discs and the surrounding medium, Safranin O staining and aggrecan immunoreactivity. The enhanced retention of newly synthesized GAGs within hybrid gels, compared to Coll gels, supports the hypothesis that the biochemical similarities of CTS to GAGs has an important role in modulating chondrocyte function, including chondrocyte differentiation [280]. A similar role for CTS has been reported following incorporation within either hydroxyethyl cellulose hydrogels, freeze-dried Coll/GAGs matrices, and silk fibroin scaffolds [136, 270, 280, 385]. Consistent with GAG synthesis, Coll II immunoreactivity was also increased by CTS content in this study.

Among the challenges now facing cartilage tissue engineering is the need of the production of constructs of a scale necessary to repair critical-sized defects (> 2 mm diameter) [16, 64, 374]. In this regard, cylindrically shaped constructs having clinically relevant diameters (3-5 mm diameter) were developed to investigate the complex interplay between scaffold geometry, microstructure, composition, mechanical properties and cell function. Previous reports have shown that chondrocytes seeded within hydrogel-based scaffolds produce mechanically functional cartilage-like scaffolds owing to the *in vitro* synthesis of cartilage specific ECM components [252, 386]. In particular, the proteoglycan

network contributes to the compressive stiffness via the repulsive electrostatic interactions amongst its fixed negative charges (GAG) [261, 387]. Thus, in this study, the effect of ECM biosynthesis by RCJ cells on the compressive modulus of dense Coll/CTS cylindrical rolls was assessed as a function of time. The compressive modulus of both cellular and acellular hydrogels at day 1 increased with CTS content. Similar to GAGs in native AC, CTS is thought to associate with the collagen network and increase the swelling pressure due to its high fluid retention capacity, resulting in higher compressive stresses for Coll/CTS when compared to Coll alone. [16, 64, 374]. Following day 1, the modulus of all specimens decreased and remained unchanged for the duration of the study. This decrease may be attributed to extended culture conditions, which may have entrapped free fluid between the spirally wrapped layers that form the cylinder, thus weakening the scaffold and reducing its compressive modulus. Therefore, the mechanical properties of cellular hydrogels were not significantly modulated by ECM deposition by seeded RCJ cells over the course of the entire culture period.

In an effort to further understand why cellular ECM deposition did not exert a detectable effect on scaffold properties, cell viability was assessed throughout the entire thickness of the cylindrical rolls at each time point using CLSM. Maximum intensity projections of Live/Dead® stained cells showed that cell viability within Coll was reduced from the middle regions of the cylinder to the core. However, this phenomenon was diminished by the incorporation of CTS.

Heterogeneous oxygen and nutrient distribution have been reported to lead to nonhomogeneous cell behaviour, with high cell growth and biosynthetic activity at the periphery and an elevated number of necrotic cells at the core regions [388]. Although studies of oxygen diffusion along a 2.3 mm diameter dense Coll roll have shown a 7-fold reduction in the oxygen levels from the periphery to the centre (from 140 to 20 mmHg), only a slight reduction in fibroblasts viability was observed at the core [307, 311]. Moreover, given that chondrocytes *in vivo* reside in a hypoxic microenvironment and that prochondrogenic effects of low oxygen

tensions have been reported [388, 389], reduction in cell viability in the core regions attributable to differences in oxygen diffusion alone are unlikely to explain the above results. In particular, the effect of low oxygen levels in the inner regions of the construct would fail to explain the temporal reduction of normalized GAG levels observed in all specimens. Indeed, it has been reported that GAG synthesis is inversely correlated to oxygen tension, resulting in a pronounced increase in the compressive stiffness of seeded constructs [390]. Nonetheless, in other studies it has been reported that nutrient availability could affect chondrocyte viability within 3D hydrogel constructs, where cell growth is significantly compromised within the core region of the constructs below a certain nutrient threshold [391, 392]. Based on these reports, nutrient availability within dense cylindrical rolls would represent a more plausible explanation for reductions in both cell viability and GAG synthesis compared to disc scaffolds. It is noteworthy that Coll/CTS cylindrical rolls of approximately 5 mm in diameter supported greater cell viability within deeper regions of the cylinder, compared to Coll rolls with diameters that were approximately 40 % smaller, therefore supporting the hypothesis that the biochemical similarities of CTS to GAGs play an important role in modulating chondrocyte function [280].

Although GAG/DNA levels decreased over time in all specimens, RCJ cells seeded in cylindrical Coll/CTS rolls synthesized greater GAG/DNA at each time point, as shown for chondrocytes seeded in dense discs. The factors contributing to the attenuated decline in GAG synthesis in constructs containing CTS remain to be determined, but may be attributable to a combination of factors, such as the ability of CTS to support chondrocyte function along with microstructural changes associated with the water retention capacity of CTS, which also contributed to a larger scaffold diameter compared to Coll rolls [132, 374]. Moreover, given that the Coll cylindrical rolls underwent a 10 % contraction at day 14 in culture (Supplementary Fig. 5.1), an increase in matrix density may have led to a decrease in both scaffold permeability and mass diffusion compared to dense Coll/CTS rolls [352, 393, 394]. Similarly, static hydrogel culture may

have caused heterogeneous distribution of nutrients within the 3D dense cylindrical rolls due to limited nutrient diffusion over long distances [393]. Strategies to enhance the biosynthetic activity of RCJ cells of these hydrogels should therefore focus on improving nutrient diffusion by using dynamic culturing modes, in analogy to conditions *in vivo* [395]. In addition, fine-tuning the geometry of such cylindrically shaped scaffolds may provide better mechanical integrity of the tissue over time [252] showing potential application as *in vitro* models for critical-sized AC defects for cartilage tissue engineering.

5.6 CONCLUSIONS

This study demonstrates that the incorporation of CTS into dense Coll hydrogel discs enhances RCJ cell growth and biosynthesis of cartilage-like ECM. Moreover, analyses of chondrocyte function in larger dense Coll/CTS constructs provided new insights into how the morphometric parameters of scaffolds regulate RCJ cell growth and differentiation. Overall, the findings reported herein provide valuable design information for the development of model scaffolds directed towards the clinical repair of critical-sized AC defects.

5.7 ACKNOWLEDGEMENTS

This work was supported by funds from Canadian Natural Sciences and Engineering Research Council, the Canadian Foundation for Innovation, and the McGill University Faculty of Engineering Gerald Hatch Faculty Fellowship (in support of SNN). Florencia Chicatun is also partly supported by McGill Engineering Doctoral Awards, Vadasz and Hatch fellowships and a Bourses Fondation Pierre Arbour scholarship. MDM is a member of the FRQ-S Réseau de Recherche en Santé Buccodentaire et Osseuse and the FRQ-S Groupe de Recherche Axé sur la Structure des Protéines.

5.8 APPENDIX: SUPPLEMENTARY INFORMATION

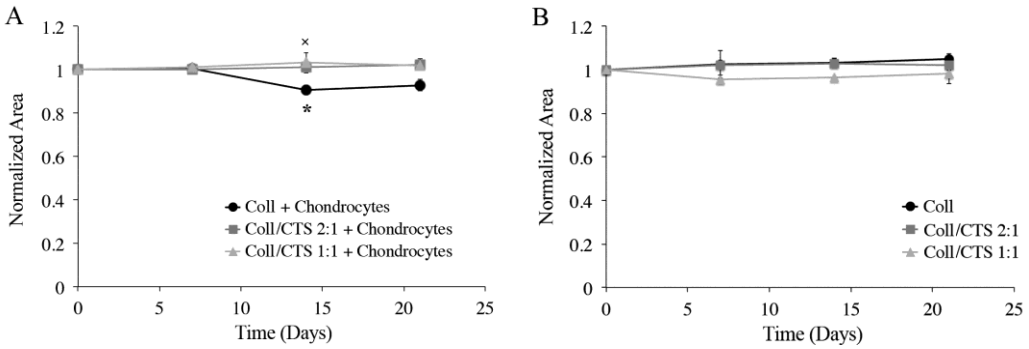

Supplementary Figure 5.1: Change in cylindrical rolls surface area up to day 21 in culture. (A) Cellular and (B) acellular cylindrical rolls of Coll (●), Coll/CTS 2:1(■) and Coll/CTS 1:1 (▲) (n = 3). There is no significant change in the acellular construct area with time. Compared to Coll, cell-mediated contraction of hybrid constructs is not significant as a function of culture time ($p > 0.05$). Coll roll area decreases at day 14 and remained unchanged for up to 21 days in culture. * indicates a significant difference ($p < 0.05$) within a given group compared to previous time point. × indicates a significant difference ($p < 0.05$) between Coll and hybrid constructs.

CHAPTER 6: A BILAYERED DENSE COLLAGEN/CHITOSAN HYDROGEL AS A THREE-DIMENSIONAL TISSUE MODEL FOR OSTEOCHONDRAL TISSUE ENGINEERING

OTE aims to fabricate complex tissues with a stratified architecture containing two or more discrete layers with specific physical and chemical properties to closely replicate the native osteochondral structure. Despite the significant advances in OTE, several challenges still remain in engineering a suitable biomimetic well-integrated matrix that mimic the native connective tissue of cartilage and bone present in the osteochondral region.

In this respect, dense Coll/CTS hydrogels developed in this dissertation indicated promising results for applications in both bone and cartilage tissue engineering. In particular, the beneficial effect of CTS incorporation to support MC3T3-E1 pre-osteoblast viability, proliferation, differentiation and mineralization under osteogenic-inducing conditions, was demonstrated in *Chapter 4*. These results showed that dense Coll/CTS hydrogels provided an efficient osteoid-like model for the study of osteoblast differentiation and BTE. As a further step towards the use of dense hybrid gels as scaffolds for TE applications, Coll/CTS gels were investigated as potential models for AC repair. The positive effect of CTS incorporation within dense Coll on RCJ3.1C5.18 chondroprogenitor-seeded cells growth, viability and differentiation, was demonstrated in *Chapter 5*. Overall, these findings provided significant evidence that dense Coll/CTS scaffolds have a stimulatory effect towards the progression from chondroprogenitors to differentiated chondrocytes, revealing the important role of CTS in stimulating ECM production.

Based on these findings and in pursuit of the aim set in the present doctoral dissertation, *Chapter 6* investigates the development of a bilayered dense hydrogel to model the complex osteochondral structure, by co-gelling cartilaginous (Coll/CTS 1:1) and osteoid-like (Coll/CTS 33:1) layers with

Coll/CTS weight ratios approaching those of Coll/GAGs in the native ECM of cartilage and bone, respectively.

This work was reported in a manuscript submitted to a peer-reviewed journal and is reproduced below.

A bilayered dense collagen/chitosan hydrogel as a three-dimensional tissue model for osteochondral tissue engineering

Florencia Chicatun,[1] Naser Muja,[1] Mari T. Kaartinen[2], Marc D. McKee [2,3] and Showan N. Nazhat [1]*

[1]Department of Mining and Materials Engineering, Faculty of Engineering, [2]Faculty of Dentistry, [3]Department of Anatomy and Cell Biology, Faculty of Medicine, McGill University, Montreal, Quebec, Canada H3A 2B2

**Corresponding author:* Showan N. Nazhat, Department of Mining and Materials, Engineering, McGill University, 3610 University Street, Montreal, Qc, Canada, H3A 2B2, Tel: 1-514-398-5524, Fax: 514-398-4492, E-mail. showan.nazhat@mcgill.ca

Keywords: Dense collagen hydrogel; chitosan; bone; cartilage; osteochondral.

6.1 ABSTRACT

Osteochondral tissue engineering (OTE) requires a scaffold system that supports the regeneration of both the articular cartilage and the underlying subchondral bone. In this study, a bilayered dense hydrogel was developed to mimic the osteochondral structure, using two defined collagen/chitosan weight ratios, which approach those of collagen/glycosaminoglycans in the native extracellular matrices of cartilage and bone. RCJ3.1C5.18 chondroprogenitor cells and MC3T3-E1 osteoprogenitor cells were selected as well-defined models of cell differentiation to be sequentially seeded within distinct, dense hydrogel layers. Culture conditions were optimized to support the simultaneous growth and differentiation of both cell types as determined by gene expression and biochemical analyses up to 35 days. Chondrogenesis was observed within the cartilage-like layer of the scaffold, as indicated by the expression of *Col2a1* and *Acan* as well as by Safranin O staining and quantification of glycosaminoglycans. In the osteoid-like layer of the scaffold, osteogenesis was shown by elevated alkaline phosphatase enzymatic activity, calcium deposition, and the expression of *Akp2, Col1a1* and *Mmp-13*. In conclusion, the integrated bilayered hydrogel scaffold supported the simultaneous differentiation of chondrocytes and osteoblasts within distinct layers, providing a relevant biomimetic construct for OTE applications and future studies using autologous stem cells.

6.2 INTRODUCTION

Articular cartilage (AC) damage, whether from trauma or arthritis, frequently transcends from the joint surface to the underlying subchondral bone through the osteochondral interface, causing severe pain and joint dysfunction [22, 24]. AC has a limited capacity for self-repair as a consequence of its avascular nature, relying upon the formation of a blood clot and an inflammatory response to recruit blood vessels and mesenchymal stem cells (MSCs) to stimulate tissue regrowth [24]. Current clinical treatments for cartilage repair include mosaicplasty [76], microfracturing [67], autograft and allograft plugs [77, 78], as well as cell-based techniques such as autologous chondrocyte implantation (ACI) [76] and matrix-induced ACI [396]. While microfracture techniques have shown functional improvement in young patients, this surgical approach often contributes to the formation of fibrocartilage tissue, which gradually deteriorates [68]. Similarly, autologous osteochondral grafts exhibit limited integration between the host and donor plug [78]. In addition, ACI techniques have not shown significant improvement over microfracture methods, although long-term graft survival is significantly increased compared to mosaicplasty [76, 80]. Therefore an alternative restorative procedure is needed to reduce donor site morbidity, promote enhanced graft-host integration and avoid mismatch between the implant and the recipient site.

Osteochondral tissue engineering (OTE) scaffolds hold promise for use in AC repair based on the rapid and effective bone-to-bone integration compared to cartilage-to-cartilage interface alone, which possess a non-adhesive matrix [25, 26]. Therefore, the osteochondral graft enables the bone to anchor the adjacent cartilage region to the host. Yet, OTE faces the challenge of engineering a scaffold that is able to maintain both chondrogenic and osteogenic phenotypes during three-dimensional (3D) co-culture [74]. Previous studies involving multi-tissue formation developed hybrid scaffolds by either suturing or gluing independently cultured constructs together [26, 28, 283]. Despite these designs, *in*

vivo studies have shown poor integration between the layers, often leading to graft failure [27, 284]. Alternative approaches have been developed to achieve integrated cartilaginous- and bone-like layers based on polymeric and ceramic constructs [27, 285, 286]. However, because of substantial differences in the mechanical properties of each layer, such constructs have weak interfacial properties, likewise leading to premature scaffold failure.

Collagen-based scaffolds have been widely applied to mimic the native connective tissue of cartilage and bone present in the osteochondral region in articulating joints [97, 112]. In particular, acid-extracted collagen type I (Coll) hydrogels have emerged as the preferred scaffold material for cartilage tissue engineering applications due to the challenges associated with processing collagen type II (Coll II) [129, 240, 241]; the dominant collagen isoform present in cartilage. However, Coll hydrogels exhibit poor mechanical properties and a high degree of cell-mediated gel contraction as a result of their highly-hydrated nature (> 99 % fluid) and low collagen fibrillar density (< 0.5 wt. %), which results in a mismatch between the implanted scaffold and the defect site [373]. Using the plastic compression (PC) technique, the collagen fibrillar density is rapidly increased by removing the excess casting fluid, and enabling the production of dense (approximately 10 wt. %) scaffolds with increased biomechanical properties and lower contraction extent, without compromising seeded cell viability [16]. In addition to this advantage, osteochondral repair can benefit from the incorporation of biomacromolecules that closely mimic the composition and microstructure of the native extracellular matrix (ECM).

Along with abundant collagenous proteins, the ECM of cartilage and bone are composed of polysaccharides such as glycosaminoglycans (GAGs) [(by weight) cartilage: ~20 % Coll II, ~10 % GAGs and ~70 % water; bone: ~33 % Coll, ~1 % GAGs and 66 % water] [46]. Attributable to similarities in structure and composition, chitosan (CTS) is commonly used as a GAG analog [99, 397]. In particular, dense collagen/chitosan (Coll/CTS) hydrogels exhibited a 2.3-fold

increase in compressive modulus (23 to 55 kPa), 3.1-fold decrease in cell-mediated contraction, and significantly increased resistance to collagenase degradation [374], while supporting chondrocyte [398] and osteoblast growth and differentiation with long-term stability up to eight weeks *in vitro*, when compared to Coll alone [374].

The aim of this study was to develop an OTE strategy that models the complex osteochondral structure and supports the simultaneous regeneration of AC and the underlying subchondral bone. Two hydrogel layers, with distinct Coll/CTS weight ratios approaching those of Coll/GAGs in the native ECMs of cartilage (Coll/CTS 1:1) and bone (Coll/CTS 33:1) were seeded with RCJ3.1C5.18 chondroprogenitors and MC3T3-E1 pre-osteoblasts, respectively, and simultaneously co-gelled. The highly-hydrated gel was then plastically compressed to produce, within minutes, a bilayered dense Coll/CTS osteochondral scaffold with solid weight percent approaching physiological values. Culturing conditions were first optimized to maintain both chondrogenic and osteogenic cell phenotypes followed by morphological and microstructural characterization. Afterwards, bilayered constructs were characterized in terms of cell viability, histochemical and biochemical analyses, as well as expression of genes associated with chondrocytic and osteoblastic differentiation and protein biosynthesis by immunostaining for Coll II and aggrecan.

6.3 MATERIALS AND METHODS

6.3.1 Bilayered osteochondral hydrogel preparation

Sterile, rat-tail tendon-derived type I collagen (2.07 mg/ml of protein in 0.6 % acetic acid, First Link Ltd., West Midlands, UK) and ultrapure CTS powder [DDA: 79.8 %, M_w: 328 kDa, Ultrasan™, BioSyntech Ltd., Montreal, QC, Canada (now Piramal Healthcare, Laval, QC, Canada)] were used as starting materials. Coll/CTS hybrid hydrogels of relative compositions of 1:1 and 33:1 (w/w) were developed by dissolving 27 and 0.8 mg of CTS, respectively, in acetic

acid (2.2 ml/0.1 M) and stirring overnight at 4 °C. Coll/CTS solutions were prepared by the addition of 12.8 ml collagen solution (27 mg) under gentle stirring at 4 °C. Coll/CTS self-assembly was achieved by mixing the solution with X10 minimum essential medium (MEM; Sigma Aldrich, Ottawa, ON, CA) at a ratio of 4:1 and neutralized with 5 M NaOH, as previously reported [374, 398]. The bilayered scaffolds were fabricated in a two-step procedure (Fig. 6.1A), where 0.5 ml of neutralized Coll/CTS 1:1 solution was pipetted first into a circular mould and left to start the self-assembly process at 37 °C for 5 min, prior to the injection of 0.5 ml of the second layer (Coll/CTS 33:1). Complete gelation was achieved by allowing the solutions to set at 37 °C in a 5 % CO_2 incubator for 30 min. Post-gelation, hydrogels were removed from the moulds and dense bilayered gels were produced by PC, as previously reported [16]. Briefly, highly-hydrated gels (6 mm height; 16 mm in diameter) were placed on a stack of blotting paper, nylon mesh and metal mesh to allow for capillary fluid flow, and subjected to PC using an unconfined compressive stress of 0.5 kPa for 5 min, to remove the excess casting fluid. After processing, the orientation of the construct was maintained throughout the study, with the top layer being the cartilage-like Coll/CTS 1:1 layer.

The solid weight percent and collagen fibrillar density before and after PC were measured by weighing the gels before and after freeze-drying for 24 hours at -102 °C and 13 mTorr (BenchTop K freeze dryer, VirTis, SP Industries, Gardiner, NY, USA), and calculated according to the following equations:

$$Solid\ weight\ percent = \frac{Total\ solid\ content\ (g)}{(Total\ solid\ content\ (g) + water\ (g))} \times 100 \quad (1)$$

and

$$Collagen\ fibrillar\ density\ (\%) = \frac{Collagen\ (g)}{(Total\ solid\ content\ (g) + water\ (g))} \times 100 \quad (2)$$

6.3.2 Structural characterization

The morphology of the bilayered hydrogels was assessed by scanning electron microscopy (FEG-SEM Model S-4700, Hitachi High Technologies America, Pleasanton, CA, USA). Gels were fixed overnight at 4 °C in a solution of 4 % paraformaldehyde and 2 % glutaraldehyde, in 0.1 M sodium cacodylate buffer. Fixation was followed by dehydration over 15 min in a series of graded ethanol solutions, and critical-point drying (Ladd Research Industries, Williston, VT, USA). SEM was performed on Au/Pd sputter-coated samples (Hummer IV Sputter Coater, Ladd Research Industries, USA).

6.3.3 Cell culture

RCJ3.1C5.18 nontransformed mesenchymal clonal chondrogenic cell line isolated originally from foetal rat calvaria (RCJ) was kindly provided by Dr. Jane E. Aubin (University of Toronto, Ontario, Canada). Cells were cultured and passaged once a week in a chondrogenic medium composed of α-MEM with ribonucleosides and deoxyribonucleosides (Gibco-Invitrogen, Grand Island, NY, USA), containing 1 % penicillin/streptomycin (Gibco), 10^{-7} M dexamethasone (DEX, Sigma, St. Louis, MO, USA) and 15 % v/v of foetal bovine serum (FBS; Hyclone, Thermo Scientific, Logan, UT, USA), named α-MEM-HDEX.

MC3T3-E1 murine calvarial osteoprogenitor cells (subclone 14) were kindly provided by Dr. Renny T. Franceschi (University of Michigan, Ann Arbor, MI, USA). Cells were cultured and passaged once a week in MEM (Gibco-Invitrogen) containing 1 % penicillin/streptomycin (Gibco), 2 mM L-glutamine (Gibco), 0.225 mM aspartic acid (Sigma), and 10 % v/v of FBS (Hyclone, Thermo Scientific). Both cell types were incubated at 37 °C in a 5 % CO_2 humidified incubator and the medium was changed at 2-day intervals.

6.3.4 Cell seeding and optimization of co-culture conditions

RCJ and MC3T3-E1 cells were mixed with Coll/CTS 1:1 and Coll/CTS 33:1 solutions, respectively, at a density of $3x10^5$ cells/ml of Coll/CTS solution prior to

gelation and PC. During the fabrication of the bilayered hydrogel, both neutralized solutions were kept on ice to avoid early polymerization. Subsequently, gels were cast as stated above (Fig. 6.1). After PC, the dense bilayered hydrogels were transferred to 12-well plates and cultured under static conditions up to 35 days. Optimization of culture medium to maximize chondrocyte and osteoblast differentiation was assessed by culturing the constructs in three different media formulations containing 10^{-7}-10^{-9} M DEX, 50 μg/ml ascorbic acid (AA, Sigma) and 10 mM β-glycerolphosphate (βGP, Sigma). AA and βGP were supplemented to enhance collagen synthesis and MC3T3-E1 differentiation as well as calcium deposition, respectively. DEX was supplemented to enhance RCJ differentiation and cell aggregate formation. Specifically, α-MEM supplemented with 10^{-7} M DEX, AA and βGP (α-MEM-HDEX), α-MEM supplemented with 10^{-9} M DEX, AA and βGP (α-MEM-LDEX), and MEM supplemented with 10^{-7} M DEX, AA and βGP (MEM-LDEX) were prepared and tested on the bilayered gel. Medium changes were performed at 2-days intervals.

Optimal medium formulation was selected based on its ability to support both chondrocyte and osteoblast differentiation. RCJ cell differentiation was assessed by GAG quantification, whereas MC3T3-E1 cell differentiation was evaluated by alkaline phosphatase (ALP) activity and calcium deposition. The optimal medium formulation was then selected for cell viability studies, RCJ and MC3T3-E1 gene expression profiles, histological and immunohistochemical analyses.

6.3.5 Biochemical analyses

Quantification of DNA and GAG content was performed using triplicate samples at days 1, 7, 14, 21, 28 and 35 as previously reported [378, 398]. Briefly, samples were washed with phosphate-buffered saline solution (PBS; Wisent, St. Bruno, QC, Canada) and freeze-dried for 24 hours followed by digestion with papainase solution (100 μg/ml papain from papaya latex (Sigma), 5 mM L-cysteine in PBE buffer (100 mM Na_2HPO_4, 5 mM Na_2EDTA, pH 7.5)) for 18

hours at 60 °C. Papain-digested constructs were centrifuged and the supernatant was immediately used for DNA quantification. A standard curve was generated using known amounts of calf thymus DNA (0-1 μg/ml) dissolved in PBE buffer. The HOECHST 33258 dye (Sigma) was added to the standards and samples prior to reading absorbance values at 360 nm excitation and 460 nm emission in a microplate reader (FLUOstar OPTIMA, BMG Labtech, Offenburg, Germany). The background fluorescence of the scaffolds was accounted for by subtracting the values of the acellular scaffolds.

For GAG quantification, the dimethyl-methylene blue (DMMB) reagent solution (40 mM NaCl; 40 mM glycine; 46 mM DMMB, pH 3) was added to the sample supernatant and standards prior to reading absorbance at 520 nm in a microplate reader equipped with two onboard reagent injectors. The results were obtained by extrapolating from the standard curve using chondroitin sulfate from shark cartilage (Sigma).

ALP activity and calcium quantification were measured in triplicates from the supernatant and cell lysate, respectively, at days 1, 7, 14, 21, 28 and 35, as previously reported [374]. Briefly, scaffolds were washed with PBS and solubilised in 10 mM Tris (pH 7.4), 0.2 % IGEPAL (Sigma), and 2 mM phenylmethylsulfonyl fluoride, followed by sonication and centrifugation. ALP activity was determined colorimetrically using a freshly prepared substrate solution (SIGMAFAST p-nitrophenyl phosphate and Tris buffer tablets; Sigma). The absorbance was read at 405 nm using a microplate reader. Calf intestinal ALP (Sigma) was used as a standard.

To assess calcium levels, the scaffold was decalcified with 0.5 N HCl for 1 hour at 4 °C on a rotator. Calcium levels were determined by measuring the supernatant spectrophotometrically (absorbance at 595 nm) from triplicate readings using a calcium assay kit (Diagnostic Chemicals Limited, Oxford, CT, USA) [399].

6.3.6 Cell viability and morphology

Cell viability (estimated pre-compression population of 1.2 x 10^5 cells/layer) was evaluated using a confocal laser scanning microscopy (CLSM, Carl Zeiss, LSM5 Exciter, Toronto, ON, Canada) prior being exposed to the Live/Dead® reagent containing 1 μM calcein AM and 2 μM ethidium homodimer-1 (EthD-1) in PBS (Invitrogen, Carlsbad, CA, USA). Maximum-intensity projections of the confocal z-stacks along the entire thickness of the dense scaffolds and 3D ortho-representations were obtained using 5 μm-thick slices with ImageJ software (1.42q, Rasband W, National Institutes of Health, Bethesda, MD, USA). Orthogonal sections were obtained using Zeiss LSM Image Browser software (Carl Zeiss, version 4.2.0.121, Germany).

6.3.7 RNA extraction and semi-quantitative RT-PCR

Semi-quantitative RT-PCR analysis was applied to measure mRNA levels of RCJ and MC3T3-E1 cells cultured within bilayered hydrogels. Cellular and acellular scaffolds in triplicates were cultured as described above and rinsed with PBS at days 1, 7, 14, 21, 28 and 35. A parallel study was performed to evaluate the characteristic gene expression trends of chondrocytes and osteoblasts cultured independently within Coll/CTS 1:1 and Coll/CTS 33:1, respectively, as compared to gene expression levels of cells simultaneously cultured within the bilayered scaffold up to 14 days.

Samples were removed from -80 °C and freeze-pulverized using a Biopulverizer (BioSpec Products Inc., Bartlesville, OK, USA). Powders were used for RNA extraction by the cetyltrimethylammonium bromide (CTAB) method, as previously described [33]. CTAB extraction buffer was comprised of 2 % CTAB (Sigma), 2 % polyvinylpyrrolidone (PVP 40; Sigma), 1.4 M sodium chloride (NaCl, Fisher Scientific), 100 mM Tris–HCl (pH 8.0; Fisher Scientific), 20 mM EDTA (Sigma) in diethylpyrocarbonate (DEPC) water, supplemented with 1 % β-mercapthoethanol (Fisher Scientific). Sample powders were thoroughly mixed with pre-warmed 600 μl of CTAB buffer and followed by

mixing with an equal volume of chloroform. The chloroform/CTAB mixture was centrifuged and the supernatant was extracted and mixed with an equal amount of isopropanol (Sigma), followed by 15 min centrifugation. The supernatant was discarded and 1 ml of 75 % ethanol in DEPC water was added to the pellet. The mix was transferred to a RNeasy spin column from Qiagen RNeasy mini kit for plants (Qiagen, Valencia, CA, USA), followed by buffer washes and RNA elution, as recommended in the manufacturer's protocol. RNA was treated with DNAse (New England Biolabs, Ontario, Canada), and 1 μg was reversed-transcribed and amplified by gene-specific primers using the Superscript III One-Step RT-PCR system with Platinum™ Taq kit (Invitrogen) in a thermocycler (MyClycler, BioRad, CA, USA). Primers (0.5 μM, Invitrogen) for aggrecan (*Acan*) and collagen type II (*Col2a1*) [34] were used to determine the expression levels from mRNA extracted from RCJ cells. mRNA extracted from MC3T3-E1 was used to determine the expression level of collagen type I (*Col1a1*), tissue-nonspecific ALP (*Akp2*) and *Mmp-13* [400]. GAPDH primers were prepared according to Foster *et al.* [36], and used as a housekeeping gene for data normalization (Table 6.1). PCR products were analyzed by electrophoresis on a 2 % agarose gel with 1.5 % ethidium bromide (E-Gel®, Invitrogen) and amplimer size was estimated with a 50 bp DNA ladder (Invitrogen). Band volume quantification was performed using ImageJ. Expression levels were normalized to the band volume for GAPDH in triplicate RNA samples.

Table 6.1: Primers used to detect RCJ3.2C5.18 chondrocytes and MC3T3-E1 osteoblast markers in bilayered scaffolds.

Gene product	*Primers (F=Forward; R=Reverse)*	*Annealing T/cycles*
GAPDH	F 5'-TGTGAACGGATTTGGCCGTA-3' R 5'-GGAAGGCCATGCCAGTGAGC-3'	55 °C/35
	RCJ3.1.C5.18	
Acan	F 5'-ATCGAAGGGGACTTCCGCTG-3' R 5'-ATCACCACACAGTCCTCTCCG-3'	62 °C/35
Col2a1	F 5'-GGAAGACCATCATCGAGTACC-3' R 5'-CCCTATGTCCACACCAAATTCC-3'	50 °C/35
	MC3T3-E1	
Col1a1	F 5'-GAGGCATAAAGGGTCATCGTGG-3' R 5'-CATTAGGCGCAGGAAGGTCAGC-3'	55 °C/30
Akp2	F 5'-CCAAGACGTACAACACCAACGC-3' R 5'-AAATGCTGATGAGGTCCAGGC-3'	45 °C/35
Mmp-13	F 5'-CCCCACCCCATACATCTGAA-3' R 5'-CTTCTGGTCTTCTGGCACAC-3'	53 °C/30

6.3.8 Histological analysis

Histological analyses were performed at day 35. Scaffolds were rinsed with PBS and fixed in 10 % neutral buffered formalin overnight at 4 °C. Fixation was followed by dehydration over 15 min in a series of graded ethanol solutions and embedded in paraffin. Sections of 5 µm thickness were cut through the center and edges of the scaffold, placed on positively charged glass slides, and stained with Safranin O/Fast Green or with Haematoxylin/Eosin (H&E) staining.

6.3.9 Immunohistochemical analysis

Unstained paraffin-embedded sections were used for Coll II and aggrecan immunohistochemistry. Deparaffinization was obtained by immersing the glass slides in a series of xylene/ethanol solutions. Antigen retrieval was performed by immersing the slides in Tris/EDTA pH 9.0 and left in a furnace at 60 °C for 24 hours. After heat-induced epitope retrieval, the samples were washed in PBS and digested with 2 % hyaluronidase (Sigma) for 30 min. After washing 3X with 0.1 % bovine serum albumin (BSA, Sigma) the sections were permeabilized with 0.25

% Triton X-100 (Sigma) for 10 min. Subsequently, the slides were placed in 2 % BSA (blocking buffer) for 30 min and then incubated overnight with rabbit anti-Coll II (1:100, Millipore, Billerica, MA, USA) or rabbit anti-aggrecan (1:100, Millipore) antibodies. The slides were further incubated with AlexaFluor 488-labelled goat anti-rabbit IgG (1:200, Invitrogen) or tetramethylrhodamine isothiocyanate goat anti-rabbit IgG (1:200, TRITC, Sigma) for 1 hour followed by nucleic acid staining with EthD-1 (1:3000; Invitrogen). Finally, samples were coverslipped with mounting medium (Geltol, Thermo Electron Corporation, Pittsburgh, PA, USA). Sections of acellular and cellular scaffolds processed without primary antibody were used as negative controls. Z-stacks of fluorescent immunoreactivity towards Coll II and aggrecan of acellular and cellular scaffolds were acquired using a CLSM. Maximum-intensity projections of the scaffolds were generated using ImageJ.

6.3.10 Statistical analysis

All data are presented as mean values ± standard deviation of the mean (± SD). Statistical significance between groups and between time points was determined using a one-way ANOVA with a Tukey-Kramer's post-hoc multiple comparison of means. The level of statistical significance was set at $p = 0.05$.

6.4 RESULTS

6.4.1 Structural evaluation of the osteochondral scaffold

There was a 14- and 36-fold increase in solid weight percent and collagen fibrillar density of Coll/CTS 1:1 and Coll/CTS 33:1 layers (Table 6.2), respectively.

Table 6.2: Solid weight percent and collagen fibrillar density of the cartilaginous-like layer (Coll/CTS 1:1) and bone osteoid-like layer (Coll/CTS 33:1) before and after PC.

Osteochodral layer	Solid weight percent (%)		Collagen fibrillar density (%)	
	Before PC	After PC	Before PC	After PC
Coll/CTS 1:1	0.42 (± 0.02)	5.84 (± 0.47)	0.21 (± 0.01)	2.92 (± 0.23)
Coll/CTS 33:1	0.24 (± 0.02)	8.87 (± 0.81)	0.24 (± 0.02)	8.61 (± 0.79)

SEM micrographs of the side edge of the bilayered hydrogel show the stratified structure of the scaffold revealing two morphologically distinct layers (Fig. 6.1B, *i*). Gross examination of the bilayered hydrogel by SEM revealed no scaffold delamination after processing, confirming the close approximation and integration of the two layers. The top view of the cartilaginous-like layer exhibited randomly oriented nanofibrils of collagen with homogenously dispersed CTS throughout the open-pore microstructure (Fig. 6.1B, *ii*). The bottom view of the osteoid-like layer, having lower CTS content, showed a more compacted structure (Fig. 6.1B, *iii*).

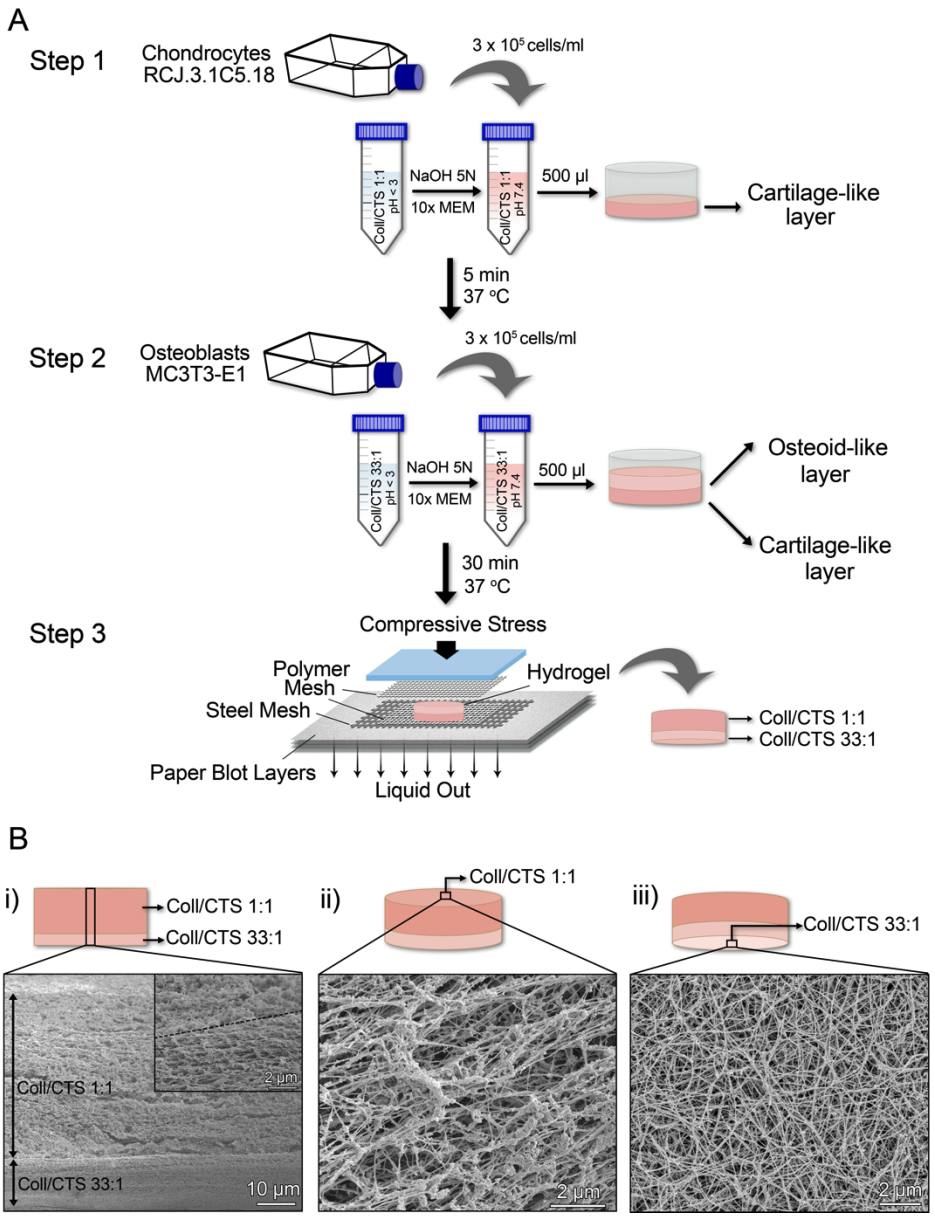

Figure 6.1: (A) Schematic of the simultaneous production of bilayered dense Coll/CTS osteochondral scaffolds. Step 1: To form a cartilaginous-like layer, a Coll/CTS 1:1 (w/w) solution containing RCJ cells ($3x10^5$ cells/ml) was placed in a mould and self-assembly was initiated for 5 min at 37 °C in a humidified incubator. Step 2: To form an osteoid-like layer, MC3T3-E1 osteoprogenitor cells ($3x10^5$ cells/ml) seeded within a Coll/CTS 33:1 (w/w) solution was then dispersed on top of the cartilaginous-like layer and the bilayered scaffold was transferred to a humidified incubator set at 37 °C for 30 min to complete the polymerization process. Step 3: Dense scaffolds were produced by PC (0.5 kPa for 5 min). (B) SEM image of the side edge of an acellular dense bilayered hydrogel after PC. SEM micrographs revealed two morphologically distinct, but integrated, layers (*i*). Top and bottom surfaces show the microstructure of Coll/CTS 1:1 (*ii*) and Coll/CTS 33:1 (*iii*), respectively.

6.4.2 Influence of culture conditions on chondrocyte and osteoblast differentiation evaluated by biochemical assays

To optimize the culture medium and concentrations of supplemental reagents (*i.e.* DEX) necessary for the simultaneous growth and differentiation of RCJ and MC3T3-E1 cells seeded in their respective layers, bilayered constructs were co-cultured either in α-MEM-HDEX, α-MEM-LDEX or MEM-LDEX for up to 35 days. The content of DNA, GAG, calcium and ALP activity within the scaffold were measured as quantitative indicators of cell differentiation (Fig.6.2). Total DNA content of the cells seeded within the bilayered construct increased up to day 21, for each medium formulation tested (Fig. 6.2A). In particular, the DNA content in scaffolds cultured in MEM-LDEX was significantly higher at each time point up to day 21, compared to α-MEM-HDEX and α-MEM-LDEX ($p < 0.05$). At day 35, a significant decrease was observed in α-MEM-LDEX and MEM-LDEX, compared to α-MEM-HDEX ($p < 0.05$). This effect can be attributed to a reduction in the DEX concentration, which is known to affect chondrocyte proliferation [37]. Compared to day 1, the DNA content was 6-fold higher in α-MEM-HDEX and 3-fold-higher in α-MEM-LDEX and MEM-LDEX at day 35.

GAG content was used as an indicator of chondrogenic differentiation within the cartilaginous-like layer (Fig. 6.2B), which was significantly increased up to day 14 for all medium formulations. In the case of scaffolds cultured in α-MEM-HDEX GAG content continued to increase over time up to day 35. Scaffolds cultured in α-MEM-LDEX and MEM-LDEX reached a plateau at day 21 and then decreased at day 35, as shown for DNA content (Fig. 6.2A). GAG content between the α-MEM-LDEX and MEM-LDEX conditions at day 35 was not statistically different ($p > 0.05$).

Calcium content and ALP activity were used as indicators of osteoblastic differentiation of MC3T3-E1 cells seeded within the osteoid-like layer. Although, RCJ cells may also induce collagen mineralization in cell culture, a regular supplementation of a high concentration of extracellular calcium (2.9 mM $CaCl_2$) is required [38]. Thus, the total calcium content measured within the bilayered

hydrogel was derived solely from the osteoblast-seeded layer. In addition, ALP activity was measured within a RCJ-seeded Coll/CTS 1:1 layer in the absence of osteoblasts for up to 14 days in order to confirm that the ALP activity measured within the bilayered construct (two orders of magnitude higher) was exclusively derived from the osteoblast-seeded layer (Supplementary Fig. 6.1).

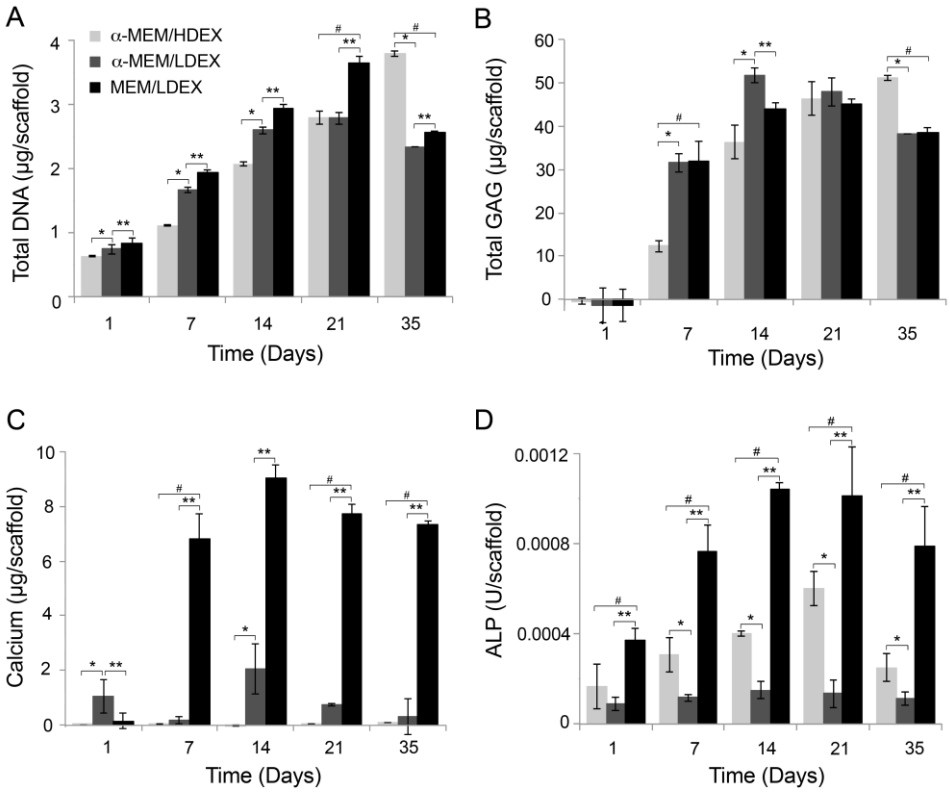

Figure 6.2: Biochemical analysis of cell proliferation as well as chondrogenic and osteogenic differentiation in a bilayered dense Coll/CTS hydrogel cultured for up to 35 days under three different medium formulations: α-MEM/HDEX, α-MEM/LDEX and MEM/LDEX. (A) Total DNA content measured by Hoechst 33258 fluorimetric detection. (B) GAG quantification via spectrophotometry with DMMB. (C) Quantification of calcium deposition within the osteogenic-layer by MC3T3-E1 cells. (D) ALP activity of MC3T3-E1 within the Coll/CTS 33:1 layer. * indicates a statistical significant difference ($p < 0.05$) between α-MEM/HDEX and α-MEM/LDEX. ** indicates a statistical significant difference ($p < 0.05$) between α-MEM/LDEX and MEM/LDEX. # indicates a statistical significant difference ($p < 0.05$) between α-MEM/HDEX and MEM/LDEX. Data are represented as the mean ± SD, n=3.

Culturing of the scaffolds in chondrogenic medium (α-MEM-HDEX) resulted in no significant calcium deposition (Fig. 6.2C). A two-order of magnitude reduction in the concentration of DEX (10^{-9} M, α-MEM-LDEX) resulted in a slight increase in calcium content. However, the content of calcium within the bilayered hydrogel cultured with MEM-LDEX significantly exceeded

that of α-MEM-HDEX (up to 9 ± 0.5 μg/scaffold at day 14, $p < 0.05$). No statistical difference was found in calcium content between days 14 and 35. Consistent with calcium quantification, MEM-LDEX medium significantly increased ALP activity, compared to α-MEM-HDEX and α-MEM-LDEX (Fig. 6.2D). ALP activity increased with time up to day 14 and remained unchanged up to day 35.

Therefore, MEM-LDEX provided the most suitable culture medium for the simultaneous differentiation of both RCJ and MC3T3-E1 cells. In view of this, MEM-LDEX formulation was chosen as the optimal culture medium for further studies of chondrocyte and osteoblast growth and differentiation in bilayered scaffolds.

6.4.3 Cell viability and morphology

The viability and morphology of RCJ and MC3T3-E1 cells were assessed using the Live/Dead® staining assay. CLSM was used to obtain images of labelled cells along the entire thickness of the bilayered scaffold (Fig. 6.3). Z-stack reconstruction of horizontal image slices covering the entire height of the ~200 μm scaffold revealed that green fluorescent calcein-AM-labelled cells were uniformly distributed throughout the hybrid scaffold (Fig. 6.3A) and the two layers were readily distinguished by the unique morphology of RCJ (Fig. 6.3B and C) and MC3T3-E1 cells (Fig. 6.3D and E) at day 7 day in culture. RCJ cells within the cartilaginous-like layer formed cartilage-like aggregates with spherical cell morphology, as early as day 7 (Fig. 6.3B, white arrows). In contrast, osteoblasts displayed a spindle-shaped morphology. Consistent with DNA quantification (Fig. 6.2A), a high density of viable cells was observed throughout the bilayered hydrogel after 35 days in culture, as evidenced by the limited number of EthD-1-stained cell nuclei. Maximum-intensity projections of the confocal z-stacks of chondrocytes and osteoblasts seeded within the top and bottom layers of the bilayered scaffold at day 35, are shown in Figs. 6.3F and G, respectively.

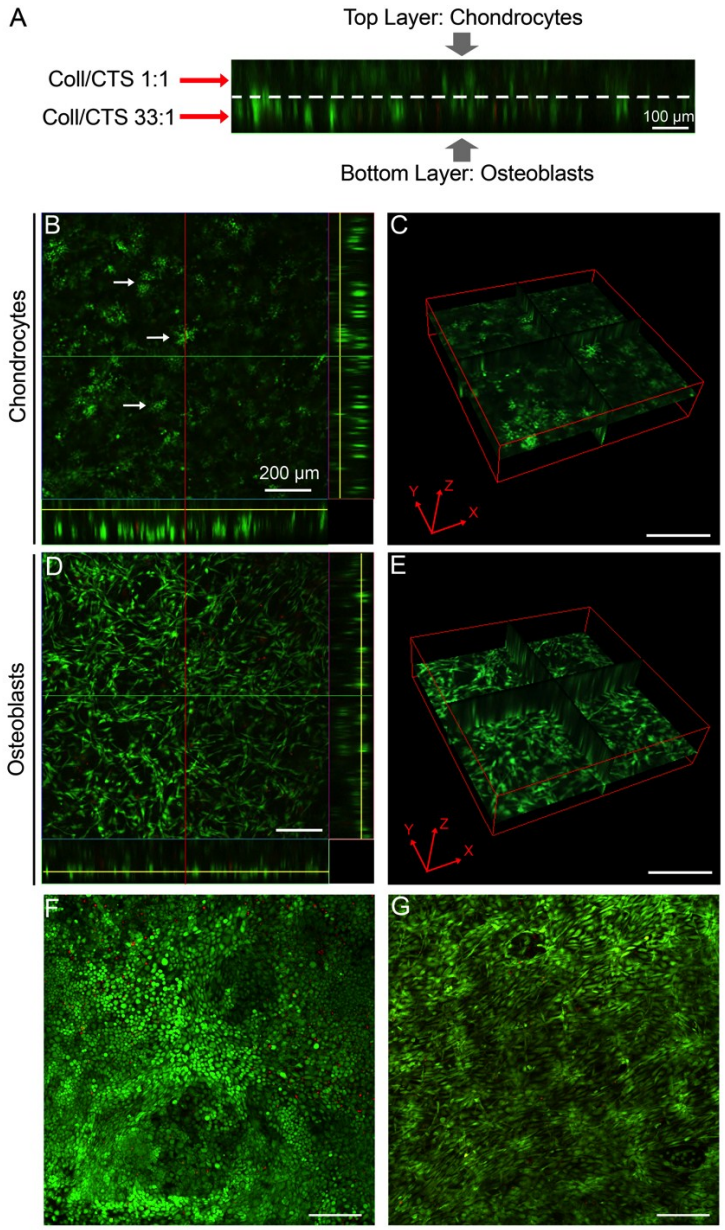

Figure 6.3: Analysis of cell viability and morphology within bilayered hydrogels. CLSM maximum-intensity projections covering the entire scaffold thickness were collected up to 35 days. Green fluorescent calcein-AM-labelled cells represent viable cells with no membrane disruption, and red fluorescent EthD-1 positive nuclei indicate cell necrosis and late apoptosis. (A) Cross-section of a 3D image stack reconstruction of the bilayered hydrogel indicating a homogeneous distribution of RCJ and MC3T3-E1 cells within top Coll/CTS 1:1 and bottom Coll/CTS 33:1 layers, respectively, at day 7 in culture (scale bar = 100 µm). (B and D) Ortho-representation of the 3D image stack reconstruction at two different heights, indicating cell viability and the characteristic morphology of (B) RCJ (cartilage-like aggregates were detected as early as day 7 (white arrows, scale bar = 200 µm)) and (D) MC3T3-E1 cells. (C and E) Ortho-representation of the confocal z-stack showing (C) cartilaginous-like top and (E) osteoid-like bottom layers of the osteochondral scaffold. (F and G) Maximum-intensity projection of the confocal z-stacks along the entire osteochondral layer showing cell viability in the (F) cartilaginous-like layer and (G) in the osteoid-like layer, at day 35 (Scale bar = 200 µm).

6.4.4 Detection of chondrogenic and osteogenic marker genes by semi-quantitative RT-PCR

Simultaneous chondrogenic and osteogenic differentiation of RCJ and MC3T3-E1 cells within the bilayered scaffold was determined by semi-quantitative RT-PCR for the expression of chondrocytic (*Col2a1* and *Acan*) and osteoblastic (*Col1a1, Akp-2* and *Mmp-13*) marker genes up to 35 days in culture (Fig. 6.4A). In particular, after normalizing gene expression relative to the GAPDH housekeeping gene, the mRNA transcription level of *Acan* within the dense hydrogel increased 5.3-fold at day 14 compared to day 1 (Fig. 6.4B; $p < 0.05$). The expression of *Acan* decreased at day 21 and remained stable thereafter. The chondrocyte-specific *Col2a1* mRNA was upregulated by 3.4-fold at day 7, followed by a downregulation at day 28, where it remained unchanged for up to 35 days (Fig. 6.4C).

The expression of *Akp2* within the dense bilayered hydrogel increased up to 2.2-fold at day 7 and remained stable up to day 21, followed by a decrease at day 28 (Fig. 6.4D). *Col1a1,* mRNA levels within the dense bilayered hydrogel increased by 8.4-fold at day 14, compared to day 1, followed by a decrease at day 21, where it remained unchanged for up to 35 days (Fig. 6.4E). Finally, *Mmp-13* expression increased at day 14 with a 1.6-fold increase above day 1 and decreased thereafter (Fig. 6.4F).

To control for the gene expression pattern of each cell type, a parallel experiment was performed using independently cultured dense cartilage-like and osteoid-like layers. Both RCJ cells (Supplementary Fig. 6.2A and B) and MC3T3 (Supplementary Fig. 6.2C-E) exhibited similar expression levels for each gene of interest when cultured either independently or simultaneously, thereby demonstrating the specificity of the PCR primers for the unique genes expressed by each cell type, and no overt effect of co-culture on gene-expression patterns.

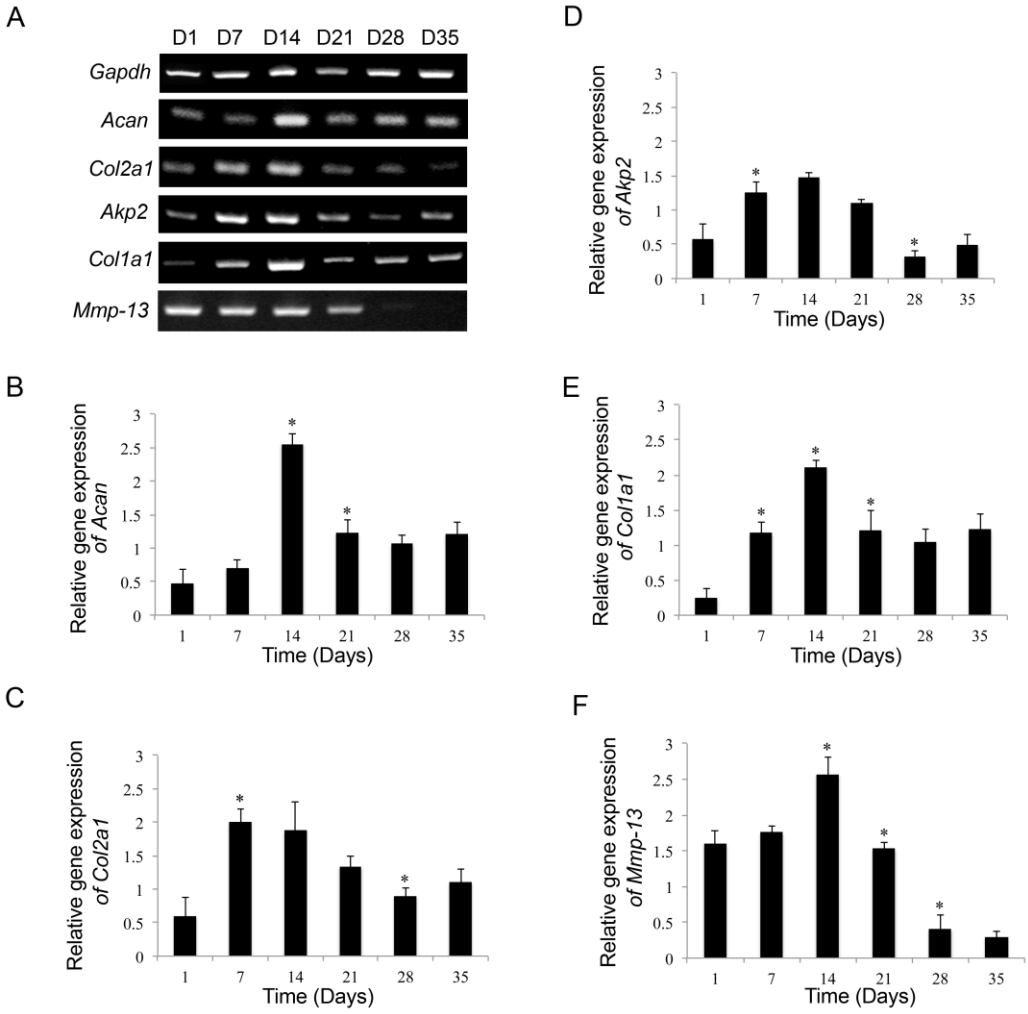

Figure 6.4: (A) RT-PCR analysis of cartilage and bone-specific gene expression of RCJ and MC3T3-E1 cells cultured for 35 days. Gene expression of (B) *Acan* and (C) *Col2a1*, from mRNA extracted from RCJ cells, revealed increased gene expression throughout the 35-day period, with peak expression for each gene at days 7 and 14, respectively. Gene expression of (D) *Akp2*, (E) *Col1a1* and (F) *Mmp-13*, three osteogenic markers, were detected at all times during the 35-day culture period. * indicates a statistical significant difference ($p < 0.05$) between the previous time point within the same group. Data are represented as the mean ± SD, n=3.

6.4.5 Histological analyses of the dense bilayered hybrid scaffold

Histological H&E staining confirmed the matrix integration at the interface of the bilayered hydrogels after 35 days in culture (Fig. 6.5). Transverse histological sections revealed two distinct layers of 154.7 ± 8.7 and 73.4 ± 8.6 μm in thickness for Coll/CTS 1:1 and Coll/CTS 33:1, respectively. Cells within the top layer (Figs. 6.5A and B) exhibited a round chondrocytic morphology that is characteristic of cells located within lacuna in native cartilage (black arrows).

There was no indication of de-differentiation into a fibroblastic phenotype as shown by an absence of flattened or ellipsoid-shaped cells. Cells seeded within the bottom layer displayed a spindle-shaped morphology, characteristic of the osteoblast/osteocyte lineage. The absence of delamination between the two layers was also confirmed in Safranin O/Fast Green-stained sections (Figs. 6.5C and D). Horizontal sections of Coll/CTS 1:1 layer stained for anionic GAG chains of proteoglycans revealed strong positive cellular and extracellular GAG staining, indicating chondrocyte synthesis of cartilage-like matrix (Figs. 6.5E and F).

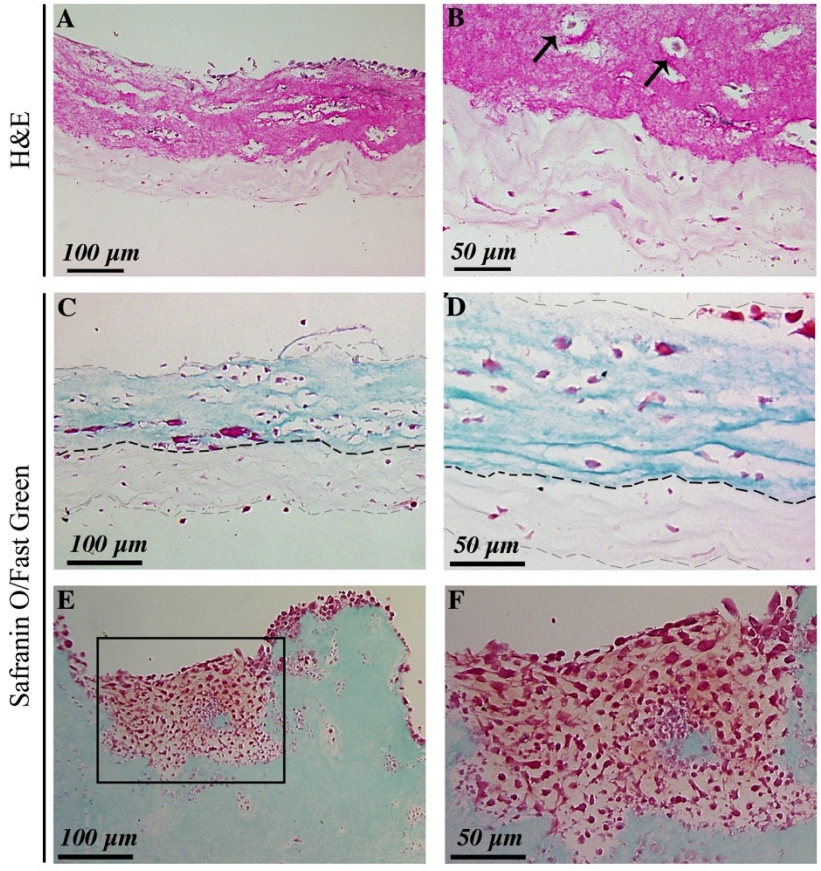

Figure 6.5: Histological analysis of chondrocytes and osteoblasts seeded within a bilayered scaffold after 35 days. Sections of paraffin-embedded scaffolds were stained with either (A, B) H&E or (C-F) Safranin O/Fast Green for GAG staining. (A) Histological examination of the construct shows two distinct layers, with greater H&E staining intensity present within the top cartilaginous-like layer, which contains greater amounts of CTS compared to the underlying osteoid-like layer. (B) Higher magnification image showing rounded chondrocyte-like cells embedded in lacuna (black arrows), a feature characteristic of native cartilage. (C, D) Cross-section of the bilayered hydrogel showing GAG localization (Safranin O staining, red) to chondrocytes in the top cartilaginous-like layer. (E, F) Horizontal sections near the surface of the scaffold in the cartilaginous-like layer showing aggregates of chondrocytes positively stained for Safranin-O, which detects cellular and extracellular GAGs.

6.4.6 Immunohistochemical analysis of chondrogenic differentiation within the cartilaginous-like layer

Immunohistochemical analyses were performed to assess the differentiation of chondrocytes and extend the semi-quantitative RT-PCR and histological findings. The newly synthetized ECM by RCJ cells was immunohistochemically localized within the cartilaginous-like layer by CLSM detection of Coll II and aggrecan immunoreactivity after 35 days in culture (Fig. 6.6). Positive immunoreactivity for Coll II was distributed extensively throughout the Coll/CTS 1:1 layer (Figs. 6.6A and B). A high magnification image shows the immunofluorescence-staining pattern of Coll II in the cartilaginous-like aggregates in greater detail (Fig. 6.6B). Antibodies directed against rat Coll II did not exhibit any immunoreactivity towards acellular scaffolds prepared using rat Coll. Furthermore, CLSM analysis of the bilayered hydrogel also revealed cell-associated aggrecan immunofluorescence within the Coll/CTS 1:1 layer (Fig. 6.6C and D). Aggrecan immunostaining was localized to the extracellular space within the Coll/CTS matrix (Fig. 6.6C inset), as well as peripherally, surrounding chondrocytes within aggregates (Fig. 6.6D inset). The negative control, in which the primary antibody was omitted, showed no evidence of immunofluorescent staining (data not shown).

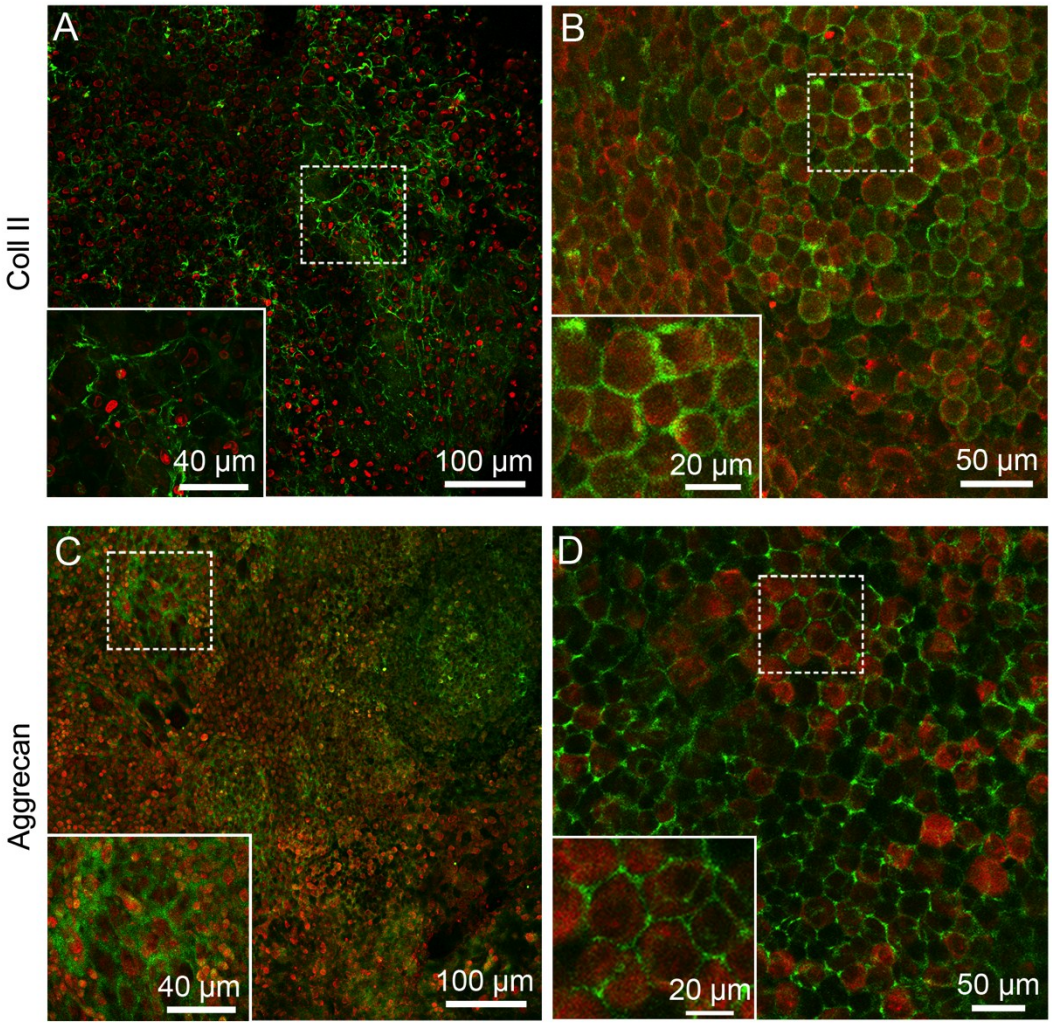

Figure 6.6: Immunohistochemical detection of cartilage-specific ECM proteins by CLSM analysis within the Coll/CTS 1:1 layer at day 35. (A, B) Horizontal paraffin sections through the cartilaginous-like layer seeded with RCJ cells immunostained for Coll II (green fluorescence). EthD-1 (red fluorescence) was used as a nuclear stain. (A) Maximum-intensity projection of extracellular Coll II immunoreactivity is extensively distributed throughout the cartilaginous-like layer. (B) In other regions, chondrocytes are closely packed, showing peripheral positive immunostaining for Coll II. (C) Immunohistochemistry of the cartilaginous-like layer shows strong immunoreactivity for aggrecan (green) expressed by chondrocytes, with an extracellular localization. (D) In other regions, aggrecan immunoreactivity is localized at the cell periphery.

Detection of Coll II (red) and F-actin (green) was also performed on transverse and horizontal sections (Fig. 6.7A) to investigate Coll II distribution within the cartilage-like layer. In transverse sections of the bilayered hydrogel, positive immunostaining for Coll II was solely present in the top cartilaginous-like layer near surface-resident cells, showing antibody specificity for

chondrocyte-produced ECM (Fig. 6.7B). Images of immunostained F-actin (Fig. 6.7C) and Coll II (Fig. 6.7D) revealed the localization of Coll II surrounding the spherically-shaped chondrocytes, providing further evidence that the ECM protein was localized at the cellular periphery (Fig. 6.7E).

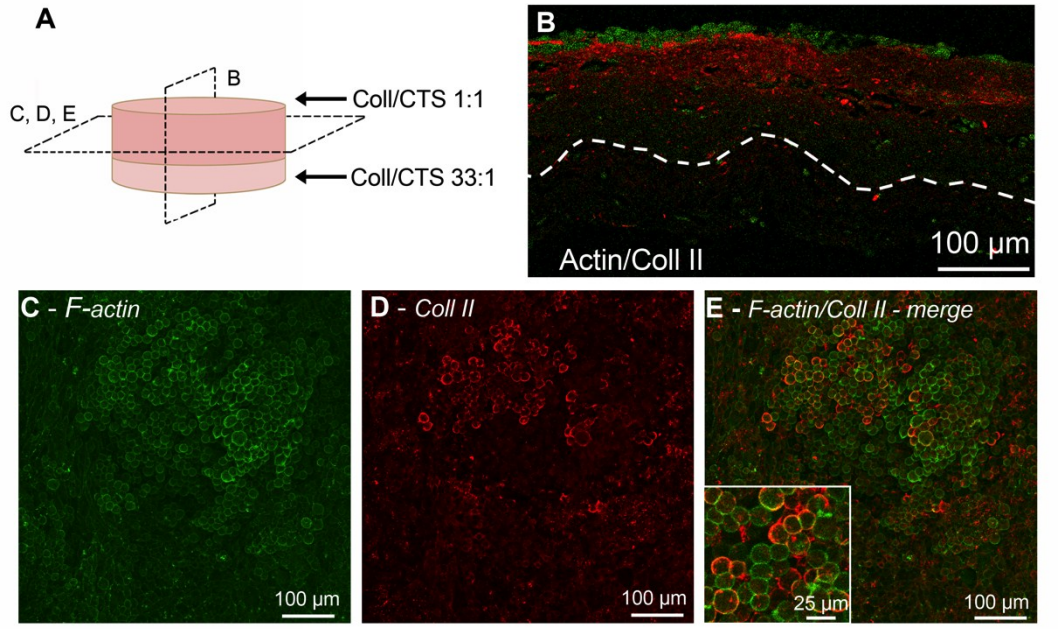

Figure 6.7: Maximum-intensity CLSM projections of immunofluorescent staining for F-actin (green) and Coll II (red) of chondrocytes seeded within the cartilaginous-like layer of the bilayered scaffold. Image planes for the subsequent panels are indicated in (A). (B) Coll II immunoreactivity (red) is greater in the upper regions of the cartilaginous-like layer near surface-resident chondrocytic cells (green). (C-E) F-Actin and Coll II staining in horizontal sections reveals the peripheral location of Coll II and F-actin in chondrocytes.

6.5 DISCUSSION

Regeneration of complex tissues comprising multiple cell types and highly organized ECM structures represents a major challenge for tissue engineering [74]. In particular, OTE relies on the fabrication of a bilayered scaffold strategy for the simultaneous replacement of the AC and the underlying subchondral bone that takes advantage of the rapid formation of an integrated graft-to-bone interface, as compared to a graft-to-cartilage interface [283]. In this study, a bilayered dense hydrogel was developed to model the complex osteochondral structure using two defined Coll/CTS weight ratios which approach those of

Coll/GAG in the native ECM of cartilage and bone, and support the simultaneous differentiation of RCJ and MC3T3-E1 cells seeded within distinct layers of the scaffold. By application of the PC technique, the solid weight percent and collagen fibrillar density of the scaffolds were increased towards physiologically relevant values approaching those found in native ECM. The scaffold design presented here mimics the unique characteristics of two distinct ECM environments rather than the development of a construct that attempts to fulfill the requirements of both cartilage and bone in a single structure [27].

In the present study, an effective and rapid strategy to homogenously seed chondrocytes and osteoblasts within different dense hydrogel layers was devised as part of the self-assembly process. Thus far, a limited number of integrated but heterogeneous hydrogel-based composite scaffolds have been described for the repair of complex stratified tissues with distinct populations of differentiated cells [316, 401, 402]. Elisseeff *et al.* [11] demonstrated that seeded chondrocytes are able to synthesize ECM in the upper, middle and lower zones of the stratified polyethylene glycol photopolymerized hydrogel. However, this approach has a limited remodelling capacity (*i.e.* nonbiodegradable) and lacks ECM-derived cellular signals (*i.e.* nonbiomimetic). Although a related yet degradable, nonbiomimetic oligo-polyethylene glycol fumarate-based scaffold supported tissue growth, the chemical cross-linking methods used for hydrogel polymerization may be cytotoxic [403]. In contrast, fully biomimetic and biodegradable compressed Coll scaffold rolls seeded with preconditioned MSCs induced cellular differentiation along chondrocytic and osteoblastic lineages within a single material for temporomandibular joint repair [316]. In another study, the repair of articular osteochondral defects in a porcine model using isolated autologous chondrocytes [404], led to the formation of neocartilage within both the cartilage layer and subchondral bone defect. This indicates that either a different cell source or simultaneous grafting of more than one cell type might be necessary, imparting several challenges to the field of OTE, such as the determination of optimal co-culture and scaffold seeding conditions [405].

Chondrogenic medium contains the synthetic glucocorticoid DEX that induces chondrogenesis and increases the number of cellular aggregates in a dose-dependent manner [406]. On the other hand, osteogenic medium contains AA and βGP, which induce the formation of a collagenous ECM, and promote calcium deposition, respectively [357, 407]. The presence of these three additives in the culture medium is necessary to support the maintenance of stable chondrogenic and osteogenic phenotype in their respective layers during co-culture. However, high concentrations of DEX (10^{-7} M) have been shown to induce apoptosis in MC3T3-E1 cultures [408]. Therefore the concentration of DEX was decreased by two orders of magnitude to prevent osteoblast apoptosis while being sufficient to support cartilage-like aggregate formation. Although the mechanisms by which DEX regulates chondrogenic differentiation are unknown, it is proposed that DEX affects various complex regulatory and signaling networks associated with the ECM and intercellular interactions [409]. Based upon analyses of total DNA content, GAG synthesis, ALP activity and calcium content, MEM-LDEX was chosen as the optimal culture medium for the study of the simultaneous growth and differentiation of both RCJ and MC3T3-E1 cells. The optimization of the culture medium was essential to achieve the phenotypic expression of both cell types as they differentiated within their respective scaffold layers.

CLSM analysis of RCJ and MC3T3-E1 cells demonstrated their long-term viability up to 35 days, as indicated by the high density of green-fluorescent calcein-AM-labelled cells. Calcein-AM staining also allowed for evaluation of cell morphology within the top and bottom layers of the bilayered hydrogel, depicting the characteristic rounded shape of RCJ cells as previously reported [377, 398], as well as evidence of cartilage-like aggregate formation as early as 7 days. The bottom layer, on the other hand, presented distinctly different cells with spindle-shape morphology, characteristic of the MC3T3-E1 osteoblasts [410].

Cell differentiation under optimized co-culture conditions within the bilayered construct was investigated by analysis of tissue-specific gene expression

by semi-quantitative RT-PCR and analysis of ECM-characteristic components production up to 35 days. The effect of co-culture on the growth and phenotypic maintenance of chondrocytes and osteoblasts was first investigated in 2D monolayer culture by Lacombe-Gleize *et al.*[411], who showed an upregulation of the mitotic potential of chondrocytes upon exposure to factors secreted by osteoblasts. Similarly, a 3D model based on the sequential culture of osteoblasts seeded on top of a chondrocyte micromass also suggested that interaction between these two cell types modulates their phenotypes, as shown by reduced proteoglycan synthesis by chondrocytes as well as decreased matrix mineralization by osteoblasts [412]. Unlike previous studies, here the gene expression levels of both RCJ cells (*Col2a1* and *Acan*) and MC3T3 cells (*Col1a1*, *Akp-2* and *Mmp-13*) were unaffected during the 14-day culture period. This may be attributed to the CTS supporting both osteoblastic and chondrogenic differentiation.

The ability of the Coll/CTS 1:1 cartilaginous-like layer to support the growth and differentiation of RCJ cells and promote cartilage-like matrix formation was demonstrated by the positive Coll II immunoreactivity, Safranin O-staining and GAG content. The results obtained by biochemical, histological and immunohistochemical analyses were consistent with the expression of the chondrocytic phenotype at the gene level, as indicated by *Acan* and *Col2a1* markers, which were strongly expressed throughout the duration of the 35-day study. *Col2a1* and *Acan* expression decreased after 14 days, which may be a late indicator of chondrocytes maturation [413]. A similar finding was reported previously [398], where the incorporation of CTS into a dense Coll hydrogel was found to stabilize the chondrocyte phenotype and increase the synthesis of cartilage-specific ECM components. In addition to analyses of ECM gene expression, confocal 3D reconstruction of the z-stack images demonstrated the pericellular deposition of Coll II and aggrecan, particularly within cartilage-like aggregates. Double staining for F-actin and Coll II confirmed the characteristic

round morphology of chondrocyte-like cells, as well as Coll II pericellular staining, consistent with this phenotype [414].

Osteoblasts seeded within a Coll/CTS 33:1 layer showed an increase in *Col1a1* and *Akp2* expression, two early differentiation markers associated with the osteoblastic differentiation phase [190, 191]. In particular, the upregulation of the mRNA expression of *Col1a1* at early time points is known to contribute to ECM synthesis and subsequent mineral deposition [191]. *Akp2* expression was in line with the onset of ALP enzymatic activity. Downregulation of *Akp2* at later time points was associated with the late osteoblast development phase, near the completion of bone ECM mineralization [190]. Indeed, the calcium content within the scaffolds was maximal (9-fold increase compared to day 1) at day 14, indicating that ALP expression and activity immediately precedes matrix mineralization where it serves to remove mineralization-inhibiting pyrophosphate [415]. The incorporation of CTS to dense Coll hydrogels has been shown to increase ALP activity, mineral deposition, and *Mmp-13* expression up to day 21 [374].

Mmp-13 (collagenase 3) is a member of a family of endopeptidases that cleave fibrillar collagens present in the ECM, and is in part responsible for matrix remodelling during tissue maintenance and repair [416, 417]. In the present study, *Mmp-13* mRNA expression was also elevated up to day 14, suggesting that the enzyme was active in degrading the Coll matrix as in normal physiological processes. *Mmp-13* was then downregulated at later time points when the calcium content within the scaffold was maximal, which is consistent with previous findings that suggest that *Mmp-13* may be involved in the mineralization process in foetal rat calvarial osteoblast culture [187]. Enzymatic degradation of the scaffold may contribute to remodelling as well as integration of the new tissue into the underlying subchondral bone *via* the creation of a bone-like layer through osteoblast-mediated mineral deposition. Ongoing studies will be necessary to quantify the performance of these scaffolds *in vivo*.

While assessment of the bilayered Coll/CTS hydrogel using a clinically relevant cell source is clearly important for clinical translation, the scope of the study conducted herein provides a strong proof-of-concept using two highly characterized and relevant cell lines grown simultaneously under well-defined conditions. Further validation of the model will be required prior to *in vivo* implantation, including the use of MSCs and specific assays to analyze the integration of the bilayered hydrogel. In addition, the PC technique [16] has recently been implemented to develop dense scaffolds using a US Food and Drug Administration approved collagen source (*i.e.* bovine dermis type I collagen) [317]. Since CTS is also a biocompatible regulatory approved biomaterial [138] and the collagen sources are interchangeable, bilayered Coll/CTS hydrogels may readily be generated for the optimization of clinical approaches. For example, hydrogel-based scaffolds may be either loaded with bioactive factors such as growth factors, or incorporated with macromolecules that induce distinct MSCs differentiation pathways in each layer. In addition, single multi-layered structures with zone-specific Coll/CTS ratios for the simultaneous differentiation of MSCs into structurally organized AC tissue may serve as an optimal model system for OTE.

6.6 CONCLUSION

A biomimetic bilayered dense Coll/CTS hydrogel, with ratios approaching those of Coll/GAG in the native ECM of cartilage and bone, was developed, within minutes, by means of plastically compressing a co-gelled two-layered hydrogel to achieve solid weight percents in the physiological range. This *in vitro* work demonstrated that the bilayered hydrogel supports simultaneous chondrogenesis and osteogenesis under optimized co-culture conditions by mimicking the complex structure of osteochondral tissue. In addition, no signs of scaffold delamination were observed throughout the 35-day study indicating an effective *in vitro* model for the study of cell-cell interactions and the production of MSCs-seeded multilayered scaffolds that resemble tissues. *In vivo* studies are

necessary to evaluate bone ingrowth and fixation (*via* the osteoid-like layer) as well as integration with surrounding cartilage for clinical translation of this system.

6.7 ACKNOWLEDGEMENTS

This work was supported by funds from the Natural Sciences and Engineering Research Council of Canada, the Canadian Foundation for Innovation, and the McGill University Faculty of Engineering Gerald Hatch Faculty Fellowship (in support of SNN). Florencia Chicatun is also partly supported by McGill Engineering Doctoral Awards, Vadasz and Hatch fellowships and a Bourses Fondation Pierre Arbour scholarship. The authors gratefully acknowledge Betty Hoac and Aisha Mousa for their assistance and useful discussions in the course of this study.

6.8 DISCLOSURES

Marc D. McKee has received consulting fees and research funding from Biosyntech, and consulting fees from Piramal Healthcare (Canada).

6.9 SUPPLEMENTARY INFORMATION

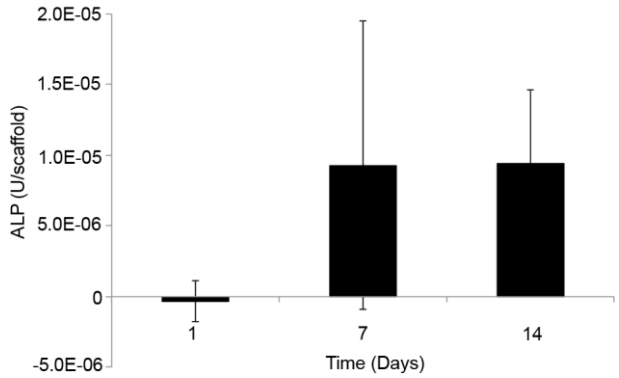

Supplementary Figure 6.1: ALP activity of RCJ cells within the Coll/CTS 1:1 layer cultured in the absence of osteoblasts up to 14 days in MEM/LDEX. Data are represented as the mean ± SD, n=3.

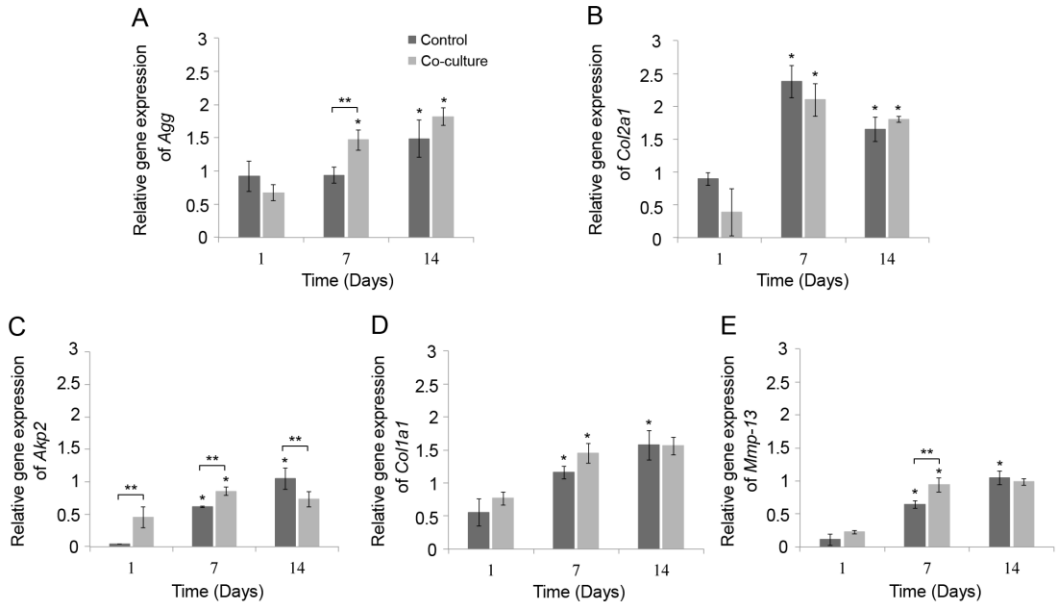

Supplementary Figure 6.2: RT-PCR analysis of cartilage and bone-specific gene expression by RCJ and MC3T3-E1 cells cultured for 14 days independently within Coll/CTS 1:1 and Coll/CTS 33:1 (control), respectively, and compared to the expression levels of both cell types simultaneously cultured within the bilayered osteochondral scaffold. Gene expression of (A) *Acan* and (B) *Col2a1*, from mRNA extracted from RCJ cells, revealed high levels at days 7 and 14. Gene expression of (C) *Akp2,* (D) *Col1a1* and (E) *Mmp-13*, three osteogenic markers, were detected at all times during the 14-day culture period. * indicates a statistical significant difference ($p < 0.05$) with previous time point within the same group. ** Indicates a statistical significant difference ($p < 0.05$) between groups at a specific time point. Data are represented as the mean ± SD, n=3.

CHAPTER 7: EFFECT OF CHITOSAN INCORPORATION ON THE CONSOLIDATION PROCESS OF HIGHLY-HYDRATED COLLAGEN TYPE I HYDROGEL SCAFFOLDS

The intercellular space of connective tissues contains a gel-like substance called the interstitium, which mainly consists of three different components: (i) a continuous fluid (water, electrolytes, nutrients), (ii) collagen fibrils and (iii) proteoglycans (GAGs) [298, 418]. The fibrous components offer high resistance to hydraulic flow to the interstitium, contributing to the compressive stiffness of tissues. In particular, the proteoglycans contribute significantly to the swelling and compressive modulus of AC [419]. From the biophysical point of view, the ECM can transmit forces, dissipate energy and provide biological signals to resident cells [420].

The use of 3D *in vitro* highly-hydrated Coll-based hydrogels to mimic the *in vivo* physiology of the interstitium has been well recognized, and its proper transport environment plays an important role in cell behaviour [298]. Analysis of fluid loss in Coll-based hydrogels undergoing either SC or PC offers the potential for the controlled production of tissue-equivalent dense hydrogels with tailored biophysicochemical properties.

In this dissertation, the use of dense Coll/CTS hybrid gels as alternative tissue-equivalent matrix that possess characteristics of connective tissue ECM, have been extensively investigated in *Chapters 4,* 5 and *6*. Therefore, the study of the biophysical properties of these hybrid gels may provide further insight on their swelling, mechanical and fluid flow properties, enabling the development of tailored scaffolds for use as tissue models for various biomedical applications.

A manuscript based upon these results has been published in the peer-reviewed journal *Soft Matter* and is reproduced below.

Effect of Chitosan Incorporation on the Consolidation Process of Highly-Hydrated Collagen Type I Hydrogel Scaffolds

Florencia Chicatun,[1] Naser Muja,[1] Vahid Serpooshan,[1] Thomas Quinn[2] and Showan N Nazhat [1]*

[1]Department of Mining and Materials Engineering, [2]Department of Chemical Engineering, Faculty of Engineering, McGill University, Montreal, Quebec, Canada H3A 2B2

**Corresponding author:* Showan N. Nazhat, Department of Mining and Materials, Engineering, McGill University, 3610 University Street, Montreal, Qc, Canada, H3A 2B2, Tel: 1-514-398-5524, Fax: 514-398-4492, E-mail. showan.nazhat@mcgill.ca

Keywords: Happel model, hydraulic permeability, swelling, fixed charge density, plastic compression, glycosaminoglycan

7.1 ABSTRACT

Collagenous body tissues exhibit diverse physicochemical and biomechanical properties depending upon their compositions (*e.g.* proteins, polysaccharides, minerals and water). These factors influence cell function and can contribute to tissue dysfunction and disease when they are either deficient or present in excess. Similarly, the constituents of tissue engineering hydrogel scaffolds must be carefully considered for the optimal design of engineered constructs for therapeutic applications. As a natural polysaccharide glycosaminoglycan-analog, chitosan (CTS) holds potential for generating highly-hydrated collagen type I hydrogel (Coll) based scaffolds that mimic the native extracellular matrix. Analysis of fluid loss in Coll/CTS hydrogels undergoing either a gravity-driven consolidation process (self-compression; SC) or plastic-compression (PC) offers the potential for the controlled production of tissue-equivalent dense hydrogels with tailored physical and mechanical properties. Herein, the effect of CTS on Coll gels microstructural evolution involved in SC and PC was investigated by detecting the spatiotemporal distribution of fluorescent beads within Coll/CTS hydrogels using confocal microscopy. The hydraulic permeability (k), pre- and post-consolidation, as a function of CTS content, was estimated by the Happel model. The effect of CTS fixed charge on dense Coll/CTS hydrogels was investigated through structural, mechanical and swelling characterizations under isotonic and hypertonic conditions. Image analysis revealed a temporal increase in bead density, with both rate and extent of consolidation, correlating strongly with increasing CTS content. k decreased from 1.4×10^{-12} to 1.8×10^{-13} m^2 and from 2.9×10^{-14} to 6.8×10^{-15} m^2 for highly-hydrated and dense hydrogels, respectively, with higher amount of CTS, resulting in a concomitant increase in the scaffold compressive modulus (from 7.65 to 14.89 kPa). In summary, understanding the effect of CTS on Coll hydrogel properties enables the development of tailored scaffolds for use as tissue models for various biomedical applications.

7.2 INTRODUCTION

Tissue engineering (TE) aims to design and develop scaffolds that model the complex structure of native tissues and support the growth and differentiation of relevant cells for therapeutic applications [421]. The availability of constructs with well-defined chemical composition, physical structure and biological functions is critical for improved understanding of the intricate mechanisms underlying physiological and pathophysiological processes, while also providing a bridge between animal models of disease and clinical studies [422]. Therefore, the success of three-dimensional (3D) tissue models depends upon the control of multiple biophysical parameters, including microstructure, hydraulic permeability (k), as well as biomechanical and swelling properties.

Type I collagen (Coll) is the major determinant of the structural and functional properties of connective tissues and has been extensively used as 3D biomimetic scaffolds for diverse biomedical applications [114, 423]. In particular, Coll-based hydrogels offer biochemical and biomechanical signals that mimic the extracellular matrix (ECM) of tissues, providing an excellent *in vitro* tissue model. In addition to the complex dense fibrillar network of collagen, connective tissues are also comprised of additional biomacromolecules that contribute to the diverse physicochemical properties of tissues, such as non-fibrillar proteins and proteoglycans containing charged glycosaminoglycan (GAG) side chains surrounded by interstitial fluid, as well as mineral, in the case of bone and calcified cartilage [56, 298]. Indeed, the repulsive electrostatic forces between the negatively charged GAGs entrapped within the collagen meshwork are directly responsible for the stiffness and swelling of the ECM [424, 425].

Chitosan (CTS) is an abundant cationic polysaccharide composed of a disaccharide repeating unit [418, 426], which has been demonstrated to be biocompatible, biodegradable, with antibacterial, wound healing and bioadhesive characteristics [427]. Since CTS is a natural biopolymer that resembles the structure, composition and biological activity of native GAGs [132, 268, 428, 429], it is hypothesized herein that modulation of its content within highly-

hydrated Coll hydrogels holds potential for engineering 3D tissue models with tailored biophysicochemical properties.

Reconstituted Coll/CTS hydrogels have been widely investigated as *in vitro* tissue models and as 3D scaffolds for several TE applications [230, 231, 374, 430, 431]. However, highly-hydrated Coll/CTS hydrogels are predominately comprised of unbound water (> 99 wt. %) and collapse due to their unstable physical structure in the absence of external support [16, 374]. This gravitational force-driven process - identified as self-compression (SC) - allows for the expulsion of the unbound water (> 95 wt. %) that results from casting. SC can be accelerated through the controlled application of an external load (plastic compression; PC) in order to rapidly generate scaffolds with physiologically relevant collagen fibrillar densities (~8 %) [14, 16]. PC has been recognized as an efficient processing method for the generation of tissue equivalent cell-seeded dense Coll gels with greatly enhanced mechanical strength [16]. A number of studies have described the microstructural evolution of Coll hydrogels undergoing SC or PC, with varied theoretical models estimating their k [432-434]. However, the effect of a charged polysaccharide, such as CTS, on the consolidation process of highly-hydrated Coll hydrogels has not been investigated. In this study, Coll/CTS hydrogels, having relative compositions of 1:0, 2:1 and 1:1 (w/w), were uniformly seeded with fluorescent beads and subjected to SC or PC. Serial confocal laser scanning microscopy was used to determine the microstructural evolution of Coll/CTS hydrogels undergoing consolidation by collecting 3D image stacks of the spatiotemporal distribution of the fluorescent beads during the collapse process. The Happel model for flow through a random array of long cylindrical fibres was used to theoretically predict k of pre- and post-compressed hydrogel [35]. In addition, compressive mechanical testing evaluated the relationship between k and compressive modulus of dense gels. Finally, the effect of CTS fixed charge on the structural, mechanical and swelling properties of dense Coll/CTS hydrogels and its contribution to k was investigated under isotonic and hypertonic conditions for charge screening. The incorporation of

CTS within dense Coll hydrogels was found to modify the biophysicochemical properties of the hydrogel, providing a reliable 3D *in vitro* tissue model that may be adapted to optimize TE scaffold design and improve therapeutic outcomes.

7.3 MATERIALS AND METHODS

7.3.1 Preparation of Coll and Coll/CTS hydrogel scaffolds

Ultrapure CTS powder (79.8 % DDA, Ultrasan™, BioSyntech Ltd., Montreal, QC, Canada (now Piramal Healthcare, Laval, QC, Canada)) was dissolved in 0.1 M acetic acid at 4 °C and stirred overnight. Coll/CTS mixtures were prepared by blending sterile, rat-tail tendon-derived collagen type I (2.10 mg/ml of protein in 0.6 % acetic acid, First Link Ltd., West Midlands, UK) and CTS at Coll/CTS weight ratios of 2:1 and 1:1, as previously described [374, 435]. Coll and Coll/CTS self-assembly was achieved by mixing the solution with 10X Minimum Essential Medium (MEM, Sigma Aldrich, Ottawa, ON, CA) at a ratio of 4:1 and by adjusting the solution pH to 7.4 with 5 M NaOH. Neutralized Coll or Coll/CTS solutions were pipetted into four-well plates (0.9 ml/well of 4.5 mm height × 16 mm diameter) to generate circular discs of highly-hydrated gels. Gelation was achieved by allowing the solutions to set at 37 °C in a 5 % CO_2 incubator for 30 min.

7.3.2 Unidirectional self- and plastic-compression of Coll and Coll/CTS hydrogels

Highly-hydrated gels were transferred to an impermeable polystyrene tube (16 mm diameter) for radial confinement on a substrate consisting of a stack of metal and nylon meshes and water-saturated paper blot. The tube allowed for unidirectional fluid flow out of the gel in the *z* direction, parallel to the driving force for flow. The wet substrate was maintained at the level of a water bath to allow for gravity driven fluid flow and avoid capillary effect. Hydrogels were allowed to undergo unidirectional SC up to 40 min or PC up to 5 min, until equilibrium was reached, using a compressive stress of 0.5 kPa at room temperature in a closed chamber maintained at 100 % humidity.

Gel weight, initially (w_0) and at various time points (w_t) during SC or PC, was measured with a digital analytical balance (n = 4; Mettler-Toledo AE 163, readability of 0.01 mg; Switzerland). Weight loss (%) was calculated using:

$$Weight\ loss\ (\%) = \frac{w_0 - w_t}{w_0} \times 100 \quad (1)$$

Pre- and post-compression solid weight percent were also verified through freeze-drying (BenchTop K freeze dryer, VirTis, SP Industries, Gardiner, NY, USA), as follows:

$$Solid\ weight\ percent = \frac{Total\ solid\ content\ (g)}{Total\ solid\ content\ (g) + water\ (g)} \times 100 \quad (2)$$

7.3.3 Microstructural evolution of Coll and Coll/CTS hydrogels undergoing consolidation

The microstructural evolution of Coll and Coll/CTS hydrogels undergoing either SC or PC was analyzed by monitoring the spatiotemporal distribution of green-fluorescent beads (2 μm in diameter, FluoSpheres® Carboxylate-modified microspheres, 2 % solids, Molecular Probes®, Oregon, USA) incorporated into the hydrogels by confocal laser scanning microscopy (CLSM, Carl Zeiss, LSM5 Exciter, Toronto, ON, CA). These carboxylate-modified fluorescent beads present carboxylic acids that can covalently link to amine-containing molecules, such as Coll and CTS, therefore ensuring that fluorescent bead position is a reliable marker of solid density. Encapsulation of the beads was achieved immediately after Coll or Coll/CTS solution neutralization. Briefly, after physiological pH (7.4) was attained, the fluorescent beads were sonicated for 3 min and added using a volume ratio of 1:450. The gel suspension was then further sonicated for 2 min at 4 °C to avoid gel polymerization and allow a homogeneous bead distribution. After gelation for 30 min at 37 °C, highly-hydrated gels were allowed to undergo SC or PC, as described above.

At 0, 5, 20 and 40 min of SC and 0, 1, 3 and 5 min of PC, gels were immediately fixed by immersion in 0.1 M sodium cacodylate buffer containing 4 % paraformaldehyde and 2 % glutaraldehyde and left overnight. Following

fixation, gels were washed with phosphate buffered saline (PBS; 3 × 10 min) and transferred to a glass dish (35 mm in diameter, MatTek, Ashland, MA, USA) for CLSM analysis (n = 3). Three-dimensional image stacks of Coll and Coll/CTS hydrogels were acquired at 1 Airy unit using a 10X objective (EC Plan Neofluoar; 0.3 NA) and argon excitation (488 nm). Image slice thickness was set to 10 μm with an image area of 1264 x 1264 μm^2. Orthogonal images of hydrogel scaffolds were generated using Zeiss LSM image browser (Carl Zeiss Inc., *v*.4.4.0.121, Germany). The number of beads in each slice was determined by transforming each slice into a binary image and performing automatic particle counting using the Analyze Particle tool in ImageJ software (1.42q, Rasband W, National Institutes of Health, Bethesda, MD, USA).

Three different regions were selected to describe the microstructural evolution of Coll gels during confined SC and PC: top 20 μm, bottom 20 μm and bottom 80 μm of the gel; with the bottom part of the gel being the fluid expulsion boundary (FEB) where the fluid flows through. The rationale for the selection of these regions was based on previous studies on Coll gels undergoing consolidation showing the formation of a dense lamella that progressively thickens from the basal surface towards the upper surface of the gel (~80 μm at the equilibrium state), in analogy to the compaction of materials at ultrafiltration surface.[22, 23]

Bead density (ρ_{bead}) was calculated by dividing the total number of beads in the top 20 μm, bottom 20 μm and bottom 80 μm of the hydrogel by the analyzed volume ((20 or 80) x 1264 x 1264 μm^3). The fold increase in density was calculated as follows:

$$Fold\ increase\ in\ density = \frac{\rho_{bead}}{\rho_{HHG}} \quad (3)$$

where ρ_{HHG} is the initial density of the highly-hydrated gels (t = 0).

7.3.3 Hydraulic permeability of Coll and Coll/CTS hydrogels

The hydraulic permeability (k) of highly-hydrated and dense gels generated by unidirectional SC or PC, were calculated using the Happel model for flow

through a random array of long cylindrical fibres [35, 352]. This model may be summarized as follows:

$$k = \frac{2}{3}k_{\perp} + \frac{1}{3}k_{\parallel} \quad (4)$$

where $k_{\perp}$ and $k_{\parallel}$ are the contributions of the perpendicular and parallel fibres to permeability [35, 298] as a function of the rod hydrodynamic radius (a) and the gel solid volume fraction (σ):

$$k_{\perp} = \frac{a^2}{8}\left[\frac{1}{\sigma}ln\left(\frac{1}{\sigma}\right) - \frac{1}{\sigma}\frac{1-\sigma^2}{1+\sigma^2}\right] \quad (5)$$

and

$$k_{\parallel} = \frac{a^2}{8}\left[4 - \sigma + \frac{1}{\sigma}\left\{2ln\left(\frac{1}{\sigma}\right) - 3\right\}\right] \quad (6)$$

σ of Coll and Coll/CTS was determined as follows:

$$\sigma = \frac{Solid\ mass(g)}{Vol_{liquid}(cm^3)\times\rho(\frac{g}{cm^3})} \quad (7)$$

Coll and CTS bulk densities (ρ) of 1.41 and 0.32 g/cm^3 [436, 437], respectively, along with the weight of solid and liquid obtained from the weight loss data and freeze-dried scaffolds pre- and post-compression, were used to calculate σ. For Coll/CTS hydrogels it was assumed that CTS was the most critical determinant of *k* and responsible for the high hydraulic resistance in the hydrogel, in analogy to the GAG chains found in cartilage which lace the interstitial space [418]; thus the totality of the fluid within the Coll/CTS hydrogel was solely associated with the CTS for the calculation of σ. *k* of the hydrogels was calculated using a collagen fibrillar radius of 50 nm [352], measured through electron microscopy investigations and using a hydrodynamic CTS radius of 39 nm [438]. Rod radius was assumed to be constant for all gel specimens.

The electrokinetic effect of the positively charged CTS on *k* of dense Coll/CTS gels was evaluated by screening its fixed charge in a saline solution of high salt concentration (hypertonic; 1.5 M NaCl), and compared to an isotonic solution (0.15 M NaCl) and non-conditioned samples (control) [439, 440]. As-

prepared highly-hydrated Coll/CTS gels were immediately placed in the saline solution to avoid a gravity-driven collapse, which is eliminated by the buoyancy force of the fluid. Highly-hydrated gels were conditioned for 1 day to allow for Donnan equilibrium and then subjected to unidirectional PC. Weight loss was gravimetrically measured to calculate σ using Equation 7. *k* of uncharged hydrogels was calculated using Equations 4 to 6.

7.3.4 Mechanical analysis of dense Coll and Coll/CTS hydrogels

Unconfined compressive mechanical tests were conducted on dense cylindrical rolls using a displacement actuator (LTA-HL, Newport, Irvine, CA, USA) mounted in a rigid frame and interfaced to a PC (LabVIEW) equipped with a 50 g-load cell (Model 31, Honeywell, Golden Valley, MN, USA) [441]. The apparatus was mounted on an antivibration table (Newport), covered by a plexiglass box and surrounded with thermal insulation (T = 23 °C). All measurements were conducted in displacement control with a cross-head speed of 0.005 mm/s. Spiral constructs were used to facilitate better handling. For this purpose, 4.5 ml of Coll or Coll//CTS solution was pipetted into a rectangular mould (18 x 40 x 6.2 mm^3), let set at 37 °C and subjected to unidirectional PC as described above. Cylindrically-shaped rolls (2.97 ± 0.09, 4.34 ± 0.35 and 5.27 ± 0.17 mm diameter; and 3.65 ± 0.45, 4.12 ± 0.37 and 3.91 ± 0.30 mm height for Coll, Coll/CTS 2:1 and Coll/CTS 1:1, respectively) were obtained by cutting the rectangular sheet in half through the short axis (9 mm width x 40 mm length x 150 to 250 μm thick), plying through the middle along the short axis and rolling along their long axis. The specimen diameter was measured using a stereomicroscope (Zeiss Stemi 2000-C) equipped with a digital camera (Canon Powershot A640) attached to a tube adapter (Zeiss MC80DX 1.0). Cylindrically-shaped rolls were conditioned by immersing the scaffolds in an isotonic or hypertonic solution for 1 day and compressed using a stainless steel plunger up to 80 % strain without any evidence of specimen unfolding (n = 3). The stress was calculated by normalizing the recorded force against the initial resistance area of the specimen, and the strain was calculated by normalizing the displacement

against the initial height of the specimen. The compressive modulus values were computed from the slope of the initial linear region of the stress-strain outputs [335, 374].

7.3.5 Swelling properties of dense Coll and Coll/CTS in saline solutions

Dense Coll and Coll/CTS gels were produced by unconfined PC, as described above, and immediately transferred to either an isotonic or hypertonic solution. Gels were allowed to move freely within the bath. At specific time points, up to 60 min, gels (n = 4) were removed from the bath with a L-shaped metal mesh and the excess fluid was absorbed using blotting paper, weighed and returned to the bath. Gel weight was recorded over time and the swelling ratio was determined as follows [442]:

$$Swelling\ ratio\ (\%) = \frac{(w_t - w_0)}{w_0} \times 100$$

(8) where w_0 and w_t are the gel initial weight (post-compression) and weight at time t, respectively.

7.3.6 Statistical analysis

All data are presented as mean values ± standard deviation of the mean (± SD). Statistical significance between scaffold groups and between time points was determined using a one-way ANOVA with a Tukey-Kramer's post-hoc multiple comparison of means. The level of statistical significance was set at p= 0.05.

7.4 RESULTS

7.4.1 Effect of CTS on the consolidation process of Coll hydrogels undergoing unidirectional SC and PC

To investigate the microstructural evolution of highly-hydrated hydrogels undergoing consolidation following the initiation of SC (Fig. 7.1) or PC (Fig. 7.2), CLSM was carried out to monitor the distribution of fluorescent beads throughout the thickness of Coll and Coll/CTS gels at defined time points. Representative orthogonal images of the *z-y* and *x-z* planes of gel specimens are shown for each hydrogel formulation in Fig. 7.1A_i-C_i. CLSM orthogonal images confirmed the

homogeneous fluorescent bead distribution throughout the initial (t = 0) 2.5 mm thickness of highly-hydrated gels. The extent of reduction in gel thickness at the equilibrium state (40 min SC) significantly decreased ($p < 0.05$) with CTS content, reaching 120 ± 8.2, 167 ± 4.7 and 200 ± 21.6 μm for Coll (Fig. 7.1A_{ii}), Coll/CTS 2:1 (Fig. 7.1B_{ii}) and Coll/CTS 1:1 (Fig. 7.1C_{ii}), respectively. A similar trend was observed after 5 min of PC, where gel thicknesses of 96.7 ± 9.4, 103 ± 12.5 and 150 ± 16.3 μm were generated for Coll (Fig. 7.2A_{ii}), Coll/CTS 2:1 (Fig. 7.2B_{ii}) and Coll/CTS 1:1 (Fig. 7.2C_{ii}), respectively. There was a significant difference between the final thickness of Coll and Coll/CTS 2:1 with Coll/CTS 1:1 gels ($p < 0.05$). Analysis of z-stack images during SC and PC of highly-hydrated gels revealed an incremental bead accumulation in both the top and bottom regions over time attributable to matrix densification (Fig. 7.3). Regions of 20-μm thickness at the top and bottom of the hydrogels undergoing SC (Fig. 7.3A-C) and PC (Fig. 7.3D-F) were analyzed, based upon previous studies that describe the formation of a dense lamella at the FEB of Coll hydrogels, in order to measure changes in ρ_{bead} over time [432]. In addition, a bottom 80-μm thickness region (comprising the bottom 20 μm) was also investigated.

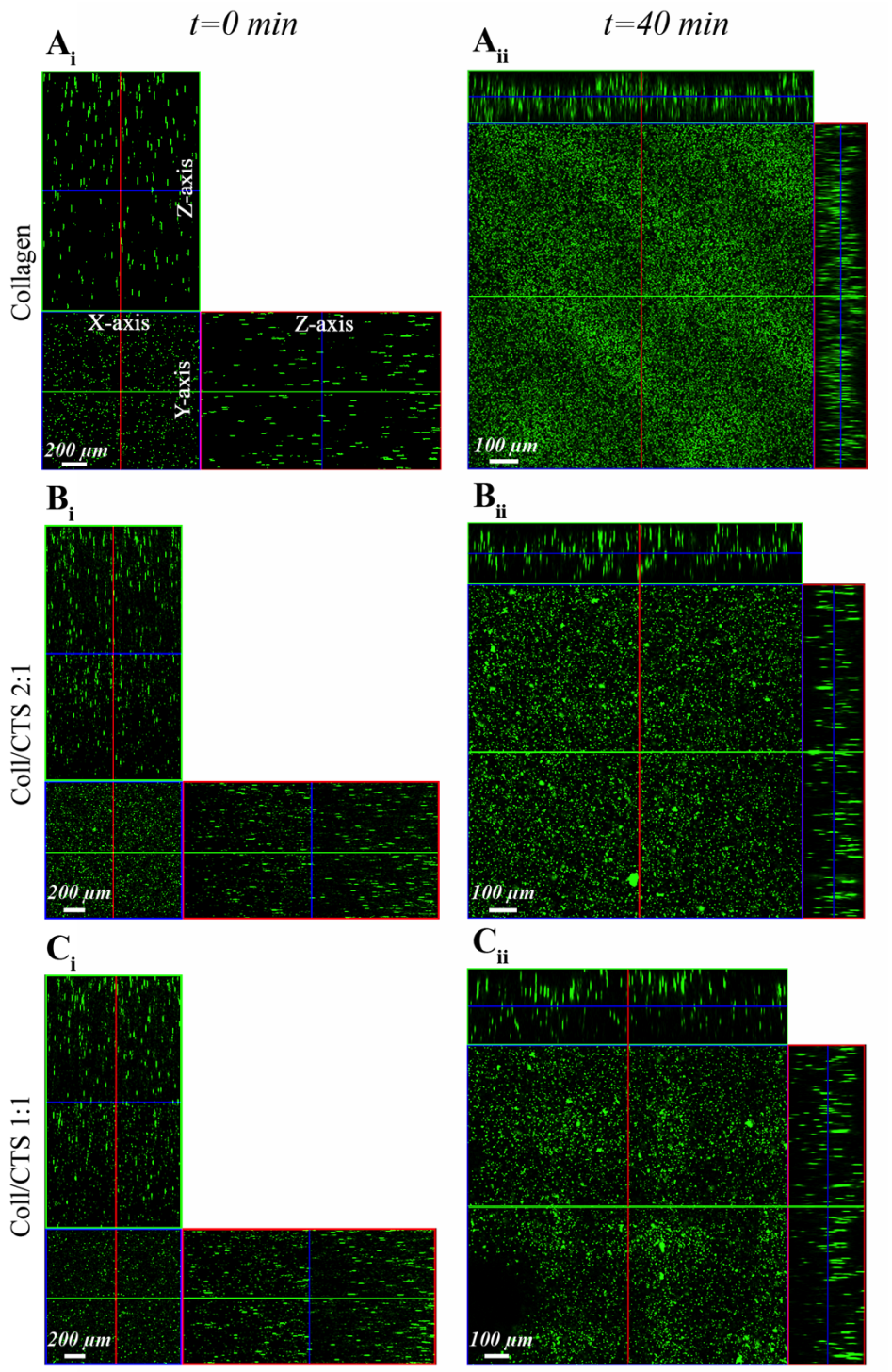

Figure 7.1: CLSM detection of fluorescent bead distribution within Coll and Coll/CTS hydrogels following SC. Ortho-representation of the confocal z-stacks throughout the entire thickness of Coll (A_i), Coll/CTS 2:1 (B_i) and Coll/CTS 1:1 (C_i) hydrogels reveals an initial uniform distribution of fluorescent beads within the gel scaffolds immediately prior to SC (t = 0, scale bar = 200 µm). After 40 min of SC, the thicknesses of the gel scaffolds decreased to 120 ± 8.2, 167 ± 4.7 and 200 ± 21.6 µm for Coll (A_{ii}), Coll/CTS 2:1 (B_{ii}) and Coll/CTS 1:1 (C_{ii}), respectively. Scale bar = 100 µm.

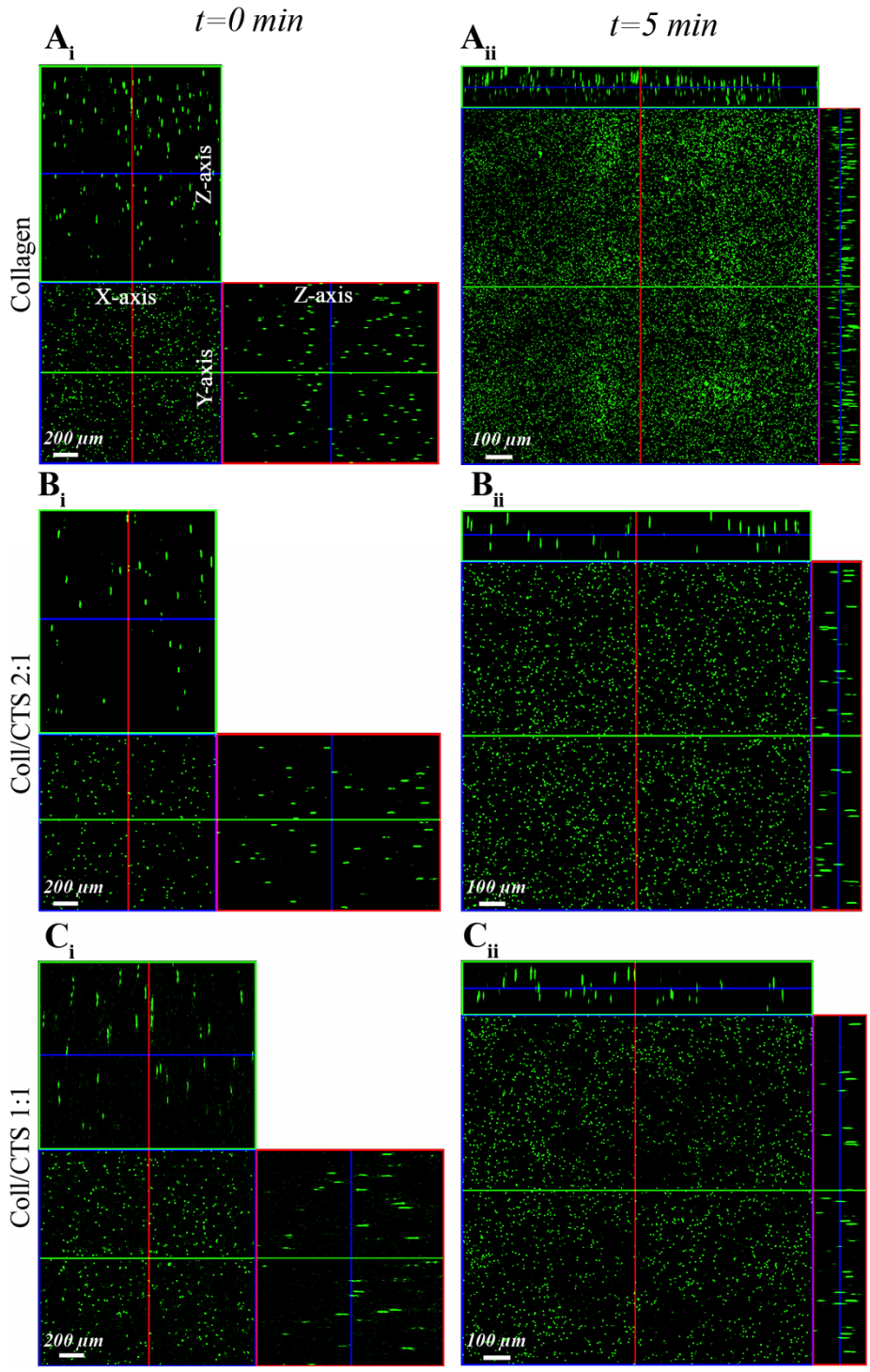

Figure 7.2: CLSM detection of fluorescent bead distribution within Coll and Coll/CTS hydrogels undergoing PC. Ortho-representation of the confocal z-stacks throughout the entire thickness of Coll (A_i), Coll/CTS 2:1 (B_i) and Coll/CTS 1:1 (C_i) hydrogels reveals an initial uniform distribution of fluorescent beads within the gel scaffolds (t = 0; scale bar = 200 µm). After 5 min of application of an external stress of 0.5 kPa for 5 min, the gel thickness decreased to 96.7 ± 9.4, 103 ± 12.5 and 150 ± 16.3 µm thickness in Coll (A_{ii}), Coll/CTS 2:1 (B_{ii}) and Coll/CTS 1:1 (C_{ii}), respectively. Scale bar = 100 µm.

After 5 min PC, ρ_{bead} within the bottom 20 μm of Coll constituted 66 % of the final density (Fig. 7.3A). There was no significant difference in ρ_{bead} between 20 and 40 min within the bottom 20 μm ($p > 0.05$). The z-stack analysis revealed that the ρ_{bead} at the bottom 80 μm followed the same trend, however the ρ_{bead} was 12.7 % lower than that of the bottom 20 μm. While ρ_{bead} within the top 20 μm exhibited a slower rate of increase when compared to that within the bottom 20 μm, after 40 min of SC it reached a similar value to ρ_{bead} within the bottom 80 μm. For Coll/CTS hydrogels, ρ_{bead} within the bottom 20 and 80 μm regions equilibrated within 5 min of SC (Fig. 7.3B and C). Relative to Coll, there was a decrease in ρ_{bead} within both top and bottom regions with an increase in CTS content. After 40 min SC, ρ_{bead} within the top 20 μm regions were 73, 28 and 24 % the value of ρ_{bead} within the bottom 20 μm regions of Coll, Coll/CTS 2:1 and 1:1 hydrogels, respectively. Also after 40 min SC, the bottom 80 μm regions underwent a 40.3 ± 0.6, 15.7 ± 1.7 and 11.9 ± 0.9 fold increase in ρ_{bead} in the case of Coll, Coll/CTS 2:1 and 1:1, respectively, compared to the initial ρ_{bead} of the highly-hydrated gels ($t = 0$).

Analysis of z-stack images during PC (Fig. 7.3 D-F) revealed an incremental bead accumulation within both top and bottom regions as early as 1 min, with the bottom 20-μm region of all hydrogels reaching a stable ρ_{bead} value. After 3 min, ρ_{bead} within the bottom 80 μm of Coll equilibrated. While Coll/CTS 2:1 exhibited a similar trend, Coll/CTS 1:1 showed no statistical difference at the bottom 80 μm between all time points ($p > 0.05$). Similar to SC, ρ_{bead} in both top and bottom regions of the gels decreased with CTS content, where the final ρ_{bead} within the bottom 80 μm of Coll, Coll/CTS 2:1 and 1:1 underwent a 35.8 ± 3.7, 21.3 ± 2.2 and 18.0 ± 1.8 fold increase, respectively. However, and in contrast to SC, there was no statistical difference in ρ_{bead} in hydrogels undergoing PC between top and bottom regions at the equilibrium state ($p > 0.05$).

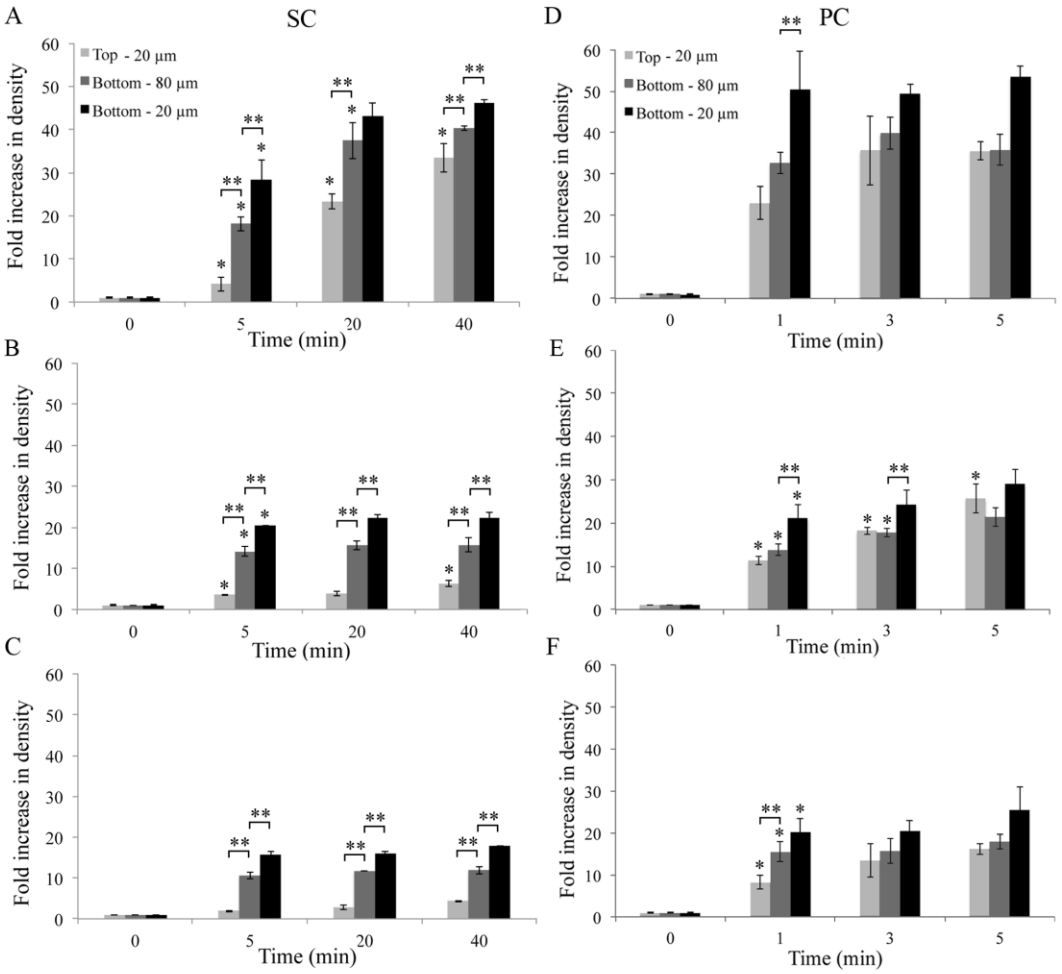

Figure 7.3: Effect of CTS on Coll hydrogel consolidation by SC and PC. The spatiotemporal distribution of fluorescent beads was studied by CLSM as an indicator of the structural evolution of highly-hydrated hydrogels when undergoing compression. ρ_{bead} within the top 20 µm and bottom 20 and 80 µm of Coll (A, D), Coll/CTS 2:1 (B, E) and Coll/CTS 1:1 (C, F) undergoing SC (A-C) and PC (D-F). Analysis of the collapse process was evaluated after 5, 20 and 40 min of the initiation of the gravity-driven process and after application of an external load for 1, 3 and 5 min. After 40 min of SC, there was a 40.3 ± 0.6, 15.7 ± 1.7 and 11.9 ± 0.9 fold increase in ρ_{bead} within the bottom 80 µm of dense Coll, Coll/CTS 2:1 and Coll/CTS 1:1 gels, respectively. The ρ_{bead} within the bottom 80 µm of all samples were significantly different ($p < 0.05$). After 5 min of PC, there was a 35.8 ± 3.7, 21.3 ± 2.2 and 18.0 ± 1.8 fold increase fold increase in ρ_{bead} within the bottom 80 µm of dense Coll, Coll/CTS 2:1 and Coll/CTS 1:1 gels, respectively. There was no significant difference between ρ_{bead} within the bottom 80 µm of dense Coll/CTS 2:1 and Coll/CTS 1:1 ($p > 0.05$). A significant difference in ρ_{bead} within the bottom 80 µm was observed between Coll and Coll/CTS hydrogels ($p < 0.05$). Both ρ_{bead} after SC or PC were in line with the fold increase in solid weight percent post-compression (42.0 ± 1.4, 23.0 ± 2.3 and 14.3 ±0.2). Hydrogels undergoing PC showed no statistical difference between top and bottom densities at the equilibrium state ($p > 0.05$). Data represented as mean ±SD, n = 3. * indicates a significant difference ($p < 0.05$) compared to previous time point. ** indicates a significant difference ($p < 0.05$) compared to a different region at the considered time point.

7.4.2 Weight loss and k of Coll and Coll/CTS hydrogels

Weight loss of highly-hydrated gels was measured as a function of unidirectional SC (Fig. 7.4A) or PC (Fig. 7.4B). Under both conditions there was

an initial rapid rate of weight loss, which was followed by a gradual reduction in weight loss towards an equilibrium state. Increasing amounts of CTS resulted in a decrease in the initial weight loss rate. After 40 min SC there was a 41.1 ± 4.1, 13.4 ± 0.6 and 9.5 ± 0.5 fold increase in solid weight percent for Coll, Coll/CTS 2:1 and 1:1, respectively, compared to the initial state (t = 0). The final solid weight percent of the hydrogels after 5 min of PC followed a similar trend, with the percentages decreasing with higher CTS content (42.0 ± 1.4, 23.0 ± 2.3 and 14.3 ± 0.2 fold increase for Coll, Coll/CTS 2:1 and 1:1, respectively).

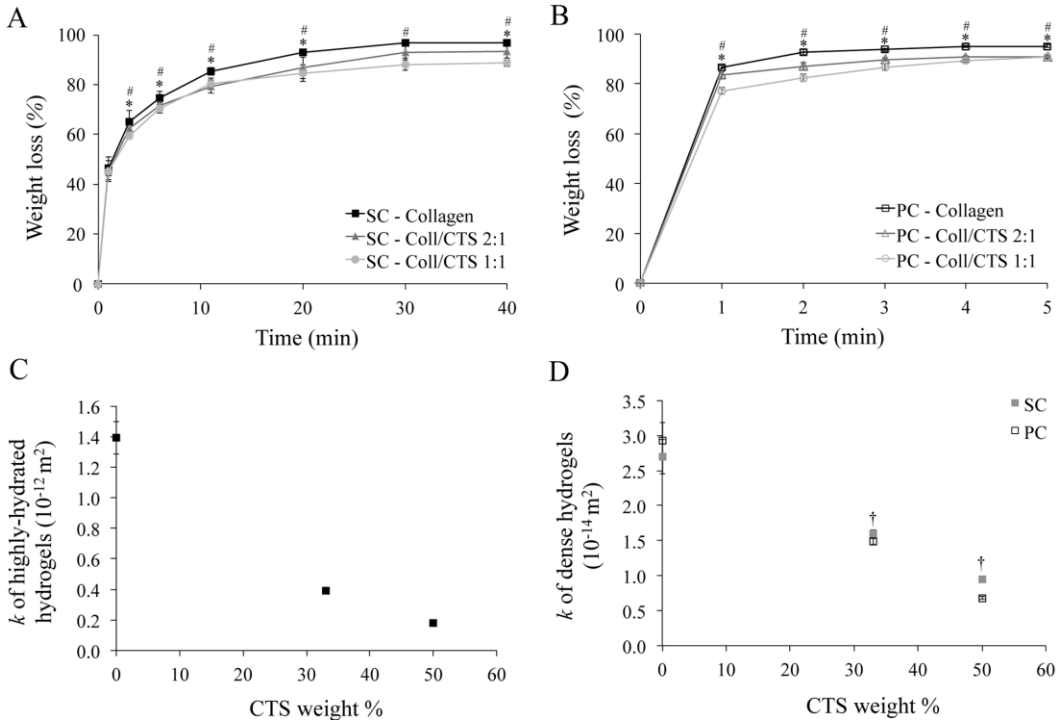

Figure 7.4: Effect of CTS on weight loss and hydraulic permeability (k) of Coll and Coll/CTS hydrogels under unidirectional SC and PC. Analysis of the effect of CTS on weight loss due to fluid expulsion and hydraulic permeability calculated using the Happel model measured up to 40 min SC and 5 min PC. Experimental data for weight loss during SC (A) and PC (B) were used to determine k for highly-hydrated (C) and dense hydrogels (D) which underwent SC or PC. There was a decrease in k with CTS content. Data represented as mean ±SD, n = 3. * indicates a significant difference ($p < 0.05$) between Coll and Coll/CTS 2:1. # indicates a significant difference ($p < 0.05$) between Coll and Coll/CTS 1:1. † indicates a significant difference ($p < 0.05$) between SC and PC.

The Happel model was used to calculate k for all hydrogels pre- and post-compression by using the weight loss and σ values (Table 7.1), along with the reported hydrodynamic radius of collagen and CTS fibres (Fig. 7.4C and D). k decreased with increasing CTS content resulting in 1.4×10^{-12} ($\pm 1.1 \times 10^{-13}$), 3.9

$\times 10^{-13}$ ($\pm$ 1.1 $\times 10^{-14}$) and 1.8 $\times 10^{-13}$ ($\pm$ 3.4 $\times 10^{-15}$) m^2 for Coll, Coll/CTS 2:1 and 1:1, respectively. A similar trend was observed for the dense hydrogels, with k decreasing from 2.7 $\times 10^{-14}$ ($\pm$ 2.5 $\times 10^{-15}$), 1.6 $\times 10^{-14}$ ($\pm$ 5.2 $\times 10^{-16}$) and 9.5 $\times 10^{-15}$ ($\pm$ 2.1 $\times 10^{-16}$) m^2 for SC and 2.9 $\times 10^{-14}$ ($\pm$ 2.7 $\times 10^{-15}$), 1.5 $\times 10^{-14}$ ($\pm$ 5.2 $\times 10^{-16}$) and 6.8 $\times 10^{-15}$ ($\pm$ 1.6 $\times 10^{-16}$) m^2 for PC for Coll, Coll/CTS 2:1 and Coll/CTS 1:1, respectively.

Table 7.1: Weight loss and solid volume fraction (σ) of Coll and Coll/CTS gel scaffolds attributable to SC and PC. σ was calculated based on gravimetric analysis of freeze-dried scaffolds pre- and post-compression and weight loss data. Values are presented as the mean ± standard deviation.

Sample	Highly-hydrated	Self-compression (SC)		Plastic compression (PC)	
	σ_{HHG}	Weight loss (%)	σ_{SC}	Weight loss (%)	σ_{pc}
Collagen	0.0016 ± 0.0001	95.4 ± 0.5	0.0325 ± 0.0006	95.1 ± 0.6	0.0320 ± 0.0022
Coll/CTS 2:1	0.0030 ± 0.0001	93.4 ± 2.8	0.0342 ± 0.0008	90.8 ± 0.4	0.0361 ± 0.0008
Coll/CTS 1:1	0.0055 ± 0.0001	88.7 ± 1.4	0.0487 ± 0.0007	90.9 ± 1.2	0.0603 ± 0.0009

7.4.3 Electrokinetic effect of CTS on k of dense Coll hydrogels

PC-induced weight loss of Coll and Coll/CTS hydrogels was evaluated by immersing as prepared highly-hydrated gels in a hypertonic solution for charge screening (Fig. 7.5A-C) and compared to those in an isotonic solution and non-conditioned hydrogels (control). After 5 min PC in isotonic solution, there was a 95.0 ± 0.2, 91.7 ± 1.4 and 91.1 ± 0.5 % weight loss for Coll, Coll/CTS 2:1 and 1:1, respectively. The weight loss of Coll/CTS hydrogels pre-conditioned in hypertonic solution increased with CTS content (95.16 ± 0.90, 93.96 ± 0.35 % and 92.85 ± 0.44 % for Coll, Coll/CTS 2:1 and 1:1, respectively), and was higher when compared to those in isotonic solution. No statistical difference was observed in the percentage weight loss of Coll between isotonic and hypertonic solutions ($p > 0.05$). Moreover, there was no statistical difference in the percentage weight loss of all formulations between control and isotonic condition.

Weight loss data was used to calculate σ of dense hydrogels under both conditions and applied into eqn. (4-6) to predict the effect of CTS fixed charge on k (Fig. 7.5D). There was no statistical difference ($p > 0.05$) between k of Coll

when pre-conditioned in either isotonic or hypertonic solutions. However, there was a significant decrease ($p < 0.05$) in k of Coll/CTS hydrogels pre-conditioned in hypertonic solution.

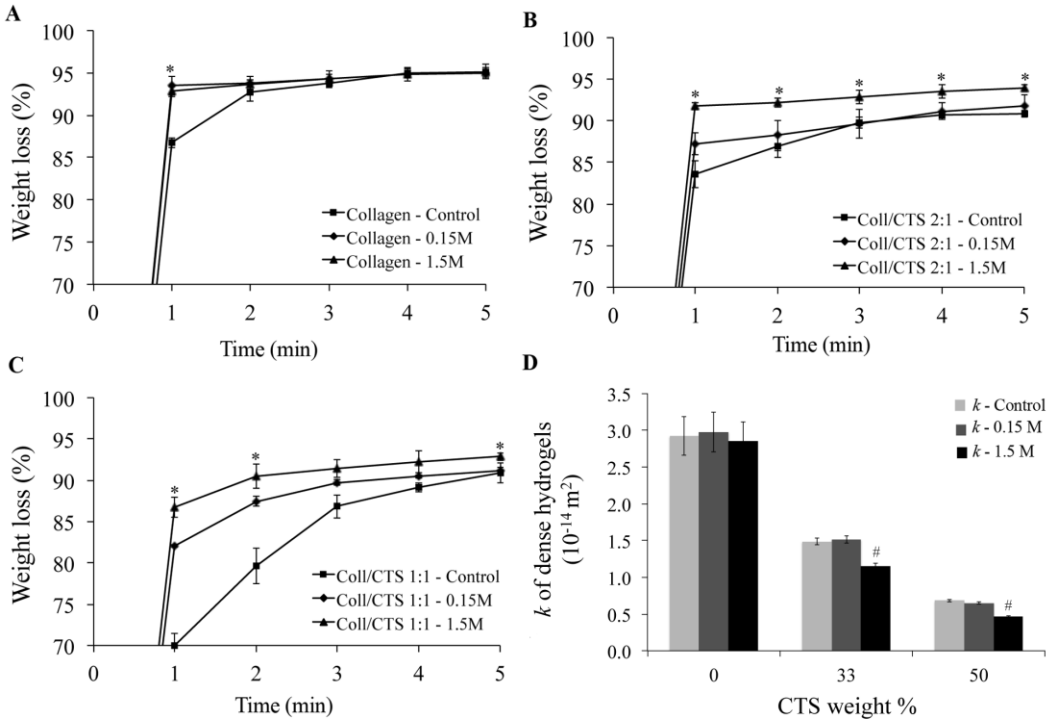

Figure 7.5: Electrokinetic effect of CTS on the weight loss (%) and hydraulic permeability (*k*) properties of Coll (A), Coll/CTS 2:1 (B) and Coll/CTS 1:1 (C) hydrogels undergoing PC without pre-conditioning (control) and pre-conditioned in isotonic (0.15 M NaCl) and hypertonic solutions (1.5 M NaCl). There was a decrease in weight loss after 5 min of PC with CTS content under both isotonic and hypertonic conditions ($p < 0.05$). There was no significant difference in Coll weight loss after 5 min PC in control, isotonic and hypertonic conditions. Coll/CTS 2:1 and Coll/CTS 1:1 hybrid gels demonstrated a significant increase in equilibrium weight loss with increasing NaCl concentration. (D) Charge screening by pre-equilibrating scaffolds in a high salt concentration solution resulted in no significant difference in Coll k values ($p > 0.05$) and up to 29 % decrease in Coll /CTS dense hydrogels. There was no significant difference between control and isotonic conditions in all scaffolds formulations. * indicates a significant difference ($p < 0.05$) compared to previous time point. # indicates a significant difference ($p < 0.05$) compared to control. Data represented as mean ±SD, n = 3.

The compressive modulus, calculated from the initial region of the stress-strain curves of dense hydrogels, tested after a 1-day pre-conditioning period in isotonic (7.65 ± 1.67, 9.94 ± 0.68 and 14.89 ± 1.53 kPa for Coll, Coll/CTS 2:1 and 1:1, respectively) and hypertonic solutions (7.50 ± 2.55, 8.68 ± 0.53 and 16.81 ± 1.71 kPa for Coll, Coll/CTS 2:1 and 1:1, respectively) significantly increased with CTS content. There was no statistical difference in the compressive modulus of Coll, Coll/CTS 2:1 and Coll/CTS 1:1 when pre-conditioned in isotonic or

hypertonic solutions ($p > 0.05$). The increase in compressive modulus with CTS content corresponded with a decrease in k of the hydrogels (Fig. 7.6).

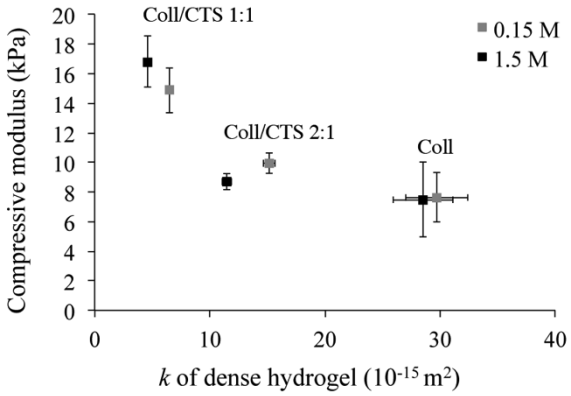

Figure 7.6: Relationship between hydrogel compressive modulus and hydraulic permeability (*k*). Cylindrically shaped dense hydrogels were pre-equilibrated in an isotonic or hypertonic solution for 1 day prior compression testing. There was a significant increase in compressive modulus with CTS content under both conditions ($p < 0.05$). An increase in CTS content also resulted in a concomitant decrease in k. Data represented as mean ±SD, n = 3.

7.4.4 Swelling of dense Coll and Coll/CTS hydrogels in isotonic and hypertonic solutions

The weight change due to water absorption of dense Coll and Coll/CTS gels was measured in either isotonic or hypertonic solutions to evaluate the electrostatic contribution of CTS to Coll hydrogels swelling properties (Fig. 7.7). The swelling of all hydrogels reached equilibrium within 5 min. Pairwise comparisons (ANOVA, $p < 0.05$) of each group of hydrogels in both solutions showed that the swelling ratio of Coll/CTS 2:1 and Coll/CTS 1:1 decreased with an increase in salt concentration, while that of Coll remained unchanged. In particular, in isotonic solution, equilibrium swelling ratio significantly increased ($p < 0.05$) with increasing CTS content, demonstrating a 48 ± 4, 88 ± 9 and 107 ± 10 % increase for Coll, Coll/CTS 2:1 and 1:1, respectively. In contrast, in hypertonic solution, there was no statistical difference ($p > 0.05$) between the equilibrium swelling ratio of Coll (49 ± 3 %) when compared to that of Coll/CTS 2:1 (49 ± 5 %), while that of Coll/CTS 1:1 was significantly lower ($p < 0.05$).

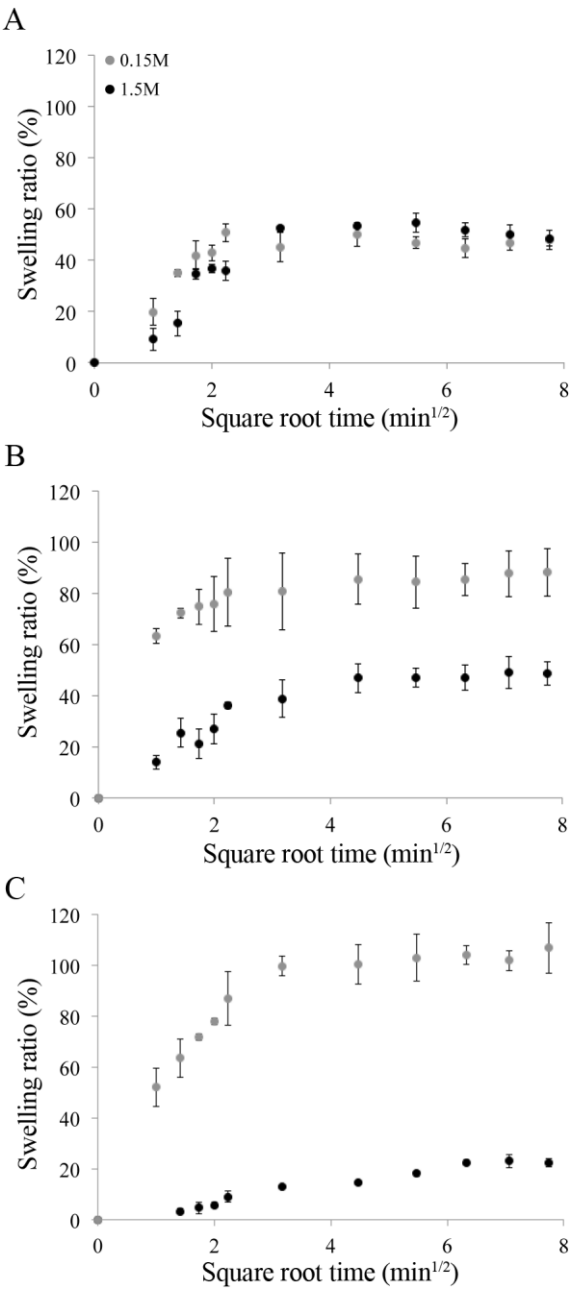

Figure 7.7: Influence of CTS on hydrogel swelling in isotonic and hypertonic conditions. Swelling of dense Coll (A), Coll/CTS 2:1 (B) and Coll/CTS 1:1 (C) hydrogels were analyzed for up to 60 min. There was a decrease in swelling ratio with increasing CTS content under hypertonic conditions. Data represented as mean ±SD, n = 4.

7.5 DISCUSSION

The distinct physicochemical properties of the 3D *in vivo* extracellular microenvironment demand the development of biomimetic scaffolds with optimal characteristics. Coll/CTS hydrogels provide an excellent ECM-mimetic milieu for

cell growth and differentiation [230, 231, 374, 430, 431]. Modulation of CTS within the Coll fibrillar structure exhibits great potential for the development of scaffolds with tailored physicochemical properties directed towards TE and drug delivery applications. However, highly-hydrated Coll hydrogels present insufficient mechanical strength and poor structural integrity on account of the unbound water that results from hydrogel casting [16]. Under unconfined conditions, highly-hydrated Coll/CTS gels undergo a gravity-driven SC process governed by interstitial fluid flow within the porous fibrillar matrix, which is accelerated by an external compressive stress (PC) to produce dense hydrogels with fibrillar densities approaching those of native ECM [16, 374]. However, the effect of CTS incorporation on the microstructural evolution of Coll/CTS hydrogels undergoing consolidation either through SC or PC has not been investigated. Having the means to understand this effect would enable greater control of hydrogel microstructure, which ultimately allows for a greater range of properties (*e.g.* hydraulic permeability, mechanics and swelling) that can be tailored to meet specific requirements for each target application.

Coll/CTS of relative compositions of 1:0, 2:1 and 1:1 (w/w) were prepared to approach the weight ratios of Coll/GAGs in the native ECM of tissues (*e.g.* bone osteoid, cartilage, tendon and ligaments) [46, 56, 374]. The consolidation process through either SC or PC of highly-hydrated Coll/CTS hydrogels was characterized by monitoring the distribution of fluorescent beads over time by CLSM. Previously, studies have determined that Coll hydrogels consist of two distinct layers following SC and PC: a highly-hydrated or bulk layer, and an underlying dense lamella [352, 433]. In analogy to the compaction of materials at ultrafiltration surfaces, the basal surface of the Coll hydrogel serves as the principal FEB, retaining the collagen fibrils [16]. In particular, Serpooshan *et al.* [433] reported that after 1 minute undergoing SC, the basal surface of the Coll hydrogel develops into a 20-μm dense lamella, which increases in thickness until reaching 80 μm at the equilibrium state. Therefore, based upon these data, the top 20 μm, the bottom 20 μm and 80 μm were selected for further analysis. In the

current work, 3D maximum intensity CLSM projections attested an initial homogeneous bead distribution throughout the entire thickness of highly-hydrated hydrogels. Image analysis revealed a temporal increase in ρ_{bead}, stabilizing at the equilibrium state. A gradient in bead density was observed from the bottom to the top of the scaffolds in accordance with a previous study using protein staining (Coomassie blue) to visualize collagen density during PC of highly-hydrated Coll hydrogels [434].

Increasing CTS content resulted in a greater difference in bead density between the top and bottom regions of hydrogels undergoing SC, suggesting that Coll gel structure is more uniform at equilibrium when compared to Coll/CTS hydrogels. Differences in bead density between the top and bottom regions of hybrid gels may be explained by an increase in the overall stiffness of the hydrogel [374, 435] in the presence of CTS (as demonstrated by the 1.9-fold increase in the compressive modulus of Coll/CTS 1:1 compared to Coll alone), which influences the mechanism of densification during the gravity-driven consolidation process. In particular, at a microstructural level, CTS is thought to interlink with the Coll network (similar to native GAGs) [443], and increase the swelling pressure due to the repulsive forces between the fixed charged groups of the hydrogel, resulting in higher compressive modulus [374, 435]. Since increasing the CTS content in Coll hydrogels results in greater stiffness, it was therefore hypothesized that ρ_{bead} throughout the hydrogel would decrease when undergoing SC. Indeed, the fold increase in density of Coll hydrogels decreased relative to CTS content. It is noteworthy that ρ_{bead} at equilibrium corresponded with the solid weight percent gravimetrically measured pre- and post-freeze drying. The correspondence between the beads and solid densities for each specimen validates the fluorescent bead imaging method as an effective and reliable indicator of solid density. Moreover, monitoring the position of fluorescent beads at different time points during the consolidation process provided an accurate measurement of bead position in space and time, offering an advantage over a previously published method based on collagen

immunoreactivity which depends on homogeneous antibody binding and fluorescent intensity stability at greater depths in the scaffold [432].

Under PC, and as early as 1 min, all formulations exhibited an increase in ρ_{bead} in the top and bottom regions. Following 1 min of compression, comparison of ρ_{bead} measured at the top 20 μm and bottom 80 μm of the scaffolds demonstrated no significant difference ($p > 0.05$). Analogous to SC, the final density within the bottom 80 μm of all scaffolds corresponded with both the densities of SC gels at equilibrium and with the solid weight percent of PC gels obtained by the freeze-drying method. However, the final density at the bottom 20 μm of the PC Coll gels was 49 % higher compared to the top and bottom 80 μm. This phenomenon can be attributed to the application of an external stress resulting in the accumulation of collagen fibrils at the gels FEB due to higher fluid flow (10-fold increase in weight loss rate under PC, compared to SC) and the unstable physical structure of the hydrogel [433]. In contrast, there was no significant difference between the three analyzed regions in Coll/CTS hydrogels at the equilibrium state, therefore suggesting a uniformly distributed solid density throughout the scaffolds thickness, compared to the gravity-driven process. Since positively charged CTS contains several hydrophilic groups, such as hydroxyl, amino and carboxyl groups, it promotes water entrapment within the hydrogel, therefore reducing the fluid flow [444] and consequently the solid density throughout the scaffold thickness, as demonstrated by the reduction in the rate and final weight loss of Coll/CTS 1:1 gels compared to Coll/CTS 2:1 and Coll alone.

The Happel model is a generalized microstructurally-based model for the calculation of k, a property that can be correlated with the inflow of nutrients and oxygen as well as the outflow of metabolic waste and biodegradation by-products within a hydrogel [36]. The Happel model describes the flow resistance as a summation of the resistance of cylindrical rods parallel and perpendicular to the flow [298], and has been particularly useful in tissues such as articular cartilage [439, 440] and fibrillar materials such as Coll, where collagen is modelled as a long cylindrical fibre [35]. Since this model assumes a constant rod cross-

sectional area along the direction of the flow, and GAG chains are the most critical determinant of the permeability in native cartilage (based on previous measurements), the Happel model has been used to calculate cartilage permeability by modeling GAG chains as rods of a constant radius "a" and assuming that the contribution of collagen to flow resistance is negligible [35, 418, 439, 445]. Since the microstructural properties are considered as one of the major signalling sources regulating cell growth and differentiation, further studies of hydrogel *k* properties are critical [446]. In analogy to cartilage, in this study, CTS – a polysaccharide of structural similarity to GAGs found in native ECM– was also modelled as a rod-like structure of a hydrodynamic radius of 39 nm [438], which in combination with experimentally measured solid volume fraction values, allowed the calculation of Coll/CTS permeability. The analysis revealed decreasing *k* values in hydrogels with higher CTS content both in highly-hydrated and dense forms, analogous to proteoglycans in articular cartilage [447]. A plausible explanation may be that an increase in fixed charge density, which originates from the protonated amino groups found in the polysaccharide structure, lowers the content of water that is free and therefore *k* [448].

In connective tissues, collagen itself is essentially neutral at physiological pH (isoelectric point at pH 7.5), whereas GAG chains possesses one to two fixed negative charges per disaccharide unit, generating the bulk flow through the interstitium to induce streaming potentials [447, 449]. In the present study, the electrostatic contribution of CTS to Coll hydrogels was investigated through structural, mechanical and swelling characterizations under isotonic and hypertonic conditions [450]. Elimination of the screening charges with high concentrations of salts (hypertonic) resulted in no significant effect on Coll hydrogel *k* ($p > 0.05$). This is in contrast to dense Coll/CTS gels, which presented up to 29 % reduction in *k*. This suggests that the electrokinetic effect does not account for the majority of the Coll/CTS *k* and that the determinant factor is the tortuosity flow-path induced by the interlinked CTS within the collagen network. *k* values obtained in this study for dense Coll hydrogels corresponded to those

previously published for Coll gel scaffolds (1×10^{-15} - 10^{-16} m^2) [451] and 3 orders of magnitude higher compared to human articular cartilage (~0.1 to 2×10^{-18} m^2) [301]. In addition, with decreasing *k*, there was a concomitant increase in the compressive modulus of the scaffolds with CTS under both isotonic and hypertonic conditions, which can be explained by CTS fixed charge increasing the osmotic pressure and resistance to compressive forces [452].

Under isotonic conditions, increasing amounts of CTS resulted in higher swelling ratios. This increment was attributed to the increased number of protonated groups, which augment the repulsive forces between the fixed charged constituents of the hydrogel, resulting in greater osmotic pressure and promotion of water intake [387, 453]. Increasing the concentration of salt resulted in a decrease in swelling ratio of Coll/CTS hydrogels, while the Coll gels remained unchanged. A likely mechanism for Coll/CTS swelling reduction is the salt's ability to increase the degree of screening of fixed charge, leading to a reduction in electrostatic repulsion and of the osmotic pressure, therefore, restricting the capacity for hydrogels to swell [453].

The ability of CTS to control and tune the permeability, mechanical and swelling properties of a biomimetic scaffold such as dense Coll hydrogels, may be utilized for various applications, including drug delivery and TE. For example, charged hydrogels have been shown to be effective drug carriers, which are able to release entrapped pharmaceutical drugs in response to a swelling trigger [454]. In addition, the positively charged molecules may facilitate cell differentiation by electrostatically binding cell membrane and negatively charged GAGs [455, 456]. In fact, it has been observed that increasing CTS content within dense Coll gels has a stimulatory effect towards the chondrocytic lineage, revealing that CTS plays an important role in stimulating ECM production [435]. Moreover, this *in vitro* model may also be used as a simple tool to measure the interaction of connective tissue GAGs with collagen, as well as with cell surfaces through a receptor-like mechanism [447].

7.6 CONCLUSION

In this study, the effect of CTS on the microstructural evolution involved in SC and PC of highly-hydrated Coll/CTS hydrogels was investigated by monitoring the spatiotemporal distribution of fluorescent beads by CLSM. Measured final bead density and solid weight percent values corresponded closely, thus validating this fluorescent-based imaging method. CTS fixed charge effect on dense Coll/CTS hydrogels was analyzed through structural (*i.e.* hydraulic permeability), mechanical and swelling characterizations under isotonic and hypertonic conditions. The results indicated the ability of a charged GAG-analog to control the physicochemical properties of Coll hydrogels, offering the potential for tailoring scaffolds for TE and other biomedical applications.

7.7 ACKNOWLEDGEMENTS

This work was supported by funds from Canadian Natural Sciences and Engineering Research Council, the Canadian Foundation for Innovation and the McGill University Faculty of Engineering Gerald Hatch Faculty Fellowship (in support of SNN). Florencia Chicatun is also partly supported by McGill Engineering Doctoral Awards, Vadasz and Hatch fellowships and a Bourses Fondation Pierre Arbour scholarship.

CHAPTER 8: GENERAL DISCUSSION

Despite the significant advances made to date in CTE, several challenges still remain in developing a suitable biomimetic matrix able to remain anchored and functional within a cartilage defect. OTE scaffolds hold promise for use in AC repair based on the rapid and efficient bone-to-bone integration compared to the cartilage-to-cartilage interface alone [25, 26]. However, OTE still faces significant difficulties in engineering a complex layered scaffold that is able to maintain both chondrogenic and osteogenic phenotypes during 3D co-culture.

Since their development by Grillo and Gross [305] in the early 1960's, *in vitro* reconstituted Coll hydrogels have been extensively utilized as scaffolds in TE studies. However, as a consequence of their highly-hydrated nature (> 99 % fluid) these hydrogels present a physically unstable structure and insufficient mechanical properties (stiffness and strength), therefore limiting their potential in clinical applications (*Figure 8.1A and D*). Dense Coll hydrogels may be readily produced by exerting a compressive mechanical stress (PC) to eliminate a significant amount of the casting fluid (*Figure 8.1B and E*) without compromising seeded cell viability [16, 18]. This simple and reproducible technique allows for the development of dense hydrogels with solid weight percent values (~8 wt. %) approaching those of native tissues, such as the ECM of bone osteoid (*Figure 8.1C*) and cartilage (*Figure 8.2F*), thus enhancing their mechanical properties.

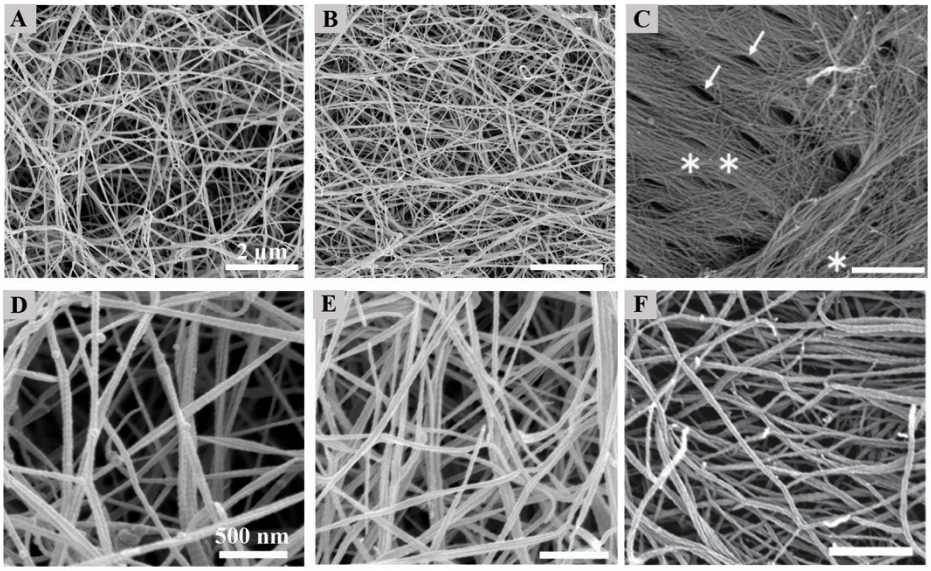

Figure 8.1: Morphological comparison between Coll hydrogels and the native ECM of bone osteoid and cartilage. SEM micrograph of: (A, D) highly hydrated Coll gel, (B, E) dense Coll gel, (C) inner bone surface of a femur of an 8-week-old rat showing the collagen fibrils loosely packed (denoted by *) and densely aggregated forming bundles (denoted by **) (Small oval pores are indicated by white arrows), and (F) normal human AC surface (grade 0) from a 77-year old patient. Adapted from [457, 458]. Copyright © 2012 Oxford University Press. Copyright © 2009 Mcmillan Publishers Limited

In an effort to provide an *in vivo*-like environment suitable for cell attachment, proliferation and differentiation, collagen-based scaffolds have been combined with different biomolecules. Because of its chemical similarity with the GAGs found in native tissue, CTS can be added as a bioactive component in collagen to better mimic the native components of the ECM. CTS is FDA approved for the use in wound dressing, and has been approved in some countries for dietary applications [138, 139]. In addition, it has the advantage of being biodegradable, biocompatible, non-immunogenic, bio-functional and haemostatic, making it a suitable natural polymer for TE applications [98, 137]. Since GAGs can interact with growth factors, receptors and adhesion proteins, it is expected that the analogous structure in CTS may also have similar bioactivities [132].

Although CTS incorporation into Coll scaffolds has been previously investigated, these studies have mainly focused on the use of freeze-dried scaffolds for bone [201, 228] and cartilage TE applications [276-282]. As a consequence of the freeze-drying process, these scaffolds have the disadvantage

of relying on cell seeding post-fabrication, which is time consuming and generally leads to heterogeneous cell distribution [229]. In contrast, Coll/CTS hydrogels have the ability to incorporate the cells during the fabrication process, allowing a homogenous cell distribution in a short time period. Coll/CTS hydrogels have been investigated by Tan *et al.* [230], as well as by Wang and Stegemann [231] for BTE applications; however, these studies have focused on the development of highly-hydrated gels (HHGs) with low CFD and solid weight percent. In particular, CFD has been discovered to be a significant parameter to control collagen mineralization *in vitro*, and has been proven to be positively correlated with the extent of carbonated hydroxyapatite formation [459].

The aim of this doctoral research was to develop an OTE strategy that models the complex osteochondral structure and supports the simultaneous regeneration of AC and the underlying subchondral bone. In this regard, an integrated bilayered model system that closely mimics the native ECM of both cartilage and bone at the osteochondral interface, was proposed based on the incorporation of a GAG-analog (*i.e.* CTS), within a dense Coll hydrogel. As a consequence of difficulties in processing hydrogels based on Coll II [129, 240, 241] acid-extracted Coll I was used instead.

The design of functional TE scaffolds for osteochondral repair involves optimization of several biophysical and biochemical properties [460]. Physical design includes scaffold architecture, ECM density, compressive modulus, cell-mediated contraction, resistance to collagenase degradation, hydraulic permeability, swelling and layer interface integration. Biochemical design concerns chemical composition and biological properties, which is related to the cell-material interaction, such as, cell viability, proliferation and differentiation. This thesis aimed to acquire insight into the role of CTS on a number of the above-mentioned aspects as part of the development of an osteochondral model system. *Figure 8.2* schematically illustrates the scaffold design parameters studied within this doctoral research.

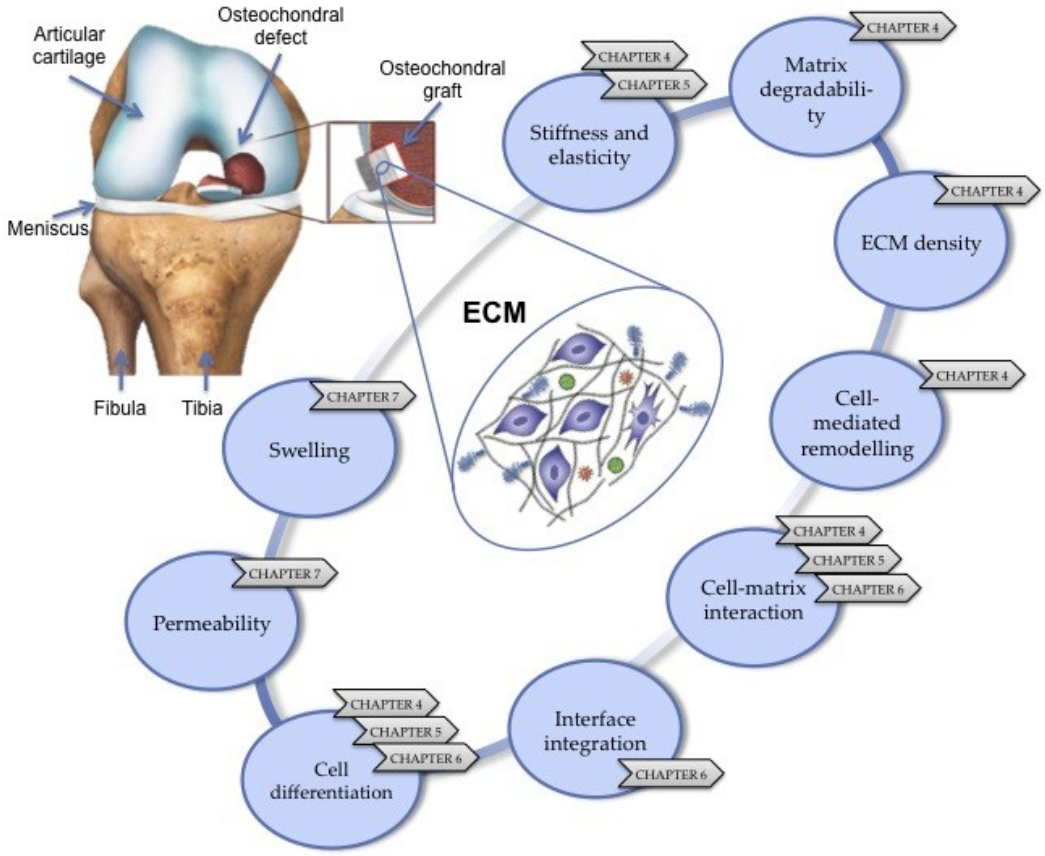

Figure 8.2: Schematic of the biophysical and biochemical properties of the complex 3D ECM environment of tissues and their study within this doctoral research.

In terms of biophysical design, an initial study investigated the development of highly-hydrated Coll/CTS hybrid gels with different CTS proportions and subjected to PC, in order to achieve dense scaffolds with compositions closer to native tissue. In this respect, PC was shown to be an effective and rapid process able to generate, within minutes, dense Coll/CTS hybrid gels with increased solid weight percent approaching physiological values. *Figure 8.3* shows the solid weight percent of the three main compositions investigated in this doctoral research in highly-hydrated and dense forms, as well as cell-seeded scaffolds after 3 weeks in culture. These results can be summarised as follows:

1. PC can be effectively applied to significantly increase the solid weight percent of highly hydrated Coll/CTS hybrid gels (up to 46.9-, 23.5- and

18.2-fold increase in as-made dense Coll, Coll/CTS 2:1 and Coll/CTS 1:1 hydrogels, respectively).

2. PC is an efficient process that allows the generation of dense scaffolds with higher solid weight percentages in a matter of minutes, compared to weeks *via* cell-action (osteoblast seeded within HHG for 21 days in culture).

3. Direct comparison of dense and HHG osteoblast-seeded scaffolds cultured for 21 days validated the increase in solid weight percentages (up to 2.8-fold increase) of dense hydrogels.

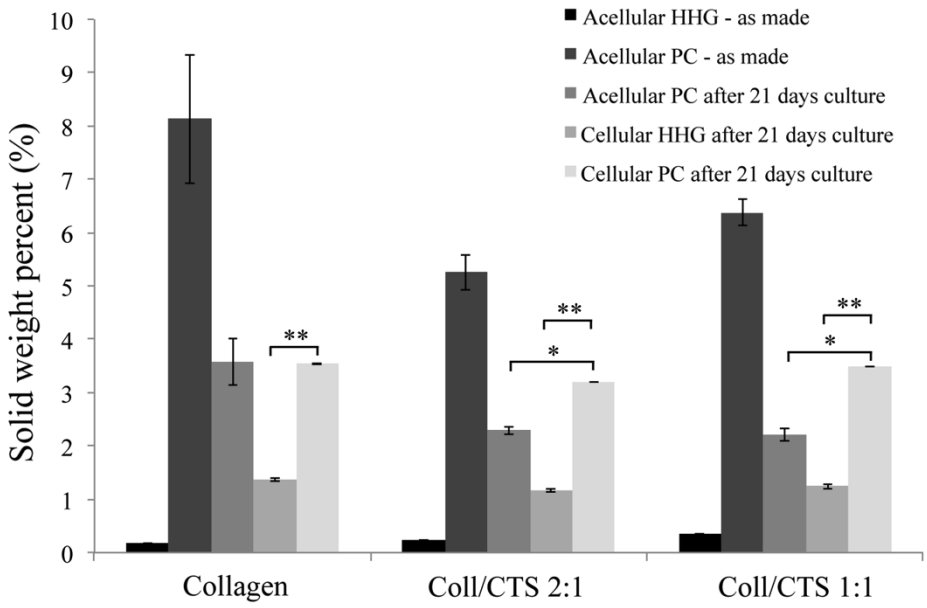

Figure 8.3: Solid weight percent of acellular and osteoblast-seeded Coll, Coll/CTS 2:1 and Coll/CTS 1:1 hydrogels after 21 days in culture in highly-hydrated and dense forms. Solid weight percent was calculated by weighing the scaffolds before and after freeze-drying. * indicates a significant difference between acellular and cellular PC after 21 days. ** indicates a significant difference between cellular HHG and PC after 21 days.

The fact that the solid weight percent of dense cell-seeded scaffolds were lower than those obtained from the as-made dense hydrogels may be attributed to a swelling effect in combination with a cell-mediated remodelling process. *Section 7.3.4* demonstrated that under physiological conditions, the swelling ratio

of the collagen-based hydrogels increased with increasing CTS content (up to 107 % for Coll/CTS 1:1), therefore reducing the solid weight percent after 21 days in culture. Moreover, osteoblast-mediated remodelling of dense scaffolds was demonstrated in *Section 4.7*, which involved the degradation of the collagenous ECM by MMPs. Further characterization by Western blotting suggested that MMP-13 was partially responsible for scaffold remodelling [358, 359]. It is noteworthy that although the cellular dense Coll/CTS 1:1 hydrogel had the highest swelling ratio (59 % more swelling compared to Coll) and presented the highest expression of MMP-13 among all the formulations assayed, the final solid weight percent of the cellular dense Coll/CTS 1:1 hydrogel was comparable to that of Coll alone. This result may be related to Coll/CTS hydrogels supporting higher cell-induced mineralization and ECM secretion within the scaffold.

The ability of dense Coll/CTS hybrid gels to withstand cell-mediated contraction was evaluated in *Sections 4.5.6* and *5.4.2*. The incorporation of CTS led to an increase in scaffold resistance to cell-mediated contraction both in osteoblast and chondroprogenitor-seeded scaffolds, regardless their initial state (*i.e.* highly-hydrated or dense) or geometry (*i.e.* sheets or rolls) as shown in *Figure 8.4* and *Figure 8.5*. It is known that depending on their external tension, cells develop a pre-stress levels to modulate their cell-matrix contacts, pseudopod lengths, cytoskeletal organization and modulus of elasticity [319]. Therefore, the mechanical tension generated by the contractile activity of the cells, plays an important role in cell differentiation, migration, morphogenesis and tissue remodelling [322].

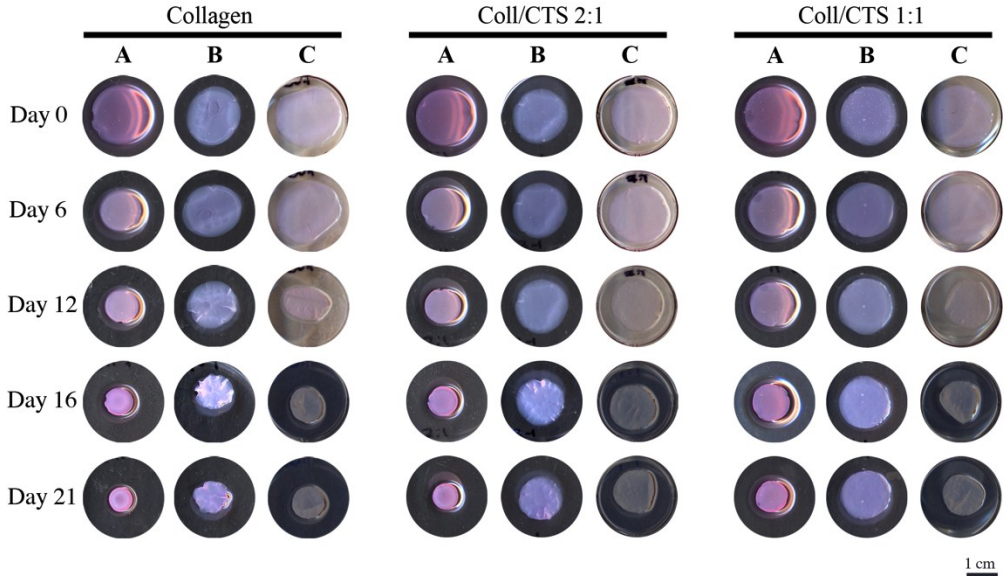

Figure 8.4: Highly-hydrated and dense Coll, Coll/CTS 2:1 and Coll/CTS 1:1 gel contraction by MC3T3-E1 pre-osteoblasts and RCJ3.1C5.18 chondroprogenitors. MC3T3-E1 cells were seeded within highly-hydrated (A) and dense hydrogels (B). RCJ3.1C5.18 chondroprogenitors were seeded within dense hydrogels (C).

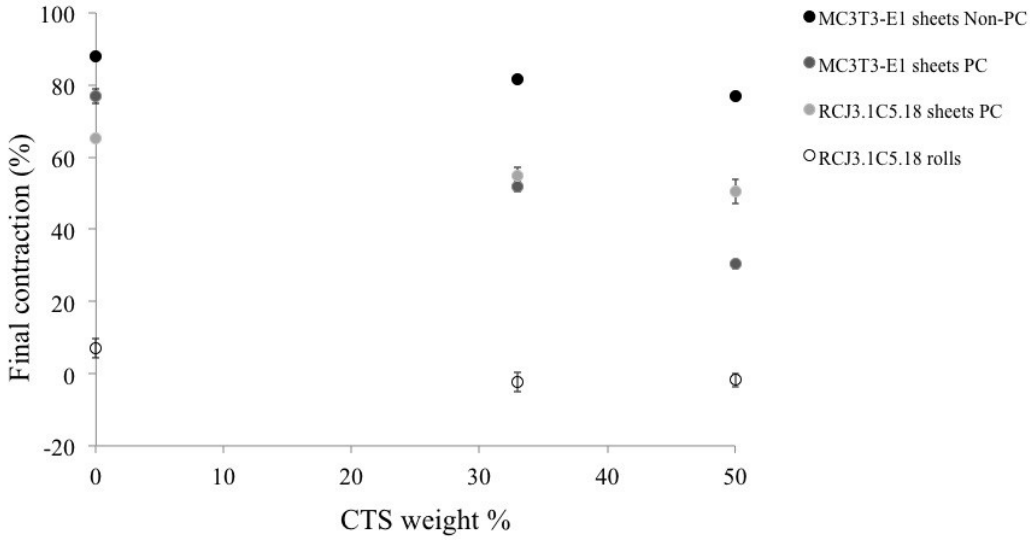

Figure 8.5: Final contraction % after 21 days in culture *versus* CTS weight %. Osteoblasts were seeded within highly-hydrated (HHG) or dense (PC) scaffolds and chondroprogenitors were seeded within dense discs or cylindrical rolls. The final contraction of all scaffolds after 21 days in culture was found to decrease with increasing amount of CTS.

Chapters 4 and *5* demonstrated that the compressive modulus of as-made scaffolds increased with CTS content and that it was inversely related to the

extent of cell-induced contraction of osteoblast and chondroprogenitor seeded cells dense sheets and dense cylindrical rolls (*Figure 8.6*). It was also found that the incorporation of CTS decreased the extent of casting fluid expulsion attributable to PC, when compared to Coll alone. CTS may be responsible for interlinking with the collagen network and increasing the swelling pressure that originates from its high fluid retention capacity (water molecules that are bound to the hydrophilic sites as well as the free water molecules that have restricted mobility) [341]. This enables Coll/CTS to resist higher compressive loads when compared to Coll (increasing from 23.5 to 55.25 kPa in the case of as-made Coll and Coll/CTS 1:1 scaffolds, respectively) [16, 64, 374]. At day 1 in MEM, although all acellular scaffolds underwent a decrease in the compressive modulus values, the hybrid scaffolds maintained a higher value when compared to Coll alone. A similar trend was observed in cell-seeded scaffolds, which was maintained throughout the culture period. The fact that there was no significant difference between the compressive modulus of acellular and cellular scaffolds over time was attributed to the long term culture, which may have allowed the entrapment of non-bound water in between the rolled sheet layers, weakening the matrix and reducing its compressive modulus.

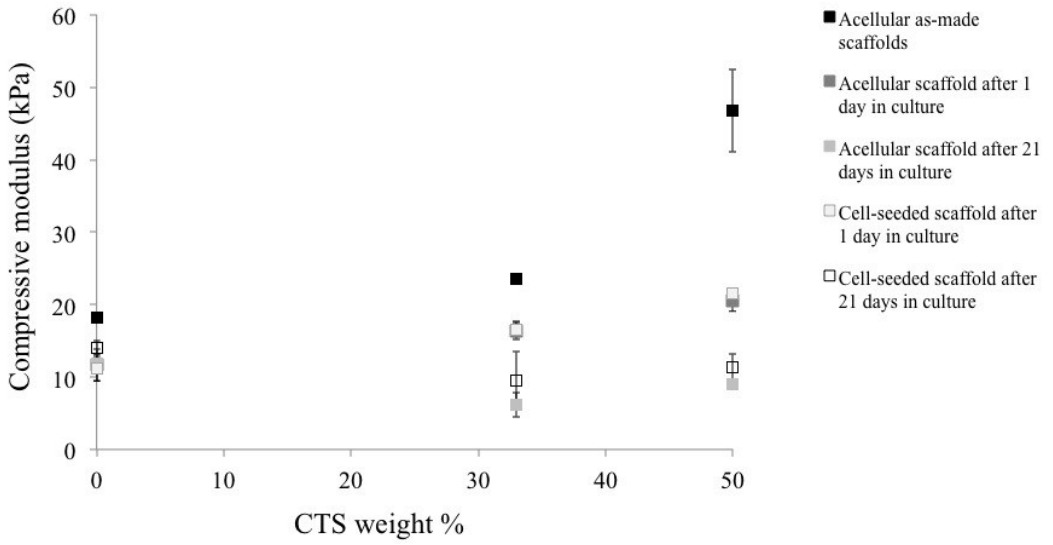

Figure 8.6: Compressive modulus *versus* CTS weight %. Compressive modulus of chondroprogenitor-seeded scaffolds and acellular dense cylindrically shaped constructs at 1 and 21 days in culture. There is a significant increase in the compressive modulus at day 1 with increasing CTS content. A significant decrease in compressive modulus is observed in all constructs at 21 days. No significant difference is observed in the acellular and cellular cylindrical rolls for all specimens at 21 days (ANOVA, $p > 0.05$).

Therefore, the results obtained in this dissertation demonstrate that the combination of CTS incorporated Coll gels and PC (*i.e.* to increase the scaffold solid weight percent), can be used as an approach to generate scaffolds that mimic the structure and composition of native tissues (*e.g.* osteoid and cartilage). Biomimetic dense Coll/CTS scaffolds provide higher compressive modulus, higher resistance to enzymatic degradation and lower cell-mediated contraction when compared to dense Coll scaffolds. In addition, in *Chapter 7* it was demonstrated that the incorporation of CTS within dense Coll gels resulted in the modulation Coll/CTS biophysicochemical properties. In particular, k was found to decrease with CTS content, resulting in a concomitant increase in the scaffold compressive modulus both under isotonic and hypertonic conditions. This was attributed to the increase in the osmotic pressure and resistance to compressive forces as a consequence of CTS fixed charge. Moreover, the electrostatic contribution of CTS to Coll hydrogels was investigated through swelling characterization. Under isotonic conditions, increasing amounts of CTS resulted in higher swelling ratios. This increase was attributed to a higher number of

protonated groups and therefore the repulsive forces between the fixed charged constituents of the hydrogel, resulting in a rise of the osmotic pressure and promotion of water intake [387, 453]. Thus, the dense Coll/CTS hydrogels developed in this doctoral research can be rapidly and easily reproduced with controlled biophysical properties through CTS incorporation, thus providing a reliable 3D *in vitro* tissue model that may be adapted to optimize TE scaffold design and improve therapeutic outcomes.

Regarding the biochemical design, dense Coll/CTS hydrogels were individually investigated for their potential use as *in vitro* model scaffolds directed towards the support of bone- and cartilage-like formation. *Chapters 4* and *5* demonstrated their ability to maintain both pre-osteoblast and chondroprogenitor growth and differentiation during long-term culture. In particular, *Chapter 4* investigated the effect of dense Coll/CTS gels on seeded MC3T3-E1 pre-osteoblast function. The results on the viability, proliferation, ALP activity, matrix remodelling capability (*via* MMP-13 expression) and its biomineralization supported the notion that dense Coll/CTS scaffolds may provide a suitable *in vitro* osteoid model able to support the normal pattern of development of bone-like tissue. In *Chapter 5* the 3D architecture, composition and structure of the native cartilage ECM was mimicked by the use of a hydrogel composed of Coll and CTS with weight ratios approaching those of Coll/GAG found in cartilage, and rapidly increasing the solid weight percent *via* PC. The incorporation of CTS to Coll scaffolds was demonstrated to have a stimulatory effect towards the differentiation of chondroprogenitors, as indicated by the higher production of Coll II and aggrecan, compared to Coll alone. The chondroprotective property of CTS, together with increased viability and metabolic activity as well as a decrease in cell-mediated gel contraction, provided a cartilage-like model for the study of chondroprogenitor differentiation toward cartilage-like ECM formation and its potential use as models for CTE.

Among the various design parameters that are necessary for CTE scaffold development is their ability to be scaled up to repair critical-sized defects (> 2 mm diameter) [68]. In this respect and in an effort to contribute to the understanding of the complex interplay between scaffold geometry, microstructure, composition, mechanical properties and cell function, cylindrically shaped constructs with clinically relevant diameters measuring 3 to 5 mm, were also developed and investigated in *Chapter 5*. The viability of RCJ3.1C5.18 cells and GAG content within each specimen was explored. While there was a decrease in cell viability within the core regions of all cylindrical constructs and a concomitant decrease in GAG content over time, the incorporation of CTS diminished both these effects. This confirmed the chondroprotective properties of CTS observed on Coll/CTS discs, which may have stabilized the chondrocytic phenotype of seeded cells closer to the core.

The findings reported in *Chapter 5* provide valuable design information for the development of model scaffolds directed towards the clinical repair of critical-sized AC defects. Furthermore, the geometry of dense Coll/CTS hydrogels may be designed to fill defects of different sizes. In this doctoral research, cylindrically shaped constructs of up to 9 mm in height were investigated, approaching human AC thickness that can vary from 0.5 to 7.1 mm [461]. Thus dense Coll/CTS scaffolds may be also transferred to generate model scaffolds able to fill a range of potential defects, from partial to full-thickness defects, providing new perspectives in the translation of *in vitro* results into *in vivo* clinical applications.

In pursuit of the aim set in the present doctoral dissertation, *Chapter 6* investigated the development of a bilayered dense hydrogel to model the complex osteochondral structure, by co-gelling cartilaginous (Coll/CTS 1:1) and osteoid-like (Coll/CTS 33:1) layers with Coll/CTS weight ratios approaching those of Coll/GAGs in the native ECM of cartilage and bone. Several attempts have been made to fabricate complex tissues with a stratified architecture containing two or more discrete layers with specific physical and chemical properties, and many

combinations of scaffolds and cell strategies have been investigated to date [28]. One strategy involves the culturing of separate layers for cartilage and bone regeneration followed by their combination by suturing or gluing before implantation [27, 28]. This strategy faces the problem of presenting poor integration between layers, increasing the probability of implant failure [27, 284]. Thus, efforts should be made to achieve well-integrated cartilaginous and bone-like layers that mimic the native connective tissue of cartilage and bone present in the osteochondral region. In *Chapter 6*, it was demonstrated by light, confocal and scanning electron microscopy, that bilayered dense Coll/CTS hydrogels presented two distinctive but integrated layers with different morphologies, which were maintained during the 35-day culture period. The bilayered hydrogel developed here was found to be an effective OTE scaffold, promoting simultaneous chondrogenesis and osteogenesis under optimized co-culture conditions as evidenced by biochemical, immunohistochemical and histological analyses, and biomarker gene expression profiles.

In particular, RCJ3.1C5.18 chondrocyte proliferation and cartilaginous ECM synthesis within the cartilage-like layer of the osteochondral construct, displayed trends similar to the *in vitro* sequence of ESC differentiation [247, 248], suggesting that the dense Coll/CTS 1:1 layer is a suitable environment for the regulation of chondrocyte differentiation and phenotype stabilization (*Figure 8.7*).

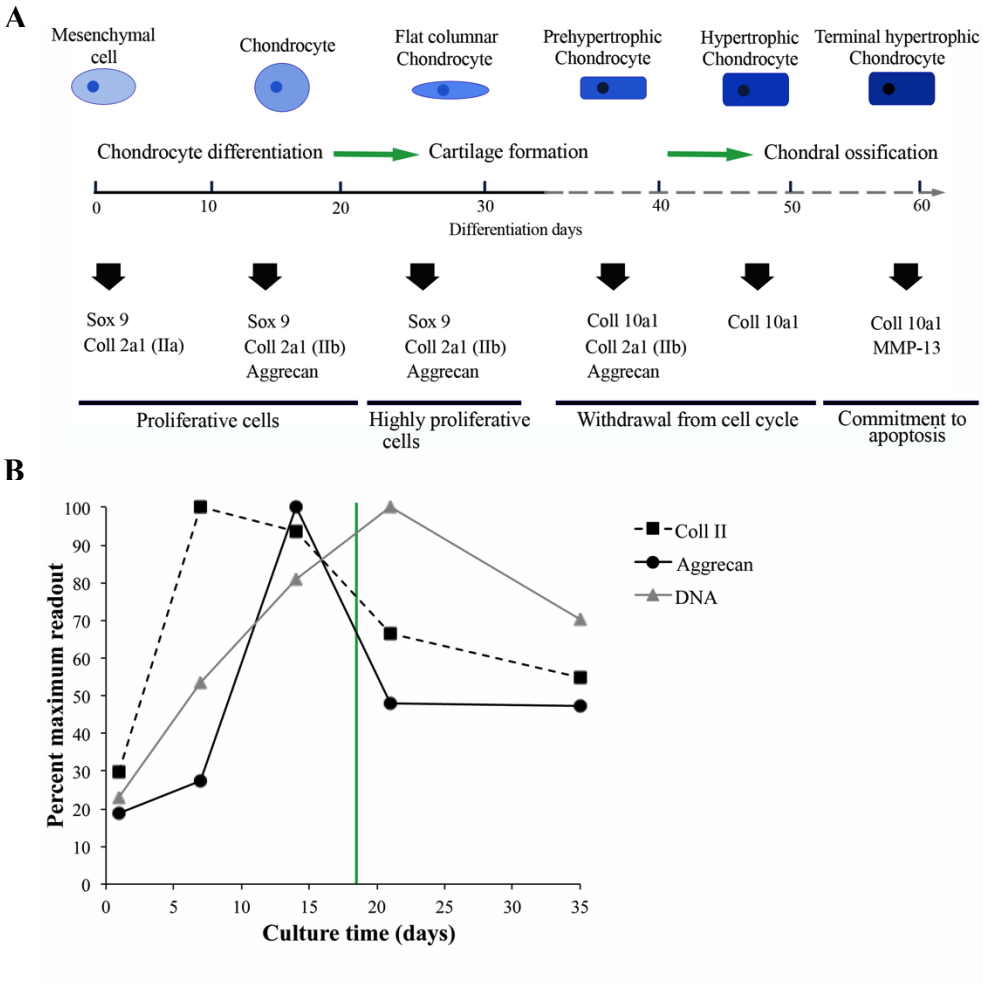

Figure 8.7: Growth and differentiation of the chondrogenic lineage. (A) The temporal morphogenetic events during ESC chondrogenesis includes: (1) condensation of progenitor, (2) chondrocyte differentiation, (3) cartilaginous ECM deposition, (4) hypertrophy and cartilage degradation, and (5) chondral ossification. (B) Chondrocyte differentiation sequence of the RCJ-seeded dense Coll/CTS 1:1 hybrid bilayered scaffold. Adapted from [247, 248]. Copyright © 2010 Yamashita et al. Copyright © 2008 The Journal of Clinical Investigation.

Moreover, the results obtained on the viability, proliferation, ALP activity, gene expression and matrix biomineralization within the osteoid-layer showed similar trends to the *in vivo* sequence of osteoblast differentiation reported in *Section 4.5.9* [190, 462], indicating that the dense Coll/CTS 33:1 layer is a suitable *in vitro* osteoid-like tissue able to support the normal pattern of development of bone-like tissue (*Figure 8.8*).

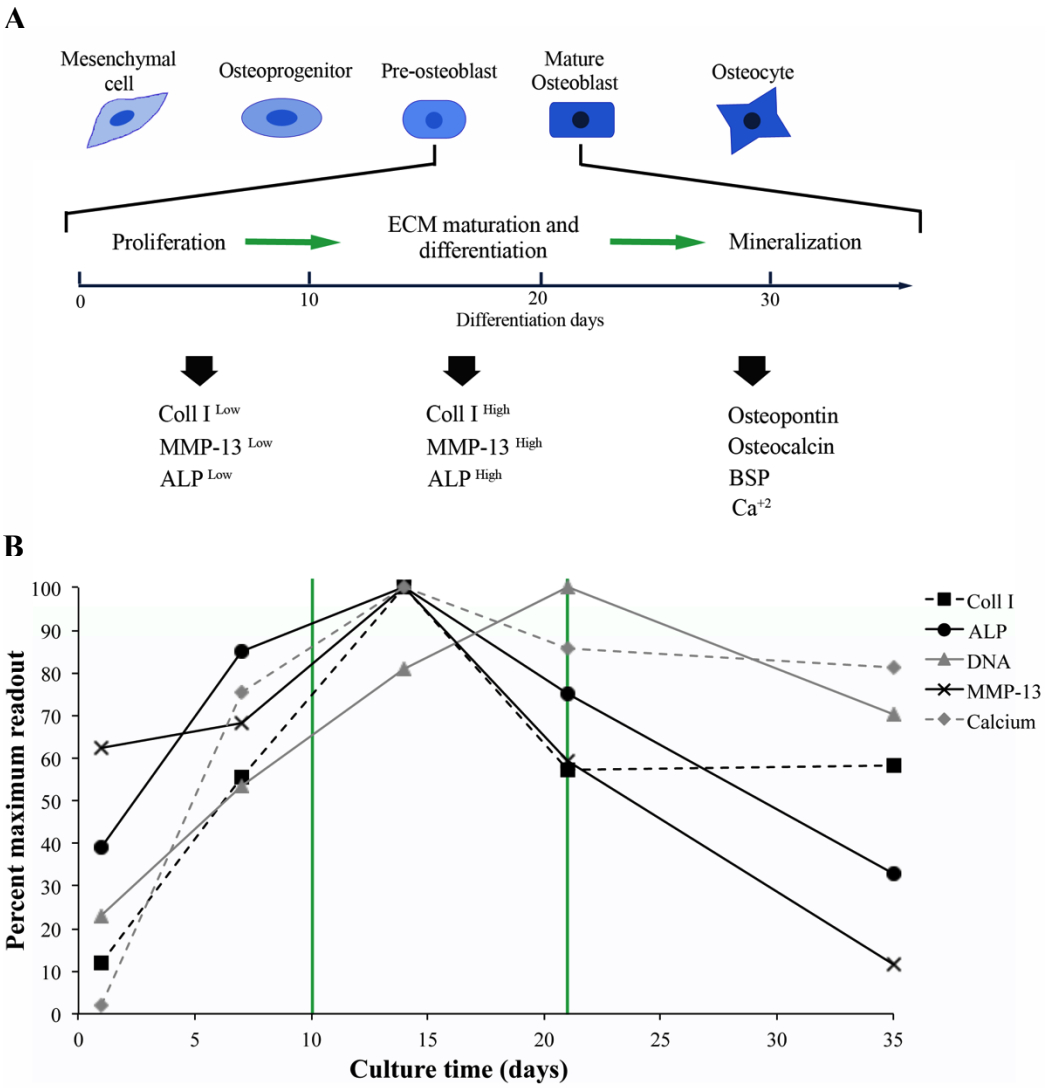

Figure 8.8: Growth and differentiation of the osteoblastic lineage. (A) Temporal morphogenetic events during osteogenesis. (B) Osteoblast differentiation sequence of the MC3T3-E1-seeded dense Coll/CTS 33:1 hybrid bilayered scaffold showing three morphologically and phenotypically distinct periods: proliferation, ECM maturation and differentiation, and mineralization. Adapted from [190, 462]. Copyright © 1993 The Endocryne Society. Copyright © 2004 Nature Publishing Group.

CHAPTER 9: CONCLUSIONS AND FUTURE PERSPECTIVES

9.1 CONCLUSIONS

The overall conclusions pertaining to the present dissertation can be summarized as follows:

- The role of GAGs in native tissues was mimicked by the incorporation of CTS into a fibrillar Coll hydrogel, resulting in a tissue-equivalent matrix with characteristics of ECMs. This tissue-like model demonstrated the transferability of the PC technique from Coll hydrogels to hybrid scaffolds, providing further control over the solid volume fraction-to-fluid composition and meso-scale structure of the scaffolds.

- The biophysical properties of dense Coll hydrogels were tailored by the incorporation of CTS. Higher CTS content led to an increase in scaffold resistance to collagenase degradation and resulted in contrasting mechanical properties when tested under tension compared to compression. Dense Coll/CTS hydrogels led to a decrease in the apparent tensile modulus and break stress and an increase in the compressive modulus compared to Coll alone.

- Hydraulic permeability of Coll/CTS hydrogels, estimated by the Happel model, decreased with increasing CTS content both in highly-hydrated and dense forms. The permeability values of Coll/CTS hydrogels depended both on the tortuosity flow-path induced by the interlinked CTS within the Coll network, as well as, on the electrokinetic effect of CTS.

- The electrostatic contribution of CTS to dense Coll hydrogels, which originates from the protonated amino groups found in the polysaccharide structure, resulted in a decrease in both the rate and final extent of weight loss when undergoing compression, as well as, in higher swelling ratios.

- Analysis of the spatiotemporal distribution of fluorescent beads-seeded highly-hydrated hydrogels by CLSM revealed a temporal increase in bead density

throughout the scaffold's thickness. Bead density of highly-hydrated Coll/CTS hydrogels undergoing compression decreased relative to CTS content, correlating strongly with increasing compressive modulus.

- Increasing CTS content resulted in a greater difference between the top and bottom densities of hydrogels undergoing SC, suggesting that at the equilibrium state, the Coll gel had a more uniform structure compared to Coll/CTS hydrogels. In contrast, Coll/CTS hydrogels under PC resulted in a more uniformly distributed solid density throughout the scaffold thickness, compared to the self-compression process.

- The correspondence between the bead density and solid weight percent values for each specimen validated the fluorescent bead method as an effective and reliable marker of collagen density.

- The modulation of CTS content in Coll/CTS hydrogels was demonstrated to engineer scaffolds with tailored permeability, swelling and mechanical properties relevant to tissue engineering applications.

- Dense Coll/CTS hydrogels individually supported MC3T3-E1 osteoblasts and RCJ3.1C5.18 chondrocytes growth, and demonstrated their ability to differentiate under osteogenic- and chondrogenic-inducing conditions, respectively, during long-term culture.

- The effect of CTS incorporation on modulating MC3T3-E1 osteoblastic cell-based remodelling of dense Coll/CTS hydrogels (*via* MMP-13 expression and cell-mediated contraction) was related to their morphological and mechanical properties.

- Seeded osteoblasts and chondrocytes showed trends similar to the *in vivo* sequence of the human osteoblast and *in vitro* sequence of ESCs differentiation, respectively; proving a potential biomimetic model as an approach towards the support of bone- and cartilage-like tissue formation.

- Dense Coll/CTS disc scaffolds were successfully scaled-up to cylindrically shaped rolls, with clinically relevant geometries (3 to 5 mm in diameter and 9 mm in height), for the repair of critical-sized defects. The viability and ECM biosynthesis of chondrocyte-seeded Coll/CTS rolls were greater along the entire radial extent of the cylindrical scaffold, when compared to Coll alone.

- Cylindrically shaped scaffolds provided new insights into the complex interplay between scaffold geometry, microstructure, composition, mechanical properties and cell function.

- Plastically compressing a stratified highly-hydrated gel, with each layer having different Coll/CTS weight ratios approaching those of Coll/GAGs in the native ECM of cartilage and bone, resulted in a bilayered dense Coll/CTS hydrogel with two distinct but integrated layers with physiologically relevant collagen fibrillar densities and solid weight percent.

- The bilayered dense Coll/CTS hydrogel model provided a strong proof-of-concept supporting simultaneous chondrogenesis and osteogenesis using two highly characterized and relevant cell lines under optimized co-culture conditions.

- Simultaneous culture of RCJ and MC3T3-E1 cells resulted in characteristic morphologies and gene expression profiles with similar trends to the *in vitro* sequence of chondrogenic differentiation of ESCs and *in vivo* sequence of human osteoblast differentiation, respectively.

- The dense stratified hydrogel provided an effective *in vitro* model for the study of cell-cell interactions and the production of multilayered scaffolds as relevant biomimetic constructs for OTE.

9.2 FUTURE PERSPECTIVES

This doctoral dissertation provides a thorough understanding of the different aspects of scaffold design and modulation of the biophysicochemical properties of dense Coll hydrogels by the incorporation of CTS, with the aim of engineering an

osteochondral model with characteristics of native ECM. Since future clinical therapies for reconstructive surgery rely on the detailed understanding of the fundamental aspects of the *in vitro* setting, it is envisaged that the outcomes achieved through this doctoral research will serve as a source for future investigations in TE. This section addresses some of the potential avenues of future investigations that deserve further examination.

The developed osteoid-mimicking dense Coll/CTS scaffold is proposed as an *in vitro* model for preclinical studies. CTS incorporation into dense Coll hydrogels improved the morphological and mechanical properties, along with higher resistance to collagenase degradation and cell-mediated contraction. In addition, *in vitro* investigation of the MC3T3-E1 osteoblast function within the developed dense hydrogels demonstrated that the Coll/CTS combination supports osteoblastic growth, differentiation and mineralization. This proposed osteoid model may be also used *in vitro* to provide new insights on bone pathologies, which involves connective tissue disorders, such as, osteogenesis imperfecta (OI), among others. GAGs (*e.g.* hyaluronic acid) have diverse functions in skeletal tissues. In particular, they participate in joint cavity formation and longitudinal bone growth, and it is believed that they regulate bone remodelling by controlling osteoclast, osteoblast and osteocyte behaviour [463]. Moreover, bone analysis from patients with OI showed a 3-fold increase in hyaluronic acid compared to normal bone [464]. Therefore, by modifying the Coll/CTS ratio to match the Coll/GAG values in normal and pathological bone may provide potential knowledge on skeletal diseases.

In this study, dense Coll/CTS hydrogels were also shown to promote chondrogenic differentiation, in particular, within hybrids with higher content of CTS. This phenomenon was attributed to the “chondroprotective” properties of CTS. However, the exact mechanisms by which it influences cell behaviour are still not fully understood. Future clinical therapies need to rely on a more detailed understanding of how CTS specifically interacts with cells and ECM components

in the body. The modification or masking of the different functional groups in CTS may provide an approach for studying this phenomenon.

Although dense Coll/CTS discs demonstrated potential as *in vitro* models directed towards the clinical repair of AC, the development of cylindrically shaped constructs of a scale necessary to repair critical-sized AC defects (> 2 mm diameter) revealed that these constructs developed a necrotic core and a reduction in GAG/DNA over time. These results were linked to the limited mass transportation along the entire thickness of the roll. In this respect, monitoring the expression of hypoxia-inducible factors (transcription factors that respond to changes in oxygen concentration) either by immunohistochemistry or PCR, can be proposed. In addition, measurements of oxygen levels along the radial direction of the cylindrically shaped construct may be performed simultaneously using an oxygen probe [465].

Another challenge for the near future is to gain further insight in the optimal geometry of dense Coll/CTS scaffolds to enhance the viability and biosynthetic activity of chondrocyte-seeded cells. Fine-tuning the geometry of these cylindrically shaped constructs should be performed alongside with optimization of the critical CTS dose to stimulate chondrocyte differentiation. Moreover, in this doctoral dissertation the effect of CTS incorporation on Coll hydrogels biopshysicochemical properties showed that CTS content is directly related to the swelling and compressive modulus, as well as to resistance to cell-mediated contraction and collagenase degradation, and inversely related to the hydraulic permeability. These effects allowed for the development of scaffolds with properties that may be tailored to meet the specific requirements of various tissue engineering and drug delivery applications. Furthermore, beyond the application proposed, it may also be anticipated that scaffolds with defined oxygen levels may be created *via* adjusting the collagen fibrillar density and CTS content, in the range of possible cell types for TE applications.

Integrated bilayered dense Coll/CTS with ratios approaching those of Coll/GAG in the native ECM of cartilage and bone was demonstrated to support simultaneous chondrogenesis and osteogenesis under optimized co-culture conditions by mimicking the complex structure of osteochondral tissue. Incorporating additional layers to recapitulate more closely the zonal organization of the osteochondral tissue may improve the proposed model. Strategies to achieve this may include the incorporation of distinct layers mimicking the superficial, middle and deep zones of cartilage by adjusting the collagen fibril orientation and density, Coll/CTS ratio and cell type and density. Moreover, the use of a pre-mineralized Coll hydrogel or the combination of a Coll hydrogel with a mineralization precursor, such as Bioglass® [335], may be used to recreate the calcified zone and/or the subchondral bone.

Future studies may also investigate different alternatives to increasing the mechanical strength of dense Coll/CTS scaffolds for their use in load bearing orthopaedic applications. Attempts to do so might involve the use of non-toxic chemical cross-linking agents, such as, 11-ethyl-3-(3-dimethylaminopropyl)-carbodiimide [164, 165], dimethyl 3,3'-dithiobisprpionimidate [166], diphenylphosphorylazide [168] and genipin [276, 281], among others. Moreover, the modulation of cross-linking may also regulate the releasing profiles of drugs or bioactive factors (*e.g.* growth factors, cytokines and genes) [269].

The results from these *in vitro* studies will be difficult to put into a clinical perspective until assessed *in vivo*. Therefore, future *in vivo* studies in small animal models should be considered to investigate the dense Coll/CTS hydrogels under physiological conditions. Medial condyle defects in rabbit femorotibial joints, of approximately 3 mm diameter and 2.5 mm deep, may be used for this purpose [466]. A defect having the same proposed dimensions should be performed in the opposite knee and implanted with a Coll alone scaffold as a control. It is proposed that acellular dense Coll/CTS hydrogels should be investigated first in order to evaluate the inflammatory host response and biostability of the scaffolds. *A*

posteriori, it is proposed that MSC-seeded bilayered dense Coll/CTS constructs may be implanted in order to evaluate the regeneration of the articular cartilage and subchondral bone regions.

CHAPTER 10: REFERENCES

[1] Langer R, Vacanti JP. Tissue Engineering. Science. 1993;260:920-6.
[2] Tsang VL, Bhatia SN. Three-dimensional tissue fabrication. Advanced Drug Delivery Reviews. 2004;56:1635-47.
[3] R.Lanza RLaJV. "Principles of tissue engineering". third edition ed: Elsevier USA; 2007.
[4] Dang JM, Leong KW. Natural polymers for gene delivery and tissue engineering. Advanced Drug Delivery Reviews. 2006;58:487-99.
[5] Nair LS, Laurencin CT. Biodegradable polymers as biomaterials. Progress in Polymer Science. 2007;32:762-98.
[6] Ramshaw JAM, Peng YY, Glattauer V, Werkmeister JA. Collagens as biomaterials. Journal of Materials Science-Materials in Medicine. 2009;20:3-8.
[7] Wakitani S, Goto T, Young RG, Mansour JM, Goldberg VM, Caplan AI. Repair of large full-thickness articular cartilage defects with allograft articular chondrocytes embedded in a collagen gel. Tissue Engineering. 1998;4:429-44.
[8] Chen GP, Sato T, Tanaka J, Tateishi T. Preparation of a biphasic scaffold for osteochondral tissue engineering. Materials Science & Engineering C-Biomimetic and Supramolecular Systems. 2006;26:118-23.
[9] Friess W. Collagen - biomaterial for drug delivery. European Journal of Pharmaceutics and Biopharmaceutics. 1998;45:113-36.
[10] Cen L, Liu W, Cui L, Zhang W, Cao Y. Collagen tissue engineering: Development of novel biomaterials and applications. Pediatric Research. 2008;63:492-6.
[11] Elisseeff J, Puleo C, Yang F, Sharma B. Advances in skeletal tissue engineering with hydrogels. Orthodontics & craniofacial research. 2005;8:150-61.
[12] Balakrishnan B, Banerjee R. Biopolymer-Based Hydrogels for Cartilage Tissue Engineering. Chemical Reviews. 2011;111:4453-74.
[13] Gentleman E, Nauman EA, Dee KC, Livesay GA. Short collagen fibers provide control of contraction and permeability in fibroblast-seeded collagen gels. Tissue Engineering. 2004;10.
[14] Abou Neel EA, Cheema U, Knowles JC, Brown RA, Nazhat SN. Use of multiple unconfined compression for control of collagen gel scaffold density and mechanical properties. Soft Matter. 2006;2:986-92.
[15] Sheu MT, Huang JC, Yeh GC, Ho HO. Characterization of collagen gel solutions and collagen matrices for cell culture. Biomaterials. 2001;22:1713-9.
[16] Brown RA, Wiseman M, Chuo CB, Cheema U, Nazhat SN. Ultrarapid engineering of biomimetic materials and tissues: Fabrication of nano- and

microstructures by plastic compression. Advanced Functional Materials. 2005;15:1762-70.
[17] Mudera V, Morgan M, Cheema U, Nazhat S, Brown R. Ultra-rapid engineered collagen constructs tested in an in vivo nursery site. Journal of Tissue Engineering and Regenerative Medicine. 2007;1:192-8.
[18] Ghezzi CE, Muja N, Marelli B, Nazhat SN. Real time responses of fibroblasts to plastically compressed fibrillar collagen hydrogels. Biomaterials. 2011;32:4761-72.
[19] Geckil H, Xu F, Zhang X, Moon S, Demirci U. Engineering hydrogels as extracellular matrix mimics. Nanomedicine. 2010;5:469-84.
[20] Nesic D, Whiteside R, Brittberg M, Wendt D, Martin I, Mainil-Varlet P. Cartilage tissue engineering for degenerative joint disease. Advanced Drug Delivery Reviews. 2006;58:300-22.
[21] Zhou J, Xu C, Wu G, Cao X, Zhang L, Zhai Z, et al. In vitro generation of osteochondral differentiation of human marrow mesenchymal stem cells in novel collagen-hydroxyapatite layered scaffolds. Acta biomaterialia. 2011;7:3999-4006.
[22] Laurencin CT, Ambrosio AMA, Borden MD, Cooper JA. Tissue engineering: Orthopedic applications. Annual Review of Biomedical Engineering. 1999;1:19-46.
[23] Matthews GL, Hunter DJ. Emerging drugs for osteoarthritis. Expert Opinion on Emerging Drugs. 2011;16.
[24] Ahmed TAE, Hincke MT. Strategies for Articular Cartilage Lesion Repair and Functional Restoration. Tissue Engineering Part B-Reviews. 2010;16:305-29.
[25] Malafaya PB, Reis RL. Bilayered chitosan-based scaffolds for osteochondral tissue engineering: Influence of hydroxyapatite on in vitro cytotoxicity and dynamic bioactivity studies in a specific double-chamber bioreactor. Acta Biomaterialia. 2009;5:644-60.
[26] Mano JF, Reis RL. Osteochondral defects: present situation and tissue engineering approaches. Journal of Tissue Engineering and Regenerative Medicine. 2007;1:261-73.
[27] O'Shea TM, Miao X. Bilayered Scaffolds for Osteochondral Tissue Engineering. Tissue Engineering Part B-Reviews. 2008;14:447-64.
[28] Martin I, Miot S, Barbero A, Jakob M, Wendt D. Osteochondral tissue engineering. Journal of Biomechanics. 2007;40:750-65.
[29] Shea LD, Wang D, Franceschi RT, Mooney DJ. Engineered bone development from a pre-osteoblast cell line on three-dimensional scaffolds. Tissue Engineering. 2000;6:605-17.
[30] Casserbette M, Murray AB, Closs EI, Erfle V, Schmidt J. Bone-formation by osteoblast-like cells in a 3-dimensional cell-culture. Calcified Tissue International. 1990;46:46-56.

[31] Menard C, Mitchell S, Spector M. Contractile behavior of smooth muscle actin-containing osteoblasts in collagen-GAG matrices in vitro: implant-related cell contractions. Biomaterials. 2000;21:1867-77.
[32] Grigoriadis AE, Heersche JNM, Aubin JE. Analysis of chondroprogenitor frequency and cartilage differentiation in a novel family of clonal chondrogenic rat cell lines. Differentiation. 1996;60:299-307.
[33] Chang WH, Tu CL, Bajra R, Komuves L, Miller S, Strewler G, et al. Calcium sensing in cultured chondrogenic RCJ3.1C5.18 cells. Endocrinology. 1999;140:1911-9.
[34] Jackson DW, Lalor PA, Aberman HM, Simon TM. Spontaneous repair of full-thickness defects of articular cartilage in a goat model - A preliminary study. Journal of Bone and Joint Surgery-American Volume. 2001;83A:53-64.
[35] Happel J. Viscous flow relative to arrays of cylinders. Aiche Journal. 1959;5:174-7.
[36] Agrawal CM, Ray RB. Biodegradable polymeric scaffolds for musculoskeletal tissue engineering. Journal of Biomedical Materials Research. 2001;55:141-50.
[37] Kartsogiannis V, Ng KW. Cell lines and primary cell cultures in the study of bone cell biology. Molecular and Cellular Endocrinology. 2004;228:79-102.
[38] Barrere F, Mahmood TA, de Groot K, van Blitterswijk CA. Advanced biomaterials for skeletal tissue regeneration: Instructive and smart functions. Materials Science & Engineering R-Reports. 2008;59:38-71.
[39] Sommerfeldt DW, Rubin CT. Biology of bone and how it orchestrates the form and function of the skeleton. European Spine Journal. 2001;10:S86-S95.
[40] Bilezikian JP, Raisz LG, Martin TJ. Principles of bone biology. USA: Academic Press; 3 edition; 2008.
[41] Martin RB, Burr DB, Sharkey NA. Skeletal tissue mechanics. New York, NY, USA: Springer-Verlag; 1998.
[42] Bronner F, Farach-Carson MC. Bone Formation. London: Springer-Verlag London Limited; 2004.
[43] Rho JY, Kuhn-Spearing L, Zioupos P. Mechanical properties and the hierarchical structure of bone. Medical Engineering & Physics. 1998;20:92-102.
[44] X.Wang, Nyman JS, X. Dong HL, Reyes aM. Fundamental Biomechanics in Bone Tissue Engineering: Morgan & Claypool Publishers; 2010.
[45] Petite H, Viateau V, Bensaid W, Meunier A, de Pollak C, Bourguignon M, et al. Tissue-engineered bone regeneration. Nature Biotechnology. 2000;18:959-63.
[46] Kawasaki K, Buchanan AV, Weiss KM. Biomineralization in Humans: Making the Hard Choices in Life. Annual Review of Genetics. 2009;43:119-42.
[47] Mescher AL. Junqueira's Basic Histology, Twelfth Edition. USA: The McGraw-Hill Companies, Inc; 2010.

[48] Fratzl P, Gupta HS, Paschalis EP, Roschger P. Structure and mechanical quality of the collagen-mineral nano-composite in bone. Journal of Materials Chemistry. 2004;14:2115-23.
[49] Weiner S, Wagner HD. The material bone: Structure mechanical function relations. Annual Review of Materials Science. 1998;28:271-98.
[50] Rosso F, Giordano A, Barbarisi M, Barbarisi A. From cell-ECM interactions to tissue engineering. Journal of Cellular Physiology. 2004;199:174-80.
[51] Springfield D. Autograft reconstructions. Orthopedic Clinics of North America. 1996;27.
[52] Finkemeier CG. Bone-grafting and bone-graft substitutes. Journal of Bone and Joint Surgery-American Volume. 2002;84A:454-64.
[53] Boyce T, Edwards J, Scarborough N. Allograft bone - The influence of processing on safety and performance. Orthopedic Clinics of North America. 1999;30:571-81.
[54] McNicol D, Roughley PJ. Extraction and characterization of proteoglycan from human meniscus. Biochemical Journal. 1980;185:705-13.
[55] De Ceuninck F, Sabatini M, Pastoureau P. Cartilage and Osteoarthitis: Structure and In Vivo Analysis. USA: Humana Press Inc.; 2004.
[56] Burdick JA, Mauck RL. Biomaterials for tissue engineering applications: a review of the past and future trends. Germany: Springer-Verlag; 2011.
[57] U.S NRC. Hierarchical structures in biology as a guide for new materials technology: National Academy Press; 1994.
[58] Burdick JA, Mauck RL. Biomaterials for tissue engineering applications: a review of the past and future trends. Germany: Springer-Verlag.
[59] Flik K. VN, Cole B. and Bach B. Articular cartilage. In: Williams IRJ, editor. Cartilage repair strategies. Totowa, New Jersey, USA: Humana Press Inc.; 2007. p. 1-12.
[60] Poole AR, Kojima T, Yasuda T, Mwale F, Kobayashi M, Laverty S. Composition and structure of articular cartilage - A template for tissue repair. Clinical Orthopaedics and Related Research. 2001:S26-S33.
[61] Sharma L, Kapoor D, Issa S. Epidemiology of osteoarthritis: an update. Current Opinion in Rheumatology. 2006;18.
[62] Sanchez-Adams KAAaJ. Engineering the knee meniscus: Morgan & Claypool; 2009.
[63] Shapiro F, Koide S, Glimcher MJ. Cell origin and differentiation in the repair of full-thickness defects of articular cartilage. Journal of Bone and Joint Surgery-American Volume. 1993;75A:532-53.
[64] Hunziker EB. Articular cartilage repair: basic science and clinical progress. A review of the current status and prospects. Osteoarthritis and Cartilage. 2002;10:432-63.
[65] Kim HKW, Moran ME, Salter RB. The potential for regeneration of articular-cartilage in defects created by chondral shaving and subchondral

abrasion - An experimental investigation in rabbits. Journal of Bone and Joint Surgery-American Volume. 1991;73A:1301-15.
[66] Bhosale AM, Richardson JB. Articular cartilage: structure, injuries and review of management. British Medical Bulletin. 2008;87.
[67] Steadman JR, Briggs KK, Rodrigo JJ, Kocher MS, Gill TJ, Rodkey WG. Outcomes of microfracture for traumatic chondral defects of the knee: Average 11-year follow-up. Arthroscopy-the Journal of Arthroscopic and Related Surgery. 2003;19.
[68] Mithoefer K, McAdams T, Williams RJ, Kreuz PC, Mandelbaum BR. Clinical Efficacy of the Microfracture Technique for Articular Cartilage Repair in the Knee An Evidence-Based Systematic Analysis. American Journal of Sports Medicine. 2009;37.
[69] Chajra H, Rousseau CF, Cortial D, Ronziere MC, Herbage D, Mallein-Gerin F, et al. Collagen-based biomaterials and cartilage engineering. Application to osteochondral defects. Bio-Medical Materials and Engineering. 2008;18:S33-S45.
[70] Alford JW, Cole BJ. Cartilage restoration, part 2 - Techniques, outcomes, and future directions. American Journal of Sports Medicine. 2005;33:443-60.
[71] Puppi D, Chiellini F, Piras AM, Chiellini E. Polymeric materials for bone and cartilage repair. Progress in Polymer Science. 2010;35:403-40.
[72] Nukavarapu SP, Dorcemus DL. Osteochondral tissue engineering: Current strategies and challenges. Biotechnology Advances. 2012.
[73] Kon E, Vannini F, Buda R, Filardo G, Cavallo M, Ruffilli A, et al. How to treat osteochondritis dissecans of the knee: surgical techniques and new trends: AAOS exhibit selection. The Journal of bone and joint surgery American volume. 2012;94.
[74] Chen J, Chen H, Li P, Diao H, Zhu S, Dong L, et al. Simultaneous regeneration of articular cartilage and subchondral bone in vivo using MSCs induced by a spatially controlled gene delivery system in bilayered integrated scaffolds. Biomaterials. 2011;32:4793-805.
[75] Rodrigues MT, Gomes ME, Reis RL. Current strategies for osteochondral regeneration: from stem cells to pre-clinical approaches. Current Opinion in Biotechnology. 2011;22:726-33.
[76] Bentley G, Biant LC, Vijayan S, Macmull S, Skinner JA, Carrington RWJ. Minimum ten-year results of a prospective randomised study of autologous chondrocyte implantation versus mosaicplasty for symptomatic articular cartilage lesions of the knee. Journal of Bone and Joint Surgery-British Volume. 2012;94B.
[77] Gross AE, Kim W, Heras FL, Backstein D, Safir O, Pritzker KPH. Fresh osteochondral allografts for posttraumatic knee defects: Long-term followup. Clinical Orthopaedics and Related Research. 2008;466.
[78] Horas U, Pelinkovic D, Herr G, Aigner T, Schnettler R. Autologous chondrocyte implantation and osteochondral cylinder transplantation in

cartilage repair of the knee joint - A prospective, comparative trial. Journal of Bone and Joint Surgery-American Volume. 2003;85A.
[79] Vijayan S, Bartlett W, Bentley G, Carrington RWJ, Skinner JA, Pollock RC, et al. Autologous chondrocyte implantation for osteochondral lesions in the knee using a bilayer collagen membrane and bone graft A TWO- TO EIGHT-YEAR FOLLOW-UP STUDY. Journal of Bone and Joint Surgery-British Volume. 2012;94B.
[80] Knutsen G, Drogset JO, Engebretsen L, Grontvedt T, Isaksen V, Ludvigsen TC, et al. A Randomized trial comparing autologous chondrocyte implantation with microfracture. Journal of Bone and Joint Surgery-American Volume. 2007;89A.
[81] MacNeil S. Progress and opportunities for tissue-engineered skin. Nature. 2007;445:874-80.
[82] Davis MW, Vacanti JP. Toward development of an implantable tissue engineered liver. Biomaterials. 1996;17:365-72.
[83] Evans GRD, Brandt K, Widmer MS, Lu L, Meszlenyi RK, Gupta PK, et al. In vivo evaluation of poly(L-lactic acid) porous conduits for peripheral nerve regeneration. Biomaterials. 1999;20:1109-15.
[84] Shinoka T, Ma PX, ShumTim D, Breuer CK, Cusick RA, Zund G, et al. Tissue-engineered heart valves - Autologous valve leaflet replacement study in a lamb model. Circulation. 1996;94:164-8.
[85] Altman GH, Horan RL, Lu HH, Moreau J, Martin I, Richmond JC, et al. Silk matrix for tissue engineered anterior cruciate ligaments. Biomaterials. 2002;23:4131-41.
[86] Awad HA, Boivin GP, Dressler MR, Smith FNL, Young RG, Butler DL. Repair of patellar tendon injuries using a cell-collagen composite. Journal of Orthopaedic Research. 2003;21:420-31.
[87] Hutmacher DW. Scaffolds in tissue engineering bone and cartilage. Biomaterials. 2000;21:2529-43.
[88] Temenoff JS, Mikos AG. Review: tissue engineering for regeneration of articular cartilage. Biomaterials. 2000;21:431-40.
[89] Cancedda R, Dozin B, Giannoni P, Quarto R. Tissue engineering and cell therapy of cartilage and bone. Matrix Biology. 2003;22:81-91.
[90] Eisenbarth E. Biomaterials for tissue engineering. Advanced Engineering Materials. 2007;9:1051-60.
[91] Dvir T, Timko BP, Kohane DS, Langer R. Nanotechnological strategies for engineering complex tissues. Nature Nanotechnology. 2011;6:13-22.
[92] Murugan R, Ramakrishna S. Design strategies of tissue engineering scaffolds with controlled fiber orientation. Tissue Engineering. 2007;13:1845-66.
[93] Yang SF, Leong KF, Du ZH, Chua CK. The design of scaffolds for use in tissue engineering. Part 1. Traditional factors. Tissue Engineering. 2001;7:679-89.

[94] Chen GP, Ushida T, Tateishi T. Scaffold design for tissue engineering. Macromolecular Bioscience. 2002;2:67-77.
[95] Hoerstrup SP, Zund G, Cheng SF, Melnitchouk S, Kadner A, Sodian R, et al. A new approach to completely autologous cardiovascular tissue in humans. Asaio Journal. 2002;48:234-8.
[96] Dietmar Werner Hutmacher JTS, Christopher Xu Fu Lam, Kim Cheng Tan, Thiam Chye Lim. State of the art and future directions of scaffold-based bone engineering from a biomaterials perspective. Journal of Tissue Engineering and Regenerative Medicine. 2007;1:245-60.
[97] Glowacki J, Mizuno S. Collagen scaffolds for tissue engineering. Biopolymers. 2008;89:338-44.
[98] Madihally SV, Matthew HWT. Porous chitosan scaffolds for tissue engineering. Biomaterials. 1999;20:1133-42.
[99] Di Martino A, Sittinger M, Risbud MV. Chitosan: A versatile biopolymer for orthopaedic tissue-engineering. Biomaterials. 2005;26:5983-90.
[100] Muzzarelli RAA. Chitins and chitosans for the repair of wounded skin, nerve, cartilage and bone. Carbohydrate Polymers. 2009;76:167-82.
[101] Jayakumar R, Menon D, Manzoor K, Nair SV, Tamura H. Biomedical applications of chitin and chitosan based nanomaterials-A short review. Carbohydrate Polymers. 2010;82:227-32.
[102] Ahmed TAE, Dare EV, Hincke M. Fibrin: A versatile scaffold for tissue engineering applications. Tissue Engineering Part B-Reviews. 2008;14:199-215.
[103] Shaikh FM, Callanan A, Kavanagh EG, Burke PE, Grace PA, McGloughlin TM. Fibrin: A natural biodegradable scaffold in vascular tissue engineering. Cells Tissues Organs. 2008;188:333-46.
[104] Breen A, O'Brien T, Pandit A. Fibrin as a Delivery System for Therapeutic Drugs and Biomolecules. Tissue Engineering Part B-Reviews. 2009;15:201-14.
[105] Wang X, Zhang Y, Wang Y. Recent progress in starch-based polymeric materials. Acta Polymerica Sinica. 2011:24-37.
[106] Allison DD, Grande-Allen KJ. Review. Hyaluronan: A powerful tissue engineering tool. Tissue Engineering. 2006;12:2131-40.
[107] Kim IL, Mauck RL, Burdick JA. Hydrogel design for cartilage tissue engineering: A case study with hyaluronic acid. Biomaterials. 2011;32:8771-82.
[108] Mori M, Yamaguchi M, Sumitomo S, Takai Y. Hyaluronan-based biomaterials in tissue engineering. Acta Histochemica Et Cytochemica. 2004;37:1-5.
[109] Augst AD, Kong HJ, Mooney DJ. Alginate hydrogels as biomaterials. Macromolecular Bioscience. 2006;6:623-33.
[110] Xiaohua Liu PXM. Polymeric Scaffolds for Bone Tissue Engineering. Annals of Biomedical Engineering. 2004;32:477-86.

[111] Ma L, Gao CY, Mao ZW, Zhou J, Shen JC, Hu XQ, et al. Collagen/chitosan porous scaffolds with improved biostability for skin tissue engineering. Biomaterials. 2003;24:4833-41.
[112] Lee CH, Singla A, Lee Y. Biomedical applications of collagen. International Journal of Pharmaceutics. 2001;221:1-22.
[113] Pignatello R. Biomaterials applications for nanomedicine. Croatia: InTech; 2011.
[114] Wallace DG, Rosenblatt J. Collagen gel systems for sustained delivery and tissue engineering. Advanced Drug Delivery Reviews. 2003;55:1631-49.
[115] Badylak SF, Freytes DO, Gilbert TW. Extracellular matrix as a biological scaffold material: Structure and function. Acta Biomaterialia. 2009;5.
[116] Chevallay B, Herbage D. Collagen-based biomaterials as 3D scaffold for cell cultures: applications for tissue engineering and gene therapy. Medical & Biological Engineering & Computing. 2000;38:211-8.
[117] Gelse K, Poschl E, Aigner T. Collagens - structure, function, and biosynthesis. Advanced Drug Delivery Reviews. 2003;55.
[118] Habermehl J, Skopinska J, Boccafoschi F, Sionkowska A, Kaczmarek H, Laroche G, et al. Preparation of ready-to-use, stockable and reconstituted collagen. Macromolecular Bioscience. 2005;5:821-8.
[119] Ricard-Blum S, Ruggiero F. The collagen superfamily: from the extracellular matrix to the cell membrane. Pathologie Biologie. 2005;53.
[120] Kadler KE, Holmes DF, Trotter JA, Chapman JA. Collagen fibril formation. Biochemical Journal. 1996;316:1-11.
[121] Hilborn J. In vivo injectable gels for tissue repair. Wiley Interdisciplinary Reviews-Nanomedicine and Nanobiotechnology. 2011;3:589-606.
[122] Silver FH, Trelstad RL. Type-I collagen in solution - Structure and properties of fibril fragments. Journal of Biological Chemistry. 1980;255:9427-33.
[123] Sionkowska A, Kaminska A. Thermal helix-coil transition in UV irradiated collagen from rat tail tendon. International Journal of Biological Macromolecules. 1999;24:337-40.
[124] Wood GC. The heterogeneity of collagen solutions and its effect on fibril formation. Biochemical Journal. 1962;84:429-35.
[125] Miller EJ, Rhodes RK. Preparation and characterization of the different types of collagen. Methods in Enzymology. 1982;82.
[126] Rubin AL, Schmitt FO, Davison PF, Pfahl D, Speakman PT. Tropocollagen - significance of protease-induced alterations. Science. 1963;139.
[127] Harris JR, Reiber A. Influence of saline and pH on collagen type I fibrillogenesis in vitro: Fibril polymorphism and colloidal gold labelling. Micron. 2007;38:513-21.
[128] Li Y, Asadi A, Monroe MR, Douglas EP. pH effects on collagen fibrillogenesis in vitro: Electrostatic interactions and phosphate binding.

Materials Science & Engineering C-Biomimetic and Supramolecular Systems. 2009;29:1643-9.
[129] Freyria A-M, Ronziere M-C, Cortial D, Galois L, Hartmann D, Herbage D, et al. Comparative Phenotypic Analysis of Articular Chondrocytes Cultured within Type I or Type II Collagen Scaffolds. Tissue Engineering Part A. 2009;15:1233-45.
[130] Dash M, Chiellini F, Ottenbrite RM, Chiellini E. Chitosan-A versatile semi-synthetic polymer in biomedical applications. Progress in Polymer Science. 2011;36:981-1014.
[131] Elder SH, Nettles DL, Bumgardner JD. Synthesis and characterization of chitosan scaffolds for cartilage-tissue engineering. Methods in molecular biology (Clifton, NJ). 2004;238:41-8.
[132] Suh JKF, Matthew HWT. Application of chitosan-based polysaccharide biomaterials in cartilage tissue engineering: a review. Biomaterials. 2000;21:2589-98.
[133] Tsai SP, Hsieh CY, Hsieh CY, Wang DM, Huang LLH, Lai JY, et al. Preparation and cell compatibility evaluation of chitosan/collagen composite scaffolds using amino acids as crosslinking bridges. Journal of Applied Polymer Science. 2007;105:1774-85.
[134] Lindahl U, Hook M. Glycosaminoglycans and their binding to biological macromolecules. Annual Review of Biochemistry. 1978;47:385-417.
[135] Dillow AK, Lowman AM. Biomimetic materials and design: biointerfacial strategies, tissue engineering and targeted drug delivery. Switzerland: Marcel Dekker Inc.; 2002.
[136] Roughley P, Hoemann C, DesRosiers E, Mwale F, Antoniou J, Alini M. The potential of chitosan-based gels containing intervertebral disc cells for nucleus pulposus supplementation. Biomaterials. 2006;27:388-96.
[137] Lee KY, Ha WS, Park WH. Blood compatibility and biodegradability of partially N-acetylated chitosan derivatives. Biomaterials. 1995;16:1211-6.
[138] Illum L. Chitosan and its use as a pharmaceutical excipient. Pharmaceutical Research. 1998;15:1326-31.
[139] Wedmore I, McManus JG, Pusateri AE, Holcomb JB. A special report on the chitosan-based hemostatic dressing: Experience in current combat operations. Journal of Trauma-Injury Infection and Critical Care. 2006;60:655-8.
[140] Kean T, Thanou M. Biodegradation, biodistribution and toxicity of chitosan. Advanced Drug Delivery Reviews. 2010;62:3-11.
[141] Rao SB, Sharma CP. Use of chitosan as a biomaterial: Studies on its safety and hemostatic potential. Journal of Biomedical Materials Research. 1997;34:21-8.
[142] Muzzarelli RA. Clinical and biochemical evaluation of chitosan for hypercholesterolemia and overweight control. Exs. 1999;87:293-304.

[143] Stone CA, Wright H, Clarke T, Powell R, Devaraj VS. Healing at skin graft donor sites dressed with chitosan. British Journal of Plastic Surgery. 2000;53:601-6.
[144] Thein-Han WW, Kitiyanant Y, Misra RDK. Chitosan as scaffold matrix for tissue engineering. Materials Science and Technology. 2008;24:1062-75.
[145] Kim I-Y, Seo S-J, Moon H-S, Yoo M-K, Park I-Y, Kim B-C, et al. Chitosan and its derivatives for tissue engineering applications. Biotechnology Advances. 2008;26:1-21.
[146] Hirano S, Tsuchida H, Nagao N. N-acetylation in chitosan and the rate of its enzymic-hydrolysis. Biomaterials. 1989;10:574-6.
[147] Kurita K, Kaji Y, Mori T, Nishiyama Y. Enzymatic degradation of beta-chitin: susceptibility and the influence of deacetylation. Carbohydrate Polymers. 2000;42:19-21.
[148] Funkhouser JD, Aronson NN. Chitinase family GH18: evolutionary insights from the genomic history of a diverse protein family. Bmc Evolutionary Biology. 2007;7:16.
[149] Hirano S, Iwata M, Yamanaka K, Tanaka H, Toda T, Inui H. Enhancement of serum lysozyme activity by injecting a mixture of chitosan oligosaccharides intravenously in rabbits. Agricultural and Biological Chemistry. 1991;55:2623-5.
[150] Sarmento B, das Neves J. Chitosan-based systems for biopharmaceuticals: delivery, targeting and polymer therapeutics. United Kingdom: John Wiley & Sons Ltd,; 2012.
[151] Khan WS, Rayan F, Dhinsa BS, Marsh D. An Osteoconductive, Osteoinductive, and Osteogenic Tissue-Engineered Product for Trauma and Orthopaedic Surgery: How Far Are We? Stem Cells International. 2012.
[152] Epple M, Baeuerlein E. Handbook of biomineralization. Germany: WILEY-VCH; 2007.
[153] Vunjak-Novakovic G, Freshney RI. Culture of cells for tissue engineering. USA: John Wiley & Sons, Inc; 2006.
[154] Burg KJL, Porter S, Kellam JF. Biomaterial developments for bone tissue engineering. Biomaterials. 2000;21:2347-59.
[155] Murata M, Huang BZ, Shibata T, Imai S, Nagai N, Arisue M. Bone augmentation by recombinant human BMP-2 and collagen on adult rat parietal bone. International Journal of Oral and Maxillofacial Surgery. 1999;28:232-7.
[156] Murata M, Maki F, Sato D, Shibata T, Arisue M. Bone augmentation by onlay implant using recombinant human BMP-2 and collagen on adult rat skull without periosteum. Clinical Oral Implants Research. 2000;11:289-95.
[157] Cochran DI, Jones AA, Lilly LC, Fiorellini JP, Howell H. Evaluation of recombinant human bone morphogenetic protein-2 in oral applications including the use of endosseous implants: 3-year results of a pilot study in humans. Journal of Periodontology. 2000;71:1241-57.

[158] Parenteau-Bareil R, Gauvin R, Berthod F. Collagen-Based Biomaterials for Tissue Engineering Applications. Materials. 2010;3:1863-87.
[159] Moore MA, Chen WM, Phillips RE, Bohachevsky IK, McIlroy BK. Shrinkage temperature versus protein extraction as a measure of stabilization of photooxidized tissue. Journal of Biomedical Materials Research. 1996;32:209-14.
[160] Ma XH, Noishiki Y, Yamane Y, Iwai Y, Marato D, Matsumoto A. Thermal cross-linking for biologically degradable materials - Preliminary report. Asaio Journal. 1996;42:M866-M71.
[161] Lee JE, Park JC, Hwang YS, Kim JK, Kim JG, Suh H. Characterization of UV-irradiated dense/porous collagen membranes: Morphology, enzymatic degradation, and mechanical properties. Yonsei Medical Journal. 2001;42:172-9.
[162] Damink L, Dijkstra PJ, Vanluyn MJA, Vanwachem PB, Nieuwenhuis P, Feijen J. Glutaraldehyde as a cross-linking agent for collagen-based biomaterials. Journal of Materials Science-Materials in Medicine. 1995;6:460-72.
[163] Jorge-Herrero E, Fernandez P, Turnay J, Olmo N, Calero P, Garcia R, et al. Influence of different chemical cross-linking treatments on the properties of bovine pericardium and collagen. Biomaterials. 1999;20:539-45.
[164] Park SN, Park JC, Kim HO, Song MJ, Suh H. Characterization of porous collagen/hyaluronic acid scaffold modified by 1-ethyl-3-(3-dimethylaminopropyl)carbodiimide cross-linking. Biomaterials. 2002;23:1205-12.
[165] Osborne CS, Reid WH, Grant MH. Investigation into the biological stability of collagen/chondroitin-6-sulphate gels and their contraction by fibroblasts and keratinocytes: the effect of crosslinking agents and diamines. Biomaterials. 1999;20:283-90.
[166] Charulatha V, Rajaram A. Influence of different crosslinking treatments on the physical properties of collagen membranes. Biomaterials. 2003;24:759-67.
[167] Charulatha V, Rajaram A. Crosslinking density and resorption of dimethyl suberimidate treated collagen. Journal of Biomedical Materials Research. 1997;36:478-86.
[168] Petite H, Frei V, Huc A, Herbage D. Use of diphenylphosphorylazide for cross-linking collagen-based biomaterials. Journal of Biomedical Materials Research. 1994;28:159-65.
[169] Orban JM, Wilson LB, Kofroth JA, El-Kurdi MS, Maul TM, Vorp DA. Crosslinking of collagen gels by transglutaminase. Journal of Biomedical Materials Research Part A. 2004;68A:756-62.
[170] Zeugois DI, Panengad PP, Yew ESY, Sheppard C, Phan TT, Raghunath M. An in situ and in vitro investigation for the transglutaminase potential in tissue engineering. Journal of Biomedical Materials Research Part A. 2010;92A:1310-20.

[171] Harley BA, Lynn AK, Wissner-Gross Z, Bonfield W, Yannas IV, Gibson LJ. Design of a multiphase osteochondral scaffold. II. Fabrication of a mineralized collagen-glycosaminoglycan scaffold. Journal of Biomedical Materials Research Part A. 2010;92A:1066-77.
[172] Du C, Cui FZ, Zhang W, Feng QL, Zhu XD, de Groot K. Formation of calcium phosphate/collagen composites through mineralization of collagen matrix. Journal of Biomedical Materials Research. 2000;50:518-27.
[173] Lynn AK, Best SM, Cameron RE, Harley BA, Yannas IV, Gibson LJ, et al. Design of a multiphase osteochondral scaffold. I. Control of chemical composition. Journal of Biomedical Materials Research Part A. 2010;92A:1057-65.
[174] Dubey DK, Tomar V. Role of the nanoscale interfacial arrangement in mechanical strength of tropocollagen-hydroxyapatite-based hard biomaterials. Acta Biomaterialia. 2009;5:2704-16.
[175] Liao S, Ngiam M, Chan CK, Ramakrishna S. Fabrication of nano-hydroxyapatite/collagen/osteonectin composites for bone graft applications. Biomedical Materials. 2009;4.
[176] Tamimi F, Kumarasami B, Doillon C, Gbureck U, Le Nihouannen D, Lopez Cabarcos E, et al. Brushite-collagen composites for bone regeneration. Acta Biomaterialia. 2008;4:1315-21.
[177] Jones JR, Gentleman E, Polak J. Bioactive glass scaffolds for bone regeneration. Elements. 2007;3:393-9.
[178] Pohunkova H, Adam M. Reactivity and the fate of some composite bioimplants based on collagen in connective-tissue. Biomaterials. 1995;16:67-71.
[179] Bernhardt A, Lode A, Boxberger S, Pompe W, Gelinsky M. Mineralised collagen - an artificial, extracellular bone matrix - improves osteogenic differentiation of bone marrow stromal cells. Journal of Materials Science-Materials in Medicine. 2008;19:269-75.
[180] Goes JC, Figueiro SD, Oliveira AM, Macedo AAM, Silva CC, Ricardo NMPS, et al. Apatite coating on anionic and native collagen films by an alternate soaking process. Acta Biomaterialia. 2007;3:773-8.
[181] Kikuchi M, Itoh S, Ichinose S, Shinomiya K, Tanaka J. Self-organization mechanism in a bone-like hydroxyapatite/collagen nanocomposite synthesized in vitro and its biological reaction in vivo. Biomaterials. 2001;22:1705-11.
[182] Kokubo T. Bioactive glass-ceramics - Properties and applications. Biomaterials. 1991;12:155-63.
[183] Rhee SH, Tanaka J. Effect of citric acid on the nucleation of hydroxyapatite in a simulated body fluid. Biomaterials. 1999;20:2155-60.
[184] Liu Y, Li N, Qi Y-p, Dai L, Bryan TE, Mao J, et al. Intrafibrillar Collagen Mineralization Produced by Biomimetic Hierarchical Nanoapatite Assembly. Advanced Materials. 2011;23:975-80.

[185] Yamauchi K, Goda T, Takeuchi N, Einaga H, Tanabe T. Preparation of collagen/calcium phosphate multilayer sheet using enzymatic mineralization. Biomaterials. 2004;25:5481-9.
[186] Meyer U, Handschel J, Meyer T, Handschel J, Wiesmann HP. Fundamentals of Tissue Engineering and Regenerative Medicine. Germany: Springer-Verlag; 2009.
[187] Pedraza CE, Marelli B, Chicatun F, McKee MD, Nazhat SN. An In Vitro Assessment of a Cell-Containing Collagenous Extracellular Matrix-like Scaffold for Bone Tissue Engineering. Tissue Engineering Part A. 2010;16:781-93.
[188] Fernandes LF, Costa MA, Fernandes MH, Tomas H. Osteoblastic Behavior of Human Bone Marrow Cells Cultured Over Adsorbed Collagen Layer, Over Surface of Collagen Gels, and Inside Collagen Gels. Connective Tissue Research. 2009;50:336-46.
[189] Yang XBB, Bhatnagar RS, Li S, Oreffo ROC. Biomimetic collagen scaffolds for human bone cell growth and differentiation. Tissue Engineering. 2004;10:1148-59.
[190] Stein GS, Lian JB. Molecular mechanism mediating proliferation differentiation interrelationships during progressive development of the osteblast phenotype. Endocrine Reviews. 1993;14:424-42.
[191] Owen TA, Aronow M, Shalhoub V, Barone LM, Wilming L, Tassinari MS, et al. Progressive development of the rat osteoblast phenotype in vitro - Reciprocal relationships in expression of genes associated with osteoblast proliferation and differentiation during formation of the bone extracellular-matrix. Journal of Cellular Physiology. 1990;143:420-30.
[192] Czekanska EM, Stoddart MJ, Richards RG, Hayes JS. In search of an osteoblast cell model for in vitro research. European Cells & Materials. 2012;24.
[193] Heath CA. Cells for tissue engineering. Trends in Biotechnology. 2000;18:17-9.
[194] Salgado AJ, Coutinho OP, Reis RL. Bone tissue engineering: State of the art and future trends. Macromolecular Bioscience. 2004;4:743-65.
[195] Blau HM, Brazelton TR, Weimann JM. The evolving concept of a stem cell: Entity or function? Cell. 2001;105:829-41.
[196] Ikada Y. Tissue engineering: Fundamentals and applications. UK: Interface Science and Technology, Elsevier; 2006.
[197] Franceschi RT. The developmental control of osteoblast-specific gene expression: Role of specific transcription factors and the extracellular matrix environment. Critical Reviews in Oral Biology & Medicine. 1999;10:40-57.
[198] Franceschi RT, Iyer BS, Cui YQ. Effects of ascorbic-acid on collagen matrix formation and osteoblast differentiation in murine MC3T3-E1 cells. Journal of Bone and Mineral Research. 1994;9:843-54.

[199] Franceschi RT, Iyer BS. Relationship between collagen-synthesis and expression of the osteoblast phenotype in MC3T3-E1 cells. Journal of Bone and Mineral Research. 1992;7:235-46.
[200] O'Brien FJ, Harley BA, Yannas IV, Gibson LJ. The effect of pore size on cell adhesion in collagen-GAG scaffolds. Biomaterials. 2005;26:433-41.
[201] Arpornmaeklong P, Suwatwirote N, Pripatnanot P, Oungbho K. Growth and differentiation of mouse osteoblasts on chitosan-collagen sponges. International Journal of Oral and Maxillofacial Surgery. 2007;36:328-37.
[202] Suphasiriroj W, Yotnuengnit P, Surarit R, Pichyangkura R. The fundamental parameters of chitosan in polymer scaffolds affecting osteoblasts (MC3T3-E1). Journal of Materials Science-Materials in Medicine. 2009;20:309-20.
[203] Marelli B, Ghezzi CE, Mohn D, Stark WJ, Barralet JE, Boccaccini AR, et al. Accelerated mineralization of dense collagen-nano bioactive glass hybrid gels increases scaffold stiffness and regulates osteoblastic function. Biomaterials. 2011;32:8915-26.
[204] Wang J, de Boer J, de Groot K. Proliferation and differentiation of MC3T3-E1 cells on calcium phosphate/chitosan coatings. Journal of Dental Research. 2008;87:650-4.
[205] Schlegel AK, Mohler H, Busch F, Mehl A. Preclinical and clinical studies of a collagen membrane (Bio-Gide(R)). Biomaterials. 1997;18:535-8.
[206] Cornell CN, Lane JM, Chapman M, Merkow R, Seligson D, Henry S, et al. Multicenter trial of Collagraft as bone graft substitute. Journal of orthopaedic trauma. 1991;5:1-8.
[207] **http://www.geistlich.com/**.
[208] Li ZS, Ramay HR, Hauch KD, Xiao DM, Zhang MQ. Chitosan-alginate hybrid scaffolds for bone tissue engineering. Biomaterials. 2005;26:3919-28.
[209] Seol YJ, Lee JY, Park YJ, Lee YM, Young K, Rhyu IC, et al. Chitosan sponges as tissue engineering scaffolds for bone formation. Biotechnology Letters. 2004;26:1037-41.
[210] Rinki K, Dutta PK. Chitosan Based Scaffolds by Lyophilization and sc.CO(2) Assisted Methods for Tissue Engineering Applications. Journal of Macromolecular Science Part a-Pure and Applied Chemistry. 2010;47:429-34.
[211] Park YJ, Lee YM, Park SN, Sheen SY, Chung CP, Lee SJ. Platelet derived growth factor releasing chitosan sponge for periodontal bone regeneration. Biomaterials. 2000;21:153-9.
[212] Muzzarelli RAA, Biagini G, Bellardini M, Simonelli L, Castaldini C, Fratto G. Osteoconduction exerted by methylpyrrolidinone chitosan used in dental surgery. Biomaterials. 1993;14:39-43.
[213] Yilgor P, Tuzlakoglu K, Reis RL, Hasirci N, Hasirci V. Incorporation of a sequential BMP-2/BMP-7 delivery system into chitosan-based scaffolds for bone tissue engineering. Biomaterials. 2009;30:3551-9.

[214] Zhang X, Hua H, Shen X, Yang Q. In vitro degradation and biocompatibility of poly(L-lactic acid)/chitosan fiber composites. Polymer. 2007;48:1005-11.
[215] Tuzlakoglu K, Bolgen N, Salgado AJ, Gomes ME, Piskin E, Reis RL. Nano- and micro-fiber combined scaffolds: A new architecture for bone tissue engineering. Journal of Materials Science-Materials in Medicine. 2005;16:1099-104.
[216] Nair LS, Starnes T, Ko J-WK, Laurencin CT. Development of injectable thermogelling chitosan-inorganic phosphate solutions for biomedical applications. Biomacromolecules. 2007;8:3779-85.
[217] Chenite A, Chaput C, Wang D, Combes C, Buschmann MD, Hoemann CD, et al. Novel injectable neutral solutions of chitosan form biodegradable gels in situ. Biomaterials. 2000;21:2155-61.
[218] Park DJ, Choi BH, Zhu SJ, Huh JY, Kim BY, Lee SH. Injectable bone using chitosan-alginate gel/mesenchymal stem cells/BMP-2 composites. Journal of Cranio-Maxillofacial Surgery. 2005;33:50-4.
[219] Couto DS, Hong Z, Mano JF. Development of bioactive and biodegradable chitosan-based injectable systems containing bioactive glass nanoparticles. Acta Biomaterialia. 2009;5:115-23.
[220] Zhang Y, Zhang MQ. Synthesis and characterization of macroporous chitosan/calcium phosphate composite scaffolds for tissue engineering. Journal of Biomedical Materials Research. 2001;55:304-12.
[221] Zhang Y, Ni M, Zhang MQ, Ratner B. Calcium phosphate-chitosan composite scaffolds for bone tissue engineering. Tissue Engineering. 2003;9:337-45.
[222] Zhang Y, Zhang MQ. Three-dimensional macroporous calcium phosphate bioceramics with nested chitosan sponges for load-bearing bone implants. Journal of Biomedical Materials Research. 2002;61:1-8.
[223] Zhang Y, Zhang MQ. Calcium phosphate/chitosan composite scaffolds for controlled in vitro antibiotic drug release. Journal of Biomedical Materials Research. 2002;62:378-86.
[224] Lee YM, Park YJ, Lee SJ, Ku Y, Han SB, Choi SM, et al. Tissue engineered bone formation using chitosan/tricalcium phosphate sponges. Journal of Periodontology. 2000;71:410-7.
[225] Kawakami T, Antoh M, Hasegawa H, Yamagishi T, Ito M, Eda S. Experimental-study on osteoconductive properties of a chitosan-bonded hydroxyapatite self-hardening paste. Biomaterials. 1992;13:759-63.
[226] Leroux L, Hatim Z, Freche M, Lacout JL. Effects of various adjuvants (lactic acid, glycerol, and chitosan) on the injectability of a calcium phosphate cement. Bone. 1999;25:31S-4S.
[227] Khor E, Lim LY. Implantable applications of chitin and chitosan. Biomaterials. 2003;24:2339-49.
[228] Arpornmaeklong P, Pripatnanont P, Suwatwirote N. Properties of chitosan-collagen sponges and osteogenic differentiation of rat-bone-marrow

stromal cells. International Journal of Oral and Maxillofacial Surgery. 2008;37:357-66.
[229] Annabi N, Nichol JW, Zhong X, Ji C, Koshy S, Khademhosseini A, et al. Controlling the Porosity and Microarchitecture of Hydrogels for Tissue Engineering. Tissue Engineering Part B-Reviews. 2010;16.
[230] Tan W, Krishnaraj R, Desai TA. Evaluation of nanostructured composite collagen-chitosan matrices for tissue engineering. Tissue Engineering. 2001;7:203-10.
[231] Wang LM, Stegemann JP. Thermogelling chitosan and collagen composite hydrogels initiated with beta-glycerophosphate for bone tissue engineering. Biomaterials. 2010;31:3976-85.
[232] Jubel A, Andermahr J, Schiffer G, Fischer J, Rehm KE, Stoddart MJ, et al. Transplantation of de novo scaffold-free cartilage implants into sheep knee chondral defects. American Journal of Sports Medicine. 2008;36:1555-64.
[233] Hu JC, Athanasiou KA. A self-assembling process in articular cartilage tissue engineering. Tissue Engineering. 2006;12:969-79.
[234] Ofek G, Revell CM, Hu JC, Allison DD, Grande-Allen KJ, Athanasiou KA. Matrix Development in Self-Assembly of Articular Cartilage. Plos One. 2008;3.
[235] Chung C, Burdick JA. Engineering cartilage tissue. Advanced Drug Delivery Reviews. 2008;60:243-62.
[236] Nehrer S, Breinan HA, Ramappa A, Young G, Shortkroff S, Louie LK, et al. Matrix collagen type and pore size influence behaviour of seeded canine chondrocytes. Biomaterials. 1997;18:769-76.
[237] Liao E, Yaszemski M, Krebsbach P, Hollister S. Tissue-engineered cartilage constructs using composite hyaluronic acid/collagen I hydrogels and designed poly(propylene fumarate) scaffolds. Tissue Engineering. 2007;13:537-50.
[238] Farjanel J, Schurmann G, Bruckner P. Contacts with fibrils containing collagen I, but not collagens II, IX, and XI, can destabilize the cartilage phenotype of chondrocytes. Osteoarthritis and Cartilage. 2001;9:S55-S63.
[239] Gibson GJ, Schor SL, Grant ME. Effects of matrix macromolecules on chondrocyte gene-expression - synthesis of a low-molecular weight collagen species by cells cultured within collagen gels. Journal of Cell Biology. 1982;93:767-74.
[240] Funayama A, Niki Y, Matsumoto H, Maeno S, Yatabe T, Morioka H, et al. Repair of full-thickness articular cartilage defects using injectable type II collagen gel embedded with cultured chondrocytes in a rabbit model. Journal of Orthopaedic Science. 2008;13:225-32.
[241] Malemud CJ, Stevenson S, Mehraban F, Papay RS, Purchio AF, Goldberg VM. The proteoglycan synthesis repertoire of rabbit chondrocytes maintained in type II collagen gels. Osteoarthritis and cartilage / OARS, Osteoarthritis Research Society. 1994;2:29-41.

[242] Pulkkinen HJ, Tiitu V, Valonen P, Jurvelin JS, Lammi MJ, Kiviranta I. Engineering of cartilage in recombinant human type II collagen gel in nude mouse model in vivo. Osteoarthritis and Cartilage. 2010;18:1077-87.
[243] Galois L, Hutasse S, Cortial D, Rousseau CF, Grossin L, Ronziere MC, et al. Bovine chondrocyte behaviour in three-dimensional type I collagen gel in terms of gel contraction, proliferation and gene expression. Biomaterials. 2006;27:79-90.
[244] Freyria AM, Yang Y, Chajra H, Rousseau CF, Ronziere MC, Herbage D, et al. Optimization of dynamic culture conditions: Effects on biosynthetic activities of chondrocytes grown in collagen sponges. Tissue Engineering. 2005;11:674-84.
[245] Speer DP, Chvapil M, Volz RG, Holmes MD. Enhancement of healing in osteochondral defects by collagen sponge implants. Clinical Orthopaedics and Related Research. 1979:326-35.
[246] Wakitani S, Goto T, Pineda SJ, Young RG, Mansour JM, Caplan AI, et al. Mesenchymal cell-based repair of large, full-thickness defects of articular-cartilage. Journal of Bone and Joint Surgery-American Volume. 1994;76A:579-92.
[247] Zuscik MJ, Hilton MJ, Zhang X, Chen D, O'Keefe RJ. Regulation of chondrogenesis and chondrocyte differentiation by stress. Journal of Clinical Investigation. 2008;118:429-38.
[248] Yamashita A, Nishikawa S, Rancourt DE. Identification of Five Developmental Processes during Chondrogenic Differentiation of Embryonic Stem Cells. Plos One. 2010;5.
[249] Mattot V, Raes MB, Henriet P, Eeckhout Y, Stehelin D, Vandenbunder B, et al. Expression of interstitial collagenase is restricted to skeletal tissue during mouse embryogenesis. Journal of Cell Science. 1995;108:529-35.
[250] Dorotka R, Bindreiter U, Macfelda K, Windberger U, Nehrer S. Marrow stimulation and chondrocyte transplantation using a collagen matrix for cartilage repair. Osteoarthritis and Cartilage. 2005;13:655-64.
[251] Willers C, Chen J, Wood D, Zheng MH. Autologous chondrocyte implantation with collagen bioscaffold for the treatment of osteochondral defects in rabbits. Tissue Engineering. 2005;11:1065-76.
[252] Buschmann MD, Gluzband YA, Grodzinsky AJ, Kimura JH, Hunziker EB. Chondrocytes in agarose culture synthesize a mechanically functional extracellular-matrix. Journal of Orthopaedic Research. 1992;10:745-58.
[253] Homicz MR, Chia SH, Schumacher BL, Masuda K, Thonar EJ, Sah RL, et al. Human septal chondrocyte redifferentiation in alginate, polyglycolic acid scaffold, and monolayer culture. Laryngoscope. 2003;113:25-32.
[254] Lin Z, Willers C, Xu J, Zheng M-H. The chondrocyte: Biology and clinical application. Tissue Engineering. 2006;12:1971-84.
[255] Pabbruwe MB, Kafienah W, Tarlton JF, Mistry S, Fox DJ, Hollander AP. Repair of meniscal cartilage white zone tears using a stem cell/collagen-scaffold implant. Biomaterials. 2010;31:2583-91.

[256] Awad HA, Butler DL, Harris MT, Ibrahim RE, Wu Y, Young RG, et al. In vitro characterization of mesenchymal stem cell-seeded collagen scaffolds for tendon repair: Effects of initial seeding density on contraction kinetics. Journal of Biomedical Materials Research. 2000;51:233-40.
[257] Zheng L, Fan HS, Sun J, Chen XN, Wang G, Zhang L, et al. Chondrogenic differentiation of mesenchymal stem cells induced by collagen-based hydrogel: An in vivo study. Journal of Biomedical Materials Research Part A. 2010;93A:783-92.
[258] Nawata M, Wakitani S, Nakaya H, Tanigami A, Seki T, Nakamura Y, et al. Use of bone morphogenetic protein 2 and diffusion chambers to engineer cartilage tissue for the repair of defects in articular cartilage. Arthritis and Rheumatism. 2005;52:155-63.
[259] Adachi N, Sato K, Usas A, Fu FH, Ochi M, Han CW, et al. Muscle derived, cell based ex vivo gene therapy for treatment of full thickness articular cartilage defects. Journal of Rheumatology. 2002;29:1920-30.
[260] Yokoyama A, Sekiya I, Miyazaki K, Ichinose S, Hata Y, Muneta T. In vitro cartilage formation of composites of synovium-derived mesenchymal stem cells with collagen gel. Cell and Tissue Research. 2005;322:289-98.
[261] Huey DJ, Hu JC, Athanasiou KA. Unlike bone, cartilage regeneration remains elusive Science. 2012;338:917-21.
[262] Ahmed TAE, Griffith M, Hincke M. Characterization and inhibition of fibrin hydrogel-degrading enzymes during development of tissue engineering scaffolds. Tissue Engineering. 2007;13:1469-77.
[263] Dare EV, Vascotto SG, Carlsson DJ, Hincke MT, Griffith M. Differentiation of a fibrin gel encapsulated chondrogenic cell line. International Journal of Artificial Organs. 2007;30:619-27.
[264] Albrecht C, Tichy B, Nuernberger S, Hosiner S, Zak L, Aldrian S, et al. Gene expression and cell differentiation in matrix-associated chondrocyte transplantation grafts: a comparative study. Osteoarthritis and Cartilage. 2011;19:1219-27.
[265] Noeth U, Steinert AF, Tuan RS. Technology Insight: adult mesenchymal stem cells for osteoarthritis therapy. Nature Clinical Practice Rheumatology. 2008;4:371-80.
[266] **http://www.tetec-ag.com/**.
[267] Bartlett W, Skinner JA, Gooding CR, Carrington RWJ, Flanagan AM, Briggs TWR, et al. Autologous chondrocyte implantation versus matrix-induced autologous chondrocyte implantation for osteochondral defects of the knee. Journal of Bone and Joint Surgery-British Volume. 2005;87B:640-5.
[268] Lahiji A, Sohrabi A, Hungerford DS, Frondoza CG. Chitosan supports the expression of extracellular matrix proteins in human osteoblasts and chondrocytes. Journal of Biomedical Materials Research. 2000;51:586-95.
[269] Liu X, Ma L, Mao Z, Gao C. Chitosan-Based Biomaterials for Tissue Repair and Regeneration. Chitosan for Biomaterials Ii. 2011;244:81-127.

[270] Griffon DJ, Sedighi MR, Schaeffer DV, Eurell JA, Johnson AL. Chitosan scaffolds: Interconnective pore size and cartilage engineering. Acta Biomaterialia. 2006;2:313-20.
[271] Breyner NM, Hell RCR, Carvalho LRP, Machado CB, Peixoto Filho IN, Valerio P, et al. Effect of a Three-Dimensional Chitosan Porous Scaffold on the Differentiation of Mesenchymal Stem Cells into Chondrocytes. Cells Tissues Organs. 2010;191:119-28.
[272] Lu JX, Prudhommeaux F, Meunier A, Sedel L, Guillemin G. Effects of chitosan on rat knee cartilages. Biomaterials. 1999;20:1937-44.
[273] Hoemann CD, Hurtig M, Rossomacha E, Sun J, Chevrier A, Shive MS, et al. Chitosan-glycerol phosphate/blood implants improve hyaline cartilage repair in ovine microfracture defects. Journal of Bone and Joint Surgery-American Volume. 2005;87A:2671-86.
[274] Hoemann CD, Sun J, McKee MD, Chevrier A, Rossomacha E, Rivard GE, et al. Chitosan-glycerol phosphate/blood implants elicit hyaline cartilage repair integrated with porous subchondral bone in microdrilled rabbit defects. Osteoarthritis and Cartilage. 2007;15:78-89.
[275] **http://bst-cargel.piramal.com/healthcare-professional/index.html**. December 28, 2012.
[276] Yan L-P, Wang Y-J, Ren L, Wu G, Caridade SG, Fan J-B, et al. Genipin-cross-linked collagen/chitosan biomimetic scaffolds for articular cartilage tissue engineering applications. Journal of Biomedical Materials Research Part A. 2010;95A:465-75.
[277] Yan J, Qi N, Zhang Q. Rabbit articular Chondrocytes seeded on Collagen-Chitosan-GAG scaffold for cartilage tissue engineering in vivo. Artificial Cells Blood Substitutes and Biotechnology. 2007;35:333-44.
[278] Yan JH, Li XM, Liu LR, Wang FJ, Zhu TW, Zhang QQ. Potential use of collagen-chitosan-hyaluronan tri-copolymer scaffold for cartilage tissue engineering. Artificial Cells Blood Substitutes and Biotechnology. 2006;34:27-39.
[279] Gong Z, Xiong H, Long X, Wei L, Li J, Wu Y, et al. Use of synovium-derived stromal cells and chitosan/collagen type I scaffolds for cartilage tissue engineering. Biomedical materials (Bristol, England). 2010;5:055005.
[280] Lee JE, Kim KE, Kwon IC, Ahn HJ, Lee SH, Cho HC, et al. Effects of the controlled-released TGF-beta 1 from chitosan microspheres on chondrocytes cultured in a collagen/chitosan/glycosaminoglycan scaffold. Biomaterials. 2004;25:4163-73.
[281] Bi L, Cao Z, Hu Y, Song Y, Yu L, Yang B, et al. Effects of different cross-linking conditions on the properties of genipin-cross-linked chitosan/collagen scaffolds for cartilage tissue engineering. Journal of Materials Science-Materials in Medicine. 2011;22:51-62.
[282] Lin Y-C, Tan F-j, Marra KG, Jan S-S, Liu D-C. Synthesis and characterization of collagen/hyaluronan/chitosan composite sponges for potential biomedical applications. Acta Biomaterialia. 2009;5:2591-600.

[283] Schaefer D, Martin I, Shastri P, Padera RF, Langer R, Freed LE, et al. In vitro generation of osteochondral composites. Biomaterials. 2000;21:2599-606.
[284] Guo X, Park H, Liu G, Liu W, Cao Y, Tabata Y, et al. In vitro generation of an osteochondral construct using injectable hydrogel composites encapsulating rabbit marrow mesenchymal stem cells. Biomaterials. 2009;30:2741-52.
[285] Taboas JM, Maddox RD, Krebsbach PH, Hollister SJ. Indirect solid free form fabrication of local and global porous, biomimetic and composite 3D polymer-ceramic scaffolds. Biomaterials. 2003;24:181-94.
[286] Kreklau B, Sittinger M, Mensing MB, Voigt C, Berger G, Burmester GR, et al. Tissue engineering of biphasic joint cartilage transplants. Biomaterials. 1999;20:1743-9.
[287] Frenkel SR, Toolan B, Menche D, Pitman MI, Pachence JM. Chondrocyte transplantation using a collagen bilayer matrix for cartilage repair. Journal of Bone and Joint Surgery-British Volume. 1997;79B:831-6.
[288] Oliveira JM, Rodrigues MT, Silva SS, Malafaya PB, Gomes ME, Viegas CA, et al. Novel hydroxyapatite/chitosan bilayered scaffold for osteochondral tissue-engineering applications: Scaffold design and its performance when seeded with goat bone marrow stromal cells. Biomaterials. 2006;27:6123-37.
[289] Frenkel SR, Bradica G, Brekke JH, Goldman SM, Ieska K, Issack P, et al. Regeneration of articular cartilage - Evaluation of osteochondral defect repair in the rabbit using multiphasic implants. Osteoarthritis and Cartilage. 2005;13:798-807.
[290] Keeney M, Pandit A. The Osteochondral Junction and Its Repair via Bi-Phasic Tissue Engineering Scaffolds. Tissue Engineering Part B-Reviews. 2009;15:55-73.
[291] Spiller KL, Maher SA, Lowman AM. Hydrogels for the Repair of Articular Cartilage Defects. Tissue Engineering Part B-Reviews. 2011;17:281-99.
[292] Lee KY, Mooney DJ. Hydrogels for tissue engineering. Chemical Reviews. 2001;101:1869-79.
[293] Van Vlierberghe S, Dubruel P, Schacht E. Biopolymer-Based Hydrogels As Scaffolds for Tissue Engineering Applications: A Review. Biomacromolecules. 2011;12:1387-408.
[294] Hoffman AS. Hydrogels for biomedical applications. Advanced Drug Delivery Reviews. 2002;54:3-12.
[295] Peppas NA, Bures P, Leobandung W, Ichikawa H. Hydrogels in pharmaceutical formulations. European Journal of Pharmaceutics and Biopharmaceutics. 2000;50:27-46.
[296] Fedorovich NE, Alblas J, de Wijn JR, Hennink WE, Verbout AJ, Dhert WJA. Hydrogels as extracellular matrices for skeletal tissue engineering: state-of-the-art and novel application in organ printing. Tissue Engineering. 2007;13:1905-25.

[297] Hillsley MV, Frangos JA. Bone tissue engineering - The role of interstitial fluid flow -Review. Biotechnology and Bioengineering. 1994;43.
[298] Swartz MA, Fleury ME. Interstitial flow and its effects in soft tissues. Annual Review of Biomedical Engineering. 2007;9:229-56.
[299] Suh JK, DiSilvestro MR. Biphasic poroviscoelastic behavior of hydrated biological soft tissue. Journal of Applied Mechanics-Transactions of the Asme. 1999;66.
[300] Ng CP, Swartz MA. Fibroblast alignment under interstitial fluid flow using a novel 3-D tissue culture model. American Journal of Physiology-Heart and Circulatory Physiology. 2003;284.
[301] O'Brien FJ, Harley BA, Waller MA, Yannas IV, Gibson LJ, Prendergast PJ. The effect of pore size on permeability and cell attachment in collagen scaffolds for tissue engineering. Technology and health care : official journal of the European Society for Engineering and Medicine. 2007;15:3-17.
[302] Neuman SP. Theoretical derivation of Darcy's law. Acta Mechanica. 1977;25.
[303] Quinn TM, Grodzinsky AJ. Longitudinal modulus and hydraulic permeability of poly(methacrylic acid) gels - effects of charge density and solvent content. Macromolecules. 1993;26.
[304] Perie D, Iatridis JC, Demers CN, Goswami T, Beaudoin G, Mwale F, et al. Assessment of compressive modulus, hydraulic permeability and matrix content of trypsin-treated nucleus pulposus using quantitative MRI. Journal of Biomechanics. 2006;39.
[305] Grillo H, Gross J. Thermal reconstitution of collagen from solution and the response to its heterologous implantation. Journal of Surgical Research. 1962;11.
[306] Ghezzi CE, Muja N, Marelli B, Nazhat SN. Real time responses of fibroblasts to plastically compressed fibrillar collagen hydrogels. Biomaterials. 2011.
[307] Bitar M, Salih V, Brown RA, Nazhat SN. Effect of multiple unconfined compression on cellular dense collagen scaffolds for bone tissue engineering. Journal of Materials Science-Materials in Medicine. 2007;18:237-44.
[308] Bitar M, Brown RA, Salih V, Kidane AG, Knowles JC, Nazhat SN. Effect of cell density on osteoblastic differentiation and matrix degradation of biomimetic dense collagen scaffolds. Biomacromolecules. 2008;9:129-35.
[309] Buxton PG, Bitar M, Gellynck K, Parkar M, Brown RA, Young AM, et al. Dense collagen matrix accelerates osteogenic differentiation and rescues the apoptotic response to MMP inhibition. Bone. 2008;43:377-85.
[310] Hu K, Shi H, Zhu J, Deng D, Zhou G, Zhang W, et al. Compressed collagen gel as the scaffold for skin engineering. Biomedical Microdevices. 2010;12:627-35.
[311] Cheema U, Brown RA, Alp B, MacRobert AJ. Spatially defined oxygen gradients and vascular endothelial growth factor expression in an engineered 3D cell model. Cellular and Molecular Life Sciences. 2008;65:177-86.

[312] Engelhardt EM, Stegberg E, Brown RA, Hubbell JA, Wurm FM, Adam M, et al. Compressed collagen get: a novel scaffold for human bladder cells. Journal of Tissue Engineering and Regenerative Medicine. 2010;4:123-30.
[313] East E, de Oliveira DB, Golding JP, Phillips JB. Alignment of Astrocytes Increases Neuronal Growth in Three-Dimensional Collagen Gels and Is Maintained Following Plastic Compression to Form a Spinal Cord Repair Conduit. Tissue Engineering Part A. 2010;16:3173-84.
[314] Levis HJ, Brown RA, Daniels JT. Plastic compressed collagen as a biomimetic substrate for human limbal epithelial cell culture. Biomaterials. 2010;31:7726-37.
[315] Mi S, Chen B, Wright B, Connon CJ. Plastic compression of a collagen gel forms a much improved scaffold for ocular surface tissue engineering over conventional collagen gels. Journal of Biomedical Materials Research Part A. 2010;95A:447-53.
[316] Brady MA, Sivananthan S, Mudera V, Liu Q, Wiltfang J, Warnke PH. The primordium of a biological joint replacement: Coupling of two stem cell pathways in biphasic ultrarapid compressed gel niches. Journal of Cranio-Maxillofacial Surgery. 2011;39:380-6.
[317] Ghezzi CE, Marelli B, Muja N, Nazhat SN. Immediate production of a tubular dense collagen construct with bioinspired mechanical properties Acta Biomaterilia. 2012;8:*1813-25*.
[318] Stevenson MD, Sieminski AL, McLeod CM, Byfield FJ, Barocas VH, Gooch KJ. Pericellular Conditions Regulate Extent of Cell-Mediated Compaction of Collagen Gels. Biophysical Journal. 2010;99:19-28.
[319] Banes AJ, Tsuzaki M, Yamamoto J, Fischer T, Brigman B, Brown T, et al. Mechanoreception at the cellular level: The detection, interpretation, and diversity of responses to mechanical signals. Biochemistry and Cell Biology-Biochimie Et Biologie Cellulaire. 1995;73:349-65.
[320] Discher DE, Janmey P, Wang YL. Tissue cells feel and respond to the stiffness of their substrate. Science. 2005;310:1139-43.
[321] Buxboim A, Ivanovska IL, Discher DE. Matrix elasticity, cytoskeletal forces and physics of the nucleus: how deeply do cells 'feel' outside and in? Journal of Cell Science. 2010;123:297-308.
[322] Fernandez P, Bausch AR. The compaction of gels by cells: a case of collective mechanical activity. Integrative Biology. 2009;1:252-9.
[323] Grinnell F, Petroll WM. Cell Motility and Mechanics in Three-Dimensional Collagen Matrices. Annual Review of Cell and Developmental Biology, Vol 26. 2010;26:335-61.
[324] Bell E, Ivarsson B, Merrill C. Production of a tissue-like structure by contraction of collagen lattices by human-fibroblasts of different proliferative potential in vitro. Proceedings of the National Academy of Sciences of the United States of America. 1979;76:1274-8.

[325] Bell E, Ehrlich HP, Buttle DJ, Nakatsuji T. Living tissue formed in vitro and accepted as skin-equivalent tissue of full thickness. Science. 1981;211:1052-4.
[326] Vernon RB, Sage EH. Contraction of fibrillar type I collagen by endothelial cells: A study in vitro. Journal of Cellular Biochemistry. 1996;60:185-97.
[327] Qi J, Chi LQ, Faber J, Koller B, Banes AJ. ATP reduces gel compaction in osteoblast-populated collagen gels. Journal of Applied Physiology. 2007;102:1152-60.
[328] Naderi H, Matin MM, Bahrami AR. Review paper: Critical Issues in Tissue Engineering: Biomaterials, Cell Sources, Angiogenesis, and Drug Delivery Systems. Journal of Biomaterials Applications. 2011;26:383-417.
[329] Castro NJ, Hacking SA, Zhang LG. Recent Progress in Interfacial Tissue Engineering Approaches for Osteochondral Defects. Annals of Biomedical Engineering. 2012;40.
[330] Gunatillake PA, Adhikari R. Biodegradable synthetic polymers for tissue engineering. European cells & materials. 2003;5:1-16.
[331] Khan SN, Tomin E, Lane JM. Clinical applications of bone graft substitutes. Orthopedic Clinics of North America. 2000;31:389-+.
[332] Badylak SF. The extracellular matrix as a biologic scaffold material. Biomaterials. 2007;28:3587-93.
[333] Badylak SE. The extracellular matrix as a scaffold for tissue reconstruction. Seminars in Cell & Developmental Biology. 2002;13:377-83.
[334] Saddiq ZA, Barbenel JC, Grant MH. The mechanical strength of collagen gels containing glycosaminoglycans and populated with fibroblasts. Journal of Biomedical Materials Research Part A. 2009;89A:697-706.
[335] Marelli B, Ghezzi CE, Barralet JE, Boccaccini AR, Nazhat SN. Three-Dimensional Mineralization of Dense Nanofibrillar Collagen-Bioglass Hybrid Scaffolds. Biomacromolecules. 2010;11:1470-9.
[336] Fung YC. Biomechanics: Mechanical properties of living tissues. 2nd ed. New York: Springer-Verlag; 1993.
[337] Koob TJ, Hernandez DJ. Mechanical and thermal properties of novel polymerized NDGA-gelatin hydrogels. Biomaterials. 2003;24:1285-92.
[338] Nakayama GR, Caton MC, Nova MP, Parandoosh Z. Assessment of the Alamar Blue assay for cellular growth and viability in vitro. Journal of Immunological Methods. 1997;204:205-8.
[339] Henning Birkedal-Hansen SY, JackWindsor, Anne Havernose Pollard, Guy Lyons,William Stetler-Stevenson, and Bente Birkedal-Hansen. Matrix metalloproteinases. Current protocols in cell biology. 2008;40:10.8.1-.8.23.
[340] Liu TY, Chen SY, Lin YL, Liu DM. Synthesis and characterization of amphiphatic carboxymethyl-hexanoyl chitosan hydrogel: Water-retention ability and drug encapsulation. Langmuir. 2006;22:9740-5.

[341] Neto CGT, Giacometti JA, Job AE, Ferreira FC, Fonseca JLC, Pereira MR. Thermal analysis of chitosan based networks. Carbohydrate Polymers. 2005;62:97-103.
[342] Guan YL, Shao L, Yao KD. A study on correlation between water state and swelling kinetics of chitosan-based hydrogels. Journal of Applied Polymer Science. 1996;61:2325-35.
[343] Lawrie G, Keen I, Drew B, Chandler-Temple A, Rintoul L, Fredericks P, et al. Interactions between alginate and chitosan biopolymers characterized using FTIR and XPS. Biomacromolecules. 2007;8:2533-41.
[344] Wang XH, Li DP, Wang WJ, Feng QL, Cui FZ, Xu YX, et al. Crosslinked collagen/chitosan matrix for artificial livers. Biomaterials. 2003;24:3213-20.
[345] Peniche C, Arguelles-Monal W, Davidenko N, Sastre R, Gallardo A, San Roman J. Self-curing membranes of chitosan/PAA IPNs obtained by radical polymerization: preparation, characterization and interpolymer complexation. Biomaterials. 1999;20:1869-78.
[346] Kim S, Nimni ME, Yang Z, Han B. Chitosan/gelatin-based films crosslinked by proanthocyanidin. Journal of Biomedical Materials Research Part B-Applied Biomaterials. 2005;75B:442-50.
[347] Kaminska A, Sionkowska A. The effect of UV radiation on the thermal parameters of collagen degradation. Polymer Degradation and Stability. 1996;51:15-8.
[348] Taravel MN, Domard A. Relation between the physicochemical characteristics of collagen and its interactions with chitosan. 1. Biomaterials. 1993;14:930-8.
[349] Engler AJ, Sen S, Sweeney HL, Discher DE. Matrix elasticity directs stem cell lineage specification. Cell. 2006;126:677-89.
[350] Ma JB, Wang HJ, He BL, Chen JT. A preliminary in vitro study on the fabrication and tissue engineering applications of a novel chitosan bilayer material as a scaffold of human neofetal dermal fibroblasts. Biomaterials. 2001;22:331-6.
[351] Nishiyama T, Tominaga N, Nakajima K, Hayashi T. Quantitative-evaluation of the factors affecting the process of fibroblast-mediated collagen gel contraction by separating the process into 3 phases. Collagen and Related Research. 1988;8:259-73.
[352] Serpooshan V, Julien M, Nguyen O, Wang HF, Li AL, Muja N, et al. Reduced hydraulic permeability of three-dimensional collagen scaffolds attenuates gel contraction and promotes the growth and differentiation of mesenchymal stem cells. Acta Biomaterialia. 2010;6:3978-87.
[353] Mariappan MR, Alas EA, Williams JG, Prager MD. Chitosan and chitosan sulfate have opposing effects on collagen-fibroblast interactions. Wound Repair and Regeneration. 1999;7:400-6.
[354] Peng L, Cheng XR, Wang JW, Xu DX, Wang G. Preparation and evaluation of porous chitosan/collagen scaffolds for periodontal tissue engineering. Journal of Bioactive and Compatible Polymers. 2006;21:207-20.

[355] Serpooshan V, Muja N, Marelli B, Nazhat SN. Fibroblast contractility and growth in plastic compressed collagen gel scaffolds with microstructures correlated with hydraulic permeability. Journal of Biomedical Materials Research Part A. 2011;96A:609-20.
[356] Almany L, Seliktar D. Biosynthetic hydrogel scaffolds made from fibrinogen and polyethylene glycol for 3D cell cultures. Biomaterials. 2005;26:2467-77.
[357] Harada S, Matsumoto T, Ogata E. Role of ascorbic-acid in the regulation of proliferation in osteoblast-like MC3T3-E1 cells. Journal of Bone and Mineral Research. 1991;6:903-8.
[358] Toriseva MJ, Ala-aho R, Karvinen J, Baker AH, Marjomaki VS, Heino J, et al. Collagenase-3 (MMP-13) enhances remodeling of three-dimensional collagen and promotes survival of human skin fibroblasts. Journal of Investigative Dermatology. 2007;127:49-59.
[359] Parreno J, Buckley-Herd G, De-Hemptinne I, Hart DA. Osteoblastic MG-63 cell differentiation, contraction, and mRNA expression in stress-relaxed 3D collagen I gels. Molecular and Cellular Biochemistry. 2008;317:21-32.
[360] Knauper V, Will H, LopezOtin C, Smith B, Atkinson SJ, Stanton H, et al. Cellular mechanisms for human procollagenase-3 (MMP-13) activation - Evidence that MT1-MMP (MMP-14) and gelatinase A (MMP-2) are able to generate active enzyme. Journal of Biological Chemistry. 1996;271:17124-31.
[361] Costa-Pinto AR, Correlo VM, Sol PC, Bhattacharya M, Charbord P, Delorme B, et al. Osteogenic Differentiation of Human Bone Marrow Mesenchymal Stem Cells Seeded on Melt Based Chitosan Scaffolds for Bone Tissue Engineering Applications. Biomacromolecules. 2009;10:2067-73.
[362] Brown WE, Eidelman N, Tomazic B. Octacalcium phosphate as a precursor in biomineral formation. Adv Dent Res. 1987;1:306-13.
[363] Viala S, Freche M, Lacout JL. Effect of chitosan on octacalcium phosphate crystal growth. Carbohydrate Polymers. 1996;29:197-201.
[364] Wang J, de Boer J, de Groot K. Preparation and characterization of electrodeposited calcium phosphate/chitosan coating on Ti6Al4V plates. Journal of Dental Research. 2004;83:296-301.
[365] Guzman-Morales J, El-Gabalawy H, Pham MH, Tran-Khanh N, McKee MD, Wu W, et al. Effect of chitosan particles and dexamethasone on human bone marrow stromal cell osteogenesis and angiogenic factor secretion. Bone. 2009;45:617-26.
[366] Sauer G. WR. Fourier transform infrared characterization of mineral phases formed during induction of mineralization by collagenase-released matrix vesicles *in vitro.* The Journal of Biological Chemistry. 1988;263:13718-24.
[367] Chou YF, Dunn JCY, Wu BM. In vitro response of MC3T3-E1 preosteoblasts within three-dimensional apatite-coated PLGA scaffolds. Journal of Biomedical Materials Research Part B-Applied Biomaterials. 2005;75B:81-90.

[368] Chang MC, Tanaka J. FT-IR study for hydroxyapatite/collagen nanocomposite cross-linked by glutaraldehyde. Biomaterials. 2002;23:4811-8.
[369] Zhang W, Huang ZL, Liao SS, Cui FZ. Nucleation sites of calcium phosphate crystals during collagen mineralization. Journal of the American Ceramic Society. 2003;86:1052-4.
[370] Honda Y, Kamakura S, Sasaki K, Suzuki O. Formation of bone-like apatite enhanced by hydrolysis of octacalcium phosphate crystals deposited in collagen matrix. Journal of Biomedical Materials Research Part B-Applied Biomaterials. 2007;80B:281-9.
[371] Farlay D, Panczer G, Rey C, Delmas PD, Boivin G. Mineral maturity and crystallinity index are distinct characteristics of bone mineral. Journal of Bone and Mineral Metabolism. 2010;28:433-45.
[372] Paschalis EP, DiCarlo E, Betts F, Sherman P, Mendelsohn R, Boskey AL. FTIR microspectroscopic analysis of human osteonal bone. Calcified Tissue International. 1996;59:480-7.
[373] Ibusuki S, Halbesma GJ, Randolph MA, Redmond RW, Kochevar IE, Gill TJ. Photochemically cross-linked collagen gels as three-dimensional scaffolds for tissue engineering. Tissue Engineering. 2007;13:1995-2001.
[374] Chicatun F, Pedraza CE, Ghezzi CE, Marelli B, Kaartinen MT, McKee MD, et al. Osteoid-mimicking dense collagen/chitosan hybrid gels. Biomacromolecules. 2011;12:2946-56.
[375] Wu H, Wan Y, Cao X, Wu Q. Proliferation of chondrocytes on porous poly(DL-lactide)/chitosan scaffolds. Acta Biomaterialia. 2008;4:76-87.
[376] Buschmann MD, Hoemann CD, Hurtig MB, Shive MS. Cartilage repair with chitosan/glycerol-phosphate stabilised blood clots. In: Williams RJ, editor. Cartilage Repair: Analysis and Strategies. Totowa, NJ: Humana Press; 2006. p. 83-106.
[377] Ciarmatori S, Kiepe D, Haarmann A, Huegel U, Toenshoff B. Signaling mechanisms leading to regulation of proliferation and differentiation of the mesenchymal chondrogenic cell line RCJ3.1C5.18 in response to IGF-I. Journal of Molecular Endocrinology. 2007;38:493-508.
[378] Hoemann CD, Sun J, Chrzanowski V, Buschmann MD. A multivalent assay to detect glycosaminoglycan, protein, collagen, RNA, and DNA content in milligram samples of cartilage or hydrogel-based repair cartilage. Analytical Biochemistry. 2002;300:1-10.
[379] Rossomacha E, Hoemann CD, Shive MS. Simple methods for staining chitosan in biotechnological applications. Journal of Histotechnology. 2004;27.
[380] Klein TJ, Rizzi SC, Reichert JC, Georgi N, Malda J, Schuurman W, et al. Strategies for Zonal Cartilage Repair using Hydrogels. Macromolecular Bioscience. 2009;9.
[381] Ohsawa S, Yasui N, Ono K. Contraction of collagen gel by dedifferentiated chondrocytes. Cell Biol Int Rep. 1982;6.

[382] Berendsen AD, Vonk LA, Zandieh-Doulabi B, Everts V, Bank RA. Contraction-induced Mmp13 and-14 expression by goat articular chondrocytes in collagen type I but not type II gels. Journal of Tissue Engineering and Regenerative Medicine. 2012;6.
[383] Quent VMC, Loessner D, Friis T, Reichert JC, Hutmacher DW. Discrepancies between metabolic activity and DNA content as tool to assess cell proliferation in cancer research. Journal of Cellular and Molecular Medicine. 2010;14:1003-13.
[384] Vacanti CA, Langer R, Schloo B, Vacanti JP. Synthetic-polymers seeded with chondrocytes provide a template for new cartilage formation. Plastic and Reconstructive Surgery. 1991;88:753-9.
[385] Bhardwaj N, Nguyen QT, Chen AC, Kaplan DL, Sah RL, Kundu SC. Potential of 3-D tissue constructs engineered from bovine chondrocytes/silk fibroin-chitosan for in vitro cartilage tissue engineering. Biomaterials. 2011;32:5773-81.
[386] Wan LQ, Jiang J, Miller DE, Guo XE, Mow VC, Lu HH. Matrix Deposition Modulates the Viscoelastic Shear Properties of Hydrogel-Based Cartilage Grafts. Tissue Engineering Part A. 2011;17.
[387] Mow VC, Ratcliffe A, Poole AR. Cartilage and diarthrodial joints as paradigms for hierarchical materials and structures. Biomaterials. 1992;13:67-97.
[388] Farrell MJ, Comeau ES, Mauck RL. Mesenchymal stem cells produce functional cartilage matrix in three-dimensional culture in regions of optimal nutrient supply. European Cells & Materials. 2012;23.
[389] Grimshaw MJ, Mason RM. Bovine articular chondrocyte function in vitro depends upon oxygen tension. Osteoarthritis and Cartilage. 2000;8.
[390] Buckley CT, Meyer EG, Kelly DJ. The Influence of Construct Scale on the Composition and Functional Properties of Cartilaginous Tissues Engineered Using Bone Marrow-Derived Mesenchymal Stem Cells. Tissue Engineering Part A. 2012;18.
[391] Heywood HK, Sembi PK, Lee DA, Bader DL. Cellular utilization determines viability and matrix distribution profiles in chondrocyte-seeded alginate constructs. Tissue Engineering. 2004;10.
[392] Heywood HK, Bader DL, Lee DA. Glucose concentration and medium volume influence cell viability and glycosaminoglycan synthesis in chondrocyte-seeded alginate constructs. Tissue Engineering. 2006;12.
[393] Ko HCH, Milthorpe BK, McFarland CD. Engineering thick tissues - The vascularisation problem. European Cells & Materials. 2007;14:1-18.
[394] Cheema U, Rong Z, Kirresh O, MacRobert AJ, Vadgama P, Brown RA. Oxygen diffusion through collagen scaffolds at defined densities: implications for cell survival in tissue models Journal of Tissue Engineering and Regenerative Medicine. Feb 2011.
[395] Martin I, Wendt D, Heberer M. The role of bioreactors in tissue engineering. Trends in Biotechnology. 2004;22:80-6.

[396] Vijayan S, Bartlett W, Bentley G, Carrington RWJ, Skinner JA, Pollock RC, et al. Autologous chondrocyte implantation for osteochondral lesions in the knee using a bilayer collagen membrane and bone graft: A two- to eight-year follow-up study. Journal of Bone and Joint Surgery-British Volume. 2012;94B.
[397] Chen Y-L, Lee H-P, Chan H-Y, Sung L-Y, Chen H-C, Hu Y-C. Composite chondroitin-6-sulfate/dermatan sulfate/chitosan scaffolds for cartilage tissue engineering. Biomaterials. 2007;28:2294-305.
[398] Chicatun F, Pedraza CE, Muja N, Ghezzi CE, McKee MD, Nazhat SN. Effect of chitosan incorporation and scaffold geometry on chondrocyte function in dense collagen type I hydrogels. Tissue Engineering, Part A; 2013 - Accepted.
[399] Addison WN, Miller SJ, Ramaswamy J, Mansouri A, Kohn DH, McKee MD. Phosphorylation-dependent mineral-type specificity for apatite-binding peptide sequences. Biomaterials. 2010;31:9422-30.
[400] Ehara A, Ogata K, Imazato S, Ebisu S, Nakano T, Umakoshi Y. Effects of alpha-TCP and TetCP on MC3T3-E1 proliferation, differentiation and mineralization. Biomaterials. 2003;24:831-6.
[401] Kim TK, Sharma B, Williams CG, Ruffner MA, Malik A, McFarland EG, et al. Experimental model for cartilage tissue engineering to regenerate the zonal organization of articular cartilage. Osteoarthritis and Cartilage. 2003;11:653-64.
[402] Sharma B, Elisseeff JH. Engineering structurally organized cartilage and bone tissues. Annals of Biomedical Engineering. 2004;32:148-59.
[403] Holland TA, Bodde EWH, Baggett LS, Tabata Y, Mikos AG, Jansen JA. Osteochondral repair in the rabbit model utilizing bilayered, degradable oligo(poly(ethylene glycol) fumarate) hydrogel scaffolds. Journal of Biomedical Materials Research Part A. 2005;75A:156-67.
[404] Liu YC, Chen FG, Liu W, Cui L, Shang QX, Xia WY, et al. Repairing large porcine full-thickness defects of articular cartilage using autologous chondrocyte-engineered cartilage. Tissue Engineering. 2002;8:709-21.
[405] Zhou G, Liu W, Cui L, Wang X, Liu T, Cao Y. Repair of porcine articular osteochondral defects in non-weightbearing areas with autologous bone marrow stromal cells. Tissue Engineering. 2006;12:3209-21.
[406] Grigoriadis AE, Heersche JNM, Aubin JE. Differentiation of muscle, fat, cartilage, and bone from progenitor cells present in a bone derived clonal cell population - Effect of dexamethasone. Journal of Cell Biology. 1988;106:2139-51.
[407] Fratzl-Zelman N, Fratzl P, Horandner H, Grabner B, Varga F, Ellinger A, et al. Matrix mineralization in MC3T3-E1 cell cultures initiated by beta-glycerophosphate pulse. Bone. 1998;23:511-20.
[408] Chua CC, Chua BHL, Chen ZY, Landy C, Hamdy RC. Dexamethasone induces caspase activation in murine osteoblastic MC3T3-E1 cells. Biochimica Et Biophysica Acta-Molecular Cell Research. 2003;1642:79-85.

[409] Owen HC, Roberts SJ, Ahmed SF, Farquharson C. Dexamethasone-induced expression of the glucocorticoid response gene lipocalin 2 in chondrocytes. American Journal of Physiology-Endocrinology and Metabolism. 2008;294:E1023-E34.
[410] Quarles LD, Yohay DA, Lever LW, Caton R, Wenstrup RJ. Distinct proliferative and differentiated stages of murine MC3T3-E1 cells in culture - An in vitro model of osteoblast development. Journal of Bone and Mineral Research. 1992;7:683-92.
[411] Lacombe-Gleize S, Gregoire M, Demignot S, Hecquet C, Adolphe M. Implication of the TGF-beta-1 in co-culture of chondrocytes-osteoblasts. In Vitro Cellular & Developmental Biology-Animal. 1995;31:649-52.
[412] Jiang J, Nicoll SB, Lu HH. Co-culture of osteoblasts and chondrocytes modulates cellular differentiation in vitro. Biochemical and Biophysical Research Communications. 2005;338:762-70.
[413] Chang WH, Tu CL, Pratt S, Chen TH, Shoback D. Extracellular Ca2+-sensing receptors modulate matrix production and mineralization in chondrogenic RCJ3.1C5.18 cells. Endocrinology. 2002;143:1467-74.
[414] Mallein-Gerin F, Garrone R, Vanderrest M. Proteoglycan and collagen-synthesis are correlated with actin organization in dedifferentiating chondrocytes. European Journal of Cell Biology. 1991;56:364-73.
[415] Addison WN, Azari F, Sorensen ES, Kaartinen MT, McKee MD. Pyrophosphate inhibits mineralization of osteoblast cultures by binding to mineral, up-regulating osteopontin, and inhibiting alkaline phosphatase activity. Journal of Biological Chemistry. 2007;282:15872-83.
[416] Abraham LC, Dice JF, Lee K, Kaplan DL. Phagocytosis and remodeling of collagen matrices. Experimental Cell Research. 2007;313:1045-55.
[417] Claudio E Pedraza BM, Florencia Chicatun, Marc D McKee, Showan N Nazhat. An *in vitro* assessment of a cell-containing collagenous extracellular matrix-like scaffold for bone tissue engineering. Tissue Entineering Part A - Ahead of print2009.
[418] Levick JR. Flow through interstitium and other fibrous matrices. Quarterly Journal of Experimental Physiology and Cognate Medical Sciences. 1987;72:409-38.
[419] Guterl CC, Hung CT, Ateshian GA. Electrostatic and non-electrostatic contributions of proteoglycans to the compressive equilibrium modulus of bovine articular cartilage. Journal of Biomechanics. 2010;43:1343-50.
[420] Kolacna L, Bakesova J, Varga F, Kostakova E, Planka L, Necas A, et al. Biochemical and biophysical aspects of collagen nanostructure in the extracellular matrix. Physiological Research. 2007;56:S51-S60.
[421] Griffith LG, Naughton G. Tissue engineering - Current challenges and expanding opportunities. Science. 2002;295:1009-14.
[422] Griffith LG, Swartz MA. Capturing complex 3D tissue physiology in vitro. Nature Reviews Molecular Cell Biology. 2006;7:211-24.

[423] Fratzl P. Collagen: structure and mechanics. New York: Springer Science + Bussiness Media, LLC; 2008.
[424] Laasanen MS, Toyras J, Korhonen RK, Rieppo J, Saarakkala S, Nieminen MT, et al. Biomechanical properties of knee articular cartilage. Biorheology. 2003;40:133-40.
[425] Kempson GE, Muir H, Swanson SAV, Freeman MAR. Correlation between stiffness and chemical constituents of cartilage on human femoral head. Biochimica Et Biophysica Acta. 1970;215:70-7.
[426] Gu WY, Yao H. Effects of hydration and fixed charge density on fluid transport in charged hydrated soft tissues. Annals of Biomedical Engineering. 2003;31:1162-70.
[427] Costa-Pinto AR, Reis RL, Neves NM. Scaffolds Based Bone Tissue Engineering: The Role of Chitosan. Tissue Engineering Part B-Reviews. 2011;17:331-47.
[428] Navarro M, Michiardi A, Castano O, Planell JA. Biomaterials in orthopaedics. Journal of the Royal Society Interface. 2008;5:1137-58.
[429] Bhat S, Tripathi A, Kumar A. Supermacroprous chitosan-agarose-gelatin cryogels: in vitro characterization and in vivo assessment for cartilage tissue engineering. Journal of the Royal Society Interface. 2011;8:540-54.
[430] Sun B, Ma W, Su F, Wang Y, Liu J, Wang D, et al. The osteogenic differentiation of dog bone marrow mesenchymal stem cells in a thermo-sensitive injectable chitosan/collagen/beta-glycerophosphate hydrogel: in vitro and in vivo. Journal of Materials Science-Materials in Medicine. 2011;22:2111-8.
[431] Song KD, Qiao M, Liu TQ, Jiang B, Macedo HM, Ma XH, et al. Preparation, fabrication and biocompatibility of novel injectable temperature-sensitive chitosan/glycerophosphate/collagen hydrogels. Journal of Materials Science-Materials in Medicine. 2010;21:2835-42.
[432] Serpooshan V, Quinn TM, Muja N, Nazhat SN. Characterization and modelling of a dense lamella formed during self-compression of fibrillar collagen gels: implications for biomimetic scaffolds. Soft Matter. 2011;7:2918-26.
[433] Serpooshan V, Quinn TM, Muja N, Nazhat SN. Hydraulic permeability of multilayered collagen gel scaffolds under plastic compression-induced unidirectional fluid flow. Acta Biomaterialia. 2013;9:4673-80.
[434] Hadjipanayi E, Ananta M, Binkowski M, Streeter I, Lu Z, Cui ZF, et al. Mechanisms of structure generation during plastic compression of nanofibrillar collagen hydrogel scaffolds: towards engineering of collagen. Journal of Tissue Engineering and Regenerative Medicine. 2011;5:505-19.
[435] Chicatun F, Pedraza CE, Muja N, Ghezzi CE, McKee MD, Nazhat SN. Effect of chitosan incorporation and scaffold geometry on chondrocyte function in dense collagen type I hydrogels. Tissue Engineering, Part A; 2013, DOI 10.1089/ten.TEA.2013.0114.

[436] Fels G. Hydration and Density of Collagen and Gelatin. Journal of Applied Polymer Science. 1964;8:1863-24.
[437] Cho YI, No HK, Meyers SP. Physicochemical characteristics and functional properties of various commercial chitin and chitosan products. Journal of Agricultural and Food Chemistry. 1998;46:3839-43.
[438] Mertins O, Dimova R. Binding of Chitosan to Phospholipid Vesicles Studied with Isothermal Titration Calorimetry. Langmuir. 2011;27:5506-15.
[439] Maroudas A. Fluid transport in cartilage. Annals of Rheumatic Disease. 1975;34:77-81.
[440] Grodzinsky AJ. Electrochemical and physicochemical properties of connective tissue. Crc Critical Reviews in Biomedical Engineering. 1983;9:133-99.
[441] Chin HC, Khayat G, Quinn TM. Improved characterization of cartilage mechanical properties using a combination of stress relaxation and creep. Journal of Biomechanics. 2011;44:198-201.
[442] Park H, Guo X, Temenoff JS, Tabata Y, Caplan AI, Kasper FK, et al. Effect of Swelling Ratio of Injectable Hydrogel Composites on Chondrogenic Differentiation of Encapsulated Rabbit Marrow Mesenchymal Stem Cells In Vitro. Biomacromolecules. 2009;10:541-6.
[443] Maroudas A. Balance between swelling pressure and collagen tension in normal and degenerative cartilage. Nature. 1976;260:808-9.
[444] Correia CR, Moreira-Teixeira LS, Moroni L, Reis RL, van Blitterswijk CA, Karperien M, et al. Chitosan Scaffolds Containing Hyaluronic Acid for Cartilage Tissue Engineering. Tissue Engineering Part C-Methods. 2011;17:717-30.
[445] Quinn TM, Dierickx P, Grodzinsky AJ. Glycosaminoglycan network geometry may contribute to anisotropic hydraulic permeability in cartilage under compression. Journal of Biomechanics. 2001;34:1483-90.
[446] Owen SC, Shoichet MS. Design of three-dimensional biomimetic scaffolds. Journal of Biomedical Materials Research Part A. 2010;94A:1321-31.
[447] Comper WD, Laurent TC. Physiological function of connective-tissue polysaccharides. Physiological Reviews. 1978;58:255-315.
[448] Maroudas A. Physicochemical properties of cartilage in light of ion exchange theory. Biophysical Journal. 1968;8:575-95.
[449] Lai WM, Mow VC, Sun DD, Ateshian GA. On the electric potentials inside a charged soft hydrated biological tissue: Streaming potential versus diffusion potential. Journal of Biomechanical Engineering-Transactions of the Asme. 2000;122:336-46.
[450] Canal Guterl C, Hung CT, Ateshian GA. Electrostatic and non-electrostatic contributions of proteoglycans to the compressive equilibrium modulus of bovine articular cartilage. Journal of biomechanics. 2010;43:1343-50.

[451] Ramanujan S, Pluen A, McKee TD, Brown EB, Boucher Y, Jain RK. Diffusion and convection in collagen gels: Implications for transport in the tumor interstitium. Biophysical Journal. 2002;83:1650-60.
[452] Korhonen RK, Julkunen P, Wilson W, Herzog W. Importance of collagen orientation and depth-dependent fixed charge densities of cartilage on mechanical behavior of chondrocytes. Journal of biomechanical engineering. 2008;130:021003.
[453] Eisenberg SR, Grodzinsky AJ. Swelling of articular cartilage and other connective tissues - Electromechanochemical forces Journal of Orthopaedic Research. 1985;3:148-59.
[454] Ostroha J, Pong M, Lowman A, Dan N. Controlling the collapse/swelling transition in charged hydrogels. Biomaterials. 2004;25:4345-53.
[455] Dadsetan M, Pumberger M, Casper ME, Shogren K, Giuliani M, Ruesink T, et al. The effects of fixed electrical charge on chondrocyte behavior. Acta Biomaterialia. 2011;7:2080-90.
[456] Bryant SJ, Arthur JA, Anseth KS. Incorporation of tissue-specific molecules alters chondrocyte metabolism and gene expression in photocrosslinked hydrogels. Acta Biomaterialia. 2005;1:243-52.
[457] Yamamoto T, Hasegawa T, Sasaki M, Hongo H, Tabata C, Liu Z, et al. Structure and formation of the twisted plywood pattern of collagen fibrils in rat lamellar bone. Journal of Electron Microscopy. 2012;61:113-21.
[458] Stolz M, Gottardi R, Raiteri R, Miot S, Martin I, Imer R, et al. Early detection of aging cartilage and osteoarthritis in mice and patient samples using atomic force microscopy. Nature Nanotechnology. 2009;4:186-92.
[459] Marelli B, Ghezzi CE, Barralet JE, Nazhat SN. Collagen gel fibrillar density dictates the extent of mineralization in vitro. Soft Matter. 2011;7:9898-907.
[460] Izadifar Z, Chen X, Kulyk W. Strategic design and fabrication of engineered scaffolds for articular cartilage repair Journal of Functional Biomaterials; 2012. p. 799-838.
[461] Kladny B, Martus P, Schiwy-Bochat KH, Weseloh G, Swoboda B. Measurement of cartilage thickness in the human knee-joint by magnetic resonance imaging using a three-dimensional gradient-echo sequence. International Orthopaedics. 1999;23.
[462] Stein GS, Lian JB, van Wijnen AJ, Stein JL, Montecino M, Javed A, et al. Runx2 control of organization, assembly and activity of the regulatory machinery for skeletal gene expression. Oncogene. 2004;23:4315-29.
[463] Bastow ER, Byers S, Golub SB, Clarkin CE, Pitsillides AA, Fosang AJ. Hyaluronan synthesis and degradation in cartilage and bone. Cellular and Molecular Life Sciences. 2008;65.
[464] Oohira A, Nogami H. Elevated accumulation of hyaluronate in the tubular bones of osteogenesis imperfecta. Bone. 1989;10.
[465] Cheema U, Rong Z, Kirresh O, MacRobert AJ, Vadgama P, Brown RA. Oxygen diffusion through collagen scaffolds at defined densities: implications

for cell survival in tissue models Journal of Tissue Engineering and Regenerative Medicine. 2012;6:77-84.
[466] Yokota M, Yasuda K, Kitamura N, Arakaki K, Onodera S, Kurokawa T, et al. Spontaneous hyaline cartilage regeneration can be induced in an osteochondral defect created in the femoral condyle using a novel double-network hydrogel. Bmc Musculoskeletal Disorders. 2011;12.